Modelling The Morphology Of

Molecular Crystals

by

Robert Docherty, BSc

A thesis submitted to Strathclyde University in part fulfilment
of the degree of Doctor of Philosophy

June 1989

Department of Pure and Applied Chemistry

University of Strathclyde

Glasgow

To my parents

Declaration

I hereby declare that the work detailed in this thesis, except where noted in the text, was carried out by me at Strathclyde University and that none of the work has been presented before for any other degree.

Signed: Robert Docherty

Date: 31-7-89

Acknowledgements

I wish to express my appreciation of the constant help, encouragement and support provided by Dr. K.J. Roberts throughout this project. I also wish to acknowledge Dr's S.N. Black and R.J. Davey (ICI Chemicals and Polymers, Runcorn) and Prof. J.N. Sherwood and Dr. D. Pugh for their guidance and help.

This work was funded jointly through a Mackie Scholarship from Strathclyde University and by ICI Chemicals and Polymers, Runcorn.

Thanks are also due to Prof. P. Bennema (University of Nijmegen) and Dr. V. Saunders (Daresbury Laboratory) for their help and advice concerning the work in chapters 9 and 7 respectively. Their expertise in their particular fields proved invaluable.

Abstract

Computer programs have been written which allow morphological calculations based on a knowledge of internal crystal structure to be carried out. Details of the programs are presented along with the guidelines developed for their use.

The programs were used to compare and contrast the current methods employed for relating crystal shape to structure and to confront specific problems in that field.

Calculations on a range of compounds show that the morphologies derived from the simple Donnay-Harker (DH) model give almost as good a fit to the observed form as the more sophisticated attachment energy (AE) calculations except when strong bonding directions were present.

In the first study of its type all the methods currently favoured in the literature including the Ising and PBC approaches as well as the DH and AE models were applied to benzophenone. All the models gave the same theoretical morphology.

One problem remaining in the field of relating crystal structure and morphology is that of polar morphology. None of the current methods can account for a polar morphology. Surface, bulk, isolated molecule charge distributions were used in a modification of the classical attachment energy model to account for urea exhibiting a polar morphology when grown from the vapour phase.

For the disruptive type of tailor made additives an improvement in the current methodology is proposed with the calculation of an additional parameter. This additional parameter accounts for the morphology with an additive present and gives good agreement with the test case of benzamide crystals grown with benzoic acid as an additive.

The additive approach also allowed the effects of toluene solvent on the crystal habit of benzophenone to be considered. By treating toluene as a tailor-made additive it was possible from calculations to identify the likely sites of toluene incorporation and the subsequent effect on crystal growth. The results from the calculation were consistent with experiment.

Table Of Contents

Chapter 1

Introduction

CONTENTS

1 The Nature of the Crystalline State

A crystal is an ordered solid bounded by a series of plane faces which are the outcome of natural processes. The fascination of crystals to early crystallographers lay in the planeness and symmetry of these faces. This regular external arrangement led these crystallographers to postulate that the shape of crystals was the result of an ordered internal arrangement. The French crystallographer Hauy [1] showed that basic crystal shapes such as cubes , octahedrons and rhombic dodecahedrons could be built up by stacking cubes, and that these cubes could be considered as the basic building blocks of the crystal. The basic building block is now referred to as a 'unit cell'. The use of X- ray diffraction allows the internal structure of crystals to be identified by describing the unit cell. The importance of this technique and the information it can provide will be discussed further in chapter 2.

Crystalline material can be divided up into a number of categories including ionic, covalent, metallic and molecular crystals. Ionic crystals are formed by interactions between oppositely charged species. In sodium chloride (NaCl) each Na^+ ion is surrounded by six Cl^- ions, held together by electrostatic interactions. Covalent crystals including diamond are formed as a result of the sharing of electrons between atoms to form a stable outer shell electron configuration. In diamond each C atom is surrounded by four other C atoms in a tetrahedral arrangement. Metallic crystals are formed by metal atoms sharing electrons with their surrounding neighbours. Molecular crystals, the crystals of interest in this thesis, are formed by molecules held together in a crystal lattice by relatively weak Van der Waals interactions and in some cases considerably stronger hydrogen bonds.

2 The Importance of Crystallisation

The crystallisation process has always played an important role in industry. Many people will be familar with the products of crystallisation they encounter in daily life, salt and sugar the most common examples. Less familiar, however will be the role of crystallisation in the body's metabolism and in industry. Crystallisation is believed to have a vital role in the formation of teeth and bones. A counter productive effect of crystallisation in the human body is the formation of 'stones' in the kidney and gallbladder which can result in health problems. In some cases surgery is required to alleviate the condition.

Crystallisation in industry has been and still is the subject of considerable study as it is one of the most important processes for the separation and purification of both bulk and speciality chemicals. Indeed the increasing importance of speciality chemicals in industry, including pharmaceuticals and agrochemicals has led to increased interest in the crystallisation of molecular crystals, the crystals of interest in this thesis. The particular aspect of crystallisation studied in this thesis is crystal shape. The importance of crystal shape to production efficiency and post production properties is considerable:

1) Product Separation - The crystal shape can affect the separation of the product from the mother liquor and the subsequent washing of the product. Plate like crystals for example can result in reduced filtration efficiency.

2) Product Handling - The handling of the product during and after the production process can be affected by crystal shape. Whenever flow through machinery is required the crystal shape must allow free-flow. Small fine crystals can be difficult to handle during production stages and during use by a customer. These types of crystals can break-up to form dust particles which may present a hazard to workers.

3) Package and Storage - It is often required that the crystal shape allows the maximum packing density. When long periods of storage are envisaged the problem of caking must be minimised.

4) Effect Property - In speciality chemicals the 'effect' or property being sold may depend on crystal shape. In pharmaceuticals the dissolution rate is often important and this depends on a number of factors including crystal shape.

It is often necessary to modify the crystal shape not only to reduce production problems but to produce a crystal with the size and shape desired by a customer. Differences in crystal shape and size may differentiate one manufacturers product from another. This change in crystal shape is often referred to as 'habit- modification'. In the oil industry habit-modifiers are used to prevent scaling in pipes in the North Sea by inhibiting the crystallisation of calcium and

barium sulphates. Habit-modifiers are also used to prevent the crystallising of flat plate like crystals in diesel fuels as the resultant plate like crystals can block fuel filters.

A systematic trial and error approach in an attempt to identify habit-modifiers is likely to be a time consuming and expensive procedure. Control experiments must be carried out to test that 'impurities' inherent to the system are not already influencing the crystal shape produced. Lahav and co-workers [2,3] at the Weizmann Institute have elegantly shown from a structural viewpoint the possibility of crystal morphology engineering by the use of tailor-made additives. The importance of understanding the fundamental crystal chemistry to industrial processes has been outlined by Davey [4].

3 Intermolecular Forces

Molecular crystals differ from the other classes of crystalline material because they are discrete units which are held together by relatively weak 'non-bonded' interactions. The attractive part of this interaction can be considered to result from dipole-dipole, dipole-induced dipole and dispersion forces. The interaction between two dipoles depends on the magnitude of the dipoles, their relative orientation and the distance by which they are separated r. It can be shown the dependence is in fact r^{-6}. When one polar species is close to another species (which may be polar or not) a dipole can be induced in the other species and vice-versa. The magnitude for this dipole-induced dipole interaction can be shown to depend on dipole magnitude, orientation, r^{-6} and the polarisability of the species in question. This accounts for interactions in polar species but not for neutral species such as the noble gases. In a neutral species the positive nucleus is surrounded by a cloud of electron density. The average over time is a sphere. At any instant in time the electron will be moving in a specific direction and this results in an instantaneous dipole. At another instant in time the electron will be moving in a different direction and so a different instantaneous dipole will result. The interaction between these instantaneous dipoles in different neutral entities results in the so-called dispersion forces, often referred to as the London forces. The dispersion forces also depend on r^{-6}. All the attractive forces show a common dependence on r^{-6}. The attractive interaction V_{att} is often written

$$V_{att} = -A/r^6 \tag{1.1}$$

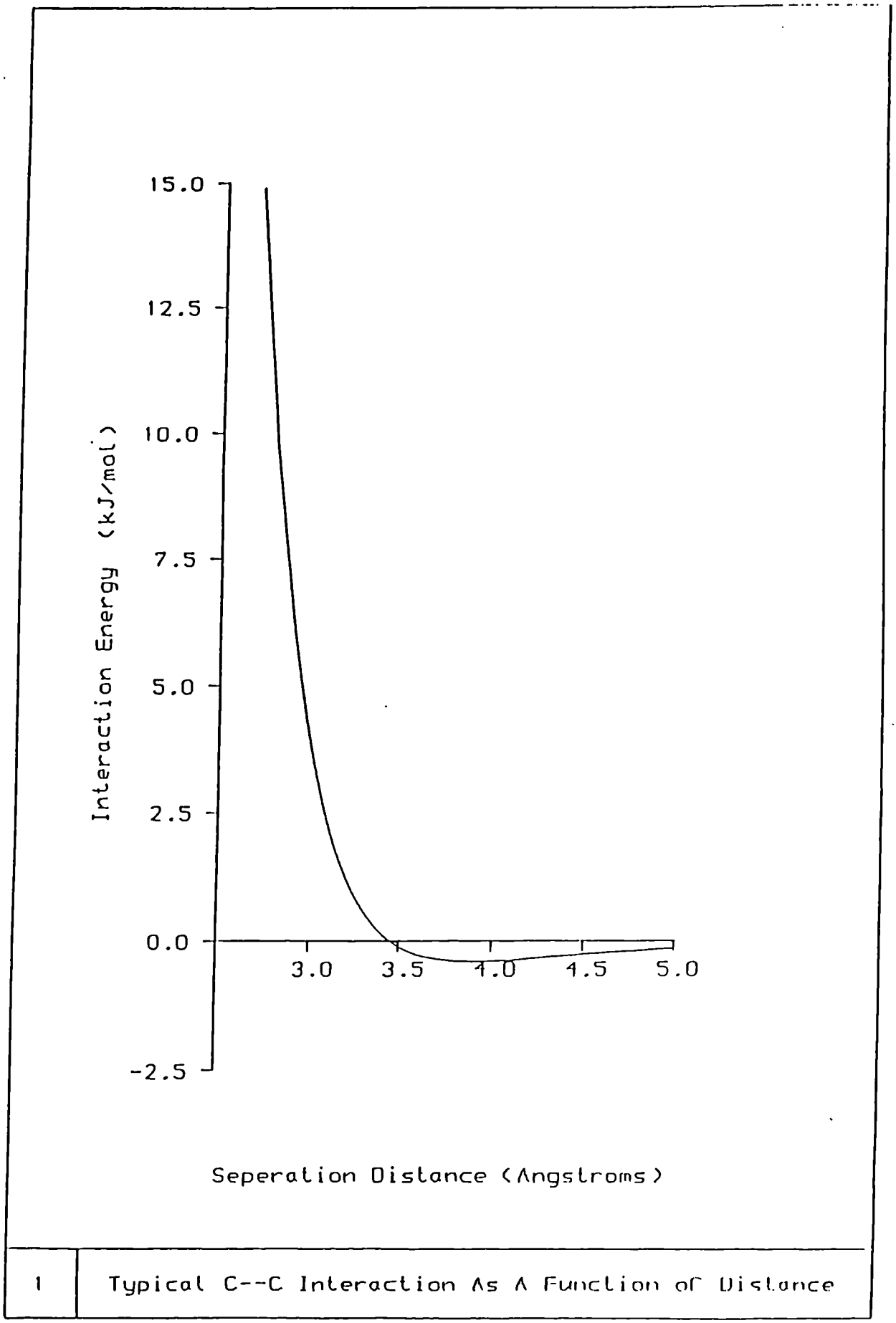

Figure 1.1 Typical C—C non-bonded Interaction as a function of separation distance r.

where A is a constant depending on the nature of the two species being considered.

Repulsive forces dominate the interactions at very short distances. This is due to the overlap of electron clouds. Calculations on this are very complex and so empirical potentials are fitted to experimental observables such as compressibility data. The most common forms of potential for describing the repulsive interactions V_{rep} are shown below

$$V_{rep} = B/r^{12} \tag{1.2}$$

$$V_{rep} = Bexp(-Cr) \tag{1.3}$$

where B and C are constants. On combination of the attractive and repulsive forces a description of the non-bonded interaction V_{nb} can be obtained. The two most common are the Lennard-Jones 6-12 (1.4) and Buckingham 6-exp (1.5) functions.

$$V_{nb} = -A/r^6 + B/r^{12} \tag{1.4}$$

$$V_{nb} = -A/r^6 + Bexp(-Cr) \tag{1.5}$$

A typical interaction curve is shown for carbon -carbon interaction in Fig 1.1. Note the dominance of the repulsive contributions at distances shorter than 3.0 Å. The minimum interaction energy is -0.4kJ/mol at an interaction distance of 3.9Å. The general shape of the curve remains the same for all atom-atom nonbonded interactions, the minimum depth and position can however vary.

4 Modelling Molecular Crystals

An understanding of the nature of the molecular crystalline state in terms of interatomic and intermolecular potentials has been of interest for a number of years. The pioneering work of Kitaigorodskii [5] and Williams [6,7] in the derivation of parameters for describing atom-atom interactions and the use of such parameters for crystal structure packing analysis has shown the applicability of this approach for organic materials. This approach is often referred to as the 'atom-atom' approximation since it assumes that the interaction between two molecules consists of the sum of all the interactions between the constituent

atoms. These two workers used the Buckingham [8] potential of the form given in equation (1.6) to initially describe the atom-atom interactions in simple hydrocarbons.

$$V_{ij} = -A/r^6 + Bexp(-Cr) \tag{1.6}$$

A, B and C are the so-called atom-atom parameters for describing the interactions between two non-bonded atoms i and j. Extension of this approach to describe the interactions in more complicated organic systems involved inclusion of electrostatic and special hydrogen bond functions as well as an update of the actual parameters [9,10]. Attempts to derive parameter sets for inorganic systems have also been made [11] and recently the atom-atom approach has been used to study organo-metallic compounds [12]. Programs for carrying out these type of calculations including PCK83 by Williams [13] and WMIN by Busing [14] have been published.

5 Internal and External Structure

The relationship between the internal arrangement of a crystal and it's external appearance has been of interest to mineralogists and chemists for a number of years. Gibbs [15] proposed that the shape of a crystal will be one in which the total free energy of the system is a minimum. Wulff [16] extended this theory. He showed that the equilibrium crystal shape is related to the surface free energies of the faces. Wulff also suggested that the relative rates at which faces grow away from the center of a crystal is related to these surface energies. The earliest attempts to understand external crystal shape in terms of internal structure tried to relate the crystal shape of mainly inorganic systems to the lattice geometry. These simple geometrical rules developed by Bravais - Friedel [17] and Donnay - Harker (DH) [18] still provide a good quick initial approach for identifying the likely crystallographic forms $\{hkl\}$ which dominate the crystal shape. The general rule is that taking into account sub-multiples of the interplanar spacing (d_{hkl}) due to space group symmetry (i.e. centering, screw axis, glide planes) the most important crystallographic forms $\{hkl\}$ will have the greatest interplanar spacing.

The advent of crystal structure determination (as discussed in the following chapter) allowed the attempts to quantify external crystal shape to be related to the internal structure not just at a geometrical level but to a molec-

ular and atomic scale. Hartman and Perdok's [19,20] Periodic Bond Chain (PBC) Theory quantified morphological theory in terms of the interaction energy between crystallising units. They identified periodic chains of strong bonds (PBC's) and defined the flat habit faces (F-faces), as those containing at least two PBC's in the growth slice of thickness d_{hkl}. They proposed that the attachment energy (the energy per molecule released on the attachment of a building block of thickness d_{hkl} to a crystal surface) is a measure of the growth rate normal to that face. Hartman and Bennema [21] have shown that under certain conditions this is a valid assumption for a number of crystal growth mechanisms.

Several predictions of morphology have been carried out by a number of workers using the PBC theory and the atom-atom approximation on a variety of materials, including diamond [22], barium sulphate [23], anthracene [24], α-alumina [25], sucrose [26] and biphenyl [27]. Recently Berkovitch-Yellin [28] has outlined a variation on this approach and predicted the morphologies of a number of carboxylic acids by calculating the attachment energies of growth slices by assuming the oncoming slice has the same structure as an equivalent slice in the bulk. This method will be referred to in this paper as the Attachment Energy (AE) model. This approach has been extended in an attempt to quantify the effects of tailor-made additives [2,3]. On the whole the predicted morphologies have shown good agreement with the observed morphologies. Differences in some cases have been accounted for by considering the preferential adsorption of solvent on certain faces [26,28] and the effects of surface relaxation [29].

6 Scope and Summary of Thesis

In this thesis investigations into modelling molecular crystal morphology are carried out. Computational models are used to predict theoretical morphologies and to attempt to quantify the effects on crystal shape of 'tailor-made' additives. When investigating morphology and morphological modification the use of computational models could provide a useful technique for concentrating time consuming experimental studies in the area's likely to yield the most fruitful results. Basic approaches are presented for carrying out the calculations along with details of the computer programs written to do these calculations. The programs and approaches are tested against a variety of examples and used to address specific problems in the field of modelling crystal morphology.

In chapter 2 a broad overview of the theories behind crystal growth and a more detailed look at the approaches for modelling morphology is given. Chap-

ter 3 is the experimental section and concentrates on crystal growth and the determination of the observed morphology. Chapter 4 provides an outline of the approaches for carrying out the calculations and where each of the programs written fit into the approaches. Details of the three programs MORANG, CRYSTLINK and PCLEMC are given in Appendices A, B and C.

Chapter 5 involves calculations on the lattice energies of molecular crystals. Particular emphasis is paid on the materials which are to be studied in subsequent chapters in this thesis. Chapter 6 has studies on four materials namely anthracene, biphenyl, β-succinic acid and benzoic acid. The reasons for the study of these materials are two fold. Firstly a comparison between the Donnay-Harker and Attachment Energy models and secondly a comparison of the calculated morphologies resulting from different choice of atom-atom parameter set.

One of the remaining problems concerning predicting crystal morphology is that of polar crystals. It has been shown that a conventional approach cannot predict a polar morphology [30,31]. In chapter 7 this problem is confronted using urea as a test case. A variation on the convential approach is suggested as a possible route for predicting polar morphology. In chapter 8 the effects of tailor made additives are considered. Small amounts of tailor-made additives can affect the shape of a crystal [2,3]. Proposed developments are outlined and the results confronted with experimental observations.

In chapter 9 the study is concentrated on one material. Benzophenone, an aromatic ketone is investigated using Donnay- Harker, PBC analysis, Attachment energy and Ising models. This chapter brings together a number of approaches and discusses the advantages of each approach. The effect of toluene solvent on the observed morphology of benzophenone is accounted for by considering toluene as a tailor-made additive. Chapter 10 includes a discussion of the results in the previous chapter an an evaluation of the approaches outlined. Suggestions for future work and development are also included.

Appendix A is concerned with the details of the program MORANG. Appendix B deals with the details of the program CRYSTLINK, Appendix C concentrates on PCLEMC including program details and sample input. Appendix D deals with the accuracy of fitting hydrogens to incomplete structures. Appendix E has a list of publications resulting from this work and details on calculations carried out by other users of the programs.

7 References

[1] R.J. Hauy, J. Phys. 19 (May 1792) 366.

[2] Z. Berkovitch-Yellin, J van Mil, L. Addadi, M. Idelson, M. Lahav and L. Leiserowitz. J. Am. Chem. Soc. 107 (1985) 3111.

[3] I. Weissbuch, L.J. Shimon, L.Addadi, Z. Berkovitch-Yellin, S. Weinstein and L. Leiserowitz. Isr. J. Chem. 25 (1985) 353.

[4] R.J. Davey. The Chemical Engineer Dec (1987) 24.

[5] A.I. Kitaigorodski. Tetrahedron 14 (1961) 230.

[6] D.E. Williams. J. Phys. Chem. 45 (1966) 3370.

[7] D.E Williams. Acta Cryst. A28 (1972) 629.

[8] R.A. Buckingham and J. Corner. Proc. Royal Soc. 189 (1947) 118.

[9] S. Lifson, A.T. Hagler and P.Dauber. J. Amer. Chem. Soc. 101 (1979) 5111.

[10] F.A. Momany, L.M. Carruthers, R.F. McGuire and H.A. Scheraga. J. Phys. Chem. 78 (1974) 1579.

[11] R. Skorczyk. Acta Cryst. A32 (1976) 447.

[12] J. Sanz-Aparicio, S. Martinez-Carrera, S. Garcia-Blanco and A. Conde. Acta Cryst. B44 (1988) 259.

[13] D.E. Williams. PCK83, A Crystal Molecular Packing Analysis Program. Quantum Chemistry Program Exchange Program No. 481.

[14] W.R. Busing. WMIN, A Computer Program to Model Molecules and Crystals In Terms of Potential Energy Functions. April 1981, Oak Ridge National Laboratory, Oak Ridge, Tennesse 37830.

[15] J.W. Gibbs. 'The Equilibrium Of Heterogenous Substances', Scientific Papers, Vol 1 (1906).

[16] G. Wulff, Z. Krist. 34 (1901) 499.

[17] A. Bravais. Etudes Crystallographiques (Paris, 1913).

[18] J.D.H Donnay and D. Harker. Amer. Miner. 22 (1937) 463.

[19] P. Hartman and W.G. Perdok. Acta Cryst. 8 (1955) 49.

[20] P. Hartman in Crystal Growth: An introduction. Ed P. Hartman (North Holland Amsterdam 1973) p367.

[21] P. Bennema and P. Hartman. J. Cryst. Growth 49 (1980) 145.

[22] P. Hartman and W.G. Perdok. Acta Cryst. 8 (1955) 521.

[23] P. Hartman and W.G. Perdok. Acta Cryst. 8 (1955) 525.

[24] P. Hartman. J. Cryst. Growth 49 (1980) 157.

[25] P. Hartman. J. Cryst. Growth 49 (1980) 166.

[26] M. Saska and A.S. Myerson. J.Cryst. Growth 61 (1983) 546.

[27] H.J Human, J.P Van der Eerden, L.A.M.J. Jetten and J.G.M Oderkerken. J. Cryst. Growth 51 (1981) 589.
[28] Z. Berkovitch-Yellin. J.Amer. Chem. Soc. 107 (1985) 8239.
[29] W.C. Mackrodt, R.J. Davey, S.N. Black and R. Docherty. J. Cryst. Growth 80 (1987) 441.
[30] L. Addadi, Z. Berkovitch-Yellin, I. Weissbuch, M. Lahav and L. Leiserowitz. Topics in Stereochemistry 16 (1986) 1.
[31] R.J. Davey, B. Milisavljevic and J.R. Bourne. J. Phys. Chem. 92 (1988) 2032

Chapter 2

Theory

CONTENTS

1 Introduction

The following chapter is split into three main sections, a general introduction, a discussion on crystal growth and a section on the relationship between internal crystal structure and morphology. In the first section a brief introduction into crystal lattices, defects, planes and an outline of the useful information that can be obtained from a full x-ray or neutron diffraction structure analysis is given. The terminology introduced is used in the subsequent sections in this chapter.

Crystal growth proceeds in two stages, nucleation followed by growth. For nucleation to occur a certain degree of supersaturation has to be attained. Once nucleation has occured growth can begin. In the second section a broad oveview of the crystal growth process is presented. The mechanisms by which growth is thought to take place are discussed.

In the final section the relationships between morphology and internal structure are introduced and outlined. The terminology introduced in the first two sections will constantly be referred to in the third section.

1.1 Crystal Lattices

A crystal is an ordered three dimensional array of entities. The asymmetric unit is the basic material entity from which the crystal is built. The asymmetric unit may consist of a an atom, a number of atoms, a molecule or a number of molecules.

It is helpful when trying to discuss crystal structure to introduce the geometric concept of the crystal lattice. A lattice is a three dimensional array of points where each point in the lattice is in the same enviroment as it's neighbours. A lattice defines the basic structure of the crystal. It is the scaffolding of the crystal. A two dimensional lattice is shown in Figure 2.1. The lattice points can be linked in a variety of ways to form regular networks, the repeating unit is called the unit cell. In a two dimensional lattice two vectors a and b are required to describe the cell. A three dimensional lattice can be broken up into unit cells requiring three vectors to describe the unit cell. In a crystal structure each lattice point is replaced by an asymmetric unit or a cluster of asymmetric units.

The unit cell is the fundamental unit from which the crystal can be built by simple displacement translations (like bricks in a wall). The unit cell is described by three dimensions a, b, c and three angles α, β and γ as shown in Fig

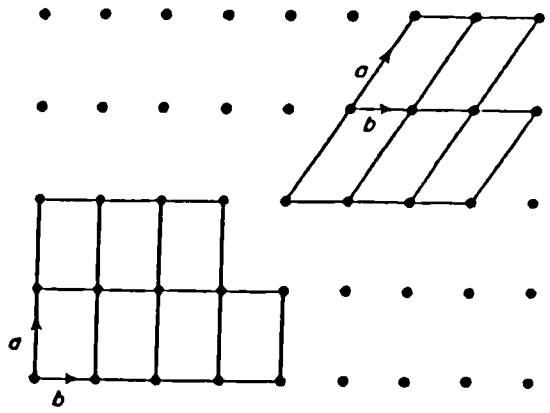

Figure 2.1 A simple two dimensional lattice.

System	Axes	Angles
Cubic	$a = b = c$	$\alpha = \beta = \gamma = 90°$
Tetragonal	$a = b, c$	$\alpha = \beta = \gamma = 90°$
Orthorhombic	$a; b; c$	$\alpha = \beta = \gamma = 90°$
Monoclinic	$a; b; c$	$\alpha = \gamma = 90°; \beta$
Rhombohedral	$a = b = c$	$\alpha = \beta = \gamma$
Hexagonal	$a = b; c$	$\alpha = \beta = 90°; \gamma = 120°$
Triclinic	$a; b; c$	$\alpha; \beta; \gamma$

Table 2.1 The seven crystal systems.

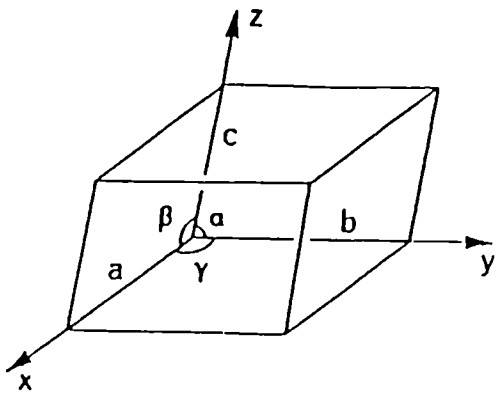

Figure 2.2 A typical unit cell.

2.2. These values are referred to as the unit cell dimensions or lattice parameters. A unit cell may contain a number of asymmetric units usually referred to as Z. The relationships between the unit cell parameters define seven crystal systems. The seven crystal systems and definitions are given in Table 2.1. They range from the unsymmetrical triclinic case with three unequal dimensions at three unequal angles to the highly symmetrical cubic system with three equal dimensions at right angles. Further background on crystal lattices can be obtained from standard texts on the subject [1].

1.2 Internal Structure of Crystals

In 1912 Max von Laue suggested that if crystals were irradiated with a wavelength as small as the distance between atoms then a diffraction pattern should result. W. Friedrich carried out an experiment passing an X-ray beam through a crystal of zinc sulphide and obtained a diffraction pattern [2]. Bragg [3] showed that the diffraction could be considered in terms of 'reflection' of the incident beam from parallel planes of atoms in the crystal structure.

The diffraction results from the interaction of the X-rays with the electrons in the crystal, the intensity of the diffraction depends on the nature of the scatter and its position. Analysis of the diffraction pattern can provide information on the internal structure of the crystal. A full crystal structure analysis can reveal a great deal of information. For molecular crystals this information can be classified into three categories:

1. Details of the Unit Cell - The analysis will give the dimensions of the unit cell (a,b,c) and the angles between the unit cell sides (α, β, γ) as shown in Figure. 2.2.

2. Molecular Information - The co-ordinates of the atoms in one molecule. These co-ordinates (x,y,z) are relative to the unit cell dimensions and are called fractional co-ordinates. These co-ordinates are the relative positions of the atoms in space and allows bond distances, bond angles and torsional angles for molecules to be calculated.

3. Symmetry Information - The analysis will also give details of the number of molecules in a unit cell and the relationship between one molecule and the other

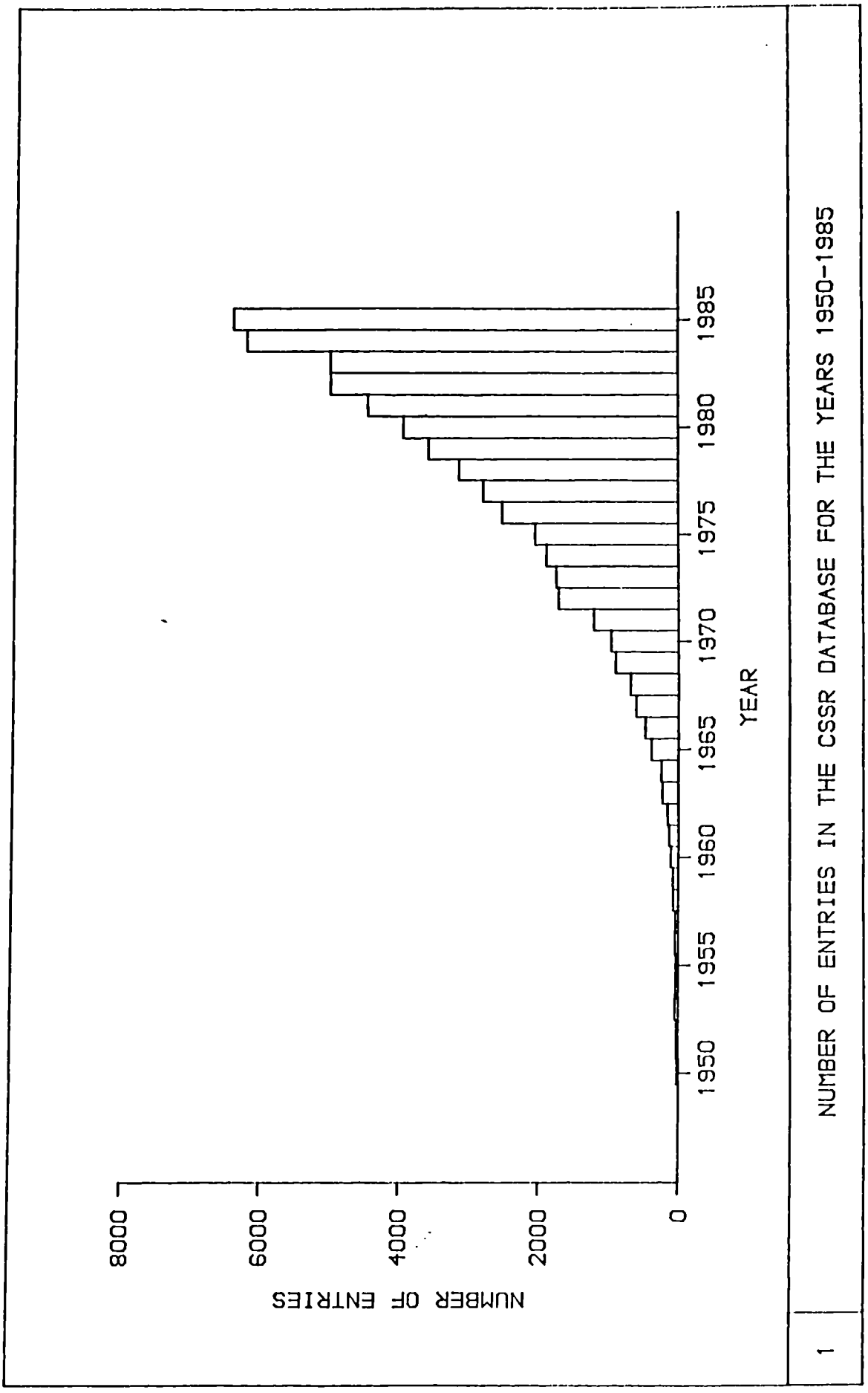

Figure 2.3 The number of entries in the Cambridge Structual Database for the years 1950-1985 inclusive.

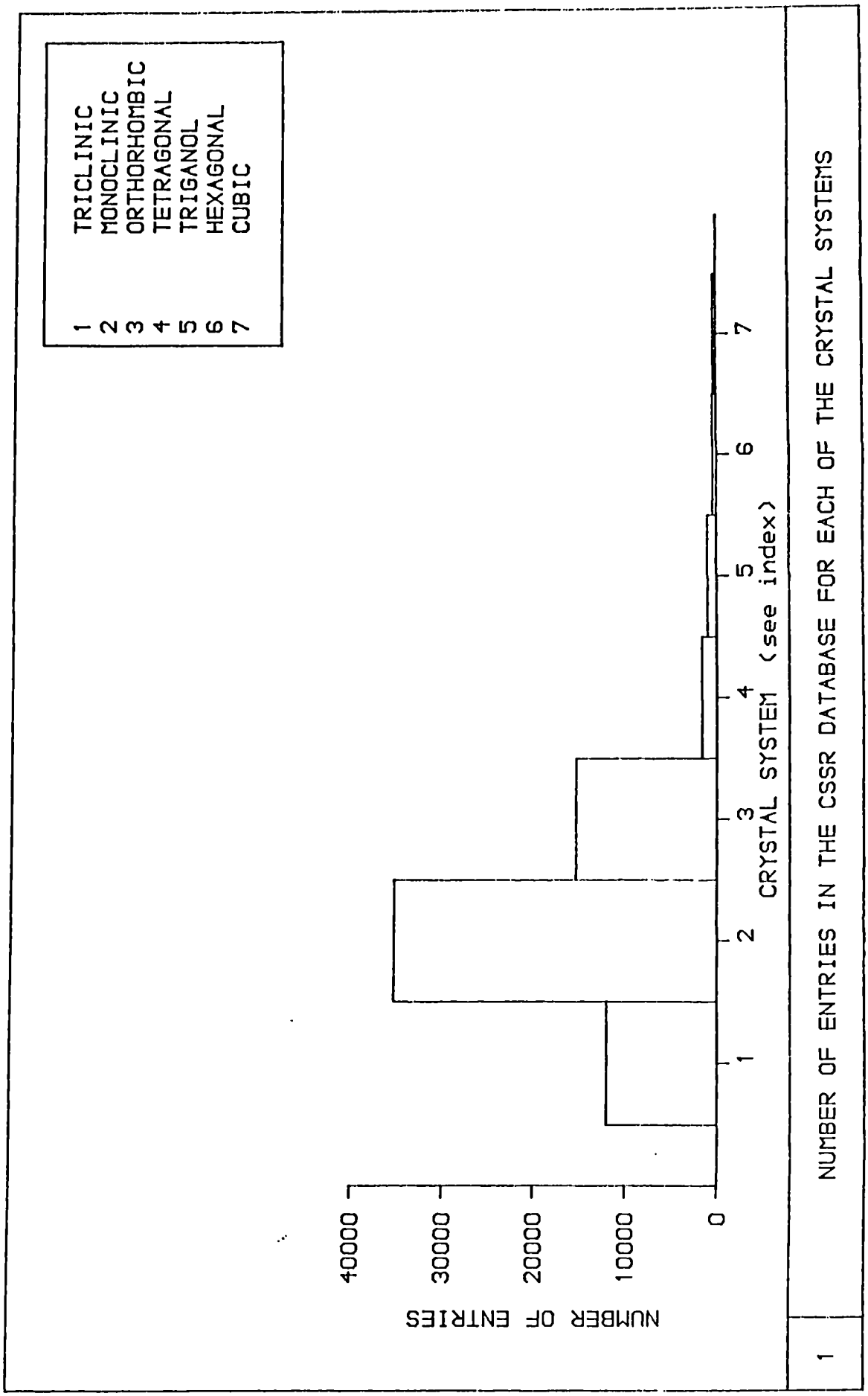

Figure 2.4 The number of entries in the Cambridge Structural Database for each of the seven crystal systems.

molecules (if any) in the unit cell.

A combination of these three pieces of information therefore gives a complete description of the structure of a crystal. This technique has over the past twenty years gained increasing importance. Computer databases have been set up to record the structures solved. Two databases have been set up for organic and inorganic structures. The Cambridge Structural Database (CSD) [4] for organic molecules has over 69000 entries in the current release (September 1988) and allows searching by formula, journal, author name and compound name. Figure 2.3 shows a histogram of the number of new entries in the database for particular years and reflects the increasing prominence of this technique. Crystals may be classified into one of seven crystal systems. Figure 2.4 shows an analysis of the database in terms of crystal system and shows a preference for monoclinic, triclinic and orthorhombic systems. The Inorganic Crystal Structure Database [5] is the corresponding database for inorganic structures, both these databases are mounted as part of the SERC Chemical Databank System at Daresbury Laboratory and are accessible via the JANET network. The Cambridge database has been slightly altered at Daresbury to allow interactive searching on a VAX computer system. This new form of the database is called the Crystal Structure Search Retrevial (CSSR) database [6].

The emergence of X-ray crystallography allows the internal structure to be obtained and this is the basis for modelling of physical properties of crystals in terms of their internal structure.

1.3 Crystal Defects

Crystals are not perfect either internally or externally. Defects present in the structure can be classified according to the degree that they extend into the crystal lattice. Point defects (zero dimensional defects) are atomic sized and can be categorised into three types, namely vacancies, interstitials and impurities. Vacancies are essentially missing crystallising entities (atoms or molecules). Interstitials are extra atoms in sites not normally occupied in the lattice. Impurities are foreign atoms occupying sites in the lattice.

Linear defects (one dimensional defects) are often referred to as dislocations. There are two basic types of dislocations called edge and screw. An edge dislocation is shown in Fig 2.5. An extra half plane of atoms has been inserted in the top half of the crystal. The inserted plane is indicated by shaded front

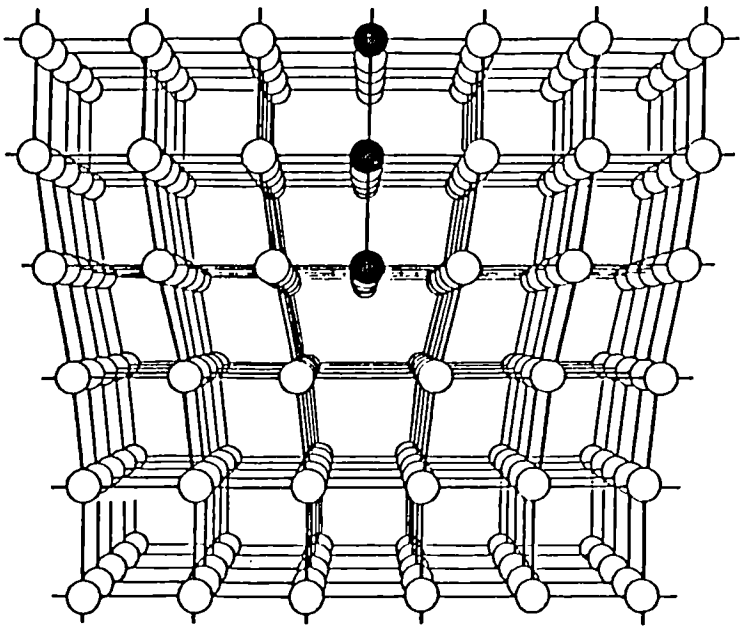

Figure 2.5 A typical edge dislocation (extra half plane of atoms are shaded for identification).

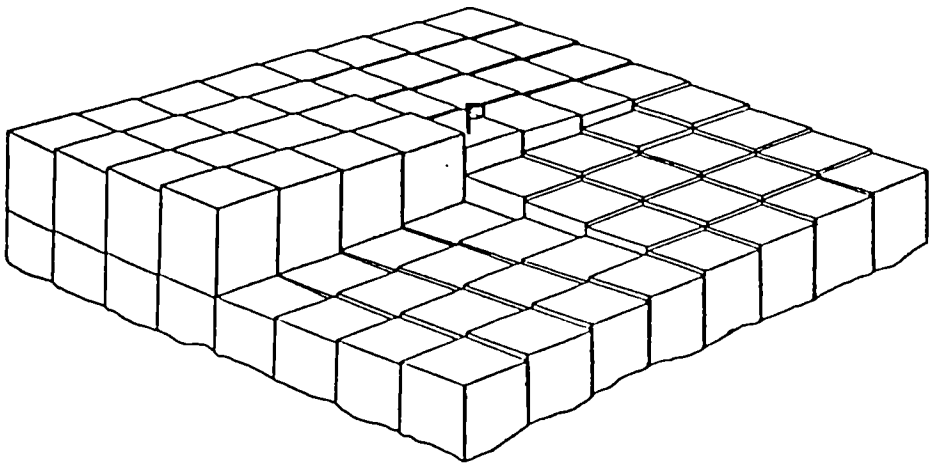

Figure 2.6 A typical screw dislocation The exposed layer rotates around the point P.

atoms. The edge dislocation results in compressed interatomic distances in the top half of the crystal and results in strain. A screw dislocation as shown in Figure 2.6 consists of a step on the surface which can be thought to result from a cut in the crystal (center to edge), the crystal to the left of the cut being pushed upwards. The exposure of this step provides a site for oncoming entities to bind. The inclined step rotates around the point P resulting in a continuous spiral. The two basic dislocation types shown are idealised cases. In most crystals a mixture of both these types of dislocation are thought to be present. The role played by dislocations in the crystal growth process will be discussed in the section 2.3.

Two dimensional defects, sometimes referred to as planar defects are mainly boundaries resulting from stacking faults or twinning. Growth sector boundaries can also occur depending on the method and conditions of growth. Three dimensional defects (volume defects) are usually the result of 'trapping' of material with a different matrix from the host crystal. This can include solvent molecules or large impurities.

1.4 Crystal Planes and Directions

The most common way of presenting details of crystal shape is the use of simple descriptive terms such as needle, plates, cubes and octahedron. Figure 2.7 shows some examples of these terms. Clearly such terms are of limited use. A more detailed definition of crystal habit is needed if attempts are to be made to relate external crystal shape to internal structure. This is achieved by characterising the faces (and the corresponding planes in the structure) relative to the crystallographic axes defining the unit cell. Consider three non- coplanar axes (a, b and c) with a plane cutting these axes at the points A, B and C as shown in Figure 2.8. If a, b and c are considered as unit lengths of crystallographic repeats in the x, y and z directions respectively then the lengths of the intercepts are OA/a, OB/b and OC/c. The reciprocal of these lengths are known as the Miller indices (hkl) i.e a/OA = h, b/OB = k and c/OC = l. In some cases a plane may be parallel to a crystallographic axes. In such a case the intercept with such an axis occurs at ∞. The Miller index is the $1/\infty$ and this is given the notation 0. Figure 2.9 shows some planes for a cubic lattice and the corresponding Miller indices. In current crystallographic notation it is common to use (hkl) to refer to a face, hkl (without brackets) to refer to a set of planes and $\{hkl\}$ to designate all the symetrically equivalent faces. The distance between

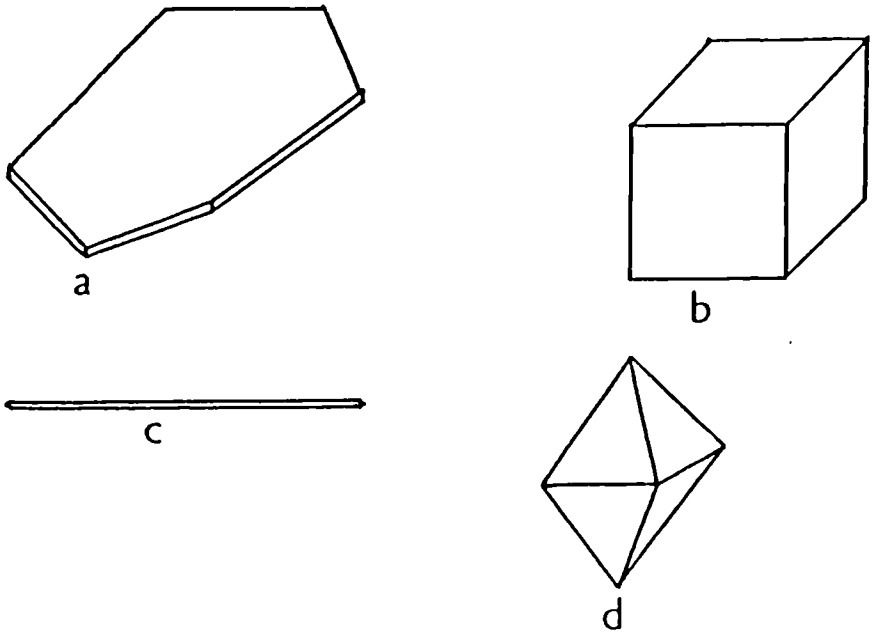

Figure 2.7 Some simple crystal shapes

a) Plate **b) Cube** **c) Needle** **d) Octahedron**

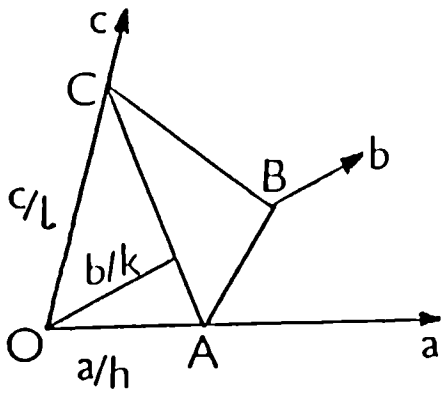

Figure 2.8 Definition of Miller Indices.

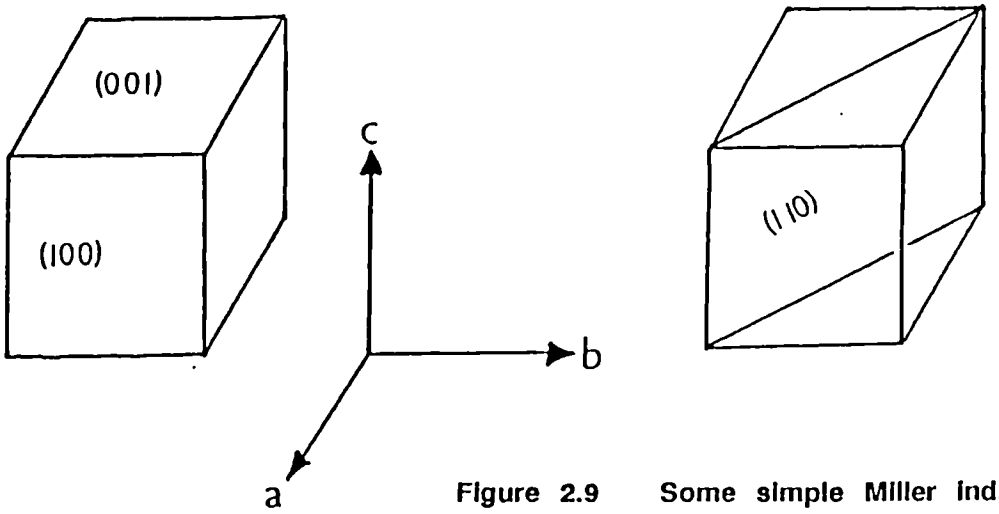

Figure 2.9 Some simple Miller Indices.

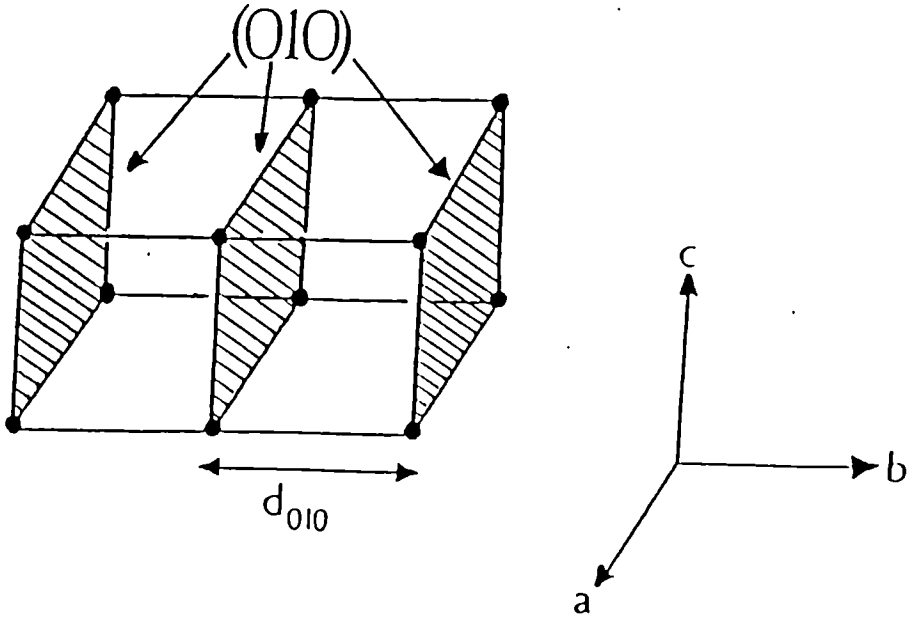

Figure 2.10 Repeating (010) planes and the corresponding interplanar spacing.

succesive planes (hkl) is called the interplanar spacing (d_{hkl}). Figure 2.10 shows succesive (010) planes and the corresponding interplanar distance. Further details on calculations of interplanar spacings is given in Appendix A and further background can be obtained from any standard text on crystallography [1].

A direction in a crystal is usually specified as [uvw] where u,v and w are the multiples of the unit cell dimensions. The direction is therefore ua+vb+wc.

One method of identifying the faces present on a crystal shape is to measure the interfacial angles and compare these measured angles with calculated angles based on unit cell dimensions and a range of Miller indices. This approach is used in the thesis to identify the morphology of l-alanine (see chapter 3). The details behind calculating the angles between crystal planes is outlined in the section on the program MORANG (see Appendix A).

2 Crystallisation

2.1 Supersaturation

The amount of material that can be dissolved in a solution depends on the nature of the material, the solvent and the temperature. Figure 2.11 shows a typical solubility curve as a function of temperature. Three area's can be defined, the stable, metastable and unstable regions. At point A the solution is described as being under-saturated and crystallisation cannot occur. On cooling from point A to C (temperature change ΔT) the metastable region is entered and the solution is said to be supersaturated. Temperature cooling is one method of achieving supersaturation. Another common method is solvent evaporation. This results in an increase in the concentration and movement into the metastable region. This is illustrated in Figure 2.11 (point X to point D).

In the metastable region nucleation can occur. The mechanisms for nucleation will be discussed in the next section. One of the 'secrets' of growing crystals of a high quality is to remain inside the metastable during growth i.e. follow the path from C to D in Figure 2.11 [7]. Care must be taken not to enter the unstable region where spontaneous nucleation can occur.

Supersaturation (σ) is often referred to as the 'driving force' for crystallisation. At low supersaturation

$$\sigma = \Delta C/C = \Delta H \Delta T/RT^2 \qquad (2.1)$$

where C is the concentration, R is the gas constant, T is the temperature

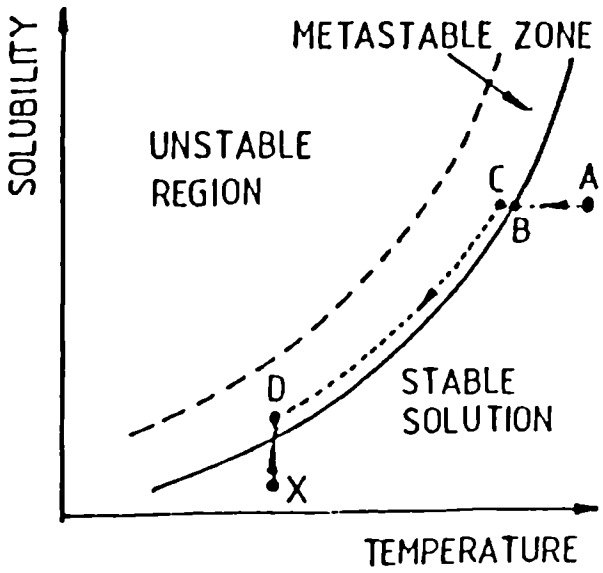

Figure 2.11 Typical solubility curve showing stable, metatable and unstable regions.

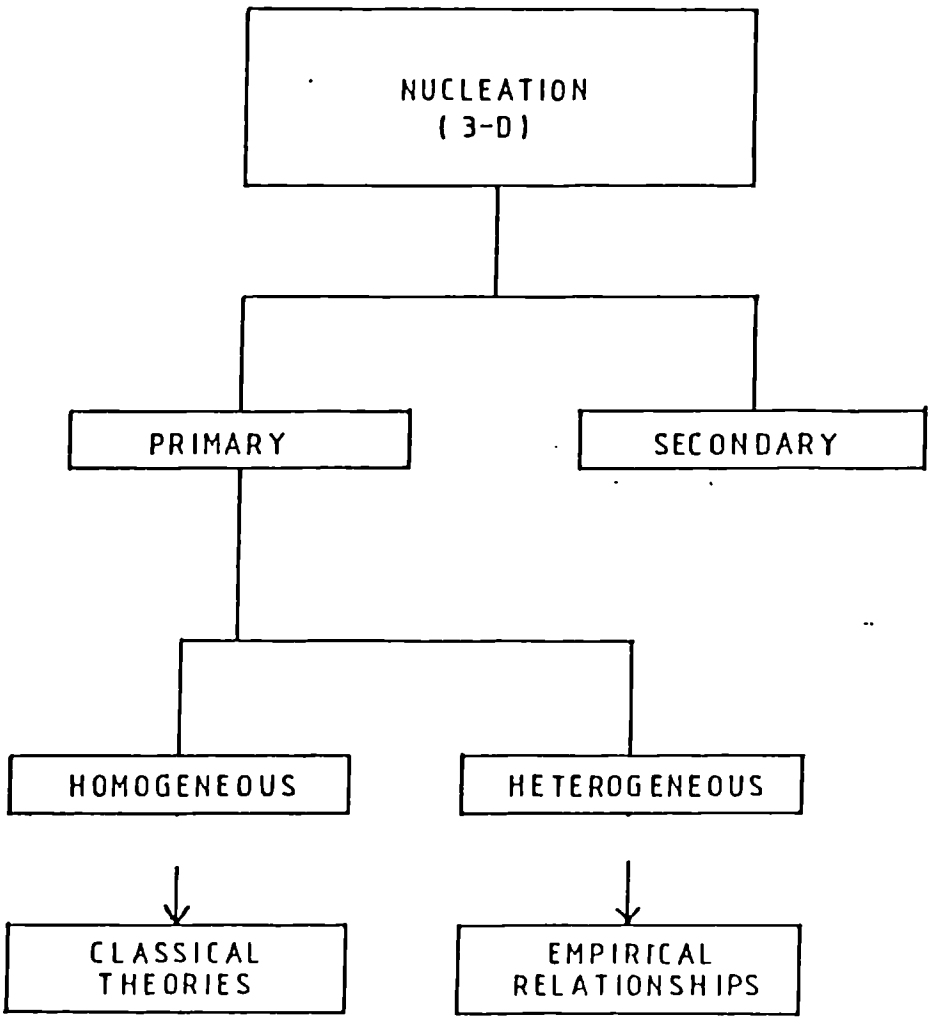

Figure 2.12 Schematic showing important stages in the nucleation process.

and ΔH is the enthalpy of dissolution [8]. Crystal growth proceeds via nucleation which is a 3D process and growth which is a 2D event. Both these depend strongly on supersaturations as will be shown in the following sections.

2.2 Nucleation

Once a certain degree of supersaturation has been achieved nucleation can occur. Nucleation is a 3D process and is thought to proceed via a progressive step by step build-up of a number of particles. Another possible mechanism for the formation of a nucleus is simultaneous collision of a number of particles. This is thought to be an unlikely event. The nucleation process can be divided into a number of categories as shown in the flowchart in Fig 2.12.

1) PRIMARY NUCLEATION

i) Homogeneous nucleation - nucleation in a completely pure solution probably via a step wise collision of a number of particles.

ii) Heterogeneous nucleation - nucleation aided by the presence of foreign bodies such as dust or the roughness of the vessel walls.

2) SECONDARY NUCLEATION - nucleation aided by the attrition of growing crystals or by the addition of a seed crystal.

2.2.1 Homogeneous Nucleation

Homogeneous nucleation can be considered to be a balance of competing free energy terms as shown in equation (2.2), where γ is the surface free energy, r is the radius on the nucleus and ΔG_v is the bulk free energy per unit volume.

$$\Delta G = 4\pi r^2\gamma - 4/3\pi r^3 \Delta G_v \tag{2.2}$$

The first term in equation (2.2) is positive and the second negative. Figure 2.13 shows the individual contribution of these terms and the summation of these contributions. Figure 2.13 shows the maximum value of ΔG at some critical radius r_c. Nuclei smaller than this critical size can only decrease their free energy by dissolving, nuclei with radii greater than the critical value can

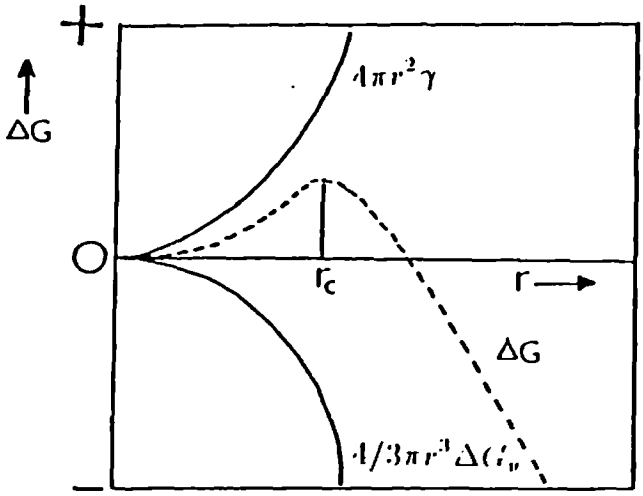

Figure 2.13 Free energy terms for nucleation as a function of radius.

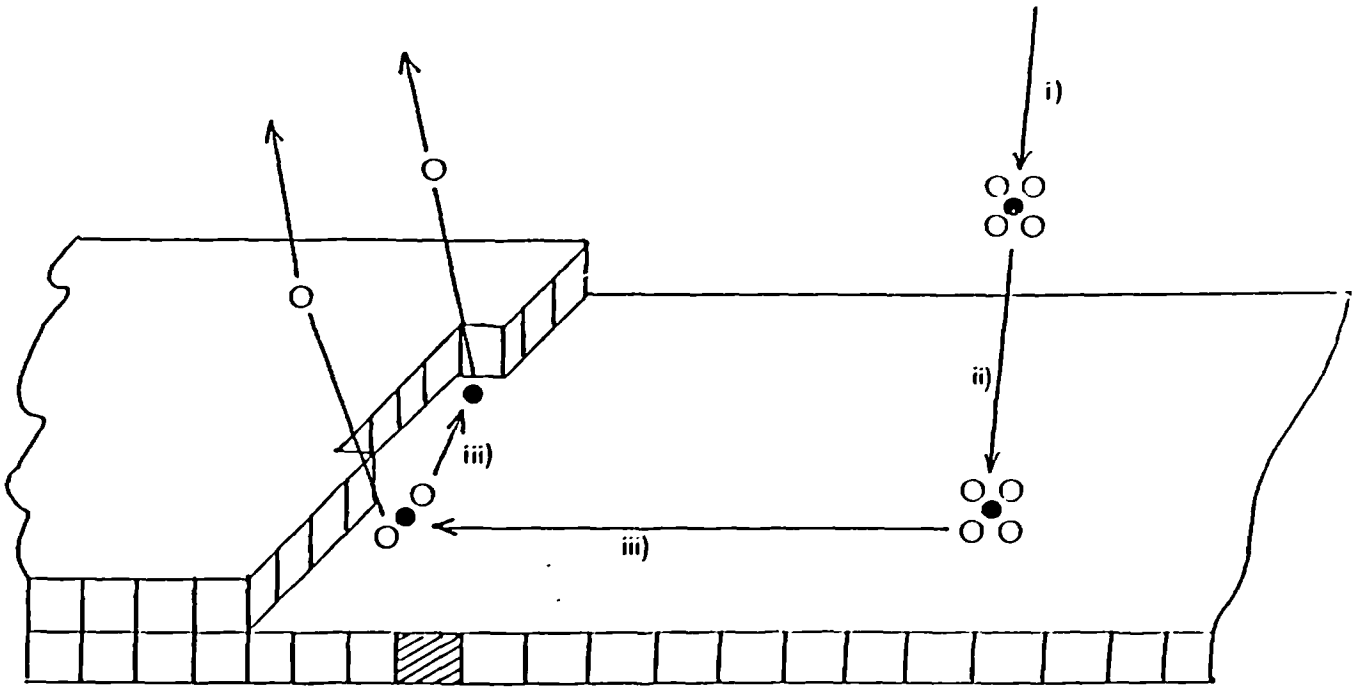

Figure 2.14 Simple schematic showing

I) Bulk transport

II) Boundary diffusion

III) Incorporation into surface.

only decrease their free energy by growing. It can be shown that the size of the critical radius and the rate of nucleation are dependent on supersaturation.

$$r^* \alpha 1/\sigma \tag{2.3}$$

$$Rate \; \alpha \; exp(-1/\sigma^2) \tag{2.4}$$

An increase in supersaturation therefore leads to a decrease in critical radius and an increase in the rate of nucleation [8].

2.2.2 Heterogeneous Nucleation

The presence of a foreign body results in nucleation taking place at lower values of supersaturation by providing a surface for nucleation. Foreign bodies can include particles of dust, added seed crystals or small crystals resulting from the attrition of growing crystals. Roughness on the vesel walls can also provide sites for nucleation. A modified version of equation (2.2) gives,

$$\Delta G = 4\pi r^2(\gamma - \gamma_s) - 4/3\pi r^3 \Delta G_v \tag{2.5}$$

where γ_s is the interfacial energy between any particle and any foreign surface. Essentially $(\gamma - \gamma_s)$ effectively reduces the positive contribution of the first term compared to the homogeneous case. The free energy change is therefore reduced [8].

2.3 Growth Mechanisms

Crystal growth from solution is a detailed process that takes place on an atomic scale. The exact details of what happens is still subject to debate and disscussion. A number of stages are thought to be involved,

i) BULK TRANSPORT - movement of crystallising entities from bulk to edge of boundary layer.

ii) BOUNDARY DIFFUSION - transport through the boundary layer to the surface of the growing crystal.

iii) INCORPORATION - adsorbsion onto the crystal surface, diffusion along the surface and attachment to the surface step. During these processes solvent molecules (when growing from solution) are lost. This is referred to as desolvation.

A summary of these steps is given in Figure 2.14. Two common mechanisms are thought to be responsible for crystal growth, the two dimensional nucleation mechanism and the screw dislocation mechanism.

The two dimensional nucleation mechanism, often called the 'birth and spread' model involves the formation of a nucleus on the surface of a growing crystal and the spreading out of the nucleus to form a new layer. This is shown in Figures 2.15(a). This results in growth normal to the suface. Each new layer has to be initiated by the formation of the nucleus on the surface. This is the rate determing step since as explained earlier this requires the step by step collision of a number of entities. It is of course possible that more than one nucleus can form on the layer or a nucleus can form on a layer that is still spreading out. This is referred to as the poly-nucleation model.

The rate of nucleation on the surface is dependendent on supersaturation (as outlined in the previous section). The rate of growth is very low at lower values of supersaturation. Discrepancies between observed rates of growth and predicted rates based on the birth and spread model led Burton, Cabrerra and Frank [9] to propose that a screw dislocation emerging at the surface as shown in Figure 2.15(b) provides a constant source of a steps onto which oncoming entities can be incorporated. This is referred to as the screw dislocation mechanism or the BCF mechanism.

Three regions of growth can be distinguished. In the first region at very low supersaturations the growth is dominated by the screw dislocation or BCF mechanism and the growth rate is dependent on the supersaturation squared i,e

$$R \alpha \sigma^2 \tag{2.6}$$

This first region is often referred to as the parabolic region. At slightly higher supersaturations growth will then be dominated by the two dimensional nucleation mechanism and the growth rate R can be shown to be roughly related to the exponential of the supersaturation i.e.

$$R \alpha \sigma^{5/6} exp(\sigma) \tag{2.7}$$

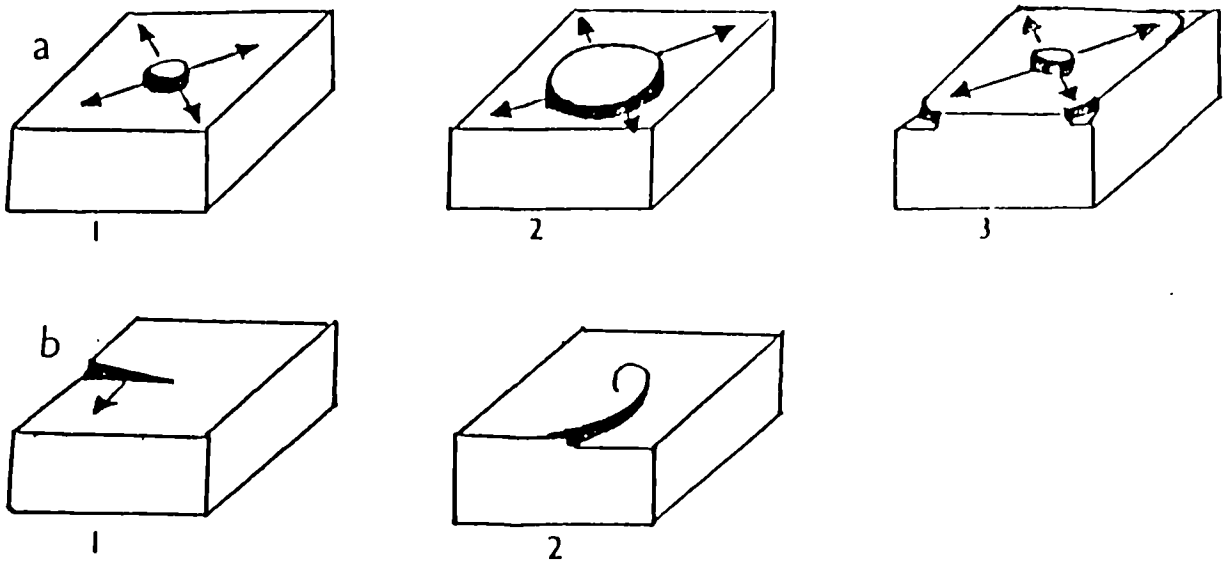

Figure 2.15 Growth by birth and spread mechanism shown in (a). Growth by prescence of screw dislocation shown in (b).

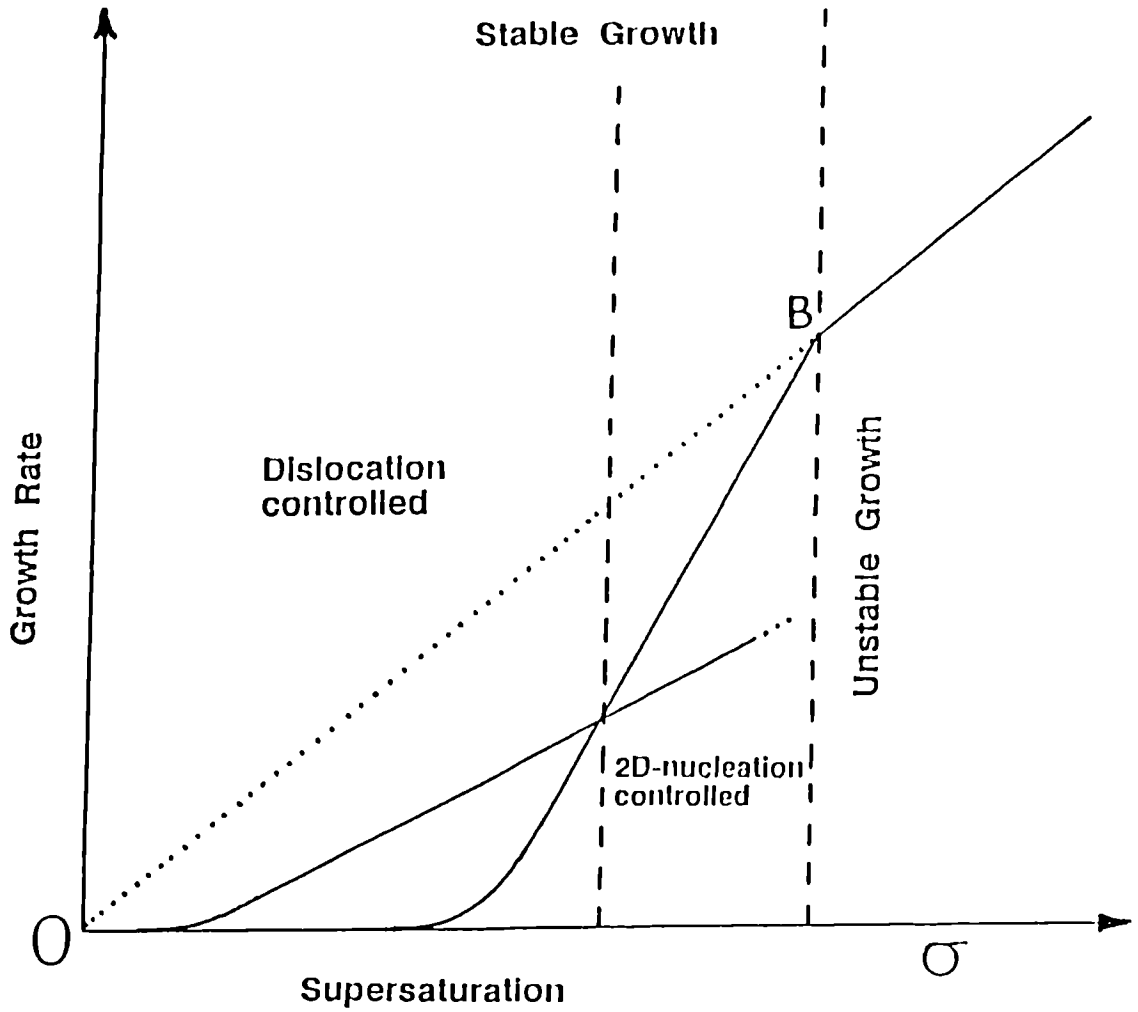

Figure 2.16 Growth rate as a function of supersaturation. The stable and unstable regions are labelled along with regions were screw-dislocation and birth and spread mechanisms dominate.

This second region is referred to as the exponential region. Increasing the supersaturation will result in entering the third region the region of rough growth. In this region the growth rate has a linear dependence with the supersaturation. i.e

$$R \alpha \sigma \tag{2.8}$$

The three regions are shown in Figure 2.16

Figure 2.17 shows a simple case of smooth and rough surfaces. Figure 2.17(a) shows a smooth surface. An oncoming entity at point A has binding energy W. On the rough surface Fig 2.17(b) an entity approaching at B and C have binding energies of 2W and 3W respectively. The growth rate at a rough surface is therfore much faster than at a smooth surface. Rough surfaces are the fastest growing faces and are not normally found on crystal forms. Growth at rough surfaces tends to result in incorporation of impurities. Figure 2.16 shows the growth rate as a function of supersaturation. The three regions are clearly defined. Computer simulations by Gilmer [10] and a recent review by Bennema and Van der Eerden [11] show these three regions. The optimum rate is labelled B, maximum growth rate without entering the rough interface region.

2.4 Crystal Growth

2.4.1 Melt Growth

Crystal growth from the melt is one of the simplest and widely used technique for the preparation of large crystals of molecular materials. The advantages of the technique are that it is a single phase system and the risk of contamination is therefore a minimum. Growth rate is high as the process involves a liquid to solid phase transformation. Supersaturation is proportional to the temperature difference across the interface and thus affords good control [7].

The melt growth technique suffers from two main disadvantages, defect generation and practical problems. Since molecular crystals have low defect formation energies (relative to inorganic solids) the technique can result in unacceptablely high defect densities. The second major disadvantage is that for some materials it may not be practical to employ the melt growth technique. The material under study may decompose before melting or the melting point may be too high for convience. The melt may contain a volatile component resulting in instability. After growth from the melt the crystal may have to be

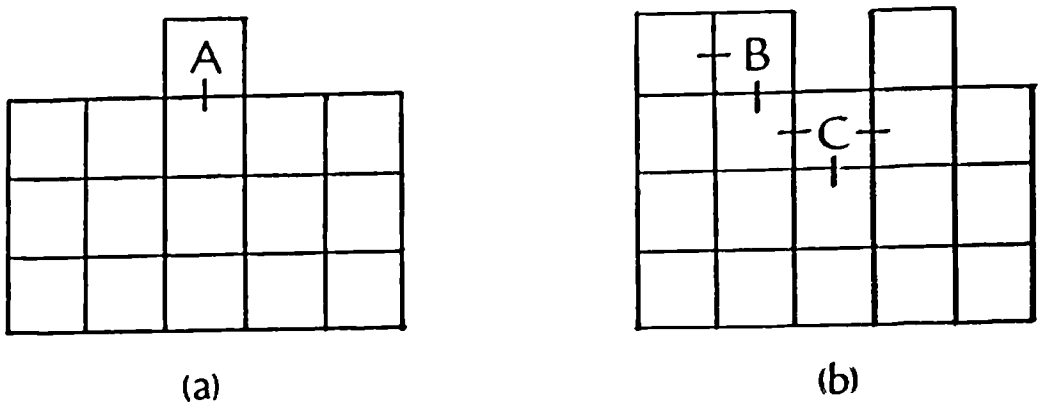

Figure 2.17 Simple models of (a) smooth and (b) rough growth surfaces.

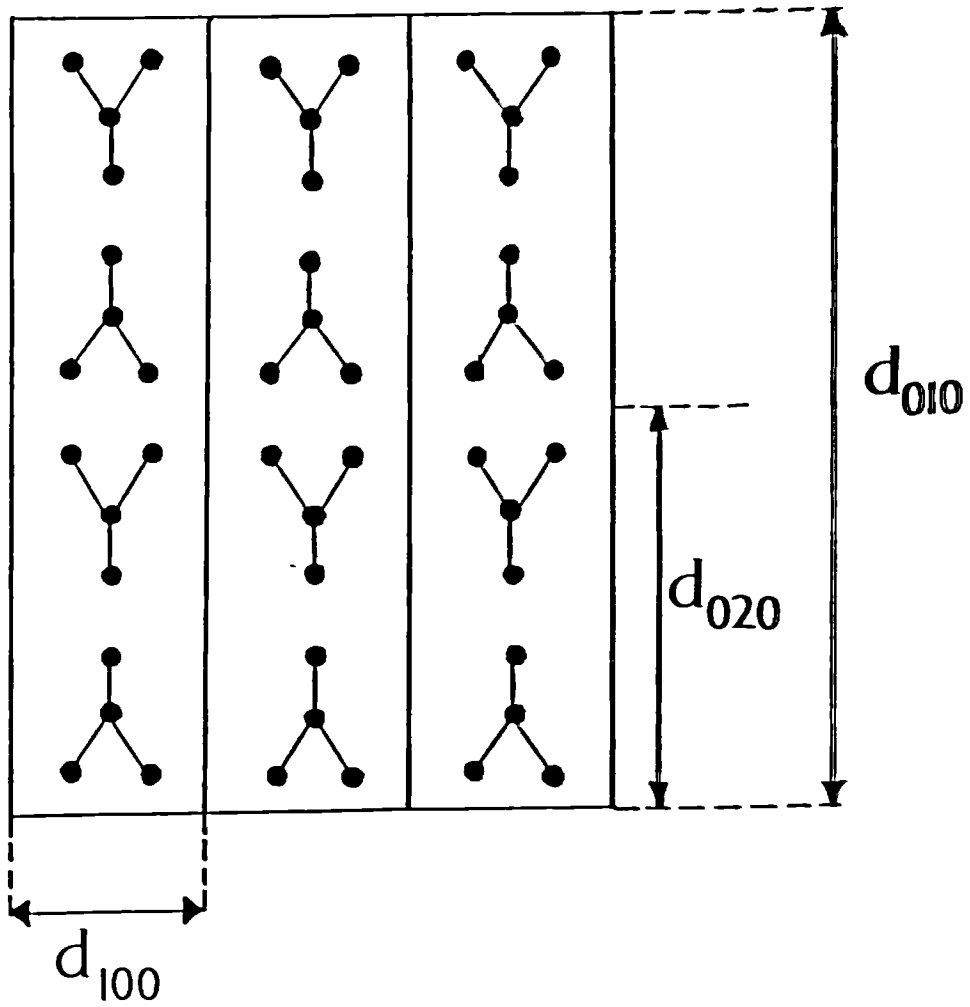

Figure 2.18 Hypothetical structure illustrating interplanar spacings.

cooled to room temperature. A structural phase transition may occur during cooling which can result in strain or even damage. In cases where these problems are present then solution or vapour growth can provide a useful alternative.

2.4.2 Growth From Solution

Growth from solution takes place at or about equilibrium conditions and enables the preparation of unstrained samples of high perfection and quality. The problems resulting from high temperature growth are not normally encountered in solution growth since it takes place at or about room temperature. However growth from solution is not a single phase system and care must be taken to minimise contamination or incorporation of solvent. Essentially the method involves seeded growth from a supersaturated solution. Changes in supersaturation needed for growth can be achieved from controlled temperature cooling or solvent evaporation. A detailed look at the experimental set-up is given in Chapter 3.

The principle factors governing the quality of the crystal are seed selection, temperature lowering rate and agitation. A good seed should be optically clear and contain no visable defects. A good seed should result in a good crystal. The aim of temperature lowering is too maintain supersaturation beyond the solubility limit but within the metastable zone (see Fig 2.12). Going beyond the metastable region results in three dimensional nucleation in the surrounding solution. These nuclei will then grow in competition with the seed.

Agitation is necessary to control the width of the boundary layer so that the growth is not dominated by diffusion and to prevent concentration gradient build up in the tank which would result in nucleation.

2.4.3 Vapour Growth

Vapour growth is an area of organic crystal growth where only a limited amount of work has been carried out. This method is likely to gain increasing importance in the field of molecular electronics . The size of the crystals currently being grown is limited by the physical size of the apparatus [7].

3 Structure and Morphology

3.1 Bravais-Friedel, Donnay-Harker Laws

The simple geometrical rules pioneered by Bravais-Friedel [12] and by Donnay-Harker [13] provide a good initial approach for identifying the forms likely to dominate the crystal habit. The rule developed by Bravais-Friedel suggested that the importance of a crystallographic form $\{hkl\}$ is directly dependent on the corresponding interplanar spacing d_{hkl}. The greater the interplanar spacing the greater the morphological importance (MI) of a form.

A number of violations of this law were observed. Some of these anomalies were accounted for by Donnay and Harker [13] who considered the effects of space group symmetry. If d_{hkl} is considered as as the period required to obtain a repeat of the surface structure and if symmetry elements are present in the unit cell then the surface structure may be repeated more than once in the period d_{hkl}. If the surface structure is repeated twice then the effective interplanar spacing is $d_{hkl}/2$. Figure 2.18 shows a sketch with four elements in a unit cell. As can be seen from the sketch the surface structure is repeated twice within the period defined by the interplanar spacing d_{010}. The 'effective' interplanar spacing is therfore defined by d_{020}. No such symmetry problems occurs in the interplanar spacing d_{100}. These reductions can have a significant effect on the relative importance of a form. If the effective interplanar spacing is halved then the relative morphological importance is also halved. The occasions when these reductions of the interplanar spacing take place are identical to the conditions for the extinction of diffracted x-rays that are listed for the 230 space groups in International Tables for X-ray Crystallography [14]. These extinction conditions and corresponding effective reductions of morphological importance of certain forms are a result of lattice centering, glide planes and screw axes. The additional periodicities introduced as a result of centering, glide planes and screw axes result in the extinction of certain reflections. For a face centered lattice the conditions for non-extinction of reflection from (hkl) planes include h+k=2n, k+l=2n and h+l=2n. The (100), (010) and (001) planes do not satisfy these conditions and their reflections are not observed. The (110) and (200) planes do satisfy the conditions and their reflections are observed.

The laws developed by Bravais, Friedel, Donnay and Harker are often quoted together as the BFDH law. The general law can be summarised thus: 'Taking into account submultiples of the interplanar spacings d_{hkl} due to space

group symmetry the most important crystallographic forms will have the greatest interplanar spacings'. If there are two forms (h_1, k_1, l_1) and (h_2, k_2, l_2),

$$\text{and } d(h_1, k_1, l_1) > d(h_2, k_2, l_2)$$
$$\text{then } MI(h_1, k_1, l_1) > MI(h_2, k_2, l_2)$$

where MI is the morphological importance of a form.

For any crystalline material given the unit cell dimensions and space group information it is possible to search through a range of Miller indices (hkl) and calculate the corresponding interplanar spacing d_{hkl}. Allowing for the extinction conditions of the space group in question, and removing the symmetrically equivalent faces it is then possible to sort out the faces in order of morphological importance (i.e. largest interplanar spacing). A computer program MORANG has been written which allows this type of calculation to be performed (see Appendix A)

The reciprocal of the slice thickness can be assumed to be a measure of the distance from the centre of a crystal to the face. This means the most important faces (hkl) will have the greatest interplanar spacing d_{hkl} and the smallest centre to face distance. Using the center to face distance for a series of faces and the basic crystallographic information such as the unit cell dimensions and space group information it is possible to compute the smallest polyhedron enclosed by these faces and produce a computer drawn picture of the morphology [15].

3.2 Hartman-Perdok Approach

The process of crystallisation is one in which the energetics of the process must play an important role. Hartman and Perdok [16] attempted to quantify crystal morphology in terms of the interaction energy between crystallising units. They identified uninterrupted chains of 'strong bonds' calling these chains Periodic Bond Chains (PBC's). A PBC can contain a number of different types of 'bonds', the influence of the chain on the overall crystal shape is governed by the weakest link in the chain which will be the rate determining step for the speed of growth along the direction of the chain.

The terms 'strong' and 'bond' require further clarification. The term 'bond' refers to an interaction between crystallising units. In the case of molecular crystals a 'bond' is an intermolecular interaction. The term 'strong' is a relative one dependent on the material of interest. Bonding in inorganic materials is much stonger than bonding in organic materials, the use of the term 'strong' is with reference to the other bonding present in the material of study.

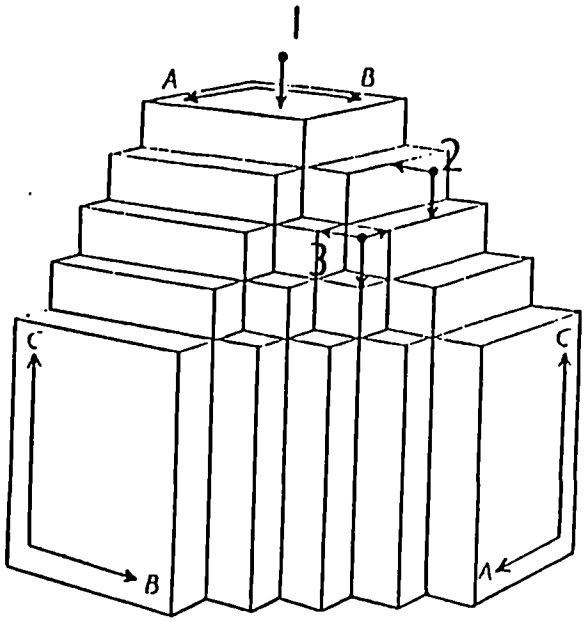

Figure 2.19 Hartman and Perdok model showing entities approaching the (100) F face (1) , the (110) S face (2) and the (111) K face (3).

Hartman and Perdok divided up the crystal faces into three categories with respect to the positions of the strong PBC's. A flat face of F-face contains one or more PBC vectors. A stepped face or S-face contains one PBC vector, a kinked face (K-face) has no PBC vectors. Consider three important PBC's along the a,b and c directions (i.e [100], [010] and [001]). Figure 2.19 shows the three classes of faces. If a crystallising entity approaches one of the main faces it can attach to only one PBC. If the face is (100) then the PBC to which the entity can attach is the one along the a-direction. If the entity approaches the (001) face it can form a bond with the PBC in the c-direction. This is shown at point (1). (010) and (001) are examples of F-faces.

Consider the (011) face, a molecule approaching this type of face is shown at point (2). The interacting entity can form 'bonds' with two PBC's along the b and c directions. The energy released is therefore greater than an entity attaching to a main face where only one bond is formed. The growth rate normal to (011) is therefore greater than normal to any main face. (011) is an example of an S-face.

An entity approaching a (111) face is shown at point (3). Approaching at this point allows the formation of bonds to three PBC's (a,b and c). This means the growth rate normal to this face is greater than that of either (011) or (010). (111) is an example of a K-face. K-faces usually grow too fast to appear on the final crystal morphology, F-faces usually dominate the crystal habit.

This approach has gained increasing importance as it has proven capable of explaining to a large degree the morphology of crystals from the internal structure. This approach has been applied to a variety of materials of which diamond [16], barite [17] and napthalene [18] are some examples. The first stage in any PBC analysis is the identification of the strong bonds present. PCLEMC (see Appendix C) allows these bonds to be identified. In lattice energy mode all the strong bonds can be identified and this will be used for the case of benzophenone in Chapter 9.

3.3 Attachment Energy Model

One of the fundamental concepts of the PBC theory was that of attachment and slice energies. The attachment energy is defined as the energy released on the addition of a slice of thickness d_{hkl} to the surface of a growing crystal. The slice energy, sometimes referred to as the layer energy, is defined as the energy released on the formation of a layer of thickness d_{hkl} [19]. The attachment energy

of a face was proposed to be a measure of how fast a crystal face grows away from the center of the crystal [20]. The faces with the lowest attachment energy will be the slowest growing and therefore the morphologically most important. If we have two faces (h_1, k_1, l_1) and (h_2, k_2, l_2) ,

$$\text{and } E_{att}(h_1, k_1, l_1) < E_{att}(h_2, k_2, l_2)$$
$$\text{then } MI(h_1, k_1, l_1) > MI(h_2, k_2, l_2)$$

It is possible to calculate the slice and attachment energies from a 3D-model of a crystal. The use of the fractional co-ordinates of one asymmetric unit and the symmetry operators for the space group in question allows one unit cell to be generated. Repeated generation of this unit cell along the directions of U V and W allow a model of the crystal to be created. For molecular crystals it is possible to calculate that lattice energy by summing all the atom-atom interactions between a central molecule and all the surrounding molecules. This is covered in more detail in Chapter 5. The slice energy by summing all the atom-atom potential interactions from a central molecule to all the molecules around within a layer of thickness of d_{hkl}. The attachment energy may be calculated by summing all the interactions between a central molecule and all the molecules outwith the slice of thickness d_{hkl} . The position of the slice can be defined as having an origin at the center of gravity of the molecule or at an atom site of each symmetrically independent molecule in the unit cell, the subsequent slice an attachment energies then being an average of all the symmetrically independent sites in the unit cell [19]. A schematic of this procedure is shown in Figure C.1 (Appendix C).

Using this approach a number of calculations on carboxylic acids and amides have been carried out. The predicted morphologies were in good agreement with observed morphologies from sublimation, though some differences were observed in crystals grown from solution. The differences were accounted for by considering the interaction of the solvent by using electrostatic potential maps of various faces and evaluating which faces have the greatest affinity for the solvent and will thus be the most affected by the solvent interaction.

Apart from the assumption that the attachment energy is a measure of the growth rate normal to that face this model also assumes that the surface is a perfect termination of the bulk and no surface relaxation or rearrangement takes place. This has been shown to have significant effect in the study of the inorganic cases of Al_2O_3 and Fe_2O_3 [20]. A futher assumption is that the on coming layer is in fact identical to a similar layer of thickness d_{hkl} in the bulk of the crystal.

Hartman and Bennema [21] have analysed the relationship between attachment energy (E_{att}) and the relative growth rate normal to a face. They showed that the attachment energy for a face could be assumed to be proportional to the relative growth rate of a face and that this assumption was particularily valid at low supersaturations when BCF and 2D nucleation mechanisms dominate. Some deviation at higher supersaturations was reported and this will be discussed in future chapters.

3.4 Tailor-Made Additives

It has been established over a number of years that impurities can affect crystal shape. Recent work by Lahav et al [22] has shown that for molecular crystals this can be accounted for by structural explanations. Tailor-made additives are 'designer' impurities which resemble the host system with differences which can affect bonding in particular directions. Changing the bonding in particular orientations changes the growth rate in a particular direction which results changes in crystal shape.

Tailor-made additives can be divided into two categories, the 'disruptive' and 'blocker' types. It is easiest to explain the the roles of these additives by considering simple schematic examples of what is believed to be happening. Disruptive additives are generally smaller than the the host system. They are structurally similar to the host system and use this structural similarity to enter the surface of the growing crystal. Additional molecules coming onto the surface then encounter a 'normal surface' except for that area due to the altered structure of the additive molecule. This is shown in Figure 2.20 (A). For a disruptive type of additive this results in a failure to complete a proper bonding sequence normally adopted by the host material. A disrpution of the bonding in a specific direction affects the growth rate in that direction. Altering relative growth rates changes crystal shape.

The 'blocker' type of additive is usually bigger than the host system. Again the additive is structurally similar to the host material but with an end group that differs significantly from the host system. The section of the molecule which is structurally similar to the host system is accepted into certain specific sites on some faces as a host molecule. The differing end group (the blocker) then prevents the oncoming molecule getting into their rightful positions at the surface. This affects the growth rate at that surface and results in changes in crystal shape. This is shown in Fig 2.20 (B).

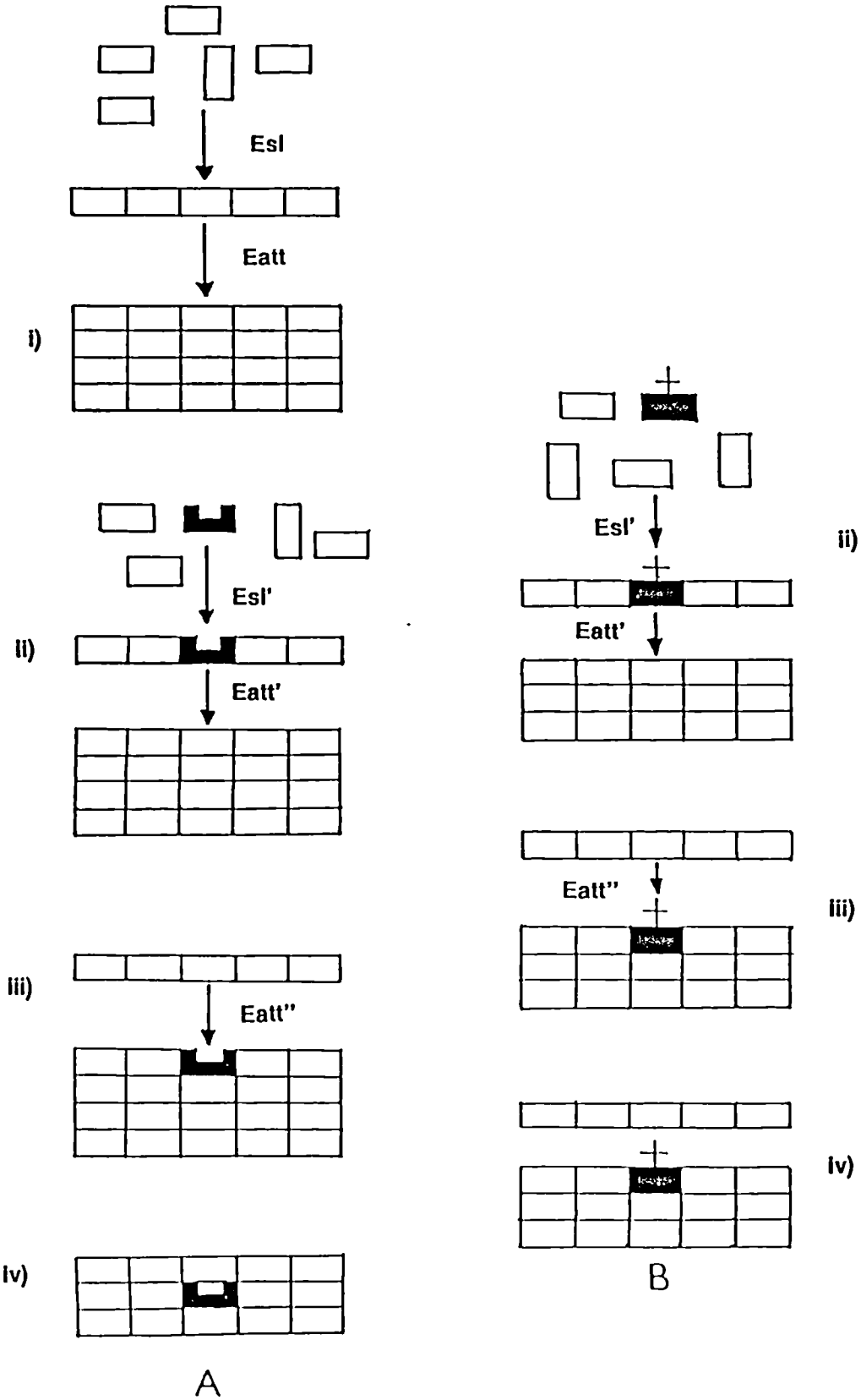

Figure 2.20 Schematic showing the important parameters in the consideration of the effects of tailor-made additives.

In order to model these changes in morphology induced by the presence of additives a number of new parameters must be calculated. Currently E_{sl} and E_{att} are calculated when carrying out a standard prediction of morphology. In order to predict the morphology with an additive present then the parameters $E_{sl'}$, $E_{att'}$ and $E_{att''}$ are calculated. $E_{sl'}$ is the slice energy calculated with an additive at the centre of the slice. This is essentially the stability of the growth slice with an additive present. It can be compared to E_{sl} as a comparsion of the stability of the slice with additive relative to the pure slice. $E_{att'}$ is the attachment energy of a growth slice containing an additive onto a pure surface. This can be compared to the E_{att} parameter for a pure material. The parameters E_{sl} and E_{att} can be compared to $E_{sl'}$ and $E_{att'}$ as a measure of the relative 'incorporation energy' of an additive at a particular surface site with reference to a pure molecule. Lahav and co-workers [22] use the term 'binding energy' instead of incorporation energy. The faces where there is minimum change in binding energy (incorporation energy) are the faces where the additives are likely to incorporate. In this work a further parameter is proposed. $E_{att''}$ is the energy released on the addition of a pure growth slice onto a surface poisoned with an additive. This additional parameter can be used as a measure of centre to face distances and calculate the morphology with an additive present. Figure 26 shows a schematic representation of the parameters discussed above, these parameters will be used to consider the effects of tailor-made additives.

3.5 Roughening Transition

3.5.1 Introduction

In section 2.3 the mechanisms of crystal growth were considered. Figure 2.17 (a) and (b) shows smooth ordered growth and rough disordered growth. These were discussed in section 2.3. When rough growth takes place the possibility of inclusion of impurities increases and consequently the quality of the crystal falls. It is therefore of importance to be able to model this transition from ordered to disordered growth. Ising models have been used to consider this transition. The aim of this section is not to consider in detail the principles behind the Ising model as it is not the main focus of this thesis and consideration of such a wide subject in detail is beyond the scope of this section. The aim is to bring to the readers attention the important parameters in such a model and to outline what is involved in such a calculation. For the interested reader the recent review by Bennema is recommended [11]. The crystal-motherphase interface has been the

subject of considerable study. In particular the study of the transition between rough and smooth crystal growth. In section 2.3 a simple look at the concept of rough and smooth growth interface was considered. Jackson [23] defined the α-factor a useful structural/thermodynamic parameter for describing the surface roughness.

$$\alpha = \xi_{hkl} \Delta H_{fus}/kT \tag{2.9}$$

where ξ_{hkl} is the surface anisotropy factor given by Esl/Ecr. The anisotropy factor can be considered to be a ratio of surface to bulk intermolecular interactions. When α is below a certain critical value the surface can be considered to be rough having unstable growth. When α is above the critical value then the growth interface is smooth and growth proceeds in an ordered manner.

At a given temperature both E_{cr} and ΔH_{fus} are constant. The parameter determing α is the slice energy. For a high slice energy, the anisotropy factor will be high and α will be high and the interface smooth. If the face is a weak face then the slice energy will be smaller in magnitude, the anisotropy factor small and the α value will be small. This means that the surface will be rough. From a simple viewpoint, the faces with the highest slice energy (lowest attachment energy) will be the most smooth. The morphologically most important faces will be the most difficult to convert to rough growth. The weaker the face in terms of morphology the easier it will roughen.

3.5.2 Physical Significance of Surface Anisotropy Factor

In order to calculate ξ_{hkl} for a molecular crystal a series of inter-molecular potential calculations based on a known crystal structure must be carried out. PCLEMC (Appendix C) can calculate the anisotropy factor. However a simple view of the importance of the anisotropy factor can be obtained from looking at simple cubic lattice.

Figure 2.21 shows a simple lattice. The intermolecular bonding from the central molecule is highlighted with dotted lines. There are six main intermoleculer bonds surrounding the central molecule. The bonding in the (100) plane is highlighted with dashes. There are four main bonds in the (100) plane. The surface anisotropy factor is therefore 4/6=0.66. This simple model considers only the nearest neighbour bonding . There is bonding of a secondary nature across the diagonals. This is however likely to be weak relative to the main bonds.

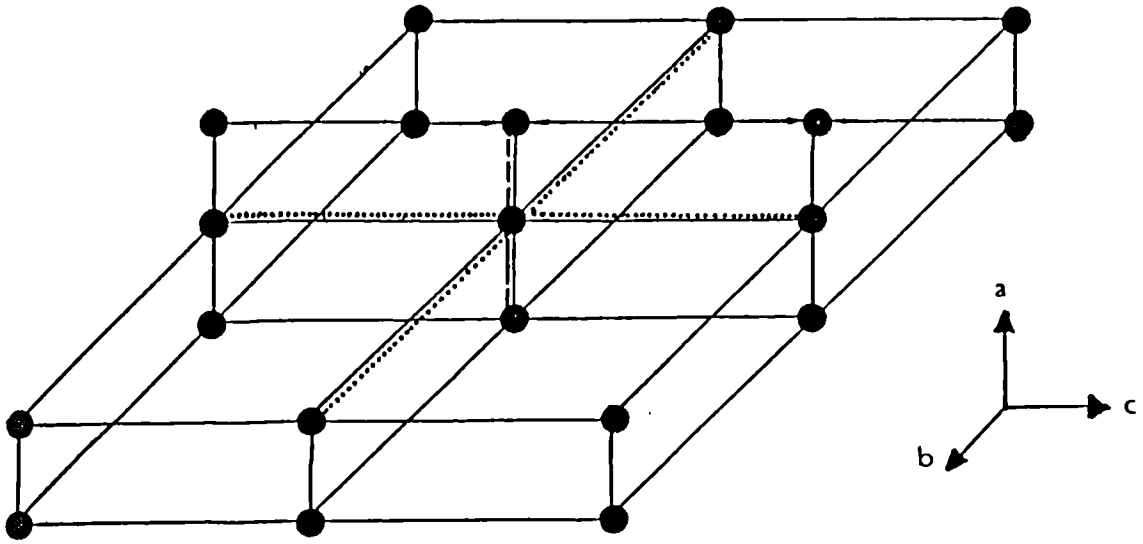

Figure 2.21 Simple crystal lattices and faces, illustating the importance of the surface anisotropy factors for a simple lattice and (100) face

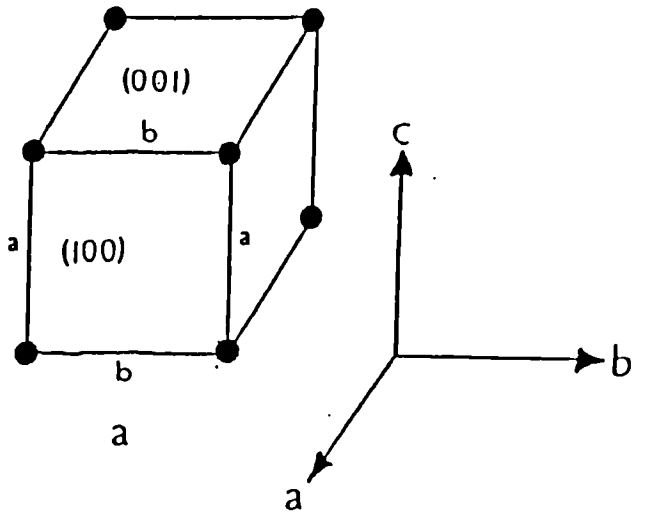

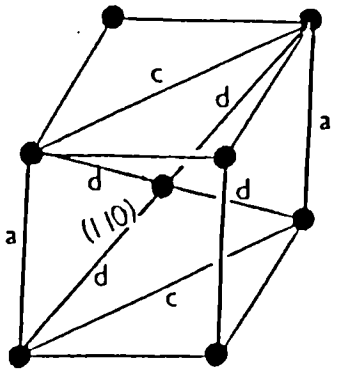

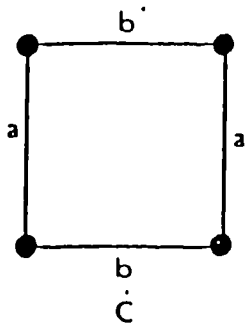

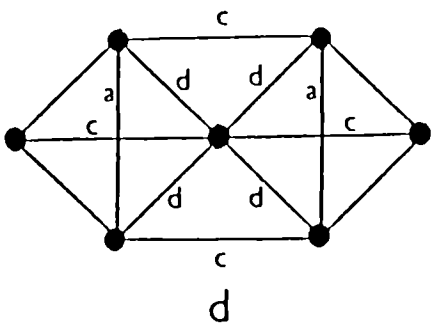

Figure 2.22 Simple crystal structures and the corresponding connected nets showing (100) and (110) surfaces.

3.5.3 Ising Models

In order to study the surface properties of crystal surfaces Ising models of the interfaces are often employed. In Ising models of crystals the crystal is partioned into cells having two possible properties only, either solid or fluid. Ising Surface models can be split into two categories [11],

i) One layer model- At -∞ the layers are completely solid. At the 1st layer there is a mixture of solid and fluid blocks. From the second layer to +∞ the layers are completely fluid. The interface has been reduced to one layer or a two dimensional mixed solid-fluid crystal.

ii) Infinite layer model- For models of this type the interface consists of infinite layers with a layer at -∞ completely solid and a layer completely fluid at +∞. The real interface consists of only a few layers. The solid on solid (SOS) model or condition is introduced which means that solid blocks occur on other solid blocks and overhangs and vacancies are ruled out.

Using this SOS approach and carrying out simulations of processes including creation (fluid units come onto surface become solid), annihilation (solid units evaporate to become fluid) and diffusion (surface diffusion to other positions on the surface) relevent properties including θ^R, the dimensionless roughening temperature can be obtained [11]. Such simulations are computationally intensive and as a consequence restricted to simple cases only.

The one layer interface is a two dimensional Ising lattice. The order-disorder phase transition in a two dimensional lattice was solved exactly by Onsager [24]. The phase transition takes place at a critical temperature θ^c. It has also been shown that for simple cases that θ^R and θ^c are numerically close to each other. It is reasonable to assume that they will also be close for more complicated structures. The theory of Onsager has recently been developed and generalised for more complicated two-dimensional crystals by Rijpkema [25]. This was a major breakthough as it was now possible to calculate θ^c for more complex crystal structures given a ratio of bond strengths. Figure 2.22 shows simple crystal structures and the corresponding nets. Figure 2.22 (a) and (b) show simple crystal structures with intermolecular bonding labelled. Figures (c) and (d) show the connected nets. The (110) connected net is clearly more

complicated than the (100) net even for these simple structures. The calculation of θ^c for a 'real' crystal structure involves a four stage process.

1. Identifying the strong bonds and relative bond strengths

2. Derivation of the connected 2D nets for the crystal structure

3. Conversion of connected nets into square planar nets

4. Use of bond energies and square planar nets to calculate θ^c

It should be noted that the exact calculation of θ^c is only possible if the two dimensional crystal is planar and there are no crossing bonds. If bonds do cross and one bond is substantially stronger than the other then the weaker of the two bonds can be ignored. If the bonds are of equal strength then they can be removed in turn and θ^c calculated within a narrow range. If the nets become complicated then calculating the value of θ^c within a narrow range can become difficult. This is the case for apatite [26].

The morphology of the crystal can now be characterised according to θ^c. The higher the value of θ^c the stronger the two-dimensional net, the slower the growth rate of the corresponding form on the crystal and the more morphologically important the form. If we have two faces (h_1, k_1, l_1) and (h_2, k_2, l_2)

$$\text{and } \theta^c(h_1, k_1, l_1) > \theta^c(h_2, k_2, l_2)$$
$$\text{then } \mathrm{MI}(h_1, k_1, l_1) > \mathrm{MI}(h_2, k_2, l_2)$$

In this thesis θ^c will be calculated for the organic crystal benzophenone using bond-strengths from PCLEMC and connected nets from Jetten [27] (see chapter 9).

4 References

[1] F.C. Phillips. 'An Introduction to Crystallography'. Third Edition, Longmans (1963).

[2] W. Friedrich, P. Knipping and M. Laue. Sitzungsberichte der (Kgl) Bayerische Akademie der Wissenschaften (1912) 303

[3] W.H. Bragg, Nature (London) 90 (1912) 360

[4] Cambridge Structural Database. O. Kennard, Crystallographic Data Centre, Cambridge England.
[5] Inorganic Structural Database. G. Bergerhoff, University of Bonn, W. Germany.
[6] Crystal Structure Search Retrevial Database. SERC Chemical Databank Systems. CSE Applications Group, Daresbury Laboratory, Warrington, England.
[7] J.N. Sherwood and B.J. Mc Ardle. Chapter 7, 'Advanced Crystal Growth', editors P.M. Dryburgh, B Cockrayne and K.G. Barraclough. Prentice Hall (1987).
[8] A.C. Stewart PhD Thesis University of Strathclyde (1987).
[9] W.K. Burton, N. Cabrera and F.C. Frank. Phil. Trans. Royal Soc. London, A243 (1951) 299.
[10] G.H. Gilmer and K.A. Jackson. Crystal Growth and Materials, edited by E. Kaldis and H.J. Scheel. North Holland Publishing Company (1977).
[11] P. Bennema and J.P. Van der Eerden. Chapter 1 in 'Morphology of Crystals', edited by I. Sunagawa. Terra Scientific Publishing Company, Tokyo (1987).
[12] A. Bravais Etudes Crystallographiques, Paris, (1913).
[13] J.D.H. Donnay and D. Harker, Amer. Miner. 22 (1937) 463.
[14] International Tables of X-ray Crystallography vol A (D. Reidel Publishing Company, 1983).
[15] E. Dowty Amer. Miner. 65 (1980) 465.
[16] P. Hartman and W.G. Perdok Acta Cryst. 8 (1955) 49.
[17] P. Hartman and W.G. Perdok Acta Cryst. 8 (1955) 521.
[18] P. Hartman and W.G. Perdok Acta Cryst. 8 (1955) 525.
[19] Z. Berkovitch-Yellin J. Amer. Chem. Soc. 107 (1985) 8239.
[20] W.C. Mackrodt, R.J. Davey, S.N. Black and R. Docherty J. Cryst. Growth 88 (1988) 159.
[21] P. Bennema and P. Hartman J. Cryst. Growth 49 (1980) 145.
[22] Z. Berkovitch-Yellin, J van Mil, L. Addadi, M. Idelson, M. Lahav and L. Leiserowitz. J. Amer. Chem. Soc. 107 (1985) 3111.
[23] K.A. Jackson, in Liquid Metals and Solidification. (American Society for Metals, Cleveland, 1958) p. 174.
[24] L. Onsager Phys. Rev. 65 (1944) 117.
[25] J.J.M. Rijpkema Thesis University of Nijmegen (1984).
[26] R.A. Terpstra, P. Bennema, P. Hartman, C.F. Woensdregt, W.G. Perdok

and M.L. Senechal J. Cryst. Growth 78 (1986) 468.
[27] L.M.A.J. Jetten, PhD Thesis (1983) University of Nijmegen

Chapter 3

Experimental

CONTENTS

1 Introduction

Crystalline materials exhibit a wide variety of properties including stability and solubility. As a result a wide range of techniques have to be employed to grow crystals of high quality [1]. At Strathclyde University melt, vapour and solution growth are used to produce highly perfect organic crystals. When materials are unstable at high temperatures solution growth at or about room temperature is usually the most successful approach (see chapter 2 section 2.4)

The method involves stirring a seed in a saturated solution. Changes in supersaturation which produce crystal growth can be obtained by temperature lowering or solvent evaporation, the former being the preferred method due to greater control. Seeds can be obtained by cooling of saturated solutions. The seed choosen for further growth studies should be optically clear and show no twinning or large areas of imperfection. The rate of temperature lowering is selected to maintain the saturation beyond the solubility limit (otherwise the crystal will start to dissolve) and within the metastable region beyond which nucleation may occur in the surrounding solution (see Figure 2.12). A knowledge of the solubility of the material as a function of temperature will help with determination of the 'best' cooling rate for crystal growth. For the interested reader a more detailed look at the growth of organic crystals and the possible methods that can be used has been presented by Sherwood and McArdle [1].

In this chapter the basic experimental set-up for crystal growth from solution along with details of the growth of crystals of the organic material l-alanine is given. L-alanine was choosen as an example because the morphological details in the literature were limited and since it has strong intermolecular bonding it would provide a good test of the calculations. It would also serve as a useful illustration on how MORANG (see Appendix B) can help in determinations of morphology. The morphology was determined using optical goniometry. Measured interfacial angles are compared with calculated angles for a range of Miller indices and the observed morphology determined. Details on the calculation of these angles is given in Appendix A as part of the write up on the computer program MORANG.

2 Experimental Set-Up

The basic experimental set-up for growth from solution is shown in Figure 3.1. A flask containing a seed in a saturated solution is held in a tank containing water.

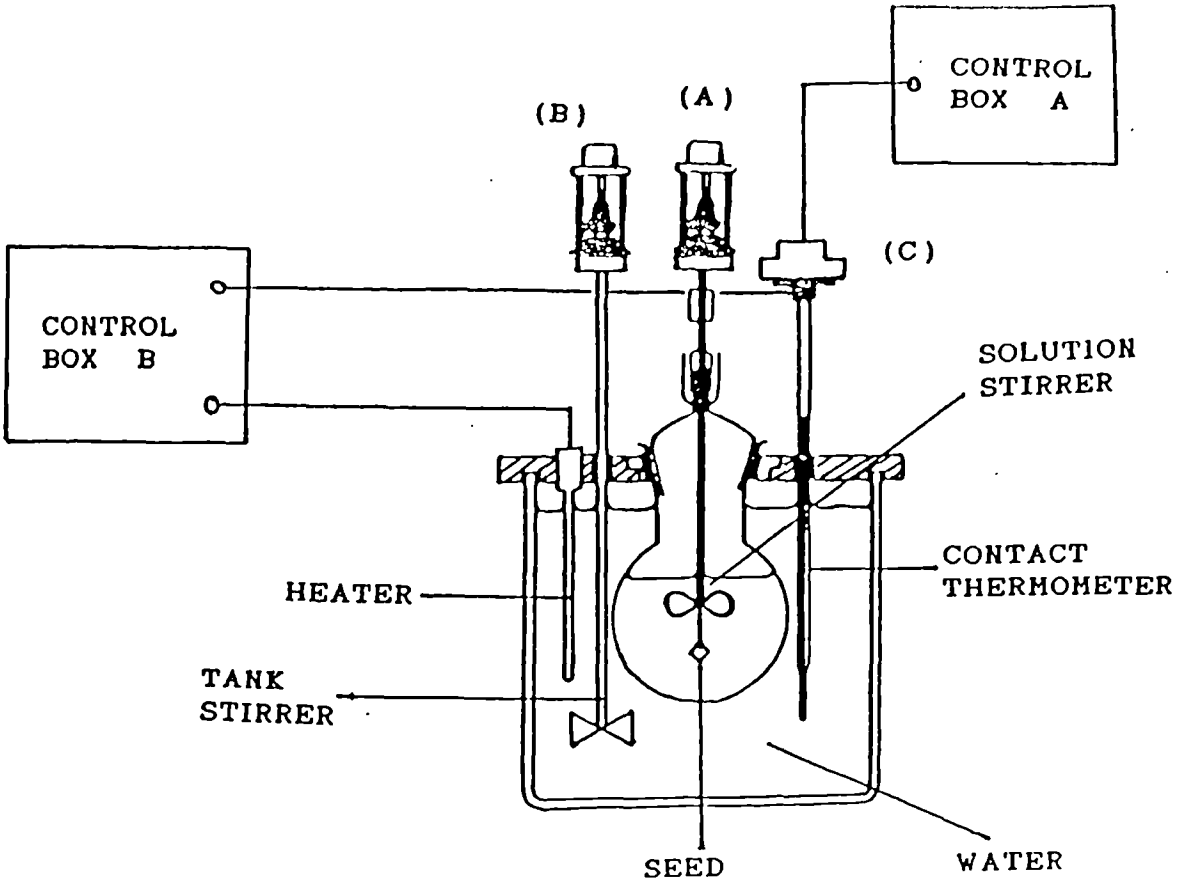

Figure 3.1 Experimental set-up adopted for growth from solution

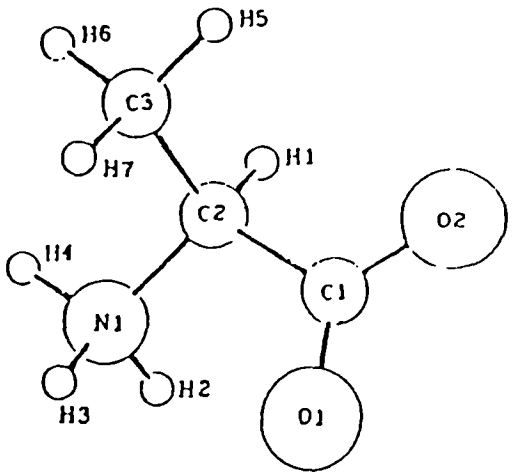

Figure 3.2 Molecule of l-alanine

The seed and solution are stirred by the simple motor (A). A larger motor (B) stirs the water to ensure even heating throughout the tank. Heat to the tank is supplied by the heater which is controlled by the contact thermometer and box B. The temperature is lowered by stepper motor (C) which is driven by control box A. Control box (A) allows the user to input the cooling rate required per day. Variations on this set-up has been used by a number of workers to grow a wide range of crystals [2,3,4]. These workers have shown this system has a high degree of temperature control and stability over long periods.

3 L- alanine

3.1 General Details

L-alanine ($CH_3CH(NH_2)COOH$) is one of the naturally occuring α-amino acids, Figure 3.2 shows the amino group at the α position relative to the carboxyl group. The α carbon is labelled 'C2' in Figure 3.2. L-alanine crystallises in the orthorhombic space group $P2_12_12_1$ with four molecules in a unit cell of dimensions a = 6.025Å b = 12.324Å and c = 5.783Å[5]. The morphology of crystals is generally described as prismatic with {120} and {011} forms dominating the morphology [5].

3.2 Experimental Procedure

The solubility data for l-alanine in water taken from [6] and plotted in Figure 3.3 shows a smooth curve indicating that 35°C to 25°C is a convenient cooling range. As l-alanine appears to be unstable at high temperatures [6] and insoluble in other convienent solvents seeds were prepared by cooling an aqueous solution saturated at 40°C to room temperature overnight. The seed was then introduced into saturated solution at 35°C. The solution was then cooled at a rate of 0.1°C per day. The cooling rate was choosen after initial experiments by Bullock [7] who grew l-alanine crystals at a cooling rate of 0.5°C. The crystal grown with the cooling rate of 0.1°C per day was smaller than that reported by Bullock but was of a higher quality. The crystal was optically clearer and had no secondary nucleation on the crystal faces.

Figure 3.4 has some computer drawn pictures of the grown crystal. The pictures were produced using the crystal drawing program SHAPE [8] and measured centre to face distances taken from the crystal. The pictures were drawn with and without back edges (Figures 3.4(a) and 3.4(b)) to give the reader

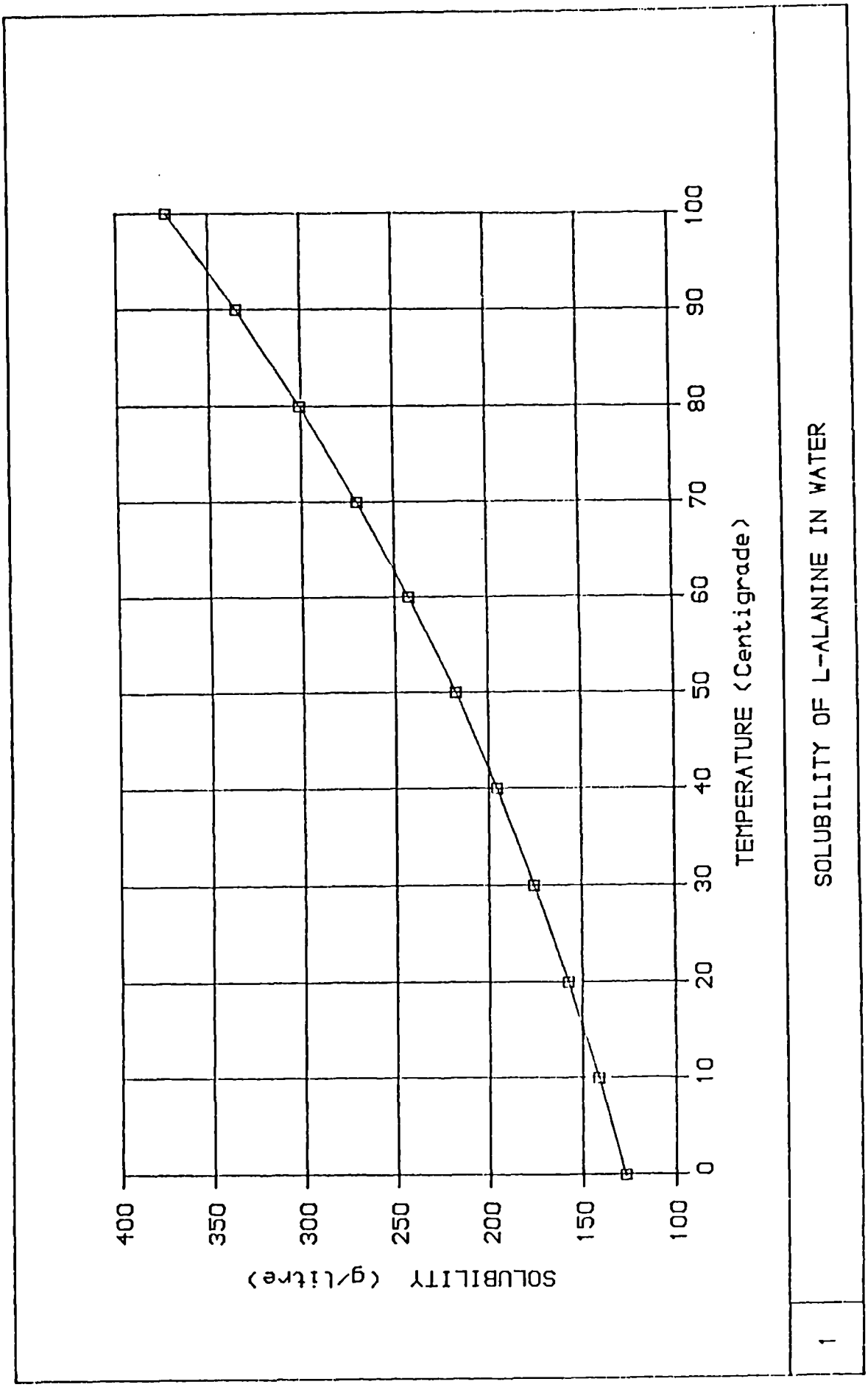

Figure 3.3 Plot of the solubility of l-alanine in water.

the clearest representation. A projection down the c-axis (Figure 3.4(c)) is also given to show the barrel like morphology.

3.3 Optical Goniometry

Initial attempts to identify the forms present on the l-alanine crystal was by the use of stereographic projections, however the closeness in the dimensions of the a and c axes meant that this method was not accurate enough to determine the morphology completely. In order to achieve this higher degree of accuracy the crystal was mounted on a STOE model J optical two circle goniometer at ICI Chemicals and Polymers, Runcorn. The use of optical goniometry and the procedure for carrying out the measurements has been explained elsewhere [9]. Essentially the use of an optical goniometer allows the angles between faces to be measured with a high degree of precision. The limiting factor to the precision is usually the quality of the crystal and its faces.

Once the angles have been obtained these can be compared to the calculated angles for sets of Miller indices allowing the forms present on the crystal to be identified. This can be time consuming and so a computer program was written as part of this thesis to help in such determinations. Details of this program MORANG is given in Appendix A. Table 3.1 has a list of the observed angles and calculated angles. This shows that the forms present on the l-alanine crystal are (120), (110), (020) and (011) in agreement with the general description given earlier [5].

The prediction of the morphology of the l-alanine crystal carried out later in this thesis shows good agreement with the observed form reported here.

4 References

[1] J.N. Sherwood and B.J. Macardle. Chapter 7, 'Advanced Crystal Growth' editors P.M. Dryburgh, B. Cockrayne and K.G. Barraclough. Prentice-Hall (1987).

[2] C.S. Yoon. PhD Thesis University of Strathclyde (1987).

[3] P.J. Halfpenny. PhD Thesis University of Strathclyde (1983).

[4] A. El-Korashy. PhD Thesis University of Strathclyde (1988).

[5] M.S. Lehmann, T.F. Koetzle and W.C. Hamilton. J. Amer. Chem. Soc. 94 (1972) 2657.

Table 3.1 Observed and calculated interfacial angles for l-alanine using program MORANG and cell parameters reported by [5].

FACES		ANGLE	
		MEASURED	CALCULATED
(120)	(020)	45.6	45.64
(110)	(120)	18.3	18.30
(020)	(011)	64.7	64.86

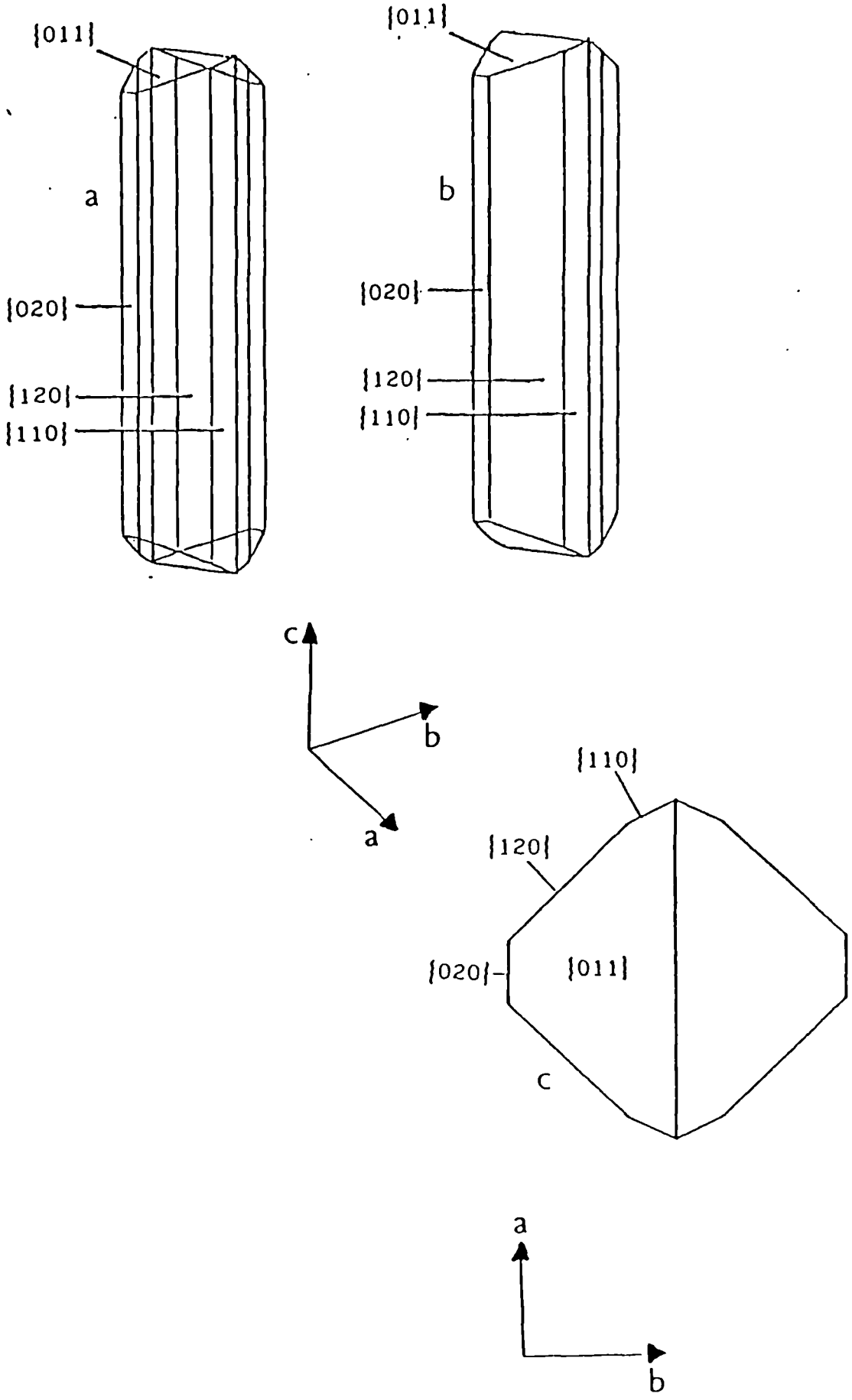

Figure 3.4 Computer drawn pictures of the morphology of l-alanine

a) with back edges drawn

b) with back edges removed

c) view along the [001] direction

[6] J.P. Greenstein and M. Winitz. 'Chemistry Of the Amino Acids'. Vol 1 J. Wiley and sons (1961)

[7] K. Bullock. Maxi Thesis. University of Strathclyde (1986).

[8] E. Dowty. Amer. Miner. 65 (1980) 465

[9] F.C. Phillips. ' An Introduction to Crystallography'. Third Edition, Longmans (1963).

Chapter 4

Basic Approaches

CONTENTS

1 Introduction

Two of the major aims of this work were to document computer code for carrying out this type of morphological study and to develop an approach and guidelines for carrying out the calculations. Three computer programs CRYSTLINK, MORANG and PCLEMC have been written as part of this work. PCLEMC was the main program written, MORANG and CRYSTLINK are ancillary programs. A summary of each of these programs is given in the following section along with brief details of other programs used. The three programs written as part of this thesis, MORANG, CRYSTLINK and PCLEMC are considered in greater detail in Appendices I, II and III respectively. The program summary is followed by a section desceribing the approaches adopted for carrying out the calculations. Particular emphasis is placed on the roles of the computer programs in the overall scheme.

2 Computer Program Summary

2.1 PCLEMC

PCLEMC (Program to Calculate the Lattice Energy of Molecular Crystals) is a computational model of a crystal and consists of a method for describing the structure of the crystal and an approach for evaluating the energy of this model of the structure. PCLEMC has been written to deal with molecular crystals. The program takes in the unit cell information, the fractional co-ordinates of the atoms in one molecule and space group symmetry and uses these to generate a three dimensional model of the crystal. The program then uses an atom-atom approximation (as discussed in Chapter 1) to describe the interactions between molecules in the crystal model. A much more detailed look at PCLEMC and its operation is carried out in Appendix C. Essentially PCLEMC outputs the lattice energy, slice energy, and attachment energies, parameters which allow morphological predictions to be carried out.

2.2 Ancillary Programs Written

2.2.1 MORANG

MORANG is a highly interactive package designed primarily to aid in determining crystal morphology. The program is written in standard Fortran-77 and has three main functions:

1). The identification of the most important crystallographic forms according to the interplanar spacings. This is essentially the Donnay-Harker approach as outlined in chapter 2.

2). The calculation of the angles between crystal planes and directions.

3). Using a combination of the above options the user can input an observed interfacial angle plus experimental error and the program will output the likely planes. This allows the identification of the forms present on the crystal habit. This approach was used in the case of l-alanine as outlined in chapter 3.

The program was developed from two existing programs MORPH [1] and ANGLE [2]. Significant modifications to both these programs were necessary to incorporate these programs into a larger, interactive standard package. Details of the modifications are given in Appendix A and in the actual source code.

2.2.2 CRYSTLINK

CRYSTLINK was written as a support program and contains a series of useful routines which carry out a variety of data manipulation procedures. The program is written in Fortran and runs on a VAX 11/782. The program utilises some of the mathematical routines available in the NAG library [3] and as a result requires linking to this library. The program could easily be modified to run on other machines with slight changes to the file handling options some of which are specific to the VAX [4]. An early version of this program has been converted to run on an IBM-AT. The program contains four sub-menus at present.

SUB MENU 1 - contains the data formatting routines. A starting file obtained from the CSSR database [5] can be used to generate partial or complete files for a variety of programs including MNDO [6], PCLEMC, CNDO [7], GAMESS [8] and ORTEP[9]. This cuts down the time used in preparing these files and reduces the errors which can be introduced when files have to be created by users at the keyboard.

SUB MENU 2 - this is part of the programs interface to molecular graph-

ics packages. Molecular graphics routines work in cartesian co-ordinate systems, when dealing with crystal systems it is much more convenient to work in crystal co-ordinates which are fractions of the unit cell dimensions (see Chapter 1, section 3). This routine has been used when fitting hydrogens to incomplete structures and when obtaining the co-ordinates of an additive. Using INTERCHEM [10] it is possible to fit hydrogens assuming standard bond lengths and geometry and then minimise the hydrogen positions with respect to the intramolecular energy using a quantum chemistry package. Both these types of programs use independent cartesian axis settings but these can be converted back to crystal co-ordinates by interfacing this routine to the molecular graphics package (INTERCHEM in this case). This routine is also used to obtain the co-ordinates of an additive in terms of a host lattice. The additive can be fitted to the host lattice using the molecular graphics package and the co-ordinates converted back to the crystal system of ther host material using this routine.

SUB MENU 3 - This subroutine allows the generation of files containing the information for slice and packing diagrams. Input required includes the standard CSSR file plus symmetry operators as given in International Tables [11]. Output is a file in the CSSR format but includes new generated co-ordinates and updated connectivity. Connnectivity is essentially the information in the file which tells the molecular drawing package which atoms are connected. The size of this file is limited by the format of the CSSR database file to 999 atoms. This file can be used as input to a variety of molecular graphic packages including CHEMX [12], VIEW [13] and INTERCHEM as well as any package that will accept the CSSR format as input.

SUB MENU 4 - This menu will contain a number of miscellaneous routines. At present it has a routine which can calculate the centre of gravity of a molecule from a CSSR file. The program outputs the centre of gravity in fractional co-ordinates.

2.3 Other Programs Used

2.3.1 TCCALC

TCCALC is a program developed by Rijpkema [14] which allows the calculation of the critical Ising temperature θ^c, from a rectangular net and a given ratio

of bond energies. The bond energies can be obtained from PCLEMC in LATT mode (see Appendix C). The procedure for obtaining rectangular nets from connected nets and connected nets from a crystal structure has been outlined in some detail by Bennema and Van der Eerden [15]. This approach will be applied to benzophenone in this thesis.

2.3.2 SHAPE

SHAPE is a crystal drawing program written by E.Dowty [16]. Given simple information such as unit cell dimensions, space group symmetry and center to face distances the program computes the smallest polyhedron enclosed by the faces and distances and produces a picture of the crystal.

If observed centre to face distances are used then a picture of the observed crystal form results. If the reciprocal of the interplanar spacings are used as measures of the centre to face distances then the Donnay-Harker (DH) model of the morphology is produced. When attachment energies as produced from PCLEMC are used as estimates of centre to face distances then SHAPE computes the Attachment Energy (AE) model.

2.3.3 INTERCHEM

INTERCHEM is Strathclyde University's 'in-house' molecular modelling package written by P. Bladon and R. Breckinridge. The package allows the display of stick, ball and stick, and space filling models of structures. Input can be accepted from standard crystallographic sources [5] or molecular orbital/mechanics calculations. Manipulation of structures includes rotation and fitting. The program runs on a VAX computer and requires a WESTWARD or PERICOM graphics screen for display purposes. The package was originally written for the display of single molecules. Crystal packing diagrams can be obtained by using the options in CRYSTLINK (see Appendix B) to produce a file that can be read in to INTERCHEM.

3 Overall Approaches

3.1 Basic Approach

The flowchart shown in Fig 4.1 can be considered to consist of two main streams, the theoretical stream (top-half) and the experimental stream (bottom-half).

Basic Approach

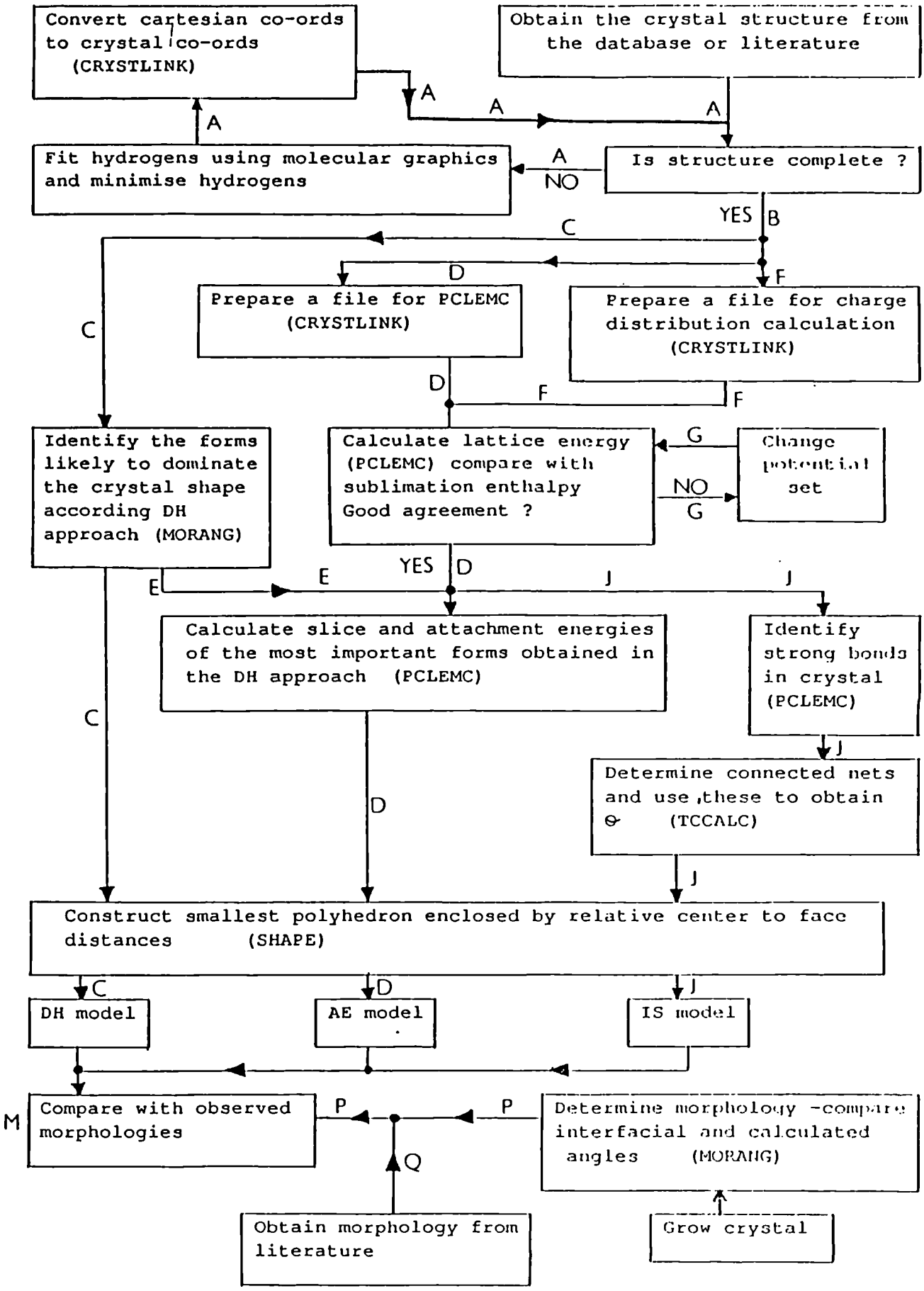

Figure 4.1 Schematic of the important pathways in the basic approach

Both streams converge at the box labelled (M) on the flowchart which is where the theoretical predictions are compared with the observed forms. The computer programs used in each step are highlighted in brackets.

The experimental stream consists of two routes for obtaining the observed forms labelled (Q) and (P). Route (P) is the route taken for identifying the morphology of l-alanine reported in Chapter 3. Interfacial angles are measured and MORANG used with these measured angles to identify the forms present. Route (Q) is the straightforward use of the forms reported in the literature.

The theoretical stream begins with a cycle labelled (A). This cycle involves fitting hydrogens to incomplete structures using a molecular graphics package (INTERCHEM). CRYSTLINK can then be used to convert the results back to crystal co-ordinates. On passing out of this cycle the flow moves onto route (B) which then splits up into two branches (C) and (D).

Branch (C) involves identifying the most important forms according to the laws of Bravais-Friedel and Donnay-Harker (see Chapter 2). The program MORANG (see previous section) performs this type of calculation. The results are then used in two ways. Firstly, along route (C) the results are used with SHAPE to produce the Donnay-Harker model of the morphology. Secondly the results are passed into route (D) via the path on the flowchart labelled (E). This allows the most effective use of cpu time. The identification of the most important forms according to the DH approach requires only a few seconds cpu time, energy calculations using PCLEMC require considerably longer. It is therefore most efficient to use MORANG to identify the important forms on which to concentrate the energy calculations.

Branch (D) begins with a cycle labelled (F). This cycle is to obtain the charge distribution over the molecule if not already available. The charge distribution can be obtained from quantum chemistry packages, files can be prepared by CRYSTLINK. A file is then prepared for PCLEMC using one of the options available in CRYSTLINK, the charges introduced and the lattice energy calculated using PCLEMC in 'LATT' mode (see Appendix C). The summation limit r is increased until no significant contribution to the lattice energy results. In Chapter 5 some profiles of the summation limit as function of lattice energy have been plotted. This is compared to the experimental sublimation enthalpy if available through cycle (G). At this point the results from route (C) are introduced to focus the energy calculations on the likely forms. PCLEMC is then used to calculate the slice and attachment energies, these attachment energies

Figure 4.2 Schematic of the additive approach

are then used with SHAPE to compute the Attachment Energy (AE) model (shown in route (D)).

After the calculation of the lattice energy branch (J) splits from path (D). Branch (J) is the Ising approach (see Chapter 2). Firstly the strong bonds in the crystal are identified. PCLEMC will output this information if flagged to do so. The connected nets for the important forms identified according to the Donnay-Harker approach (stream F) are then obtained. These nets can, with the relative bond strengths be used as input to TCCALC which will calculate θ^c . This can be used as a measure of relative centre to face distances and used to compute the Ising model of the crystal (see route labelled (J)). Routes (C), (D) and (J) converge on box (M) where the morphologies are compared.

3.2 Additive Approach

The approach for the additive calculation is shown in the schematic given in Figure 4.2. The diagram consists of two streams labelled (A) and (B). Stream (A) starts with the design of the additive. This process involves using a molecular graphics package to build the additive and then to fit the additive onto the host system. CRYSTLINK can then be used to produce crystal co-ordinates in terms of the host lattice system from the cartesian co-ordinates used by the molecular graphics package. The file produced can then be converted into a file in the format for PCLEMC using another option available in CRYSTLINK. This is used as input to stream (B) at box (C). Stream (B) begins with a straight-forward prediction of the morphology. This is essentially the previous schematic reduced into one box. The new parameters for predicting the new morphology with the presence of an additive can then be calculated using PCLEMC. The nature of the model has been explained earlier (Chapter 2), the format of the input and output for PCLEMC will be discussed in the following chapter. The new parameters can be used with SHAPE to compute the model of the morphology with the additive present.

4 References

[1] E. Dowty Amer. Miner. (1976) 61 448.

[2] K.J. Roberts (unpublished results).

[3] National Alogrithms Group. NAG Central Office, Mayfield House, 256 Banbury Road. Oxford OX2 7DE.

[4] Vax Fortran Reference Manual April (1982) Digital Equipment Corporation. Maynard, Massachusetts, USA.
[5] Crystal Structure Search Retervial Database. SERC Chemical Databank Systems. CSE Applications Group, Daresbury Laboratory, Warrington, England.
[6] M. J. S. Dewar and W. Theil. J. Amer. Chem. Soc. 99 (1979) 4899.
[7] CNDO. QCPE Program Library (Number 19).
[8] GAMESS - General Atomic and Molecular Electronic Structure System. M.F. Guest and J. Kendrick. University of Manchester Regional Computer Centre. (June 1986).
[9] ORTEP-II C.K. Johnson Oak Ridge National Laboratory, Oak Ridge, Tennessee. Rep ORNL-3704 US.
[10] INTERCHEM. P. Bladon and R. Breckinridge. University of Strathclyde.
[11] International Tables of X-ray Crystallography. (D. Riedel publishing company, 1983).
[12] CHEM-X, developed and distributed by Chemical Design Ltd, Oxford, England.
[13] VIEW. SERC Chemical Databank Systems. CSE Applications Group, Daresbury Laboratory Warrington England.
[14] J.J.M . Ripjkema. Thesis, University of Nijmegen (1984).
[15] P. Bennema and J.P. Van der Eerden. Chapter 1 in Morphology of Crystals, edited by I. Sunagawa. Terra Scientific Publishing Compan Tokyo (1987).
[16] E. Dowty Amer. Miner. (1980) 65 465.

Chapter 5

Lattice Energy Calculations

CONTENTS

1 Introduction

The lattice energy, often referred to in the literature as the crystal binding energy or cohesive energy, can for molecular crystals be calculated by summing all the interactions between a central molecule and the surrounding molecules. Each intermolecular interaction can be considered to consist of the sum of constituent atom-atom interactions [1,2]. If there are n atoms in the central molecule and n' atoms in each of the N surrounding molecules then the lattice energy E_{latt} can be calculated through the summation shown in equation (1).

$$E_{latt} = 1/2 \sum_{k=1}^{N} \sum_{i=1}^{n} \sum_{j=1}^{n'} V_{kij} \qquad (5.1)$$

V_{kij} is the interaction between atom i in the central molecule and atom j in the k^{th} surrounding molecule. V_{ij}, the interaction between two non-bonded atoms i and j can be described by Lennard-Jones and Buckingham type potentials as shown earlier in chapter 1. Equation (5.2) shows a simple Lennard-Jones 6-12 potential function plus an additional Coulombic description of the electrostatic interaction (the third term in equation (5.2)).

$$V_{ij} = -A/r^6 + B/r^{12} + q_i q_j / r \qquad (5.2)$$

A and B are the atom-atom parameters for describing a particular atom-atom interaction (eg. C—O or C—-H), q_i and q_j are the fractional charges on atoms i and j separated by a distance r. The selection of potential function and the sources of atom-atom parameters is discussed in greater detail at the start of chapter 6.

A number of published programs including WMIN [3] and PCK83 [4] use this type of approach for calculating the lattice energies. These packages also allow the minimisation of lattice energies with respect to the structural variables (lattice constants and atomic co-ordinates) and have been used to investigate packing analysis problems [5].

The lattice energy is a valuable parameter to calculate since it can be compared against the experimentally determined sublimation enthalpy (see section 3 in this chapter). It therefore serves as a useful check for any new program/ parameter set being written or tested.

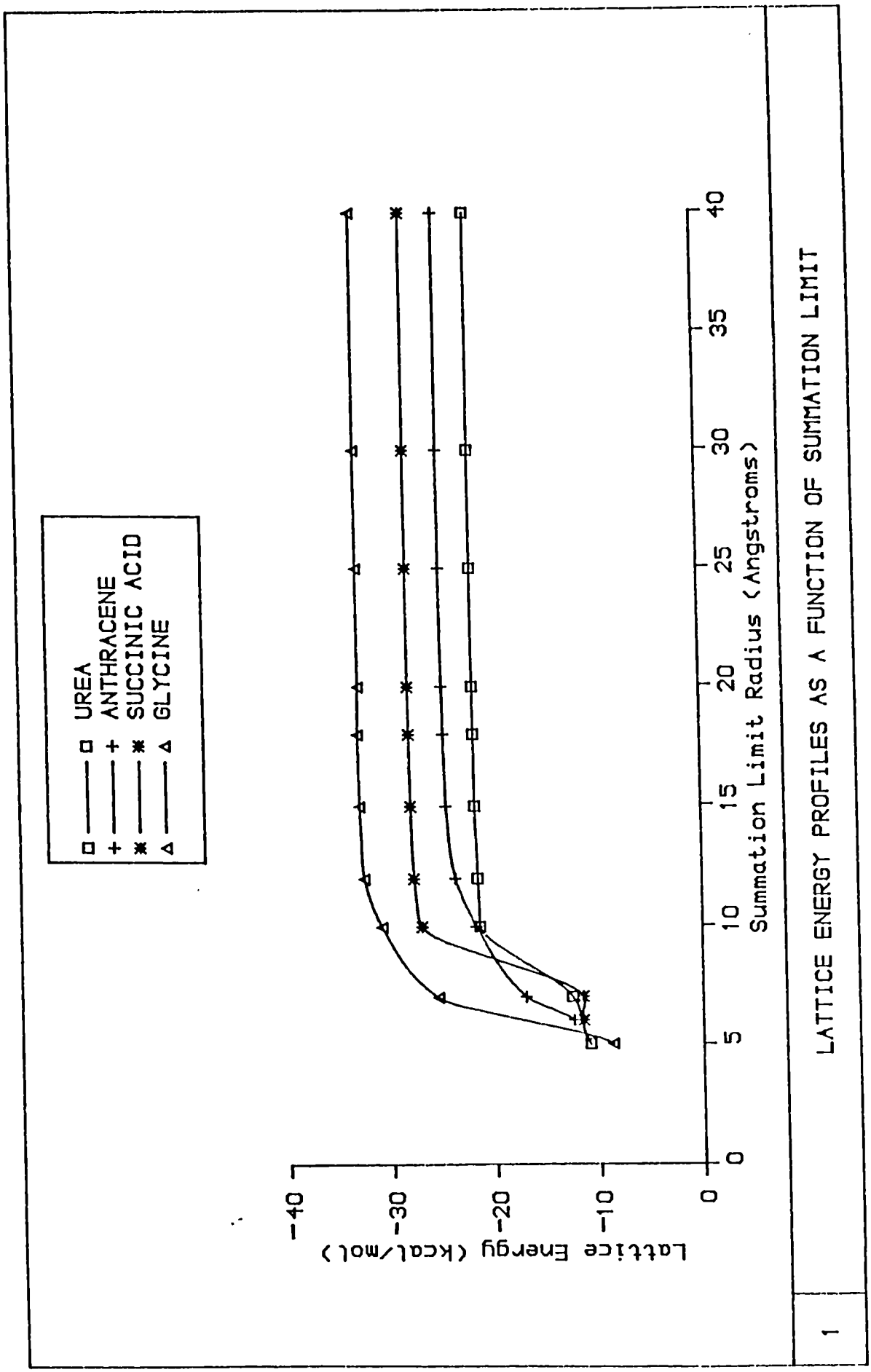

Figure 5.1 Calculated lattice energy as a function of summation limit for a selection of organic compounds.

2 Lattice Summation Limit

Calculation of all the interactions between a central molecule and all the surrounding molecules in a crystal is clearly a huge computational task. On inspection of the potential function shown in equation (2), it is clear that since A,B, q_i and q_j are constants for a particular atom-atom interaction the magnitude of the interaction energy depends on the distance between the atoms r. At large seperation distances the interaction energy will be small. The Van der Waals interactions will act over a small range depending as it does on the inverse powers of r. The electrostatic interaction will be a longer range interaction depending as it does on 1/r (see third term of equation (5.2)). Clearly at certain distances the interaction between two molecules will become negligble. An intermolecular interaction is just the sum of the interatomic interactions present between two molecules.

In 'LATT' mode PCLEMC allows the lattice energy to be calculated using various sizes of summation limit (see Appendix C). The summation limit is the radius of the sphere inside which the summation between the central and surrounding molecules is carried out. This allows the identification of the limit beyond which increasing the the sphere size results in no further significant contribution to the lattice energy [6]. Figure 5.1 shows the profiles of the lattice energy as a function of summation limit for α-glycine, anthracene, β-succinic acid and urea. These materials exhibit a range of intermolecular bonding (including hydrogen bonding) and different degrees of electrostatic interactions. The electrostatic contribution varies from negligible in the case of anthracene to over 60 percent in the case of urea.

The plots all show the same general trend. An initial increase is followed by a levelling off after 20Å. The lattice energy beyond this limit shows little change resulting from increasing the summation limit. The lattice energy on this plateau can be compared against the sublimation enthalpy.

3 Comparison with Sublimation Enthalpy

In Table 5.1 the calculated lattice energies are given along with the experimental sublimation enthalpies for a range of organic molecules [7]. The range studied includes not only a variety of intermolecular interactions (hydrocarbons through to amino acids) but also a selection of the most important crystal classes (monoclinic, triclinic and orthorhombic) as reflected in the analysis of the CSSR

Table 5.1 Calculated Lattice Energies and Experimental Sublimation Enthalpies for Some Organic Compounds.

Material	Calculated Lattice Energies -(kcal/mol)	Experimental Sublimation Enthalpies (kcal/mol)	Further Calculation Details
Anthracene	25.1	25.0	Chapter 6
Biphenyl	21.6	19.5	Chapter 6
Urea	22.0	21.0	Chapter 7
Benzoic Acid	20.4	21.9	Chapter 6
Succinic Acid	28.2	28.1	Chapter 6
Glycine	33.0	32.6	Chapter 8
L-alanine	31.7	33.0	Chapter 8
Benzophenone	24.5	22.7	Chapter 9

Experimental sublimation enthalpies taken from [7].

database in Chapter 2 section 1.2. The table also includes details on the parameter sets used and where in the thesis to find further details on the calculations.

The lattice energy and sublimation enthalpy should be of the same order of magnitude but be of opposite signs. Table 5.1 shows excellent agreement between the calculated and experimental values through the range of materials.

4 References

[1] A.I. Kitaigorodski, Tetrahedron, 14 (1961) 230.

[2] D.E. Williams, J. Phys. Chem. 45 (1966) 3370.

[3] W.R. Busing. WMIN, A Computer Program To Model Molecules and Crystals In Terms of Potential Energy Functions. April 1981, Oak Ridge, Tennesse 37830.

[4] D.E. Williams PCK83, A Molecular Crystal Packing Analysis Program. Quantum Chemistry Exchange Program no. 481.

[5] W.R. Busing Acta Cryst A39 (1983) 340.

[6] Z. Berkovitch-Yellin, J. Amer. Chem. Soc. 107 (1985) 8239.

[7] Thermochemistry Of Organic and Organometallic Compounds. J.D. Cox and G. Pilchard (Academic Pres, New York 1970).

Chapter 6

The Importance of Potential Function Choice

Anthracene, Biphenyl, Succinic Acid and Benzoic Acid

As Case Studies

CONTENTS

1 Introduction

In this chapter studies of the morphologies of anthracene, biphenyl, β-succinic acid and benzoic acid are carried out. The theoretical morphologies using Donnay-Harker (DH) and Attachment Energy (AE) models are calculated and compared with the observed morphologies. Details of the principles behind these calculations have been presented earlier (see chapter 2), the basic approach for carrying out these calculations has also been presented (see chapter 4). The purpose of these calculations is three-fold.

1) A further test of the computer programs and the guidelines outlined earlier.

2) A comparison of the DH and AE models for materials where there is isotropic bonding such as anthracene and biphenyl and materials where stong bonding directions occur such as β- succinic acid and benzoic acid.

3) An investigation of the variation in predicted morphology from energy calculations with choice of atom-atom potential fuction.

In order to carry out these investigations a small 'database' of potential parameter sets was used. These potentials reflect the different approaches for describing the interactions between atoms. Three different approaches are used for describing the hydrogen bonding interactions for the cases of β-succinic and benzoic acid.

2 Atom - Atom Potential Parameters

A variety of atom- atom potential parameters have been derived by a number of authors to describe interactions in particular classes of compounds [1]. The interaction between two non- bonded atoms can be considered to consist of a simple electrostatic interaction (V_{elec}), a Van der Waals attractive and repulsive contribution (V_{vdw}) and in some cases a hydrogen bond contribution . The electrostatic contribution is commonly described by a simple coulombic interaction as shown by equation (6.1) where q_i and q_j are the fractional charges on atoms i and j separated by a distance r. D is the dielectric constant.

$$V_{elec} = \frac{q_i \cdot q_j}{Dr} \tag{6.1}$$

The non - bonded Van der Waals interactions can be described by a number of potential functions all of which have the same basic form, consisting of an attractive and repulsive contribution. Two of the most common are the so-called Lennard- Jones 6-12 [2] and the Buckingham 6-exp [3] functions illustrated by equations (6.2) and (6.3) where A,B and C are the parameters to describe interactions between particular pairs of atoms.

$$V_{vdw} = -A/r^6 + B/r^{12} \tag{6.2}$$

$$V_{vdw} = -A/r^6 + Bexp(-Cr) \tag{6.3}$$

In this chapter five different parameter sets are used to evaluate atom-atom interactions and a short summary of these parameter sets follows.

2.1 Parameter Set I

This set of parameters derived by Scheraga et al [4,5] were applicable to both hydrocarbons and carboxylic acids and so they were applied to all four cases studied in this chapter. This was the only set which was applied to all four cases. The authors used the 6-12 potential to describe the interactions between atoms except for the case of a hydrogen bond where a 10-12 potential (similar in structure to the 6-12 function) was used. The attractive parameter for the 6-12 potential function was determined by these authors from experimental measurements on atom polarisabilities, the repulsive parameter determined by an energy minimisation procedure. The attractive part of the 10-12 potential was determined from quantum chemistry calculations on hydrogen bond strengths the repulsive part determined again by an energy minimisation procedure, similar to the procedure adopted in the 6-12 case. The electrostatic contribution was described by the simple coulombic interaction outlined earlier (equation (6.1)).

2.2 Parameter Sets II and III

Parameter sets II and III were derived by Williams [6] and Kitaigordski [7]. Both sets use the 6-exp function (see equation 6.3)) and were derived for hydrocarbons only and so were not applied to the cases of β-succinic acid and benzoic

acid in this chapter. Williams used compressibility measurements of the interplanar spacings in graphite to obtain the exponent of the repulsive part of the C–C interaction potential, the corresponding value for the H–H interaction being obtained from quantum chemistry calculations. The other parameters were obtained from a fitting of calculated properties to some experimentally observed properties including structural details and sublimation enthalpies.

2.3 Parameter Set IV

This set of parameters from Hagler [8] were derived to deal specifically with carboxylic acids and use the 'classic' 6-12 potential function (see equation (6.2)) . Unlike set I or set V the authors found that no special hydrogen bonding function needed to be introduced. The authors use the consistent force field (CFF) approach which involves evaluating the constant parameters for a particular potential fuction to describe interactions in particular classes of compounds by a least squares fitting of the calculated to experimentally observed properties. This requires the use of all the available relevant experimental data for a particular family of compounds including structural details, sublimation energies and dimerisation energies. The parameters obtained by these authors including charges (Set III in reference [8]) were applied to the cases of β-succinic and benzoic acid.

2.4 Parameter Set V

Like set IV this set of parameters derived by Smit [9] is particular to carboxylic acids. These workers used the 6-exp function to describe the interactions between atoms except in the case of hydrogen bonds of the form OH-O where the interactions (V_{hb}) are described by a Lippincott - Schroeder potential [10] of the type shown in equation (6.4) below.

$$V_{hb} = D[1 - exp[-n(r_{OH} - r_{OH})^2)/2r_{OH}] - 1/gexp[(-ng(r_{H-O} - r_{H-O})^2)/2r_{H-O}] + Aexp(-br_{O-O}) - Br_{O-O}^{-m} \quad (6.4)$$

In equation (4) the variables D, n, g, A, B, b, m,r_{OH} and r_{H-O} are empirical parameters introduced by Lippincott and Schroeder [10] and r_{OH}, r_{H-O} and r_{O-O} are the observed distances in the crystal of interest. Smit and co-workers [9] used these parameters for the hydrogen bond and starting parameters for the

TABLE 6.1 The major faces for anthracene, biphenyl and succinic acid identified according to their slice thickness

ANTHRACENE FACE	d(hkl)	BIPHENYL FACE	d(hkl)
(0 0 1)	9.195	(0 0 1)	9.472
(1 1 $\bar{1}$)	4.888	(1 1 0)	4.621
(1 1 0)	4.583	($\bar{1}$ 1 1)	4.239
(2 0 $\bar{1}$)	4.174	($\bar{1}$ $\bar{1}$ $\bar{1}$)	4.072
(2 0 $\bar{2}$)	4.164	(2 0 0)	4.043
(1 1 $\bar{2}$)	4.091	($\bar{2}$ 0 1)	3.845
(1 1 1)	3.603	($\bar{2}$ 0 $\bar{1}$)	3.605
(2 0 0)	3.520	($\bar{1}$ 1 2)	3.395
(0 2 0)	3.019	($\bar{1}$ $\bar{1}$ $\bar{2}$)	3.226
(0 2 1)	2.863	($\bar{2}$ 0 2)	3.220

β-SUCCINIC ACID FACE	d(hkl)	BENZOIC ACID FACE	d(hkl)
(1 0 0)	5.517	(0 0 2)	10.89
(1 1 0)	4.683	(1 0 0)	5.46
(0 2 0)	4.431	(1 0 $\bar{2}$)	5.16
(0 1 1)	4.420	(0 1 1)	5.02
(1 1 $\bar{1}$)	3.491	(0 1 2)	4.66
(1 2 0)	3.454	(1 0 2)	4.65
(1 1 1)	3.409	(0 1 3)	4.20
(0 2 1)	3.344	(1 0 $\bar{4}$)	4.13
(1 2 $\bar{1}$)	2.883	($\bar{1}$ $\bar{1}$ 1)	3.75
(1 2 1)	2.837	(1 1 0)	3.75

TABLE 6.2 - Calculated lattice energies for anthracene, biphenyl B-succinic acid and benzoic acid for various parameter sets.

	LATTICE ENERGY (kcal/mol)				
MATERIAL	SET I	SET II	SET III	SET IV	SET V
Anthracene	-25.1	-24.9	-23.0	-	-
Biphenyl	-23.0	-22.7	-21.6	-	-
β-Succinic Acid	-28.2	-	-	-30.8	-31.9
Benzoic Acid	-18.9	-	-	-20.4	-20.1

6-exp function from other authors to derive parameters for carboxylic acids by fitting the parameters to experimental observations on structures and dimerisation energies of a family of carboxylic acids. The authors derived four parameter sets, they expressed a slight preference for their third set and so this set was used for the cases of succinic and benzoic acids in this chapter.

3 Anthracene

3.1 Structural Details of Anthracene

Anthracene ($C_{14}H_{10}$) shown in Figure 6.1 is an aromatic hydrocarbon which crystallises in the monoclinic space group $P2_1/a$ in a bimolecular unit cell of dimensions a = 8.562Å, b = 6.038Å, c = 11.184Å with β=124.7° [11]. Figure 6.2 shows the arrangement of the molecules in the unit cell. The general extinction conditions for the space group in question were given in International Tables [12] as:

h0l h=2n, 0k0 k=2n, h00 h=2n.

Since the anthracene molecules are situated at special positions (i.e centers of symmetry) an additional special extinction condition must be considered i.e (hkl h+k=2n.)

3.2 Results Of Anthracene Calculations

The ten major faces according to slice thickness for anthracene were identified using MORANG (see Appendix A and Chapter 4) and are listed in Table 6.1 and the morphology based on these results is given in Figure 6.3(b). Parameter sets I,II and III were used along with a charge distribution given by Scheraga [4] to perform energy calculations on anthracene, the calculated lattice energies V_{latt} for anthracene are given in Table 2. The electrostatic contribution to this lattice energy was found to be negligible. The lattice energy can be related to the energy of sublimation by the equation:

$$V_{exp} = -\Delta H_s - 2RT \qquad (2.5)$$

where V_{exp} is the 'experimental' lattice energy, Δ imersH_s is the enthalpy of sublimation and 2RT represents a correction factor for the difference between the gas phase enthalpy and the vibrational contribution to the crystal enthalpy [6]. Two sublimation enthalpies of 22.5 and 24.5 kcal/mol have been reported

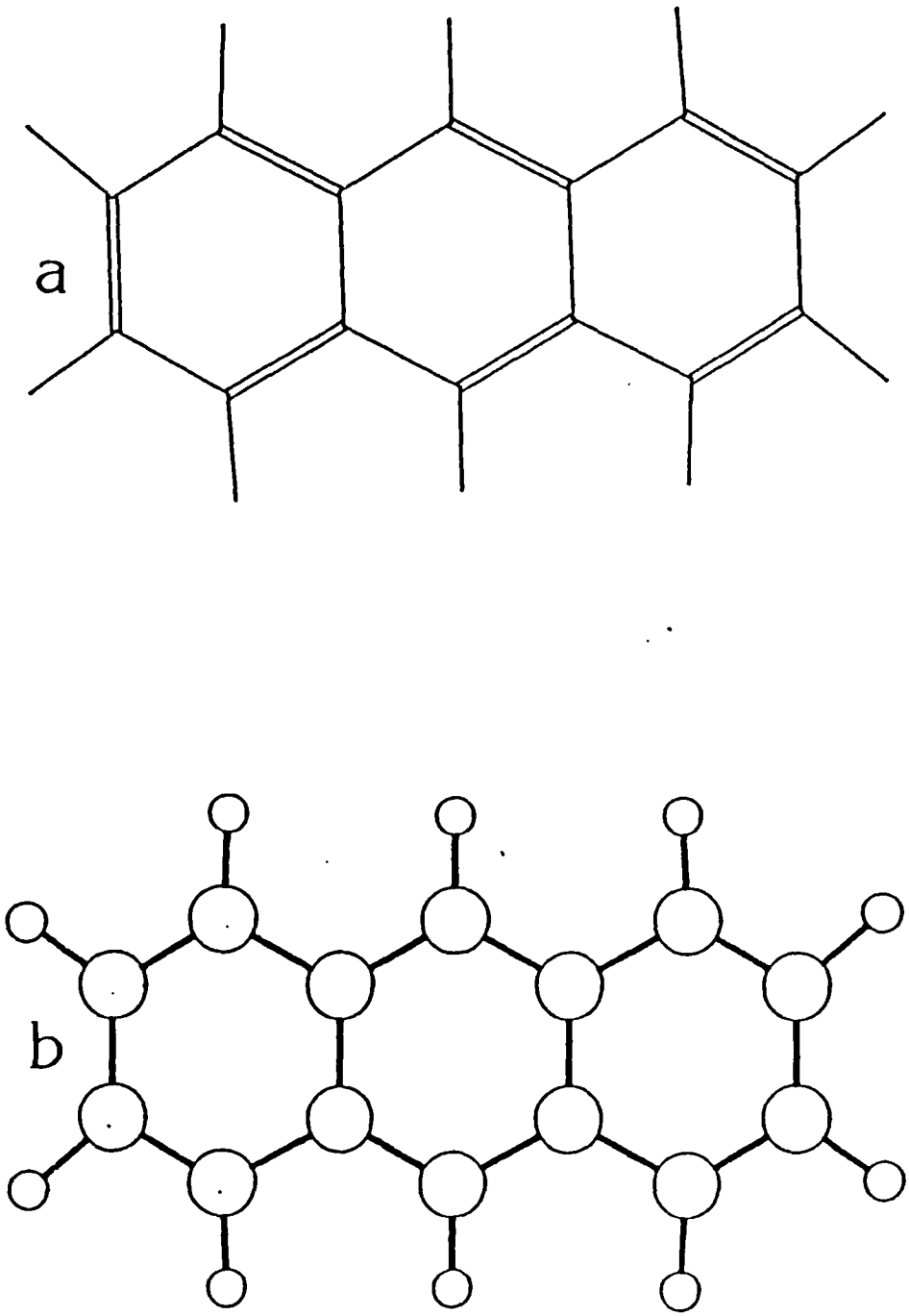

Figure 6.1 Anthracene molecule, (a) stick diagram with double bonds highlighted, (b) ball and stick model

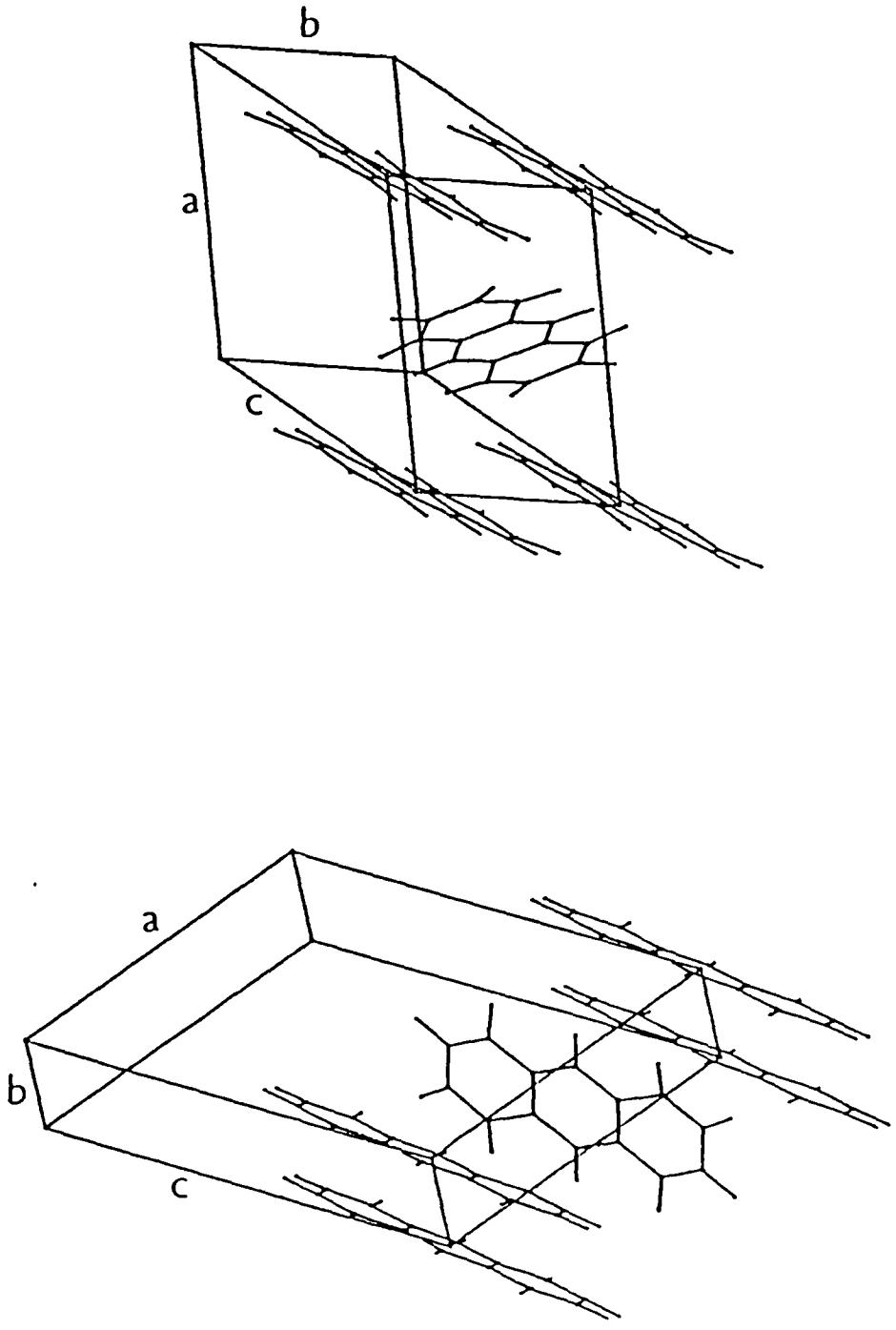

Figure 8.2 Anthracene molecules arranged in the unit cell.

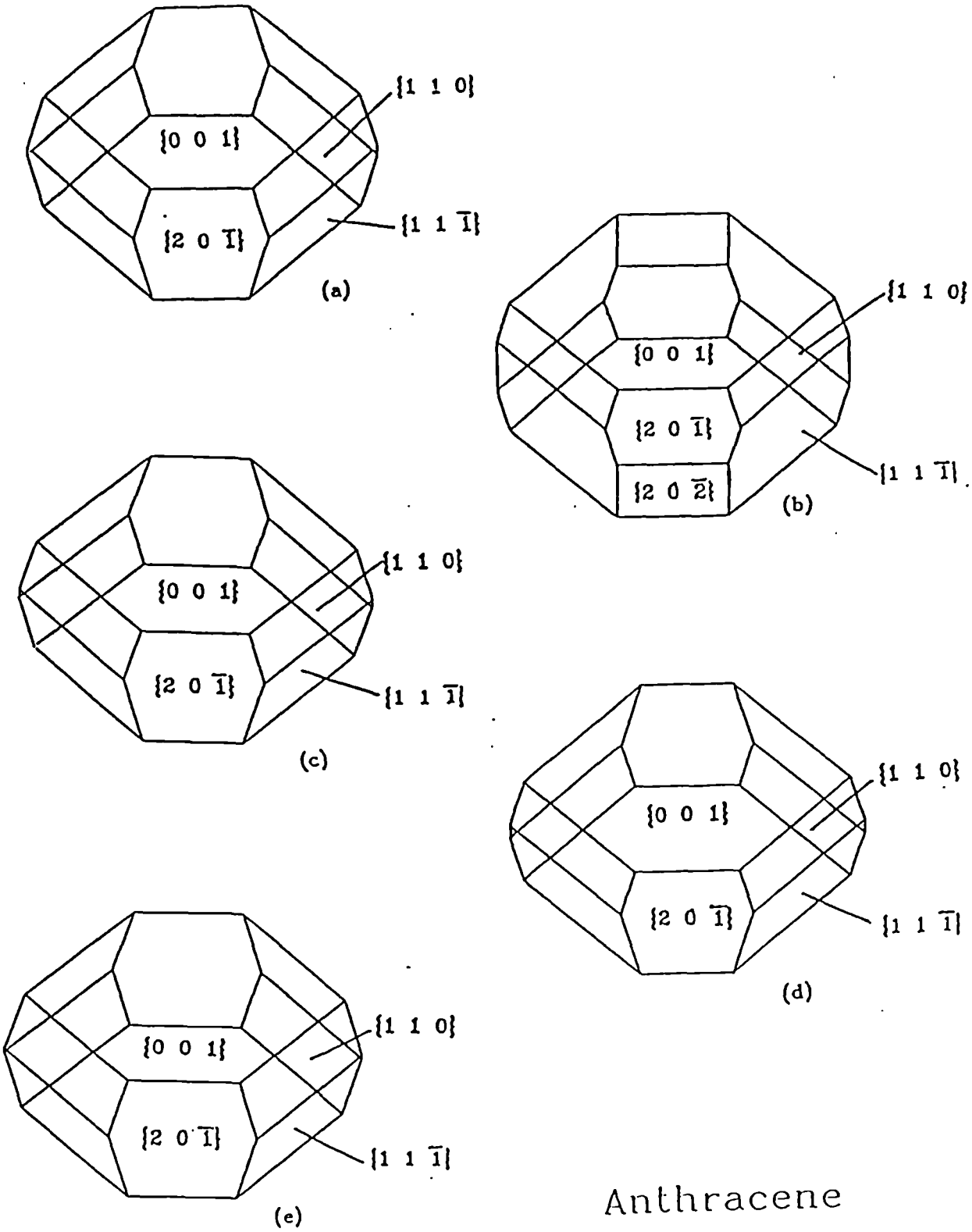

Figure 6.3 Morphologies of anthracene, (a) observed
(b) Donnay-Harker model (c) Attachment Energy model (set I)
(d) Attachment Energy model (set II)
(e) Attachment Energy model (set III)

Table 6.3 Calculated slice and attachment energies for the major faces in anthracene using all three parameter sets (results in kcal/mol).

FACE	SET I		SET II		SET III	
	Esl	Eatt	Esl	Eatt	Esl	Eatt
(0 0 1)	-21.6	-3.4	-21.8	-3.1	-19.7	-3.3
(1 1 $\bar{1}$)	-16.5	-8.6	-16.5	-8.4	-15.1	-7.9
(1 1 0)	-16.9	-8.2	-16.7	-8.2	-15.5	-7.5
(2 0 $\bar{1}$)	-16.1	-9.0	-15.7	-9.2	-15.0	-8.0
(2 0 $\bar{2}$)	-13.9	-11.2	-13.8	-11.1	-12.8	-10.2
(1 1 $\bar{2}$)	-13.7	-11.3	-14.0	-10.9	-12.4	-10.6
(1 1 1)	-14.1	-11.0	-14.3	-10.6	-12.8	-10.2
(2 0 0)	-14.7	-10.4	-14.4	-10.5	-13.8	-9.2
(0 2 0)	-10.4	-14.7	-10.3	-14.6	-9.5	-13.5
(0 2 1)	-9.6	-15.4	-9.7	-15.2	-8.7	-14.2

for anthracene [4] . Using equation (2.5) this gives the 'experimental' lattice energies of -23.7 and -25.7 kcal/mol which are in reasonable agreement with the calculated lattice energies listed in Table 6.2.

The calculated slice and attachment energies for the top ten faces listed in Table 6.1 are given in Table 6.3 for parameter sets I,II and III, the resultant morphologies constructed from these results are given in Figures 6.3(c),(d) and (e). A comparison of these morphologies follows.

3.3 Morphologies of Anthracene

Anthracene grows in a number of forms but generally it has a hexagonal like tabular habit with the (001) faces being the major faces with the (110), $(11\bar{1})$ and $(\bar{2}01)$ side faces as shown in Figure 2(a) [13]. It sometimes grows without the $(11\bar{1})$ faces and with a increased importance of $(\bar{2}01)$ faces, occasionally the (200) faces are observed. The DH model (Fig 6.3(b)) shows all the same faces as in the growth form except that the $(20\bar{2})$ faces are predicted in the model but not observed. The DH model is also slightly thicker than the observed form. The AE models all show excellent agreement with the observed form, the results from SET II showing a slightly thinner morphology than that observed or that produced by the other two parameter sets. There is only a slight variation in crystal shape due to changes in parameter sets. These results are in good agreement with the surface energy calculations by Hartman [14].

4 Biphenyl

4.1 Structural Details Of Biphenyl

Biphenyl ($C_{12}H_{10}$) crystallises in a bimolecular unit cell of dimensions a = 8.120Å, b = 5.630Å, c = 9.510Å with β=95.10° [15]. The space group is $P2_1/a$ and the same extinction conditions which applied to the anthracene case can be applied to biphenyl. The biphenyl molecule is shown in Figure 6.4 , a picture of the unit cell is shown in Figure 6.5.

4.2 Results Of Biphenyl Calculations

The ten major faces according to slice thickness obtained from MORANG are listed in Table 6.1. In the biphenyl case the charge distribution over the biphenyl molecule was not available from any of the parameter set sources and so a charge

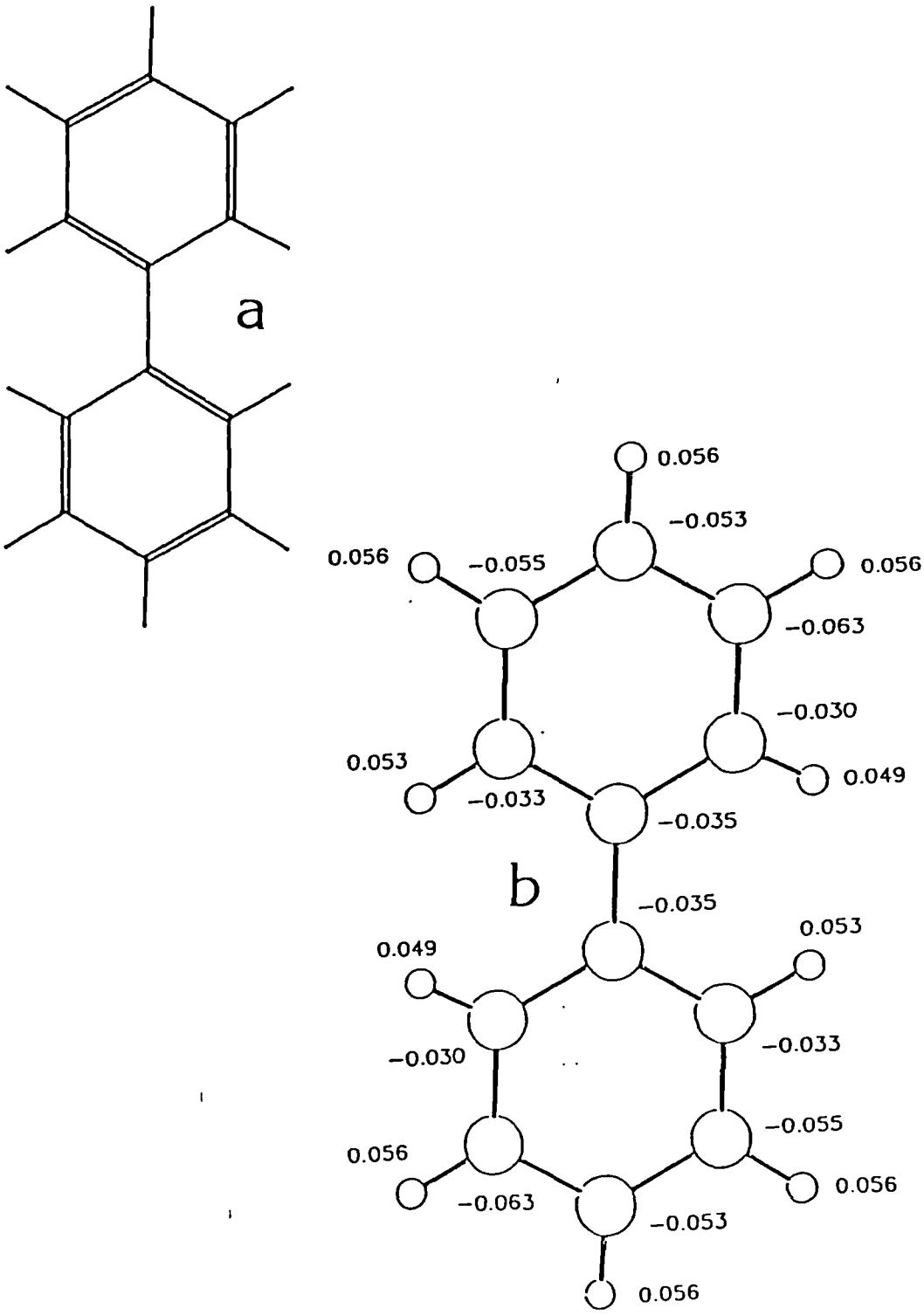

Figure 6.4 Biphenyl molecule, (a) stick model with double bonds, (b) ball and stick model with corresponding MNDO charge distribution.

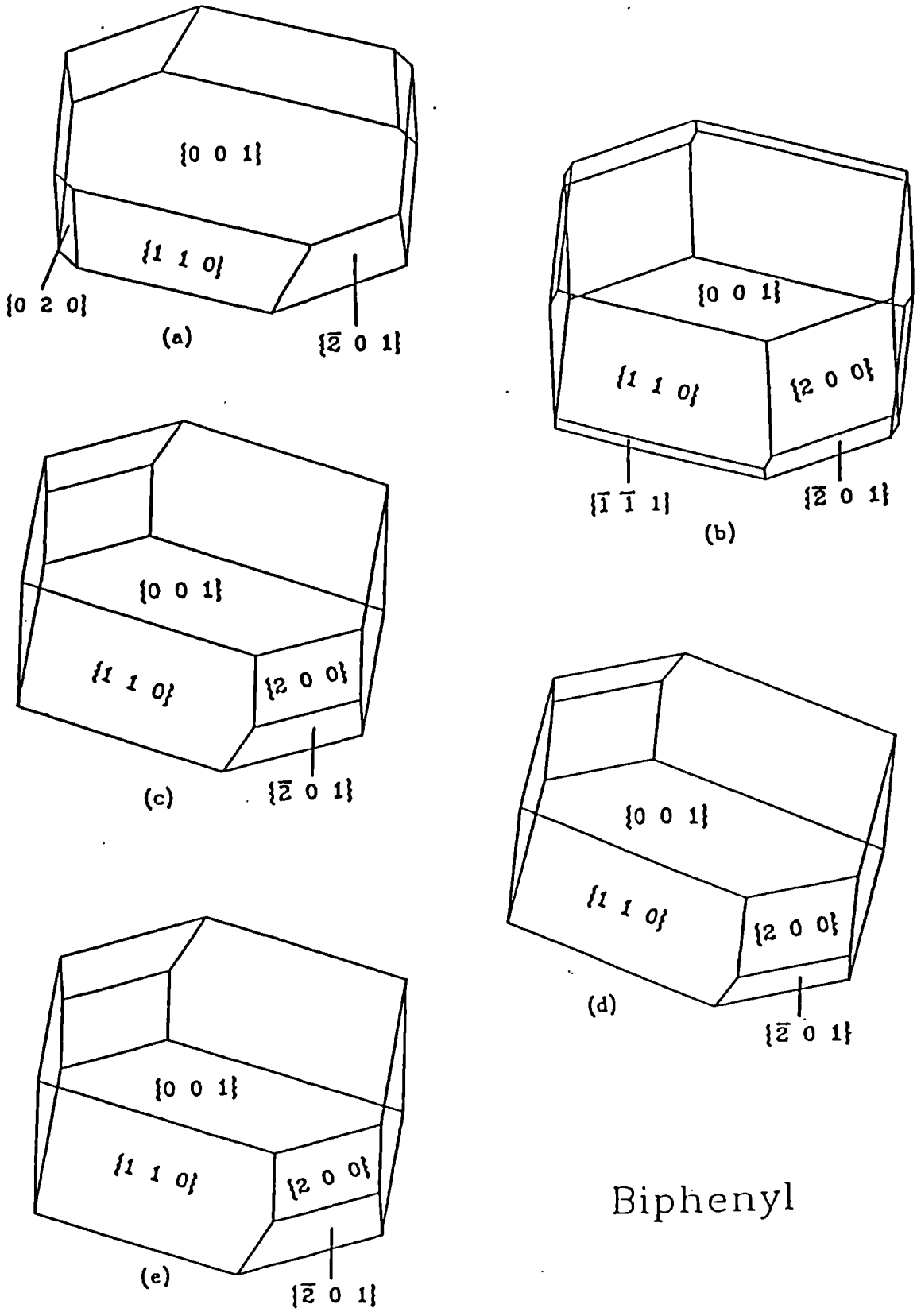

Figure 6.6 Morphologies of biphenyl, (a) observed
(b) Donnay-Harker model (c) Attachment Energy model (set I)
(d) Attachment Energy model (set II)
(e) Attachment Energy model (set III)

Table 6.4 Calculated slice and attachment energies for the major faces in biphenyl using all three parameter sets (results in kcal/mol).

FACE	SET I		SET II		SET III	
	Esl	Eatt	Esl	Eatt	Esl	Eatt
(0 0 1)	-19.9	-3.1	-19.9	-2.8	-18.6	-3.0
(1 1 0)	-15.8	-7.2	-15.5	-7.2	-14.9	-6.7
($\bar{1}$ 1 1)	-14.9	-8.1	-14.6	-8.1	-14.0	-7.6
($\bar{1}$ $\bar{1}$ $\bar{1}$)	-13.4	-9.6	-13.5	-9.2	-12.5	-9.1
(2 0 0)	-14.0	-9.0	-13.8	-8.9	-13.3	-8.4
(2 0 $\bar{1}$)	-14.3	-8.8	-13.9	-8.8	-13.6	-8.0
($\bar{2}$ 0 $\bar{1}$)	-11.6	-11.4	-11.8	-10.9	-10.9	-10.8
($\bar{1}$ 1 2)	-12.4	-10.6	-12.4	-10.3	-11.5	-10.1
(1 1 2)	-11.6	-11.5	-11.8	-10.9	-10.7	-10.9
(2 0 $\bar{2}$)	-11.9	-11.1	-11.8	-10.9	-11.3	-10.4

Table 6.5 Reported and calculated interfacial angles for biphenyl. Reported angles [19] and calculated using MORANG (Appendix A) and cell parameters from [15]

FACES	REPORTED ANGLE	CALCULATED ANGLE A	CALCULATED ANGLE B
(110) ($\bar{1}$10)	69.63	69.64	69.68
(110) (001)	87.28	87.28	87.09
(101) (001)	70.62	70.23	46.57
(100) (001)	85.25	85.24	84.90
($\bar{2}$01) (001)	-	-	71.25

CALCULATED ANGLE A - cell ratio reported in Groth [19]

CALCULATED ANGLE B - cell ratio reported by Trotter [15]

distribution from an MNDO [16] calculation was used. The charge distribution over a biphenyl molecule is shown in Figure 3. The calculated lattice energy of biphenyl using the three parameter sets I,II and III listed in Table 6.2 compare quite well with the 'experimental' lattice energy of -20.7 kcal/mol derived from the reported sublimation energy of 19.5 kcal/mol [17] and equation (5). The slice and attachment energies for the three parameter sets are listed in Table 6.4 , the corresponding morpholgies are shown in Fig 6.6(c),(d) and (e).

4.3 Morphologies of Biphenyl

Biphenyl is generally reported as crystallising as (001) plates with (110) as the major side faces [18,19]. Human and co-workers [18] report that the ($\bar{2}$01) and the (200) faces are occasionally observed on crystals grown from low supersaturations. This is in good agreement with the DH and AE models shown in Figure 4. In Groth [19] however the (020) and (101) faces are reported as being in the crystal form. A comparison with the axial ratios reported in Groth [a:b:c=1.442:1:5.483] with β=94.77° and those of Trotter [a:b:c=1.442:1:1.689] with β=95.10° shows a discrepancy. The reported and calculated interfacial angles (using both cell ratios and the program MORANG) are listed in Table 6.5. Good agreement is found between the angles except in the case of the (101) and (001) where the reported angle and the calculated angle (using Trotters cell ratios) differ by 23.6°. Calculations of the interfacial angles between (001) and the other faces show the best fit to the reported angle of 70.62° occurs between the ($\bar{2}$01) and the (001). Since the calculations carried out in this chapter were done so using Trotters cell dimensions we have re-indexed the (101) face as the ($\bar{2}$01) face and used this modified form as observed morphology for biphenyl (see Fig 6.6(a)).

None of the models predicts the presence of the (020) form reported in [19]. The (020) form is not in the top ten faces according to DH calculations and even when included in energy calculations it's relative centre to face distance is too high to have any effect on the constructed morphology. There is some slight variation in the size of faces in the AE models, the maximum changes being the slight differences in face area being observed in the ($\bar{2}$01) and (200) faces (see Fig 6.6(c),(d) and (e)).

5 β-Succinic Acid

5.1 Structural Details of β-succinic acid

Succinic acid (HOOC – CH_2 – CH_2 – COOH) is a dicarboxylic acid which crystallises in the monoclinic space group $P2_1/c$ in a unit cell of dimensions a = 5.519Å, b = 8.862Å, c = 5.101Å with β=91.59° [21] with two molecules in the unit cell. A picture of a succinic acid molecule is given in Figure 6.7 the arrangement of the molecules in the unit cell is given in Figure 6.8. Allowing for the change in setting the extinction conditions are the same as those outlined for the anthracene case.

5.2 Results Of β-succinic acid Calculations

The ten faces with the greatest interplanar spacings are listed in Table 1 along with the results for anthracene and biphenyl. The lattice energy for β-succinic acid was calculated using parameter sets I,IV and V the results listed in Table 2. For sets I and V the charge distribution was taken from Scheraga [4] the charges for set IV being taken from Hagler [8]. The calculated lattice energies again show good agreement with the 'experimental' lattice energy of -30.1 kcal/mol derived from the sublimation energy of 28.9 kcal/mol [4]. The morphologies given in Figures 6.6 (c), (d) and (e) are the morphologies derived from the attachment energy calculations on succinic acid given in Table 6.6

5.3 Morphologies Of β-Succinic acid

The morphology of β-succinic acid crystals grown by sublimation [21] shows a crystal with the (020),(100),(011),(111) and small (110) faces (see Fig 6.9(a)). The DH model identifies most of these faces as present in the theoretical form although it underestimates the importance of the (020) faces and overestimates the importance of the (100) and (011) faces. This is clearly shown in Fig 6.9(b). The AE models (Fig 6.9(c), (d) and (e)) show much better agreement identifying all the faces and reflecting the general shape of the crystal much better than the DH model even though all these models overestimate and underestimate the importance of the (111) and (011) faces respectively. Between the AE models there is some slight variation in the size of the faces, SET I and SET V giving a slightly better fit to the observed morphology than SET IV. The results are in excellent agreement with the calculations of Berkovitch-Yellin [21].

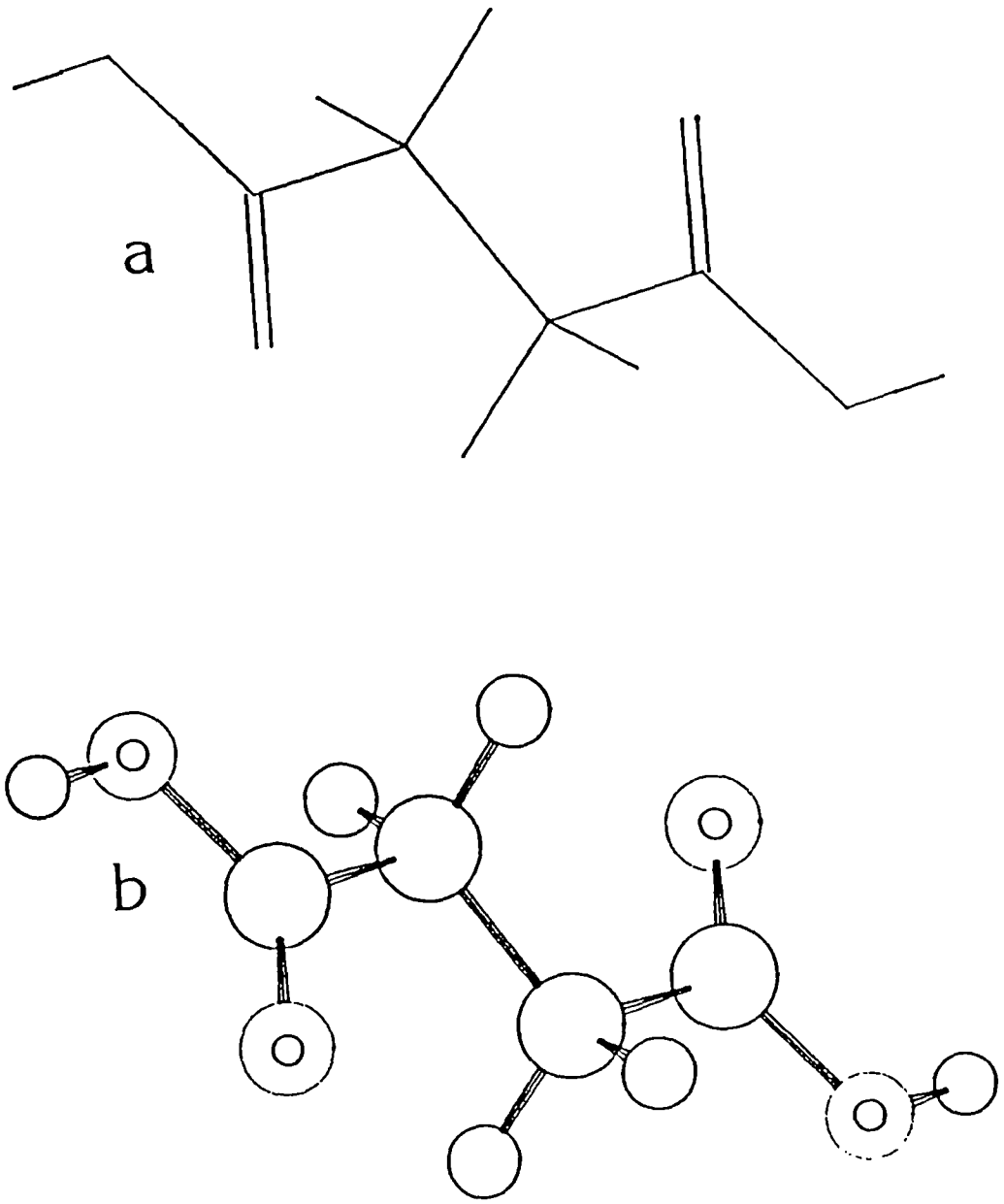

Figure 6.7 Molecules of succinic acid, (a) stick model with double bonds highlighted, (b) ball and stick model with heteroatoms labelled.

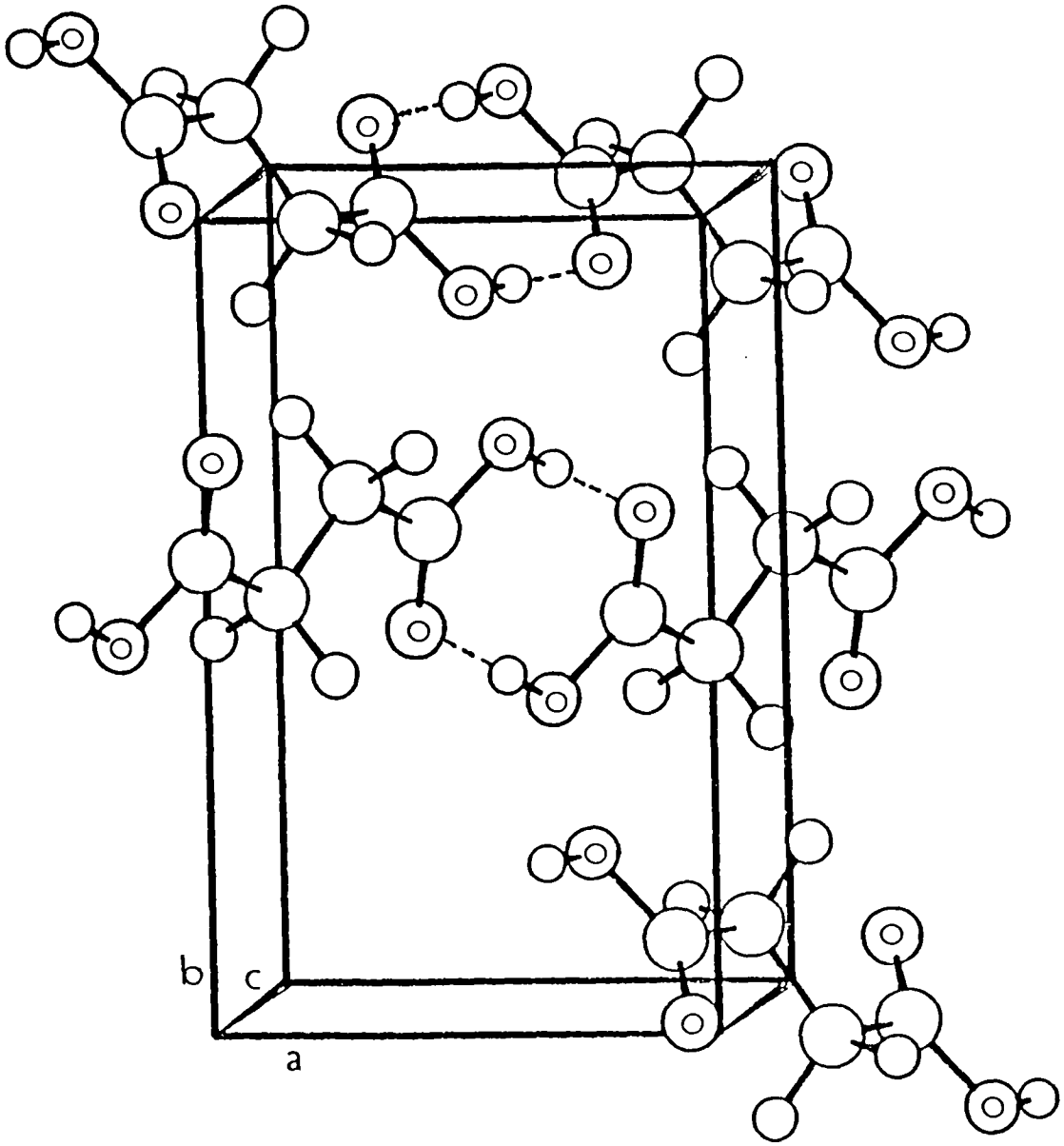

Figure 6.8 Ball and stick model showing the arrangement of the succinic acid molecules in the unit cell. The hydrogen bonding is labelled along with the heteroatoms.

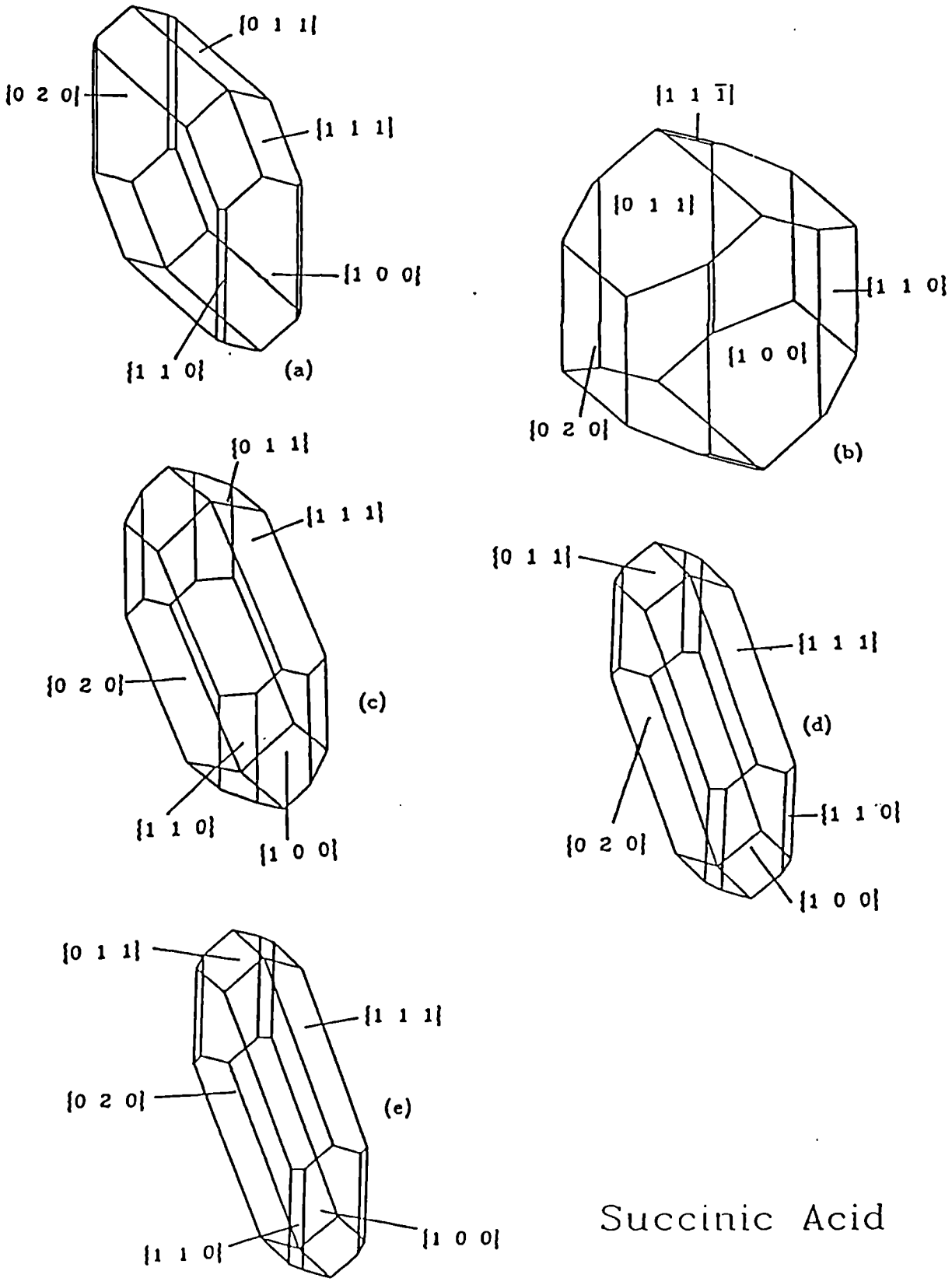

Figure 6.9 Morphologies of succinic acid, (a) observed
(b) Donnay-Harker model (c) Attachment Energy model (set I)
(d) Attachment Energy model (set IV)
(e) Attachment Energy model (set V)

Table 6.6 Calculated slice and attachment energies for the major faces in succinic acid using all three parameter sets (results in kcal/mol).

FACE	SET I		SET II		SET III	
	Esl	Eatt	Esl	Eatt	Esl	Eatt
(1 0 0)	-18.5	-9.8	-20.0	-10.8	-21.0	-10.9
(1 1 0)	-18.4	-9.8	-20.0	-10.8	-20.9	-11.0
(0 2 0)	-23.9	-4.3	-24.7	-6.0	-27.4	-4.5
(0 1 1)	-17.0	-11.2	-18.6	-12.2	-19.0	-12.9
(1 1 $\bar{1}$)	-8.3	-19.9	-9.4	-21.3	-9.2	-22.7
(1 2 0)	-15.7	-12.5	-16.9	-13.9	-17.9	-14.0
(1 1 1)	-21.7	-6.5	-21.0	-7.8	-24.7	-7.2
(0 2 1)	-15.3	-12.9	-16.0	-14.7	-17.3	-14.6
(1 2 $\bar{1}$)	-7.3	-21.0	-7.9	-22.8	-7.9	-24.0
(1 2 1)	-20.1	-8.0	-20.8	-10.0	-22.9	-9.0

6 Benzoic Acid

6.1 Structural Details Of Benzoic Acid

Benzoic acid (C_6H_5COOH) shown in Figure 6.10 is an aromatic carboxylic acid which crystallises in the space group $P2_1/c$ with four molecules in a unit cell of dimen sions a = 5.510Å, b = 5.157Å, c = 21.973Å with β= 97.41° [22]. Figure 6.11 shows the arrangement of the molecules in the unit cell. The dimers formed in the crystal are clearly visable. The extinction conditions for the space group in question given in International Tables for X-ray Crystallography [12] are:

h0l l=2n and 0k0 k=2n

6.2 Results Of Benzoic Acid Calculations

The important planes likely to dominate the crystal form were identified according to interplanar spacing and are listed in Table 6.1 . Energy calculations were carried out using parameter sets I,IV and V. A charge distribution was not available for sets IV and V and so an MNDO distribution was obtained [16]. The charge distribution over the benzoic acid molecule is given in Figure 6.10. The lattice energies listed in Table 2 are in reasonable agreement with the reported 'experimental' lattice energy of -23.0 kcal/mol derived from the sublimation enthalpy of 21.8kcal/mol [17]. The slice and attachment energies for the top ten forms listed in Table 6.1 were obtained for three parameter sets and are listed in Table 6.7.

6.3 Morphologies of Benzoic Acid

The observed morphology for benzoic acid taken from [22] and outlined in Fig 6.12(a) shows a (001) main face with smaller (011),(100) and $(10\bar{2})$ side faces. The DH model of the morphology has all these faces present in the computer drawn picture but is much thicker along the c-axis than the observed morphology. The DH model also has additional (110) and $(\bar{1}\bar{1}1)$ faces present.

The AE models (Figs 6.12(c),(d),(e)) are in good agreement with each other and with the observed form. The AE models give much better agreement than the DH model. The only differences between the observed morphology and the predicted morphologies from energy calculations are the overestimation and underestimation of the (100) and $(10\bar{2})$ faces respectively.

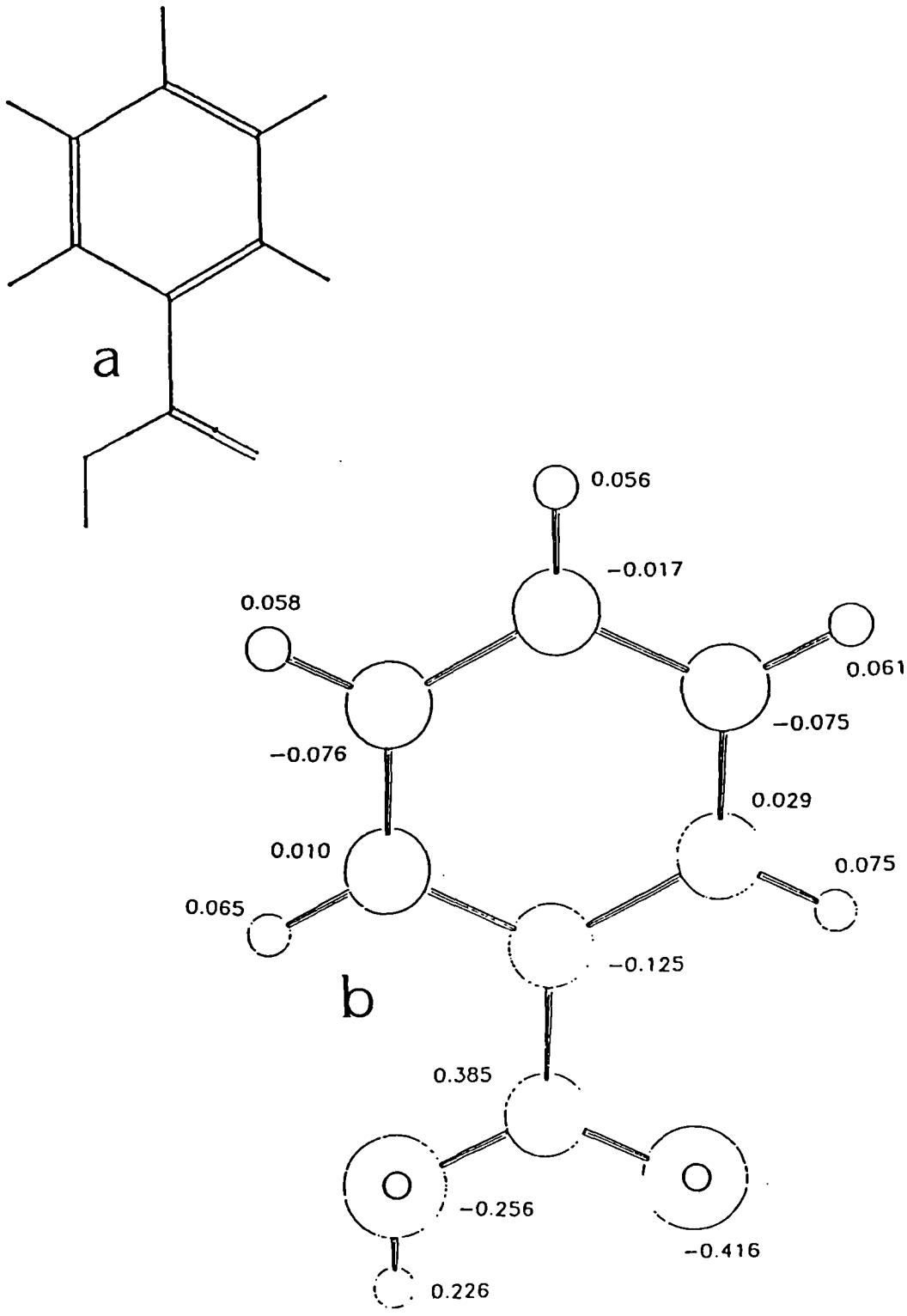

Figure 6.10 Benzoic acid molecules, (a) stick model with double bonds, (b) ball and stick arrangement with heteroatoms labelled and an MNDO charge distribution.

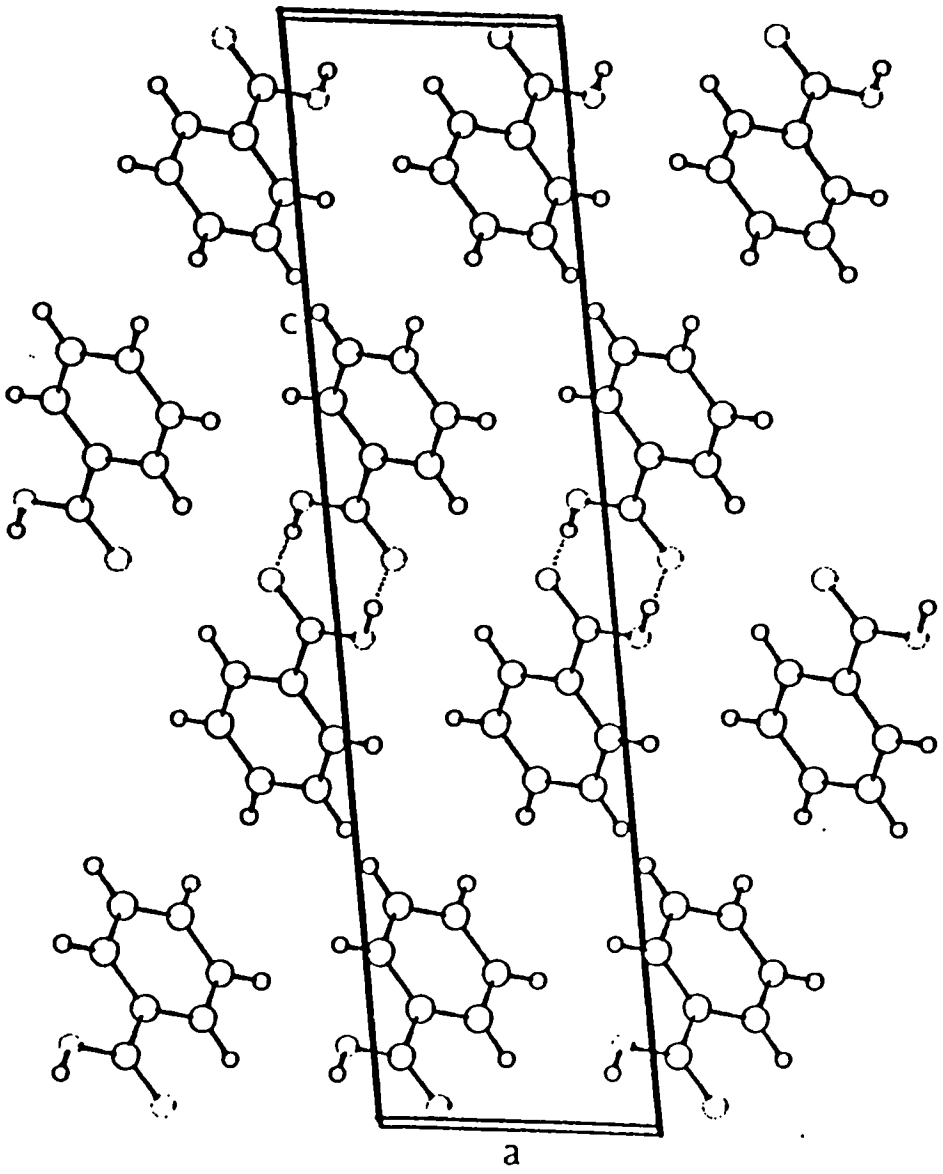

Figure 6.11 Arrangement of benzoic acid molecules in the unit cell.

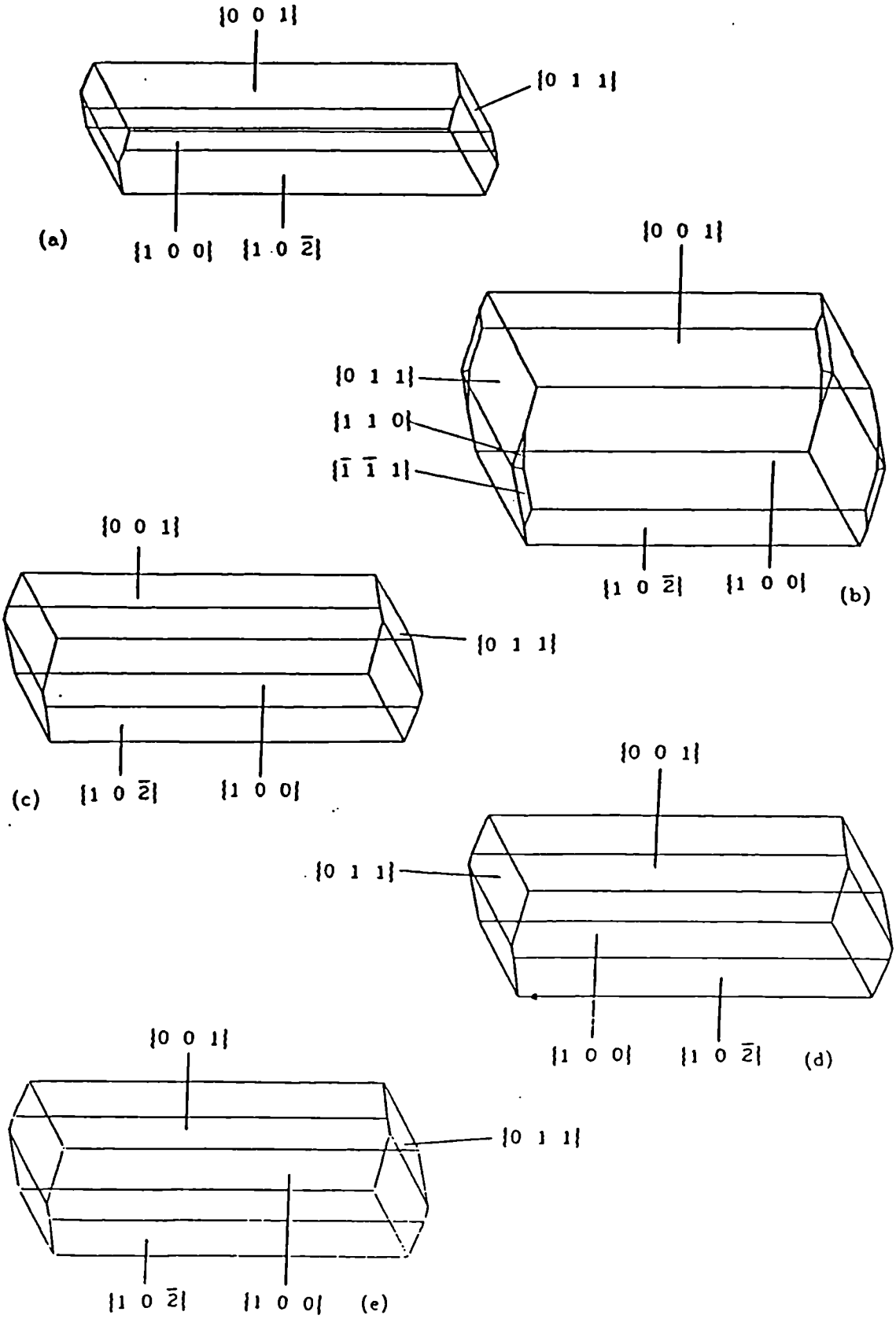

Figure 6.12 Morphologies of benzoic acid, (a) observed
(b) Donnay-Harker model (c) Attachment Energy model (set I)
(d) Attachment Energy model (set IV)
(e) Attachment Energy model (set V)

Table 6.7 Calculated slice and attachment energies for the major faces in benzoic acid using all three parameter sets (results in kcal/mol).

FACE	SET I		SET II		SET III	
	Esl	Eatt	Esl	Eatt	Esl	Eatt
(0 0 2)	-17.3	-3.1	-15.7	-3.2	-15.2	-4.8
(1 0 0)	-13.9	-6.5	-11.5	-7.4	-10.1	-9.1
(1 0 $\bar{2}$)	-13.9	-6.5	-11.7	-7.2	-10.9	-9.1
(0 1 1)	-6.6	-13.8	-7.3	-11.6	-9.3	-10.7
(0 1 2)	-6.6	-13.8	-7.3	-11.6	-9.3	-10.7
(1 0 2)	-5.8	-14.5	-5.4	-13.5	-8.4	-11.6
(0 1 3)	-7.3	-13.1	-6.9	-12.0	-6.3	-13.7
(1 0 $\bar{4}$)	-12.6	-7.8	-10.3	-8.6	-8.9	-11.2
($\bar{1}$ $\bar{1}$ 1)	-3.7	-16.7	-3.8	-15.1	-4.8	-15.2
(1 1 0)	-3.7	-16.7	-3.8	-15.1	-4.8	-15.2

7 Discussion

In the four studies present in this chapter the attachment energy (AE) calculation models give a better fit to the observed morphologies than the simple Donnay-Harker (DH) approach . The improvement is particularily apparent in the cases of succinic and benzoic acid where there is directionally strong bonding. In benzoic acid the hydrogen bonding is contained inside dimers (see Fig 6.11) and consequently the DH model for benzoic acid is not as bad a fit as for succinic acid. It is however not as good as in the anthracene and biphenyl cases. In the cases of biphenyl and anthracene the bonding is isotropic and consequently the DH models give almost as good a fit as the AE models. This is in agreement with the work of Terpstra [23] on apatite and Dowty [24] on silicates. The authors report that the Donnay-Harker predictions give agreement with observed forms in both cases. The bonding in these materials is stronger than in the molecular crystals considered in this chapter but the bonding is uniform in all directions i.e there is no relatively strong bonding directions.

Even though the DH models do not give as good a fit as the AE models to the observed morphologies, the DH models can still be used as a initial guess of the important forms before refinement by energy calculations. This procedure was outlined in the basic approach flowchart earlier (see Chapter 4). This procedure allows the energy calculations to be concentrated on the most important forms and therefore the most efficient use of computing time. The top ten symmetrically independent forms identified from the DH approach were used for energy calculations in this study. From the results of this study it appears that the cut-off limit of the top ten forms appears to be high enough to allow all the forms likely to dominate the crystal habit to be considered. This cut-off limit will be reviewed in future studies and the 'guidelines' presented in this thesis modified accordingly.

The results indicate very little variation in the theoretical morphology from choices of potential parameter sets. This indicates that as long as the parameter set choosen reflects the bonding present in the material i.e. the calculated lattice energy is in reasonable agreement with the sublimation enthalpy the approach of predicting morphology is independent of the choice of potential function.

8 Conclusions

1. The Donnay-Harker (DH) model gives results comparable with the Attachment Energy (AE) model except in cases with directionally strong bonding where the AE model results are significantly better.

2. The AE model results are largely independent of the potential parameter set choosen to describe the intermolecular interactions.

3. The artificial cut-off limit of considering only the top ten forms identified in the DH analysis for further energy calculations appears to be high enough to capture the most important forms.

9 References

[1] S. Ramdas and J.M. Thomas, Chem. Phys. Solids Surf. 7 (1978) 31.

[2] J.E. Lennard-Jones. Proc. Royal Soc. A106 (1924) 442

[3] R.A. Buckingham and J. Corner. Proc. Royal Soc. 189 (1947) 118

[4] F.A. Momany, L.M. Carruthers, R.F. McGuire and H.A. Scheraga. J. Phys. Chem. 78 (1974) 1579

[5] G. Nemethy, M.S. Pottle and H.A. Scheraga. J. Phys. Chem. 87 (1983) 1883

[6] D.E. Williams. J. Phys. Chem. 45 (1966) 3370

[7] A.I. Kitaigorodski, K.V. Mirskaya and A.B. Tovbis. Sov. Phys. Crystallogr. 13 (1968) 176

[8] S. Lifson, A.T. Hagler and P. Dauber. J. Amer. Chem. Soc. 101 (1979) 5111

[9] P.H. Smit and J.L. Derissen. Acta Cryst. A34 (1978) 842

[10] E.R. Lippincott and R.Schroeder. J. Chem. Phys. 25 (1955) 1099

[11] R. Mason. Acta Cryst. 17 (1964) 547

[12] International Tables of Crystallography vol A (D. Reidel Publishing Company, 1983)

[13] P. Groth. Chemische Kristallographie, Vol 5 p437 (Engelmann, Leipzig, 1919)

[14] P. Hartman. J. Cryst. Growth 49 (1980) 157

[15] J. Trotter. Acta Cryst. 14 (1961) 1135

[16] M.J.S. Dewar and W. Thiel. J. Amer. Chem. Soc. 99 (1979) 4899

[17] Thermochemistry of Organic and Organomettallic Compounds. J.D. Cox and G. Pilchard. (Academic Press, New York, 1970)
[18] H.J Human, J.P Van der Eerden, L.A.M.J. Jetten and J.G.M Oderkerken. J. Cryst. Growth 51 (1981) 589
[19] P. Groth. Chemische Kristallographie, Vol 5 p7 (Engelmann, Leipzig, 1919)
[20] J.L. Leviel, G. Auvert and J.M. Savariault. Acta Cryst. 37 (1981) 2185
[21] Z. Berkovitch-Yellin. J.Amer. Chem. Soc. 107 (1985) 8239
[22] G. Bruno and L. Randaccio. Acta Cryst. B36 (1980) 1711
[23] R. Terpstra, J.J.M. Ripkema and P. Bennema. J. Cryst. Growth (1986) 76 494
[24] E. Dowty. Private Communication.

Chapter 7

Modelling Polar Morphology

An Investigation of Urea

CONTENTS

1 Introduction

One problem that remains in relating internal structure to crystal morphology is that of polar morphology. Some crystals have polar directions and the growth rates at opposite ends of these polar directions can be different. The conventional Donnay-Harker, Hartman-Perdok or Attachment energy models of the morphology are based on the bulk crystal structure and therefore always give the same growth rates at the different ends of a polar direction. Addadi and his co-workers [1] have recently reviewed the problem of polar morphology and detailed the effects of tailor-made additives on the different surfaces exposed at the opposite ends of a polar direction. Furthermore *Addadi [1]* summarised the factors that could result in polar growth including the effects of solvent at opposite ends of the polar direction and the result of flexible entities exposed at opposite faces adopting different conformations. Recently Davey et al [2] have accounted for the polar morphology in the case of α-resorcinol in terms of the solvent interactions at the surfaces of the faces growing at opposite ends of the polar direction. For resorcinol the $\{011\}$ faces are benzene rich and the $\{0\bar{1}\bar{1}\}$ faces are hydroxy rich. These faces will therefore have different degrees of interactions with different solvents.

Figure 7.1 shows a model molecule aligned along the polar b direction. The (010) surface consists of a layer of exposed A atom types. The $(0\bar{1}0)$ surface consists of a layer of B atom types. Clearly these surfaces are different in chemical nature. Solvents will therefore have different interactions with these surfaces, and the exposed entities at the different surfaces may adopt different conformations.

Figure 7.2 has oncoming molecules approaching the (010) and $(0\bar{1}0)$ surfaces. The result is the same interaction on both sides, two (A-B) interactions. Since bulk properties are used to determine the magnitude of the (A-B) interaction this results in $E_{att}(010) = E_{att}(0\bar{1}0)$. A classical attachment energy cannot therefore predict a polar morphology.

Urea is an important commodity chemical in the fertilizer and plastics industry. When grown from sublimation and solution urea crystals exhibit a polar morphology [3]. During growth by sublimation there are no solvent effects present. It suggests that polar morphology in this case is a result of the properties of the molecules in the crystal and at the crystal surface. Charge distributions over isolated urea molecules and urea molecules in the enviroment of the crystal bulk and at the surface are calculated using quantum chemistry

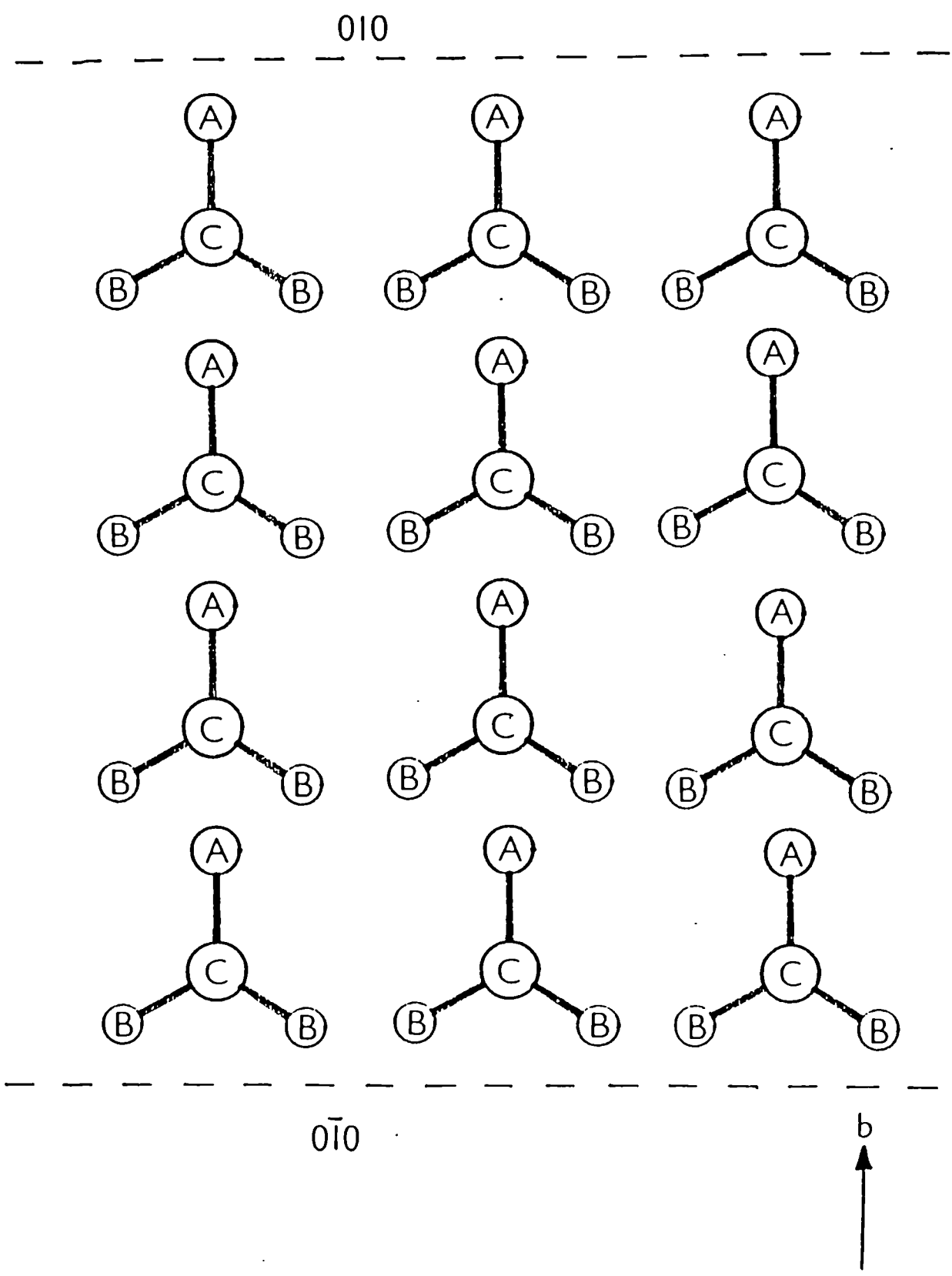

Figure 7.1 Schematic showing the packing of a model structure along a polar direction. The different nature of the surfaces at the opposite ends of a polar direction is shown.

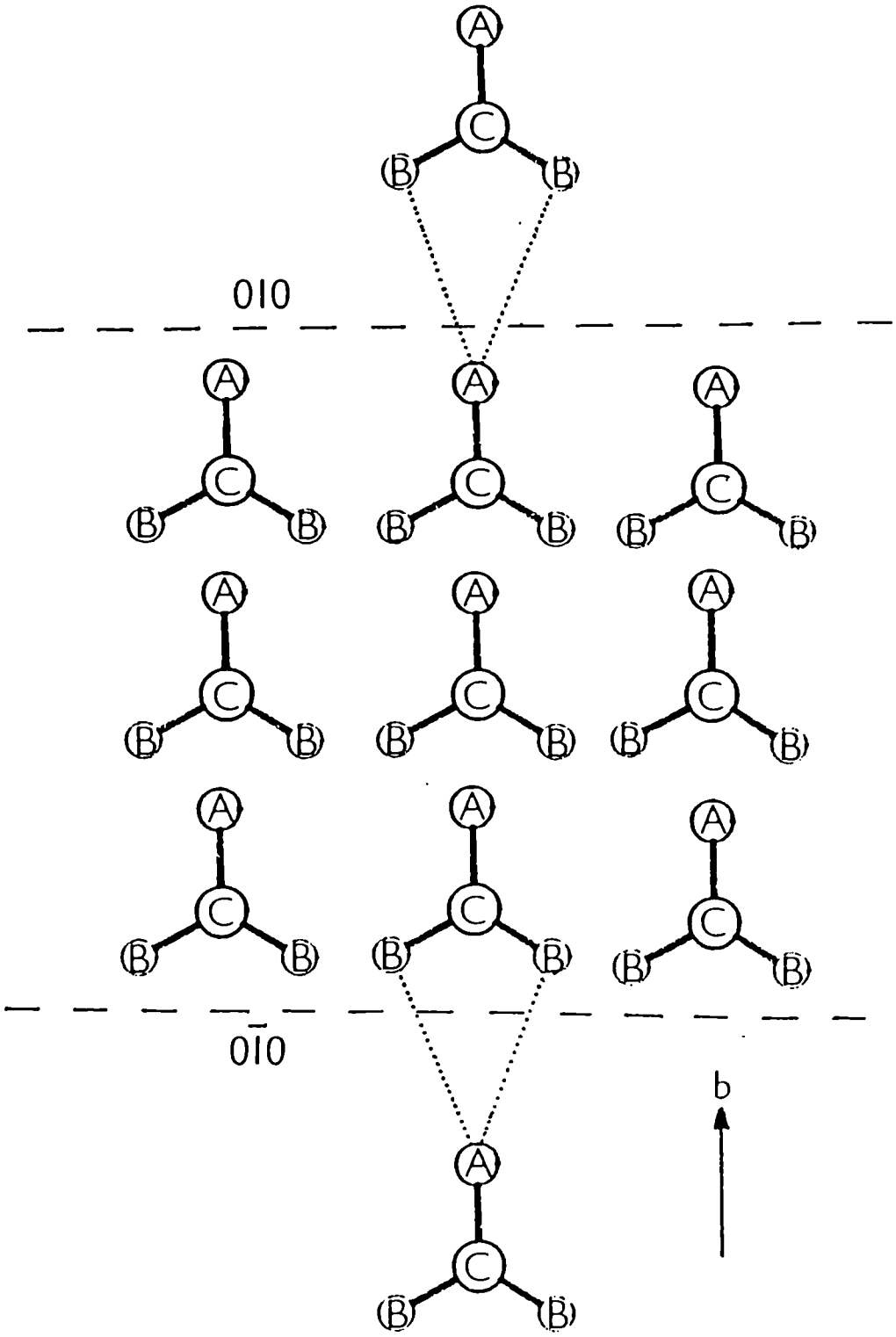

Figure 7.2 Schematic showing why classical attachment energy approach cannot predict a polar morphology.

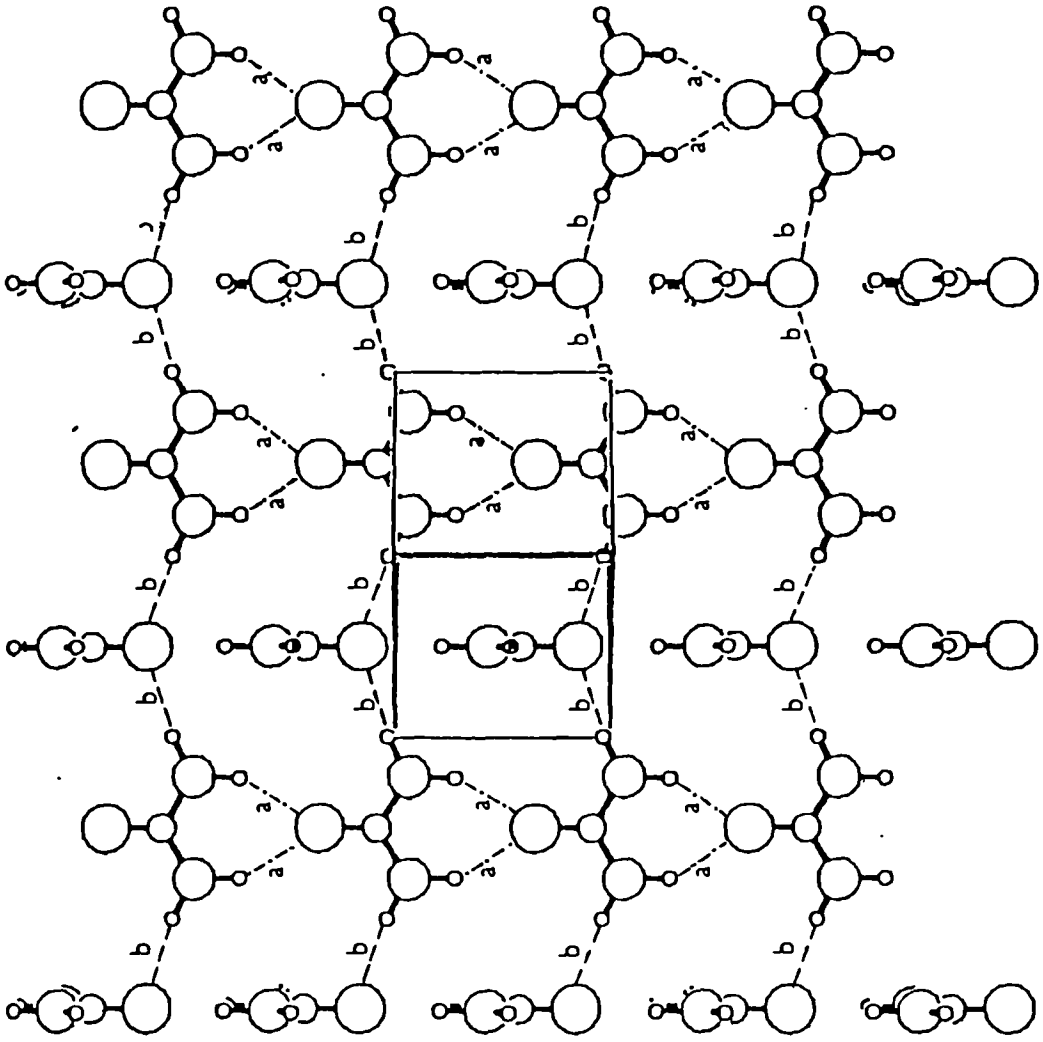

Figure 7.3 Projection of the urea structure

The two types of intermolecular bonds are labelled.

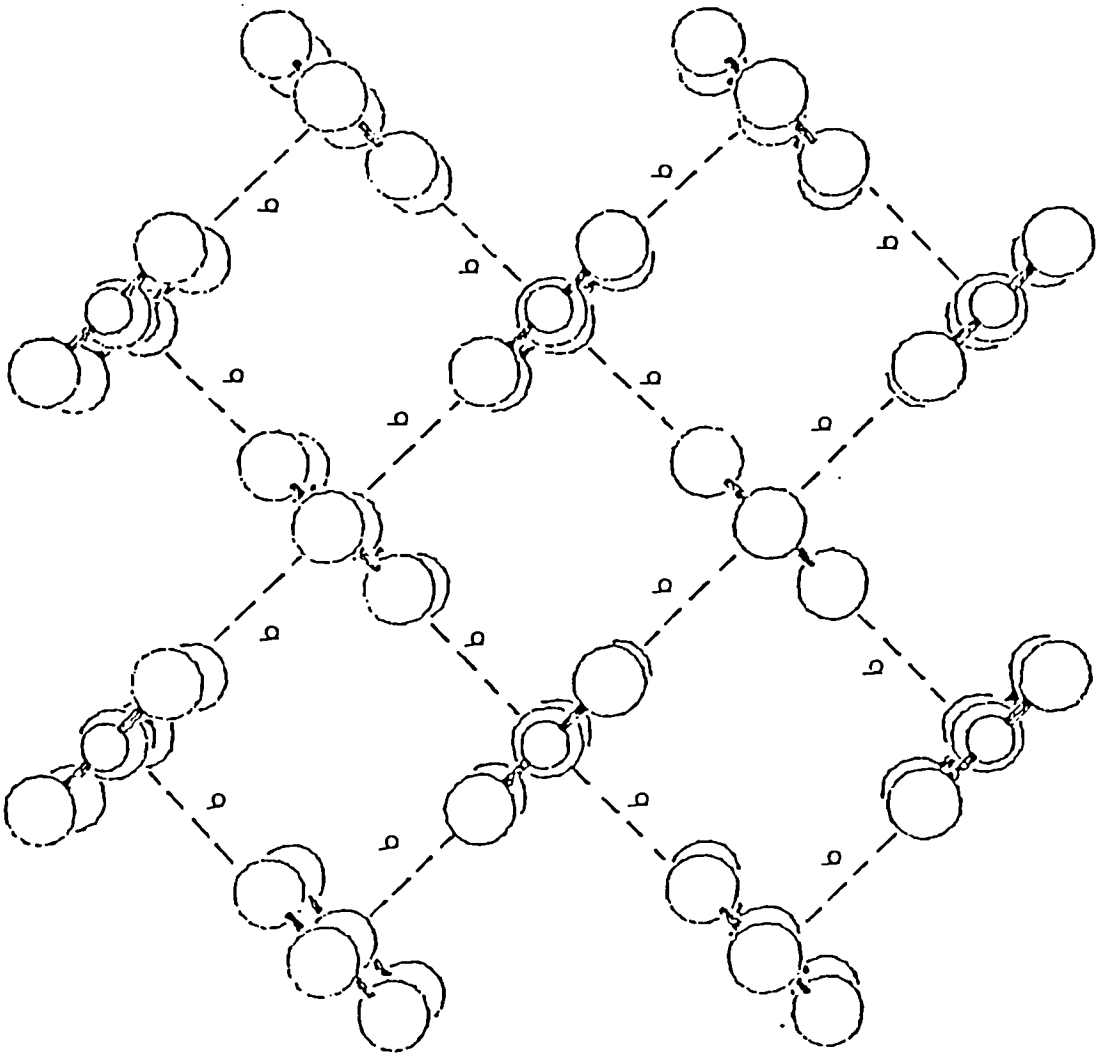

Figure 7.4 Projection down the c-axis showing that each urea molecule is surrounded by four neighbours via b-type contacts.

code currently under development [4]. These distributions are used in a modification of the classical attachment energy approach to attempt quantify the role of surface/bulk/isolated molecular charge on polar morphology.

2 Structural Details Of Urea

Urea $O = C(NH_2)_2$ as shown in Fig 7.3 is one of the simpler organic molecules. It was one of the earliest structures solved and has been the subject of a number of structural studies. Urea crystallises in the highly symmetrical tetragonal space group $P\bar{4}2_1m$ with two molecules in a cell of dimensions a=5.576 and c=4.684Å[5]. The co-ordinates reported in this investigation were used for all the calculations in this chapter. Figs 7.3 and 7.4 show the arrangement of the urea molecules in the crystal viewed down the [110] and [001] projections. The important intermolecular hydrogen bonding (see section 4) is labelled in these plots. The cluster shown in Fig 7.5 shows the important molecules surrounding one urea molecule. Details on the generation of this cluster are given in section 4.

3 Observed Morphologies of Urea

Like the structure, the morphology of urea has been the subject of considerable investigation. When grown from solution the morphology is dominated by the {110} and {111} forms as shown in Fig 7.6(a). When the growth rate from solution is reduced the resultant morphology is shown in Fig 7.6(b) [6]. The {110} forms still dominate but the {001} form has begun to appear at the expense of the {111} and occasionally occurs to the exclusion of the {111} forms [6]. Grown from sublimation the same forms dominate the crystal habit but the overall shape is more bulkier [3] . A computer drawn picture (using estimated center to face distances) of the morphology from sublimation is shown in Fig 7.6(c). The observed morphology taken by electron microscope is shown in Fig 7.7 [3]. In all these cases the crystal exhibits a polar morphology.

Fig 7.6(d) is a hypothetical sublimation morphology with polar morphology prevented by setting the growth rates of {111} and $\{\bar{1}\bar{1}\bar{1}\}$ as the same. On comparison with Fig 7.6(c) the effects of polar morphology are clear. For Fig 7.6(a) this would produce a crystal with pointed ends.

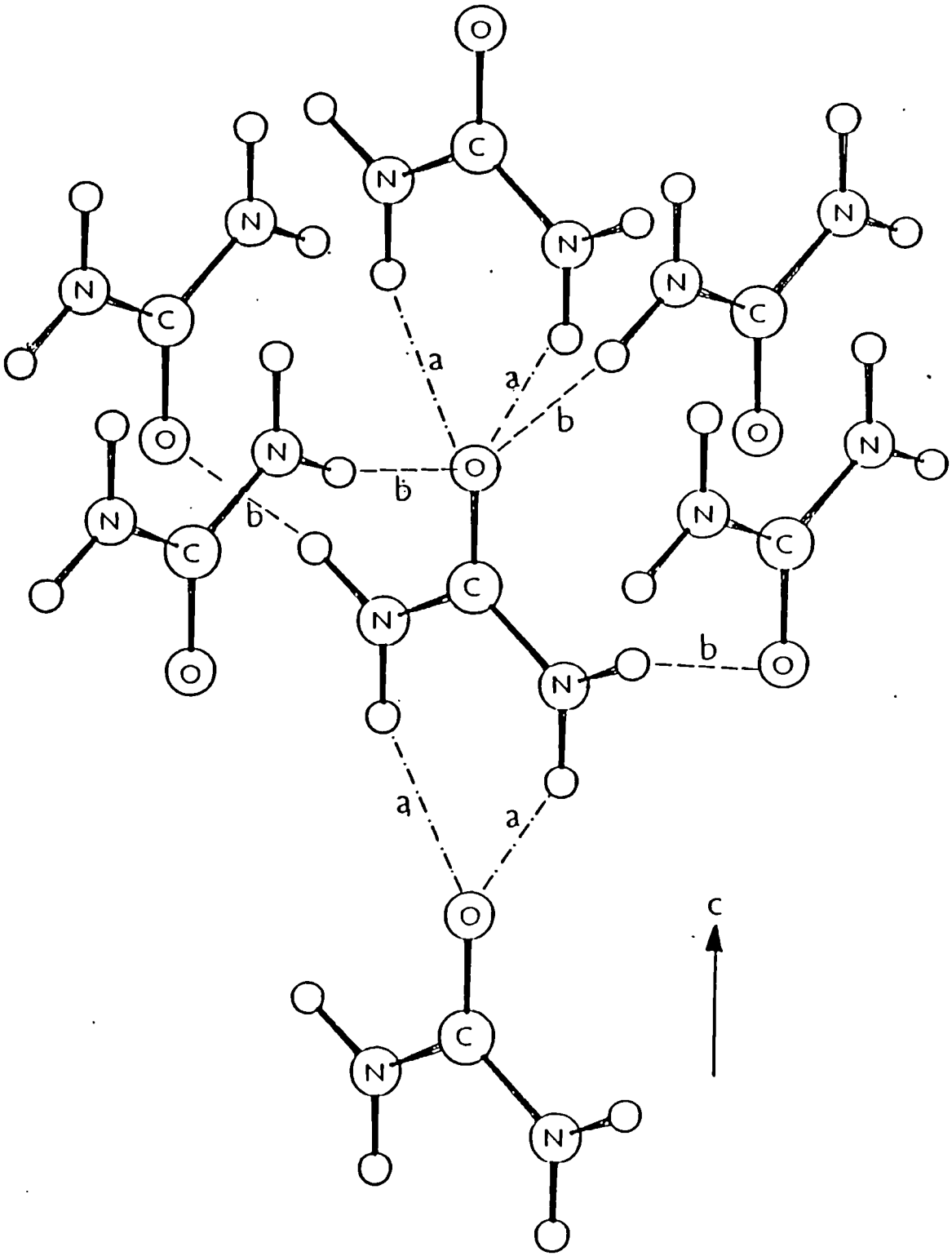

Figure 7.5 Urea cluster with a central molecule surrounded by the important molecules identified in the bonding analysis using PCLEMC.

OBSERVED MORPHOLOGIES OF UREA

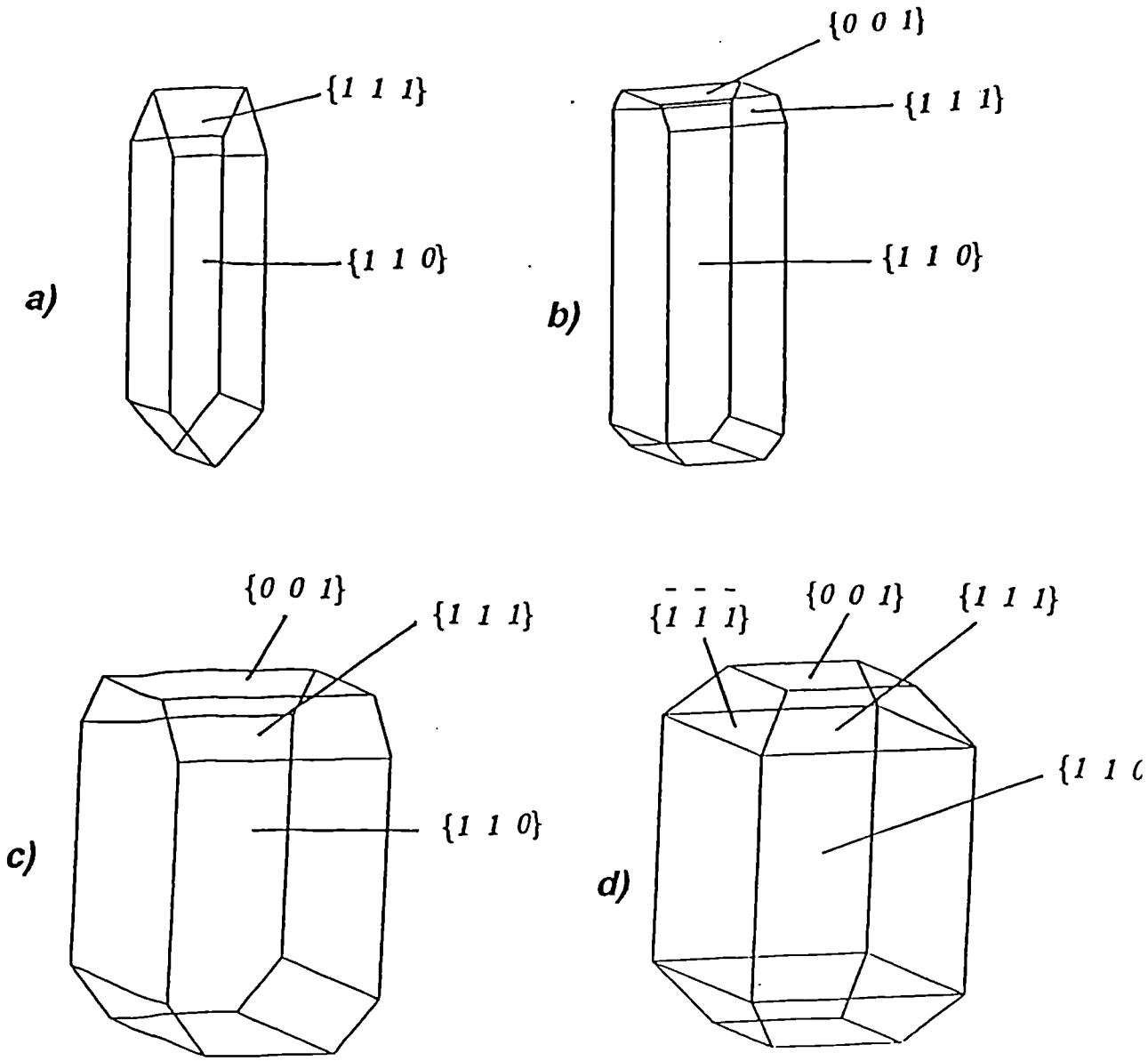

Figure 7.6 Morphologies of urea

a) Observed from solution

b) Observed from solution with reduced growth rates

c) Observed from sublimation [3]

d) Hypothetical morphology from sublimation with polar morphology prevented.

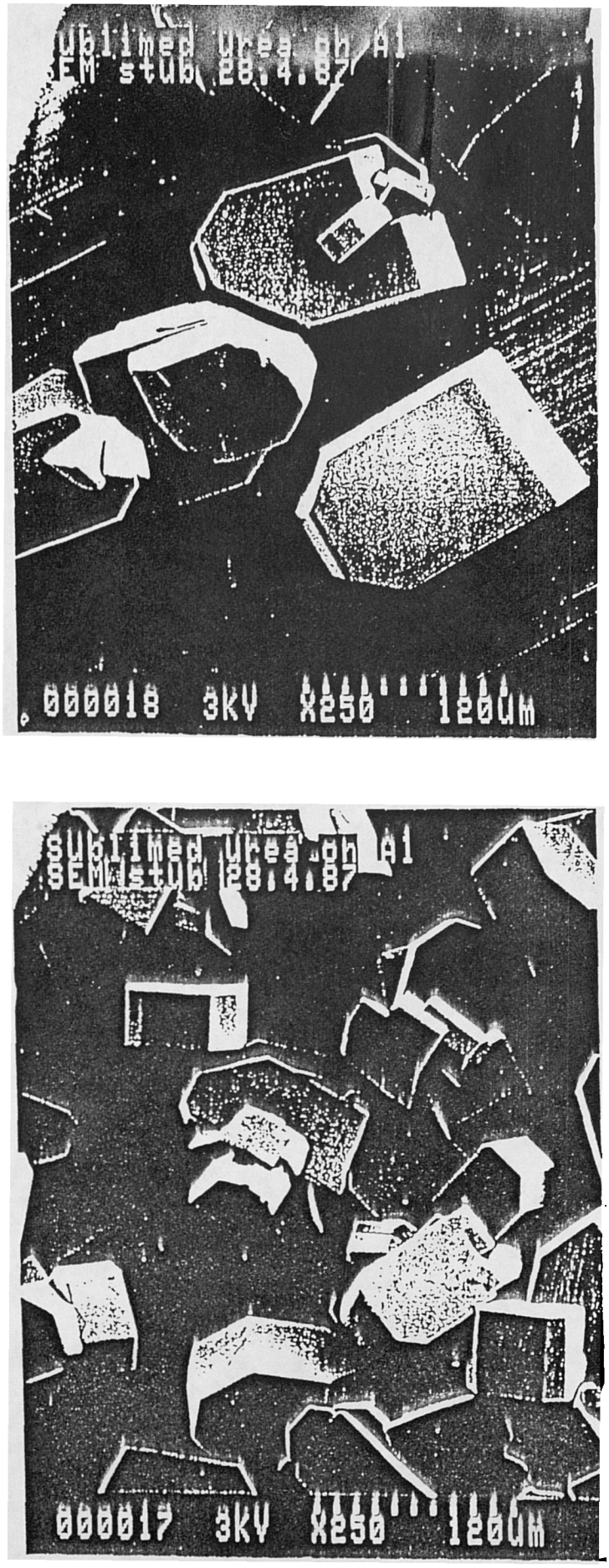

Figure 7.7 Scanning electron microscope pictures of urea crystals grown by sublimation [3]

4 Energy Calculations

The parameter sets of Hagler and Lifson [7] derived for the study of amides were used for the calculations on urea. Charges are supplied with the parameters. The lattice energy calculated of -22.6 kcal/mol is in good agreement with the experimental sublimation enthalpy of 21.0 kcal/mol reported in the literature [8]. PCLEMC was used in 'LATT' mode to analyse the intermolecular bonding in urea. The results are listed in Table 7.1. Two types of hydrogen bonding can be identified. Bonds of type (a) as shown in Fig 7.3 link the urea molecules together along the c-axis. Bonds of type (b) as shown in Fig 7.4 hold the urea molecules together in the (001) plane. For each urea molecule there are 6 main intermolecular bonds, four of type (b) and two of type (a). Fig 7.4 shows a projection down the [001] direction showing the four b type hydrogen bonds. The six bonds from one urea molecule to the surrounding molecules accounts for over 90 percent of the lattice energy. Figure 7.5 shows the 6 important bonds surrounding one urea molecule. The important contacts were determined using PCLEMC and the cluster generated using CRYSTLINK (see Appendix B).

5 Charge Distribution Calculations

Traditionally the charges on atoms in a molecule are obtained from gas phase molecular orbital calculations. The molecule is essentially being regarded as isolated in space. These charges are then used for packing studies of the crystal state with no consideration of the effect on the charges over the molecule of the crystal enviroment. Some authors have noted this and commented on the difficulty of obtaining the charge distribution over a molecule in the field of a crystal [9].

An ab-initio quantum chemistry package CRYSTAL is currently being developed for the study of three dimensionally periodic systems [4]. This allows the charge distributions over molecules in a crystal to be calculated. The current development version of CRYSTAL is limited to systems with only 20 atoms in the unit cell and using only a STO-3G basis set. An improved version under development will have the capacity to deal with 30 atoms and a range of basis sets [10].

Charge distributions over both isolated and crystal urea molecules were calculated using a STO-3G basis set. CRYSTAL was run on the CRAY XMP/48 at Rutherford Appleton Laboratory. The resultant charge distributions are

Table 7.1 The strong intermolecular interactions identified using PCLEMC in bonding analysis mode. Central molecule can be regarded as 1(000) where 1 represents the molecule in the unit cell and (000) represents the translations in the lattice directions U , V and W.

Second Molecule	Interaction Energy (kcal/mol)	Bond type
1(001)	-4.51	a
1(00$\bar{1}$)	-4.51	a
2(100)	-3.16	b
2($\bar{1}$10)	-3.16	b
2(000)	-3.16	b
2(010)	-3.16	b

shown in Fig 7.8, the isolated distribution in round brackets and the CRYSTAL bulk distribution in square brackets Differences in charges are found for all atoms the most significant differences being found on hydrogens. The differences result from the close hydrogen bond interactions in the crystal which are not considered in an isolated molecule model.

Some feeling for these interactions can be obtained by using simple dimers and trimers as models. The charge distribution over a urea trimer along the c-axis is shown in Fig 7.9. The trimer was built using the packing options in CRYSTLINK (see Appendix B). The calculations were carried out using a STO-3G basis set and the package GAMESS [11]. The hydrogens on the bottom molecule of the trimer in Fig 7.9 have a charge that is very similar to the isolated molecule given in round brackets in Fig 7.8 (0.196 isolated, 0.206 in trimer). However for the same hydrogens in the molecule at the center of the trimer the charge is 0.230 (see Fig 7.9) which is much closer to the bulk value of 0.233, square brackets in Fig 7.9. The trimer is a simplified model of the structure since it contains molecules pointing in only one direction and only one type of hydrogen bonding (i.e type a).

Using the packing options in CRYSTLINK a more reasonable model of the solid state can be generated. The six important surrounding molecules (identified in the intermolecular bonding analysis in section 4) were generated around a central molecule and the charge distribution over these molecules calculated using GAMESS [11] and a STO-3G basis set. Fig 7.5 shows the cluster built using the CRYSTLINK packing options detailed in Appendix B. The central molecule in the model should feel the same effects as a molecule in the bulk crystal enviroment. The resultant charges are shown in Fig 7.8 in curly brackets along with the isolated and bulk distribution. The cluster calculation model served two purposes. Firstly a test of the results from CRYSTAL as this package is still under development and secondly to investigate the possibilty of using the GAMESS package and CRYSTLINK to produce simple models in order to mimic the effects of the crystal enviroment.

Using the slice packing options in CRYSTLINK (see Appendix B) it is possible to generate slices of specific orientation $\{hkl\}$ and of a given depth (usually specified as a factor of the interplanar spacing d_{hkl}). A double layer of {111} was generated for urea and the charge distribution calculated using GAMESS [11] at a STO3G basis level. Figure 7.10 shows a urea {111} slice. The charge distributions over the two molecules in the unit cell on that surface

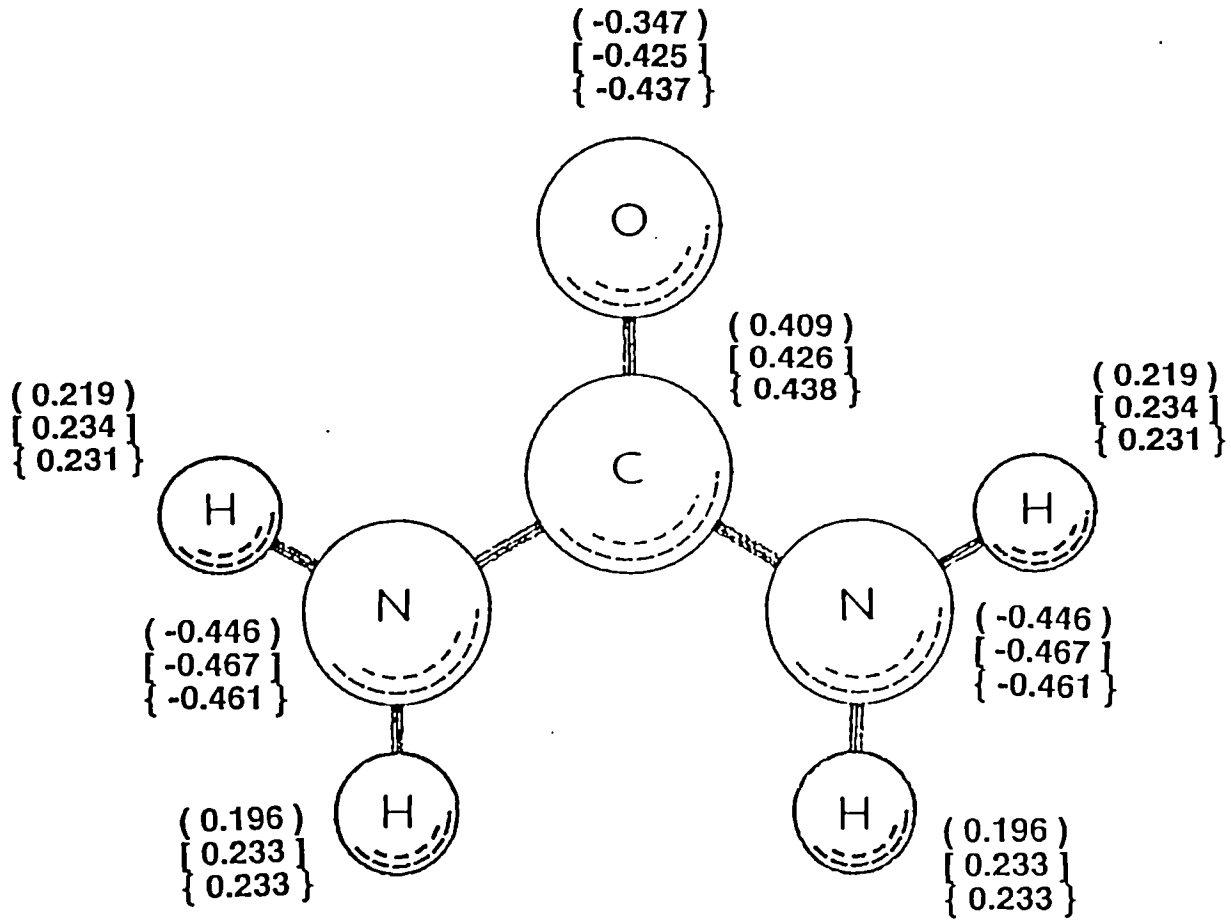

Figure 7.8 Charge distribution over urea molecule. Round brackets indicate isolated molecule values, square brackets indicate CRYSTAL bulk results and curly brackets indicate charges on central molecule in the cluster calculation.

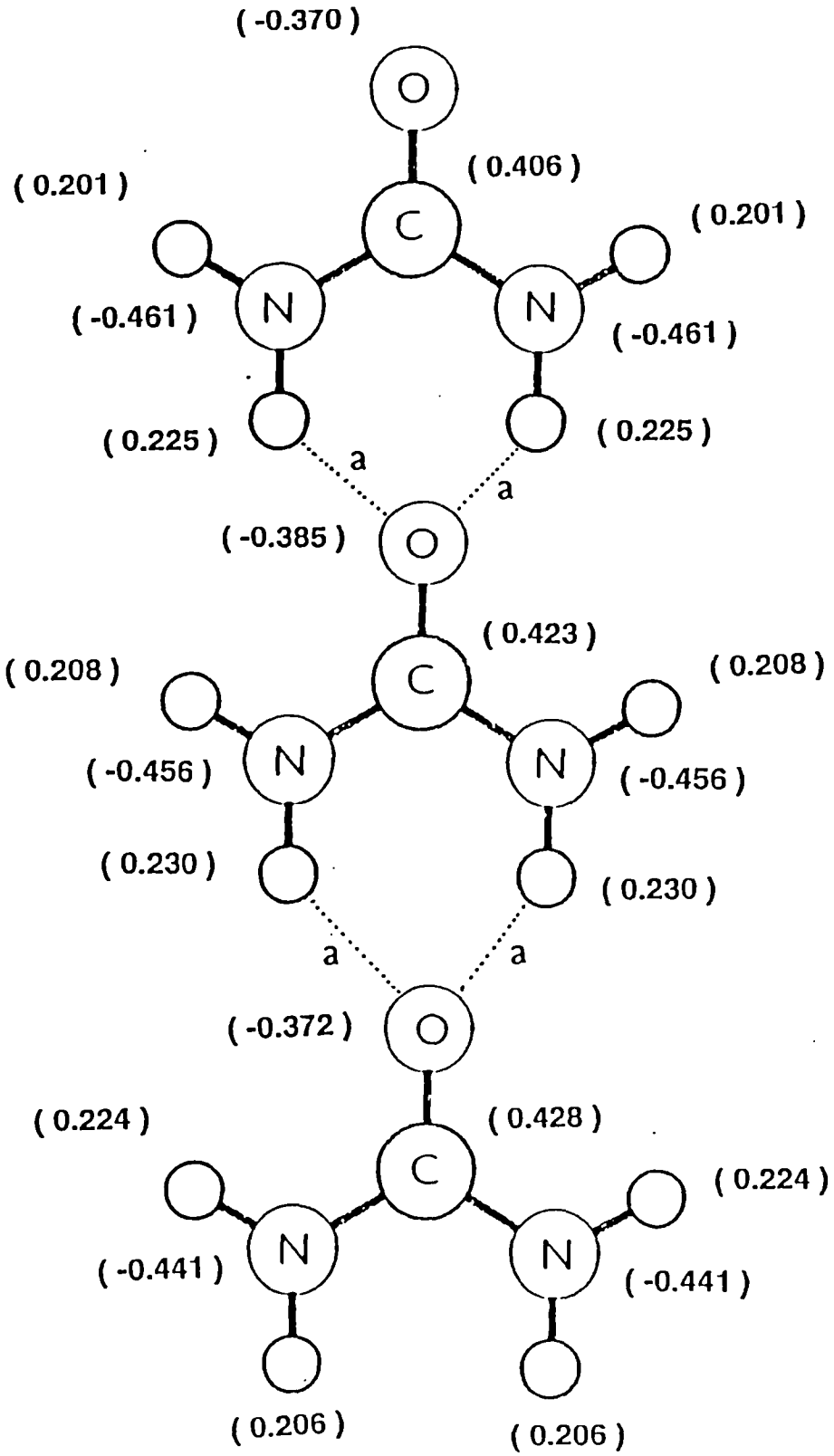

Figure 7.9 Charges on a trimer along the c-axis. The charges on the central molecule reflects trends in the bulk, the outer molecules reflect the monomer distribution.

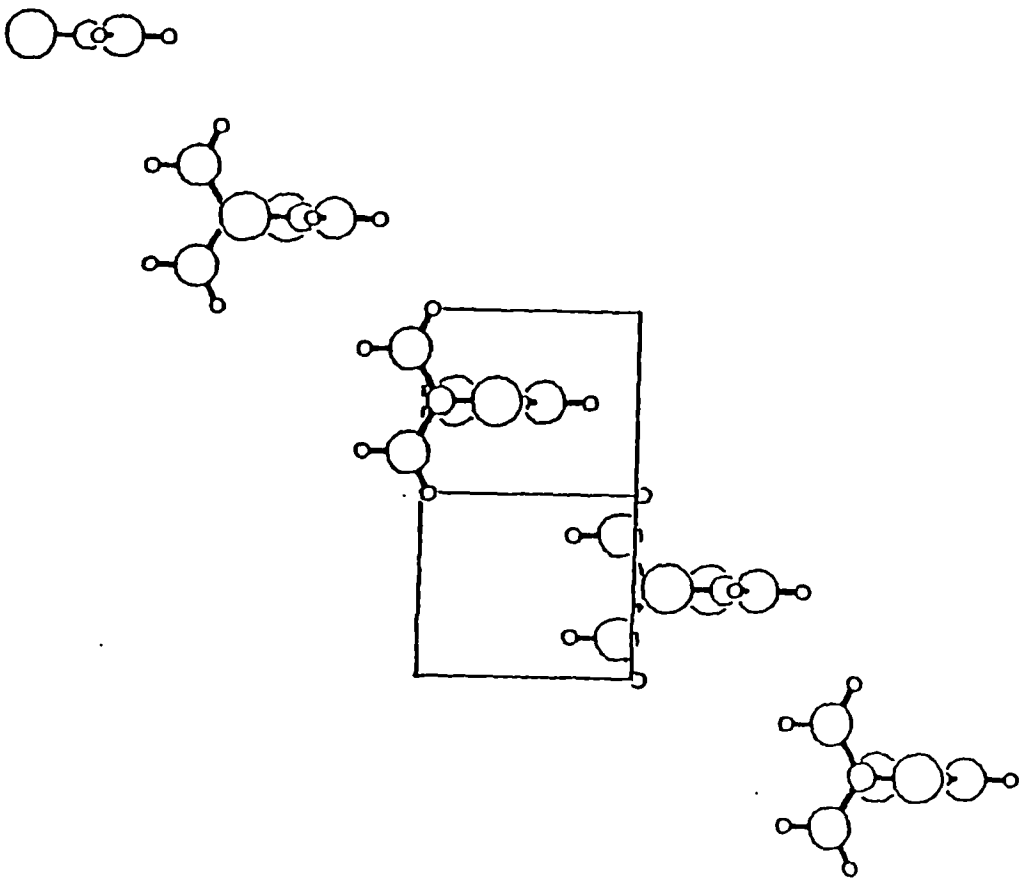

Figure 7.10 Urea {111} slice

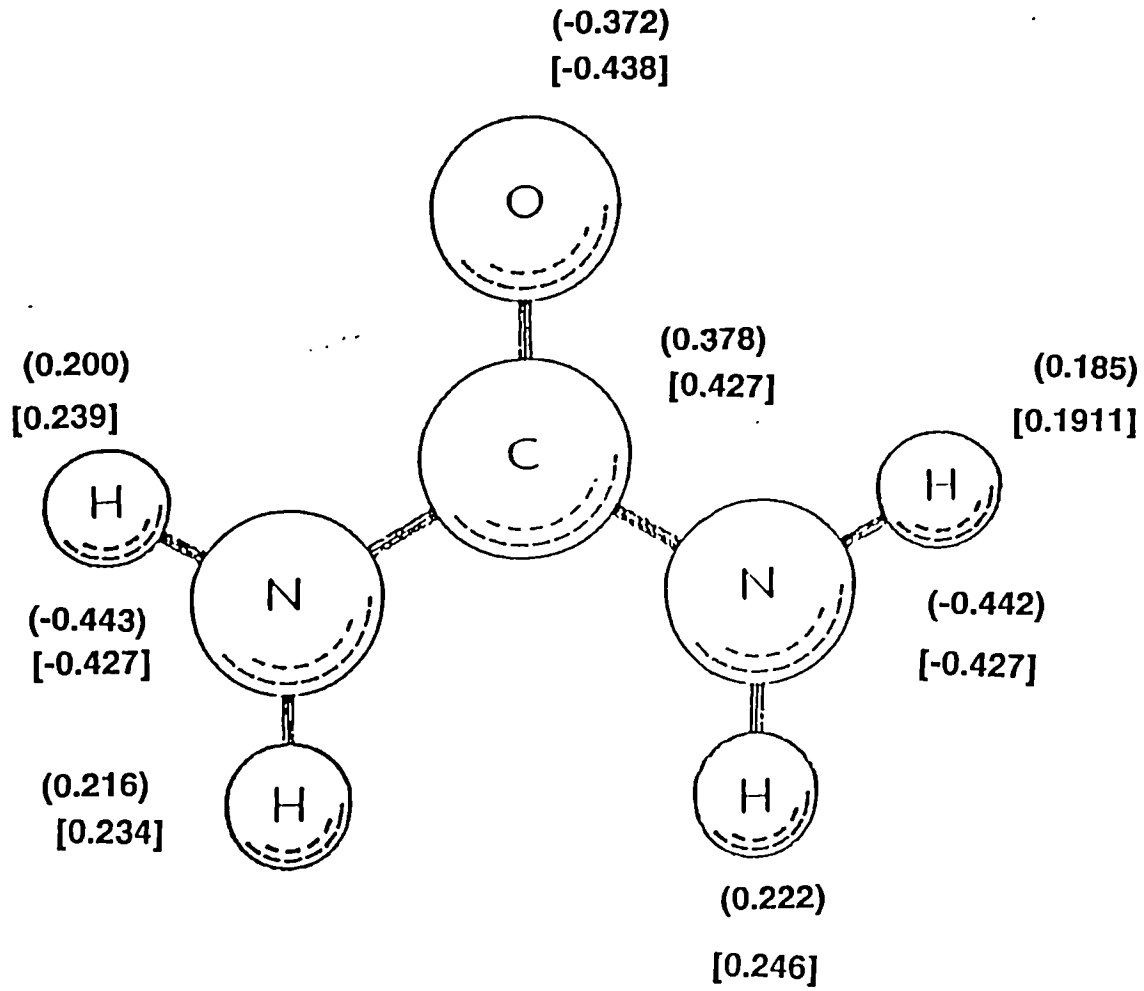

Figure 7.11 The surface charge distribution for the {111} face. The molecules in the unit cell are represented by round brackets for molecule 1 and square brackets for molecule 2.

is shown in Fig 7.11.

The charges calculated were carried out using a STO-3G basis set. It is not the actual values that are important but the differences. The force field which gives the best description for amides is that of Hagler and Lifson [7]. The published force field has it's own charge distribution. In order to be consistent with the force field the differences in the STO-3G isolated/bulk/surface charges were used to scale those published by Hagler. Haglers published charges were assumed to be that of the bulk for two reasons. Firstly the charges had been derived for a force-field describing bulk properties. Secondly the published charges trends were in better agreement with the calculated bulk charges than with the isolated gas phase molecule calculations. Haglers published charges were assumed to be bulk and then scaled to produce surface and isolated molecule charges. The scaled isolated molecule charges are given in Fig 7.12.

6 Morphological Calculations

6.1 Classical Attachment Energy

The theory behind and the methods for carrying out the classical attachment energy calculations have been detailed in previous chapters (2 and 4 respectively). In this chapter calculations will be concentrated on the main forms observed in urea i.e. the {110}, {001}, {111} and $\{\bar{1}\bar{1}\bar{1}\}$. A classical prediction was carried out, both using the Hagler parameter set [7] mentioned in section 4.

The slice and attachment energies were calculated using PCLEMC in 'FULL' mode , the resultant relative growth rates are given in Table 7.2. The computed morphology are given in Fig 7.13(a). In Table 7.2 both {111} and $\{\bar{1}\bar{1}\bar{1}\}$ have the same relative growth rates for the classical approach. This is reflected in the computed morphology which has both forms present. The computed morphology is in reasonble agreement with the observed form from sublimation (see Fig 7.6(c)). The computed morphology shows {110} as the major form with {001}, and {111} as less important. It is the presence of the $\{\bar{1}\bar{1}\bar{1}\}$ forms that is the major difference. A comparison with the hypothetical structure in Fig 7.6(d) where polar morphology has been prevented illustrates the point.

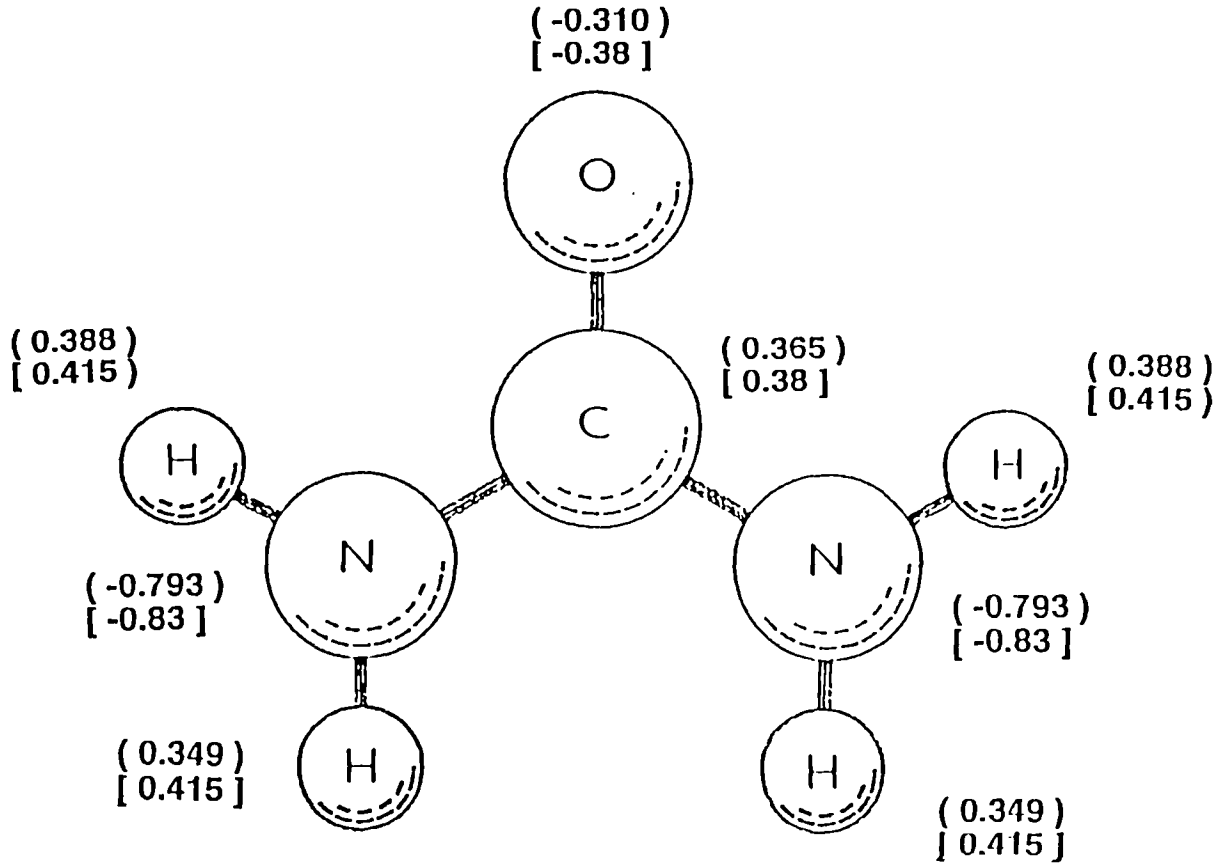

Figure 7.12 Hagler and Lifson's charge set [7] scaled.
The charges as published by Hagler are in square brackets, the scaled charges are in round brackets.

6.2 Polar Attachment Calculations

In 'POLR' mode PCLEMC allows the charges on the oncoming molecules to be different from that in the bulk of the crystal. PCLEMC decides on the charge distribution over a molecule through it's slice assignment routine (see Appendix C). The bulk and isolated molecule distributions from CRYSTAL (see previous section) are shown in Fig 7.8. These charges were then used to scale the published charges of Hagler [7] to produce 'bulk' and 'isolated' charges. These are shown in Fig 7.12 .

The resultant growth rates in 'POLR' mode are shown in Table 7.2. The resultant morphology is shown in Fig 7.13(b) . Table 7.2 shows for both charge sets that in 'POLR' mode the growth rates for $\{111\}$ and $\{\bar{1}\bar{1}\bar{1}\}$ are not the same. This is reflected in the plots where the surface area's of the faces of the two forms are different. The $\{\bar{1}\bar{1}\bar{1}\}$ are smaller. This indicates that the $\{111\}$ forms are more important than the $\{\bar{1}\bar{1}\bar{1}\}$. This is in agreement with what is observed except that the $\{\bar{1}\bar{1}\bar{1}\}$ forms are not actually observed because of their decreased importance.

The surface charges shown in Fig 7.11 were used to scale Hagler's published charges to produce surface and isolated charges for Hagler's parameters sets. The surface charges were assigned to the $\{111\}$ layer in PCLEMC, the isolated distribution to the oncoming molecules. The resultant growth rates are shown in Table 7.2. Using the surface charges/*isolated charges the growth rates* of $\{111\}$ and $\{\bar{1}\bar{1}\bar{1}\}$ forms are different. The computed morphology reflects this with the computed polar morphology shown in Figure 7.13(c). The growth rates of $\{110\}$ and $\{001\}$ are unaltered in this plot.

7 Discussion

The predicted morphology of urea from a classical attachment energy approach shows reasonable agreement with the observed form from sublimation. The main forms $\{110\}$, $\{001\}$ and $\{111\}$ are all predicted and observed as being present. The main difference is the prediction of the appearance of the $\{\bar{1}\bar{1}\bar{1}\}$ forms. The modification of the classical approach to assign the oncoming molecules the isolated molecule charge distribution shows some reduction in the importance of the $\{\bar{1}\bar{1}\bar{1}\}$ forms. This reduction is not large enough to to make these forms disappear. The model is also a much simplified one since as the oncoming molecules approach the surface both their and the molecules at the surface charge

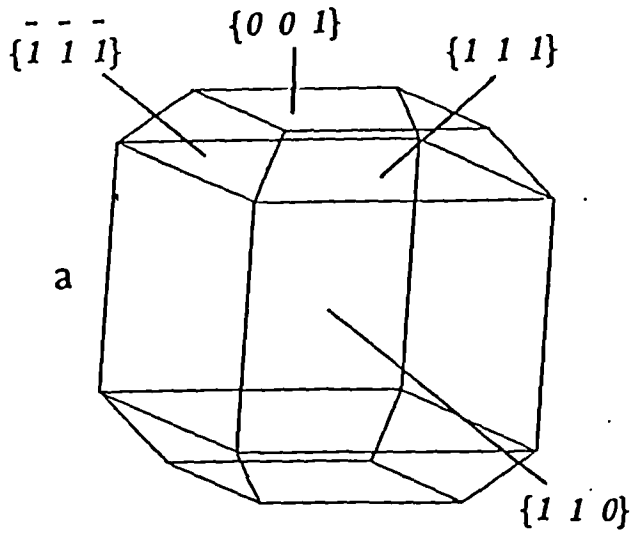

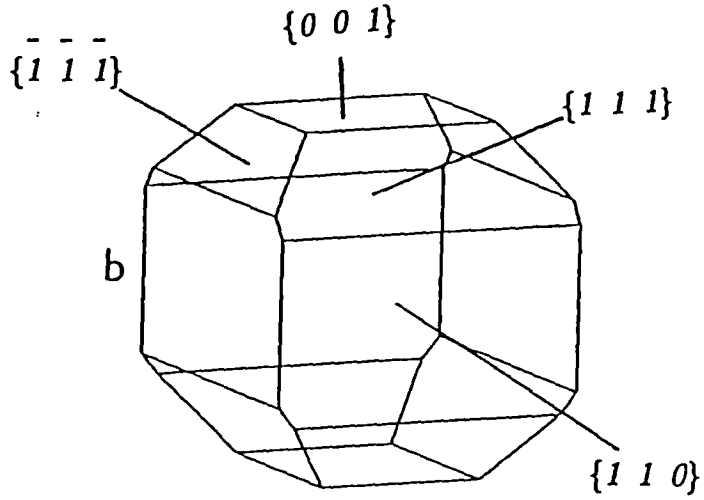

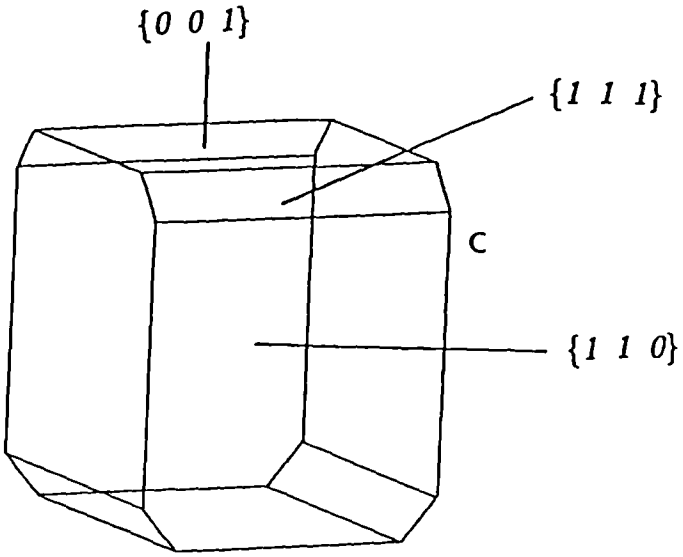

Figure 7.13 Theoretical morphologies for urea.

a) Classical approach

b) Bulk/isolated charges employed

c) Surface/isolated charges employed.

Table 7.2 Attachment energies for the important forms in urea calculated using various models. Results in kcal/mol.

FACE	CLASSICAL	BULK/ISOLATED	SURFACE/ISOLATED
(1 1 0)	-4.5	-4.2	-4.5
(0 1 1)	-5.2	-4.5	-5.2
(1 1 1)	-5.7	-4.5	-6.0
($\bar{1}$ $\bar{1}$ $\bar{1}$)	-5.7	-4.9	-7.0

distributions are likely to undergo gradual changes rather than the 'black and white' or bulk and isolated distribution approach adopted initially. The use of surface charges to describe the charge distribution in the {111} layer and isolated distribution on oncoming molecules does provide a polar morphology. This approach should be tried against another small molecule, γ-glycine a possible candidate.

An interesting result from this chapter is the agreement between the CRYSTAL charges and the charges from the model cluster. This allows the possibility of modelling the charge distributions over more complicated systems that CRYSTAL cannot handle as yet by constructing simple clusters. Most organic materials crystallise in less symmetrical space groups than urea. Monoclinic systems seem to be the preferred crystal system. This would mean smaller clusters in terms of molecule numbers than was necessary in the urea case.

8 Conclusions

1. Polar morphology in the case of urea grown from the vapour phase is not an effect of solvent or flexible entities but can be accounted for from a structural viewpoint by modification of the classical attachment energy approach to consider bulk, surface and gas phase molecular charge distributions.

2. Quantum chemistry code is being developed to allow molecular charge distributions in the solid state to be considered. Results in this chapter suggest that by constructing simple clusters an effective mimic of the solid state packing can be achieved and hence the bulk molecular charge distribution evalulated and compared against the traditional gas phase calculation.

9 References

[1] L. Addadi, Z. Berkovitch-Yellin, I.Weissbuch, M. Lahav and L. Leiserowitz. Topics In Stereochemistry Vol 16 pages 1-85.

[2] R.J. Davey, B. Milisavljevic and J.R. Bourne, J. Phys. Chem. 92 (1988) 2032

[3] R.J. Davey and S.N. Black (private communication).

[4] CRYSTAL V. Saunders, Theory Section, Daresbury Laboratory, Warrington WA4 4AD.

[5] S. Swaminathan, B.M. Craven, R.K. Mullan. Acta. Cryst. B40 (1984) 300.
[6] F. Anwar, PhD Thesis, University of Strathclyde (1989).
[7] S. Lifson, A.T. Hagler and P. Dauber J. Amer. Chem. Soc. 101 (1979) 5111.
[8] Thermochemistry of Organic and Organometallic Materials. J.D. Cox and G. Pilchard (Academic Press, NY 1970).
[9] F.A. Monamy, L.M. Carruthers, R.F. McGuire and H.A. Scheraga. J. Phys. Chem. 78 (1974) 1579.
[10] V. Saunders, private communication.
[11] GAMESS General Atomic and Molecular Electronic Structure. M.F. Guest and J. Kendrick, University of Manchester Regional Computing Centre (June 1986).

Chapter 8

Modelling the Effects Of Tailor-Made Additives

On Crystal Morphology

CONTENTS

1 Introduction

Tailor-made additives are impurities specially designed to alter crystal shape in a desired manner. The additives work by incorporating into the crystal faces at specific sites. Once in the surface the additive affects the growth rate by hindering the oncoming molecules from getting into their rightful sites on the surface. The additives hinder on coming molecules by either disrupting the expected bonding sequence or actually blocking the molecules from getting close to their required surface site. This alters the growth rate in a specific direction and consequently changes crystal shape. The disruptive type of additive will be considered through the benzamide/benzoic acid, adipic/succinic acid and l-alanine/glycine host/additive systems. The 'blocker' type additive will be considered via the glycine/l-alanine host/additive system. The theory behind the calculations has been discussed already in Chapter 2 (see Fig 2.20). The important parameters to be used are the $E_{sl'}$ and $E_{att'}$ which can be compared with the E_{sl} and E_{att} as a measure of the ease relative to the pure host material that an additive can get into the surface at a specific site [1]. $E_{att''}$ a new parameter is proposed as a useful value that can in some cases be used to re-compute the morphology with the effects of an additive considered.

2 Benzoic Acid/Benzamide System

2.1 Structural Details

Benzamide ($C_6H_5CONH_2$) shown in Fig 8.1 crystallises in the monoclinic space group $P2_1/c$ with four molecules in a unit cell of a=5.607, b=5.460 and c=22.053$\AA$ with $\beta = 90.66°$ [2]. A picture of the arrangement of the unit cell is shown in Fig 8.2. Crystallographic details concerning the structure of benzoic acid have been given in Chapter 6. Fig 8.1 shows a benzoic acid and a benzamide molecule, the structural similarity is clear.

2.2 Morphological Calculations

The additive approach detailed in chapter 4 was adopted. A Donnay-Harker analysis (DH) was carried out using MORANG (see Appendix A). The extinction conditions for benzamide are identical to those for benzoic acid given in chapter 6. The important forms are given in Table 8.1. These important forms were used in the attachment energy calculations (AE). The parameters of Hagler and Lifson

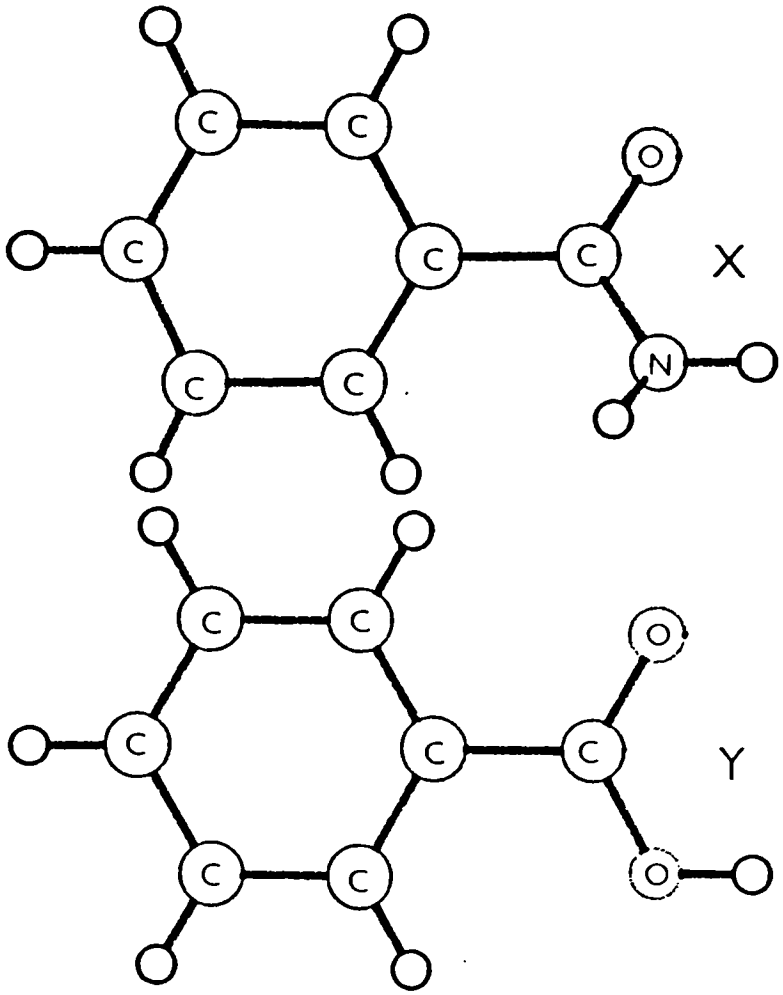

Figure 8.1 Molecules of benzamide (X) and benzoic acid (Y)

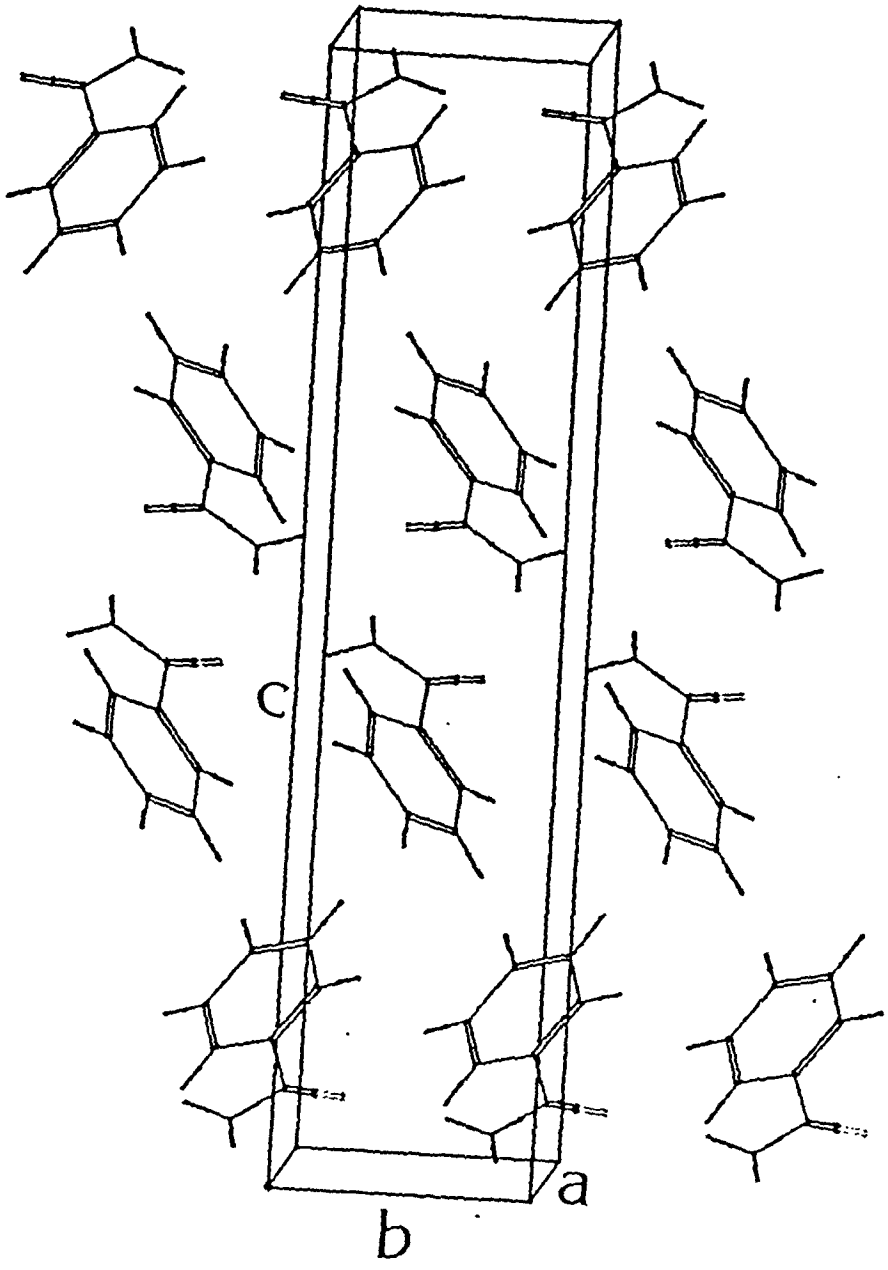

Figure 8.2 Molecules of benzamide packing in the unit cell along the b-axis

[3] were used to describe the interactions between benzamide molecules in the crystal. The calculated lattice energy is -20.9 kcal/mol. This in agreement with the calculations on benzoic acid. Benzoic acid packs in a similar arrangement to benzamide. The calculated lattice energy for benzoic acid is -20.4 kcal/mol (see Chapter 6). The difference could result from the difference in the amide and carboxylic acid dimers.

The slice and attachment energies for the important faces are given in Table 8.1. The DH and AE models of the morphology were computed using SHAPE [4] and are shown in Fig 8.3(b) and (c). The observed morpholgy is shown in Fig 8.3(a). This was computed using estimated center to face distances taken from work by Lahav [1].

The results show generally good agreement between the computed morphologies and observed with the {001} dominating the crystal habit with the {100}, {011} and $\{10\bar{2}\}$ forms completing the morphology.

2.3 Benzoic Acid Additive Calculation

INTERCHEM [5] was used to build a benzoic acid molecule from a benzamide molecule. CRYSTLINK was used to convert the co-ordinates of the benzoic acid molecule into the fractional co-ordinates of the host benzamide lattice and to prepare a file for input to PCLEMC. PCLEMC was used in 'ADDT' mode (see Appendix C). The calculations were concentrated on the most important forms. The important parameters detailed in section 8.1 and in chapter 2 were calculated and are given in Table 8.2. The change in binding energy is the change in energy for an additive to get into a specific site relative to the pure material [4]. The least change in binding energy is the one where additives are most likely to get into the surface site. The change in binding energy for each of the crystallographic sites on the four main faces is given in Table 8.2. From these results it seems that sites 3 and 4 for the (011) face is the most likely site for the benzoic acid additive to get into since there is no loss in incorporation energy at these sites. The additive going into other sites results in a slight loss in incorporation (binding) energy.

The $E_{att''}$ parameter is a measure of the relative growth rate with an additive present in the surface site. Two models can be developed . In model (2) it can be assumed that the additive only gets into the (011) faces then there is a reduction in the growth rate of these faces relative to the other faces. This is shown in Table 8.2. The morphology computed for model (2) is shown in

Table 8.1 Table of important forms in benzamide from a Donnay Harker analysis. The slice and attachment energies for these forms are also given.

FACE	d(hkl) (Angstroms)	Esl (kcal/mol)	Eatt (kcal/mol)
(0 0 2)	10.96	-17.6	-1.7
(1 0 0)	5.59	-12.3	-4.3
(1 0 $\bar{2}$)	5.01	-11.6	-4.6
(1 0 2)	4.95	-10.7	-5.1
(0 1 $\bar{1}$)	4.88	-10.0	-5.4
(0 1 $\bar{2}$)	4.56	-5.8	-15.1
(0 1 $\bar{3}$)	4.13	-1.3	-9.9
(1 0 $\bar{4}$)	3.94	-12.1	-4.4
(1 0 4)	3.89	-8.3	-6.3
(1 $\bar{1}$ 0)	3.73	-5.2	-7.9

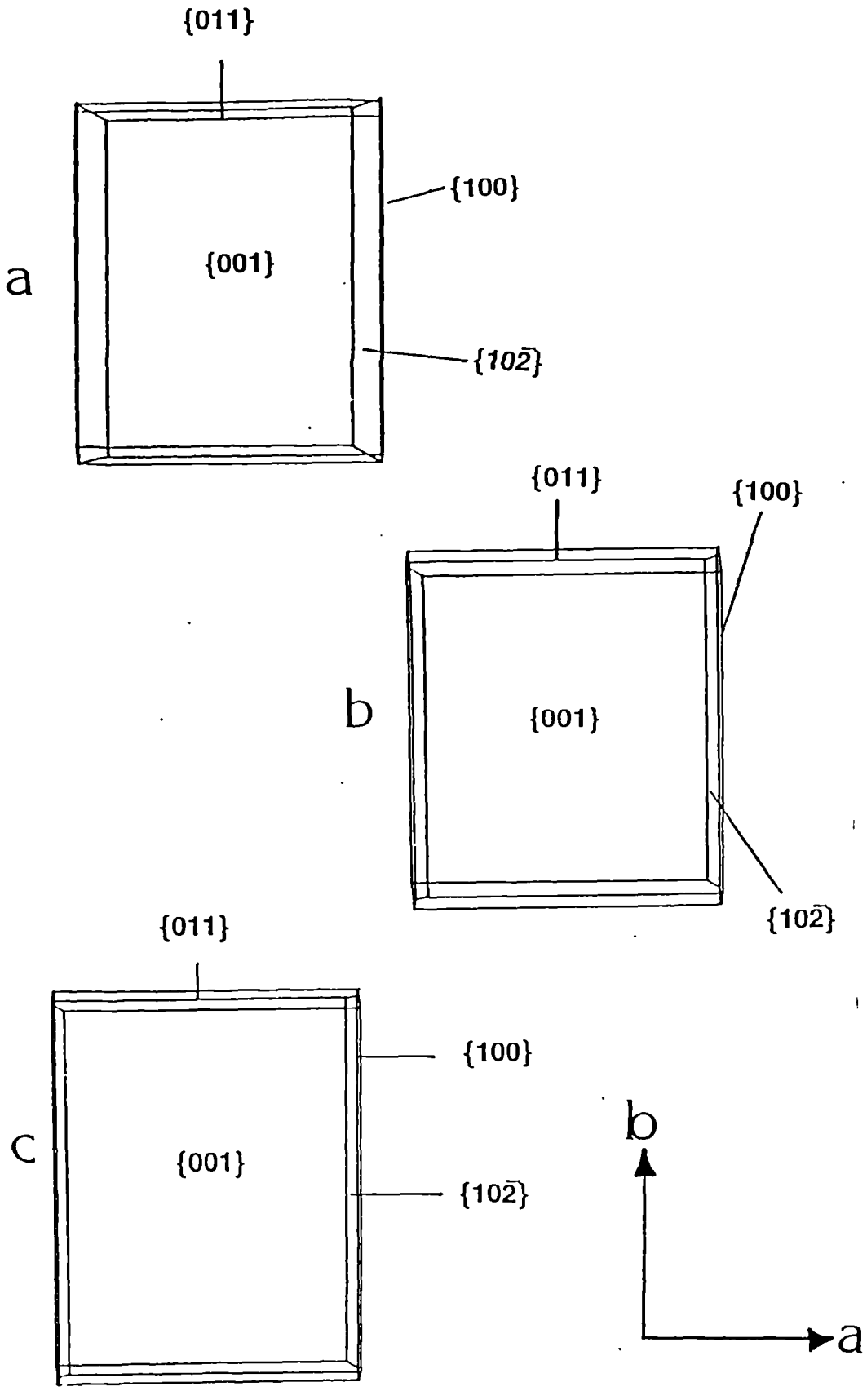

Figure 8.3 Morphologies of benzamide

a) observed

b) Donnay-Harker model

c) attachment energy model

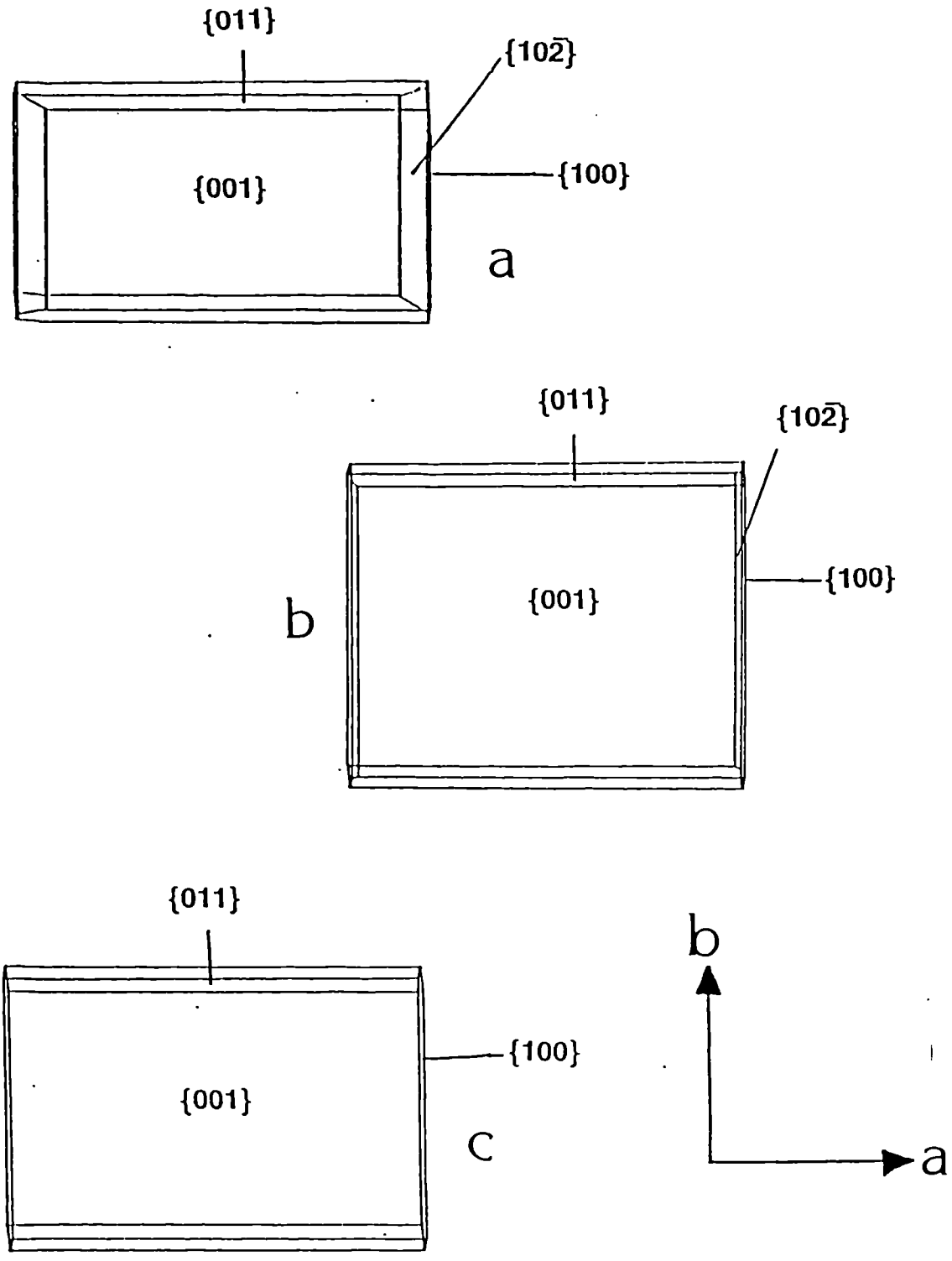

Figure 8.4 Morphologies of benzamide with benzoic acid present.

a) observed

b) calculated using model 1

c) calculated using model 2

Table 8.2 Changes in incorporation energy and relative growth rates for benzamide crystal host system with benzoic acid additive.

FACE	SYMM	CHANGE IN INCORPORATION ENERGY (kcal/mol)	Eatt'' MODEL 1 (kcal/mol)	Eatt'' MODEL 2 (kcal/mol)
(002)	1	+1.7	-1.6	-1.7
	2	+1.7		
	3	+1.7		
	4	+1.7		
(100)	1	+2.6	-4.8	-4.3
	2	+2.2		
	3	+2.2		
	4	+2.6		
(10$\bar{2}$)	1	+2.5	-5.2	-4.6
	2	+2.3		
	3	+2.3		
	4	+2.5		
(011)	1	+1.3	-4.2	-3.5
	2	+1.3		
	3	-0.3		
	4	-0.4		

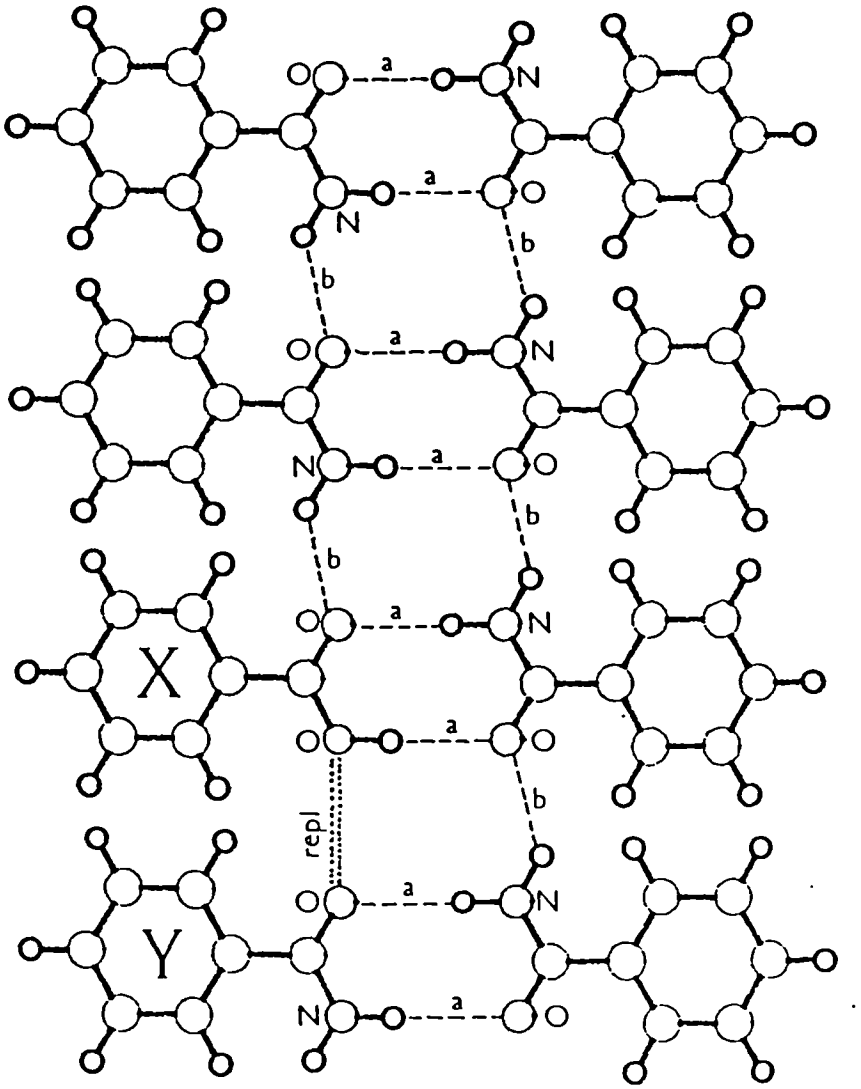

Figure 8.5 Schematic showing growth along the b-direction of a benzamide crystal. A disruptive benzoic acid molecule (X) is shown affecting growth along this direction.

Figure 8.4(c). Since the energy loss at the other faces is small it seem possible that the additive gets into the other faces to a lesser extent. In model (1) the $E_{att''}$ parameter was used for all faces. The relative growth rates are shown in Table 8.3, the computed morphology is shown in Figure 8.4(b). For both models there is a reduction in the growth rates along the b-direction. In model (2) the effect is more noticible. This is in good agreement with the results observed in experiments. Figure 8.4(a) shows the observed morpholgy with an additive present [1]. A comparison the relative growth rates given in Tables 8.1 and 8.2. the reduction of growth rates is clear. Estimated centre to face distances *from* the work of Lahav [1] were used to compute the observed morphologies.

2.4 Discussion

The computed morphologies from both the DH and AE models show good agreement with the observed form with the {001}, {100}, {011} and $\{10\bar{2}\}$ forms dominating the morphology. The observed effect of benzoic acid additive is to reduce the growth rate along the b-direction [1]. This is reflected in the calculations. The additive appears most likely from energetic considerations to be able to get into the (011) faces. Once in the faces it is growth along the b-direction that the additive will have most effect. The observed extent of reduction in growth rate appears to be between the two models. Figure 8.2 shows the packing arrangement of benzamide molecules in the unit cell. Figure 8.5 shows an idealised representation of a benzamide crystal growing along the b-direction. A benzoic acid molecule can get into the growing direction at point (X) where it completes the normal bonding sequence. A further benzamide molecule trying to continue the growth rate at point (Y) cannot complete the proper bonding sequence as it encounters O:::O repulsion when expecting a H atom to complete an N-H:::O hydrogen bonding sequence.

3 Succinic/Adipic Acid System

3.1 Structural Details

Adipic acid is one of a family of di-carboxylic acids with a general formula $(HOOC-(CH_2)_n-COOH)$. For adipic acid n=4 and succinic acid n=2. Adipic crystallises in a monoclinic cell of dimensions a=10.01, b=5.15, c=10.06Å with $\beta = 136.75°$[6]. There are two adipic molecules in each unit cell. Fig 8.7 shows molecules of adipic and succinic acid. Fig 8.7 shows a unit cell of adipic acid,

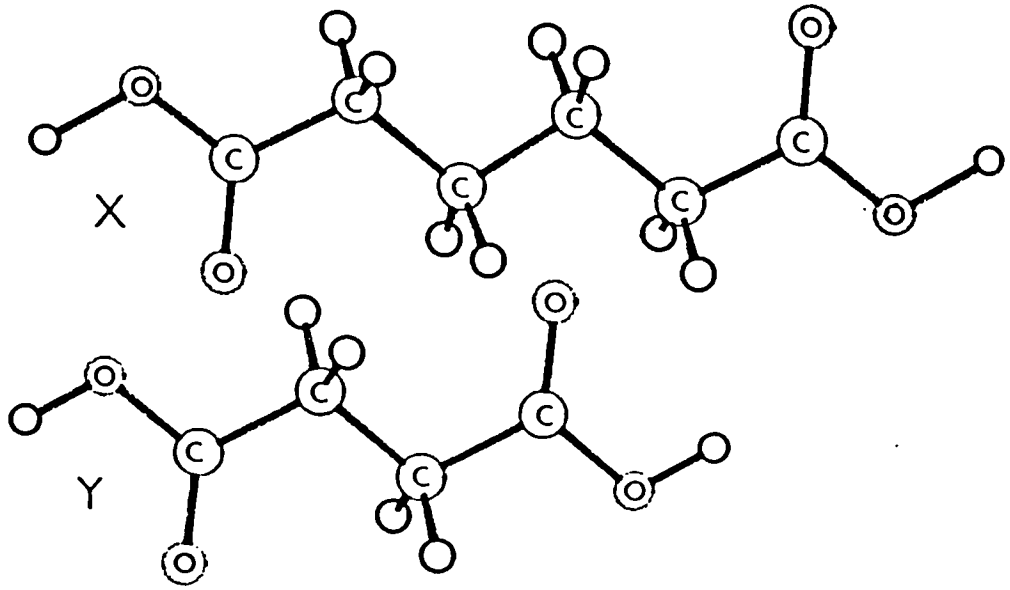

Figure 8.6 Molecules of adipic acid (X) and succinic acid (Y).

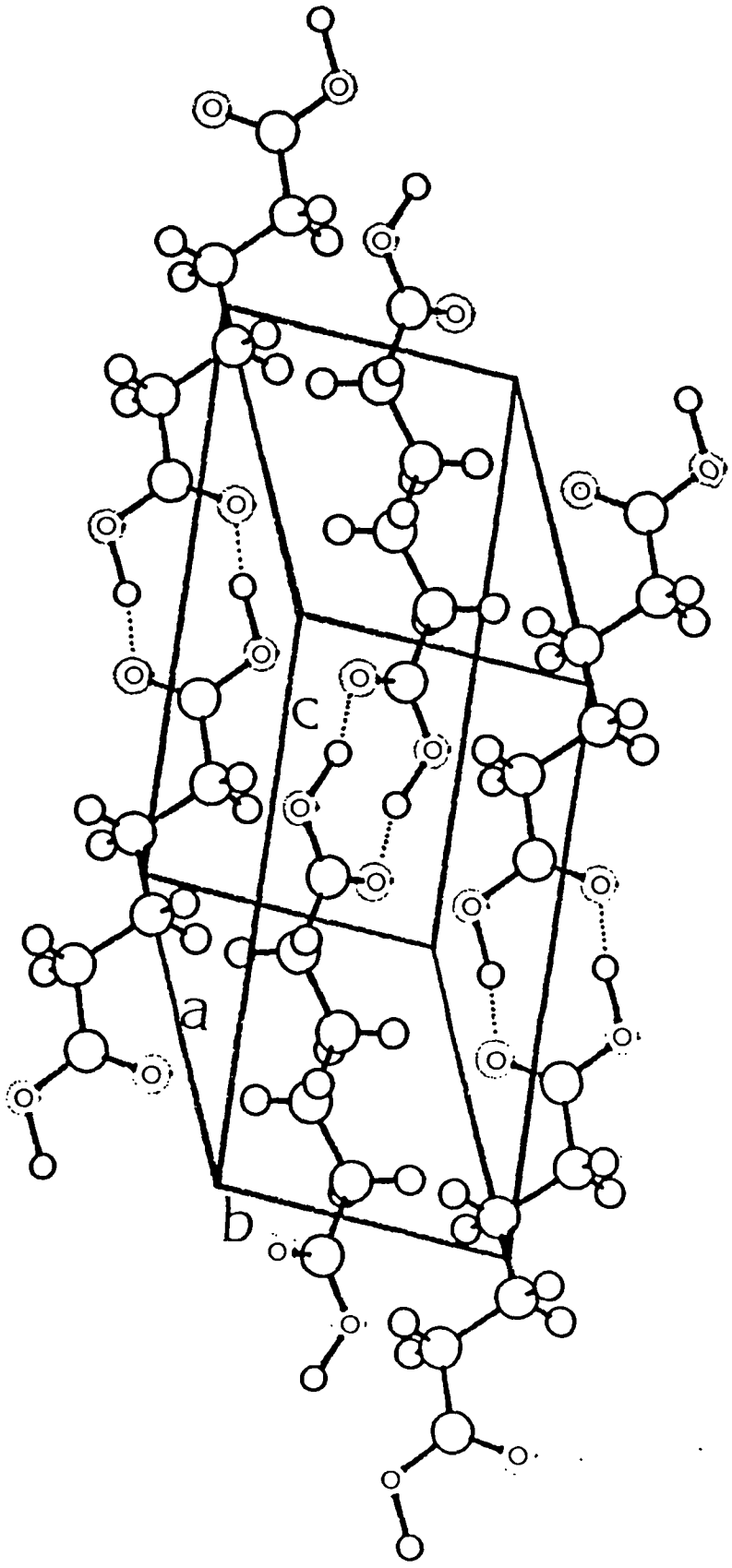

Figure 8.7 Adipic acid packing in the unit cell. The heteroatoms and hydrogen bonding has been labelled.

Table 8.3 Important forms for adipic acid morphology determined by Donnay-Harker analysis and attachment energy calculations.

FACE	d(hkl) (Angstroms)	Esl (kcal/mol)	Eatt (kcal/mol)
(1 0 0)	6.86	-10.0	-12.8
(1 0 $\bar{2}$)	4.78	-8.7	-13.4
(2 0 $\bar{2}$)	4.66	-4.3	-15.6
(1 1 $\bar{1}$)	4.51	-8.3	-13.9
(0 1 1)	4.12	-22.4	-6.5
(2 $\bar{1}$ $\bar{1}$)	3.49	-4.1	-15.7
(0 0 2)	3.45	-20.1	-7.7
(3 0 $\bar{2}$)	3.32	-2.8	-16.4
(1 $\bar{1}$ 1)	3.00	-4.8	-15.3
(2 1 $\bar{3}$)	2.80	-3.2	-16.1

the heavy atoms and hydrogen bonding has been labelled. A comparison with succinic acid unit cell shown in Fig 6.8 illustrates the similarity in crystal packing of the two systems. The structural details of succinic acid are available in chapter 6.

3.2 Morphological Prediction

A Donnay-Harker (DH) analysis of the adipic acid system was carried out using MORANG and the same extinction conditions as those for succinic acid (see chapter 6). The important forms according to the DH model are listed in Table 8.3. The resultant DH model of the morphology is shown in Fig 8.8(b). Energy calculations were carried out using the parameters and charges of Hagler and Lifson [3]. The calculated lattice energy of -35.5 kcal/mol can be compared with the calculated lattice energy of -30.8 kcal/mol for succinic acid. Since adipic acid adopts a similar packing arrangement to succinic acid and adipic acid is larger molecule this means n and n' (see equation 5.1) are increased and a greater lattice energy expected. The important forms identified in this analysis were used for attachment energy (AE) calculations. The AE results are listed in Table 8.3 along with the DH results. The resultant computed morphologies are shown in Figure 8.8(b) and (c). The observed morphology is shown in Fig 8.8 (a) [7,8,9]. The AE model shows good agreement with the observed form with the {100}, {110} and {001} faces dominating the hexagonal shaped morphology. In the observed form the {001} faces are the major forms. The DH model of the morphology identifies the most important forms such as {100} but does not produce the observed overall hexagonal shape.

3.3 Additive Calculation

INTERCHEM [5] was used to fit a succinic acid molecule onto an adipic acid molecule using the heavy atom backbones of both molecules. CRYSTLINK used to obtain co-ordinates for succinic acid in terms of the host adipic acid lattice. PCLEMC was then used in ADDT mode to calculate the important parameters $E_{sl'}$, $E_{att'}$ and $E_{att''}$. The binding energy terms shown in Table 8.4 indicate that the additive can get into a number of faces with small losses in the energy relative to the pure material occupying the same site. The additive can get into $\{10\bar{2}\}$ and {100} forms which are two of the main faces. It seems unlikely that the additive can get into the {011} or {002} forms since the loss in binding energy is greater than 10 kcal/mol. The $E_{att'}$ parameter for the faces with the

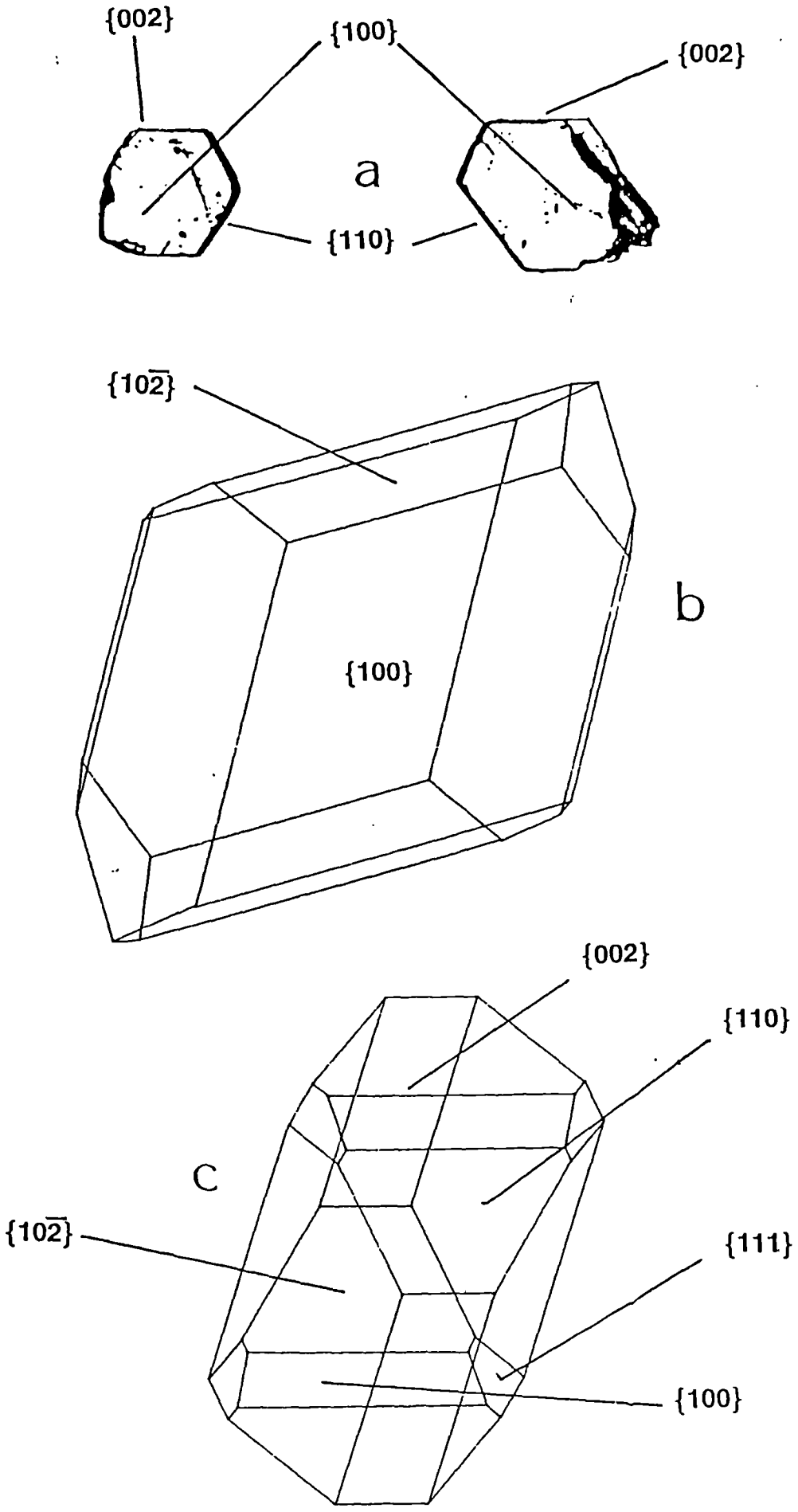

Figure 8.8 The morphologies of adipic acid.

a) observed

b) Donnay-Harker model

c) attachment energy model

a

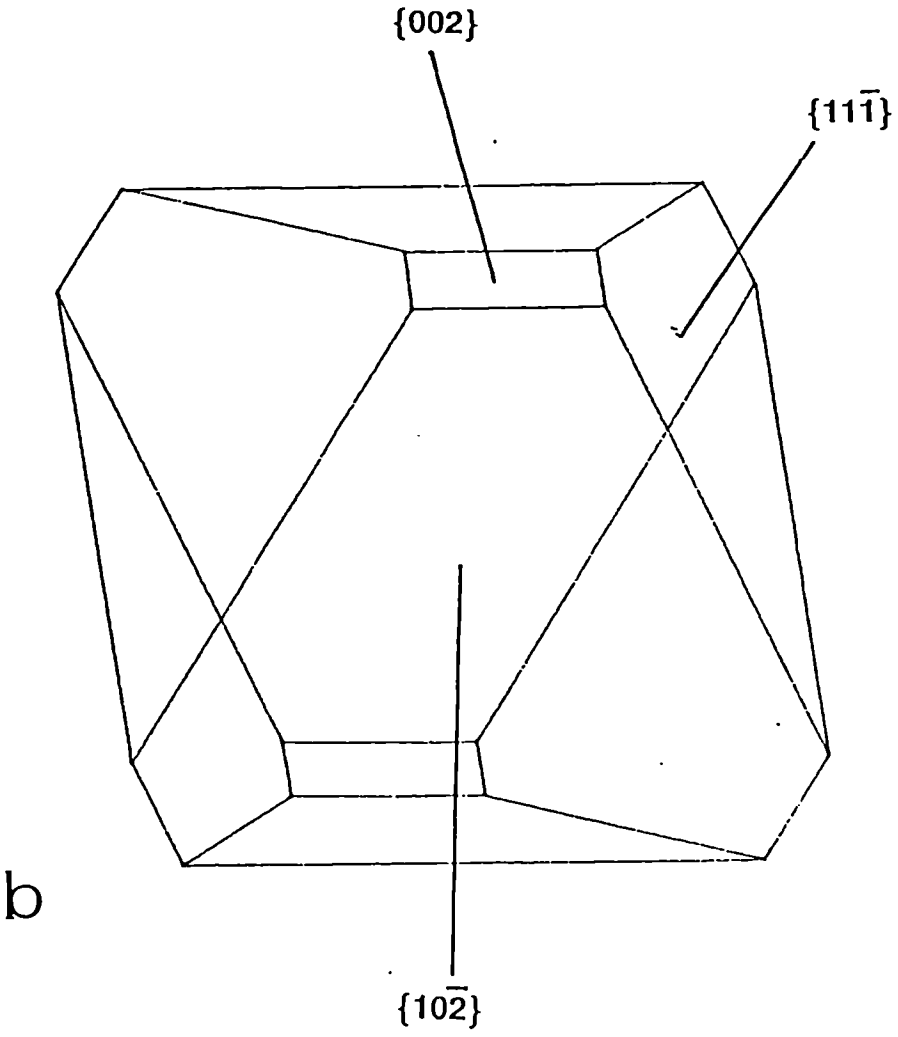

b

Figure 8.9 The morphologies of adipic acid with succinic acid present.

a) observed

b) calculated.

Table 8.4 Table of change in incorporation energy and new relative growth rates for adipic acid with succinic acid present.

FACE	CHANGE IN INCORPORATION ENERGY (kcal/mol)	Eatt'' (kcal/mol)
(1 0 0)	+2.0	-2.6
(1 0 $\bar{2}$)	+1.1	-2.8
(2 0 $\bar{2}$)	+1.5	-4.0
(1 1 $\bar{1}$)	+2.3	-3.7
(0 1 1)	+10.7	-6.5
(2 $\bar{1}$ $\bar{1}$)	+1.2	-4.8
(3 0 $\bar{2}$)	+0.2	-4.6
(1 $\bar{1}$ 1)	+0.6	-5.9
(2 1 $\bar{3}$)	+0.5	-4.9
(0 0 2)	+10.8	-7.7

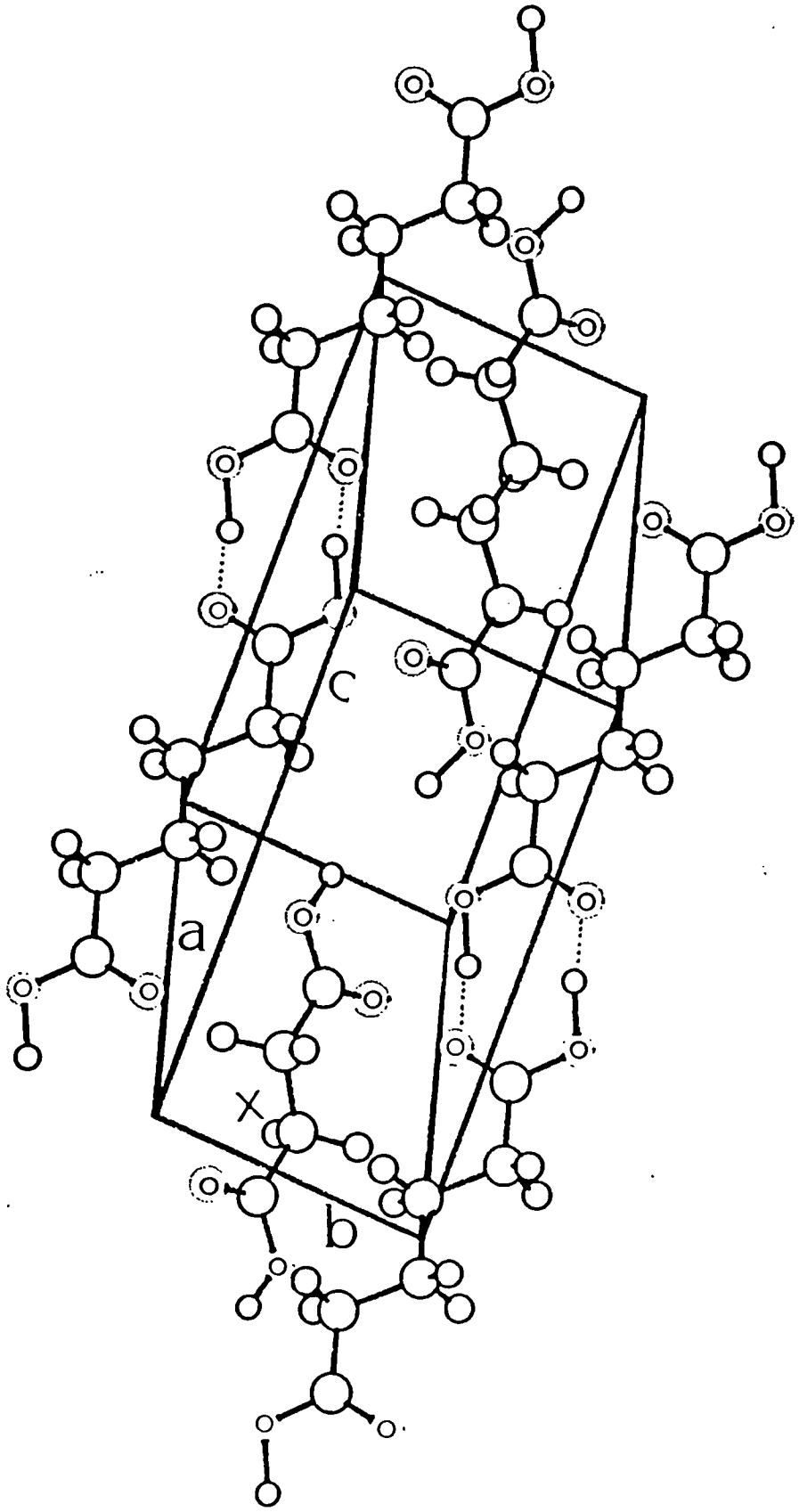

Figure 8.10 Adipic acid unit cell in similar arrangement to previous figure. A succinic acid molecule has been introduced at point X.

relatively small loss in binding energy, listed in Table 8.4 was used to compute a morphology with the additive present. The resultant morphology is shown in Fig 8.9(b), the $\{10\bar{2}\}$ and $\{11\bar{1}\}$ forms dominate the morphology with small $\{100\}$ forms present. Figure 8.9(a) shows the effect of succinic acid on adipic acid crystal morphology.

3.4 Discussion

The predicted morphologies from DH and AE models show good agreement with the observed morphology. The $\{001\}$ is the most important with the $\{110\}$ and $\{100\}$ forming a hexagonal shape. The AE model shows a good agreement but with extended growth along the c-direction. The calculated effect of succinic acid is to reduce the growth rate along the c-direction. This can be seen by comparing the growth rates with and without additive given in Tables 8.4 and 8.3. The resultant plotted morphology makes the $\{10\bar{2}\}$ and $\{11\bar{1}\}$ forms dominate the crystal shape as shown in Figure 8.9(b). These faces were small faces in the original prediction (see Fig 8.8(c)). The calculations suggest that the $\{100\}$ face has also a reduced importance, the rate along the c-direction being reduced as shown in Figs 8.8(c) and 8.9(b). The observed effects of succinic on adipic acid morphology can be seen by comparing Figs 8.8(a) and 8.9(a). The experimentally observed effects on adipic acid morphology of succinic acid have not been detailed fully in terms of the adipic acid morphology and so do not allow a detailed comparison. However the change in morphology is consistent with a structural explanation. Figure 8.8 shows the arrangement of adipic acid molecules in the unit cell. The H-bond distances of $1.5\mathring{A}$ are labelled. Figure 8.10 shows a similar view except at point X a succinic acid molecule has replaced an adipic acid molecule. There has been a corressponding increase in the H-bond distance to $3.9\mathring{A}$. At this distance the hydrogen bond distance no longer exists. This means that interactions along this direction are reduced. This affects growth particularily along the c-axis and the a axis to some extent an hence results in the increased importance of the $\{10\bar{2}\}$ forms.

4 L-alanine/ α-glycine

L-alanine and α-glycine are the first two members of a family of compounds known as the naturally occuring α amino acids. The general formula for this family of compounds is $(R - CH_2(NH_2)COOH)$. For l-alanine $R = CH_3$ and for

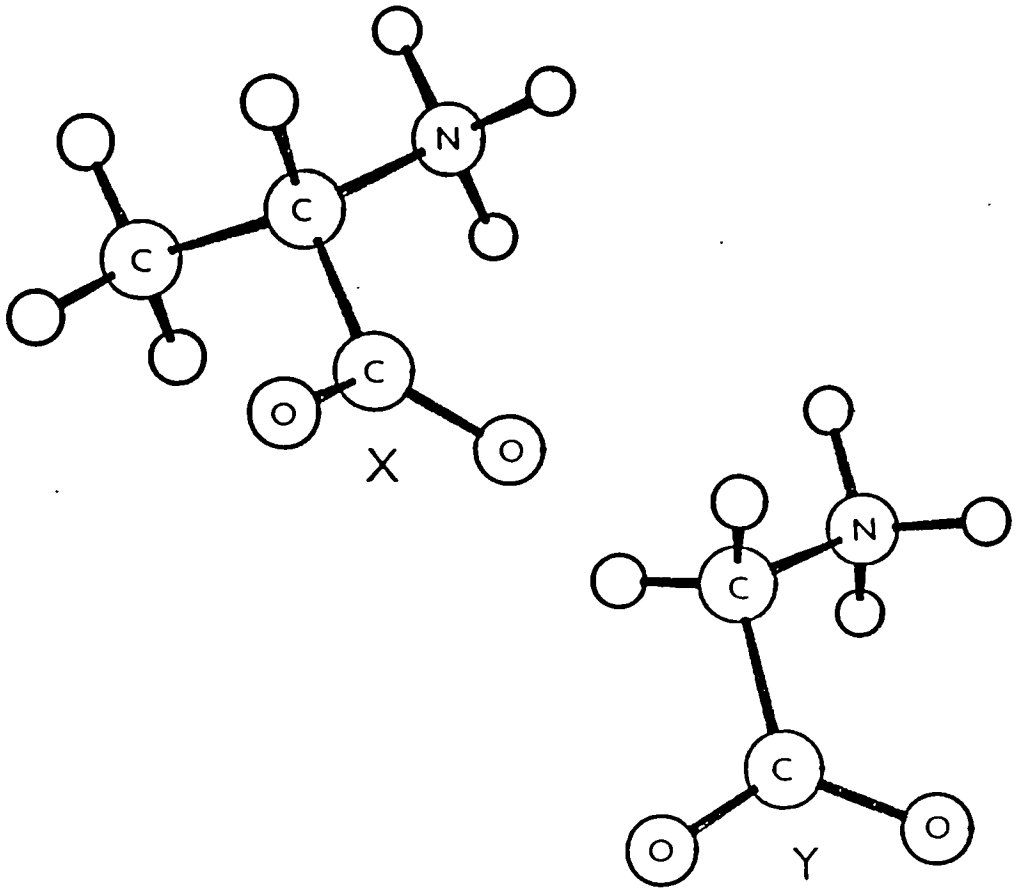

Figure 8.11 L-alanine (X) and glycine (Y) molecule.

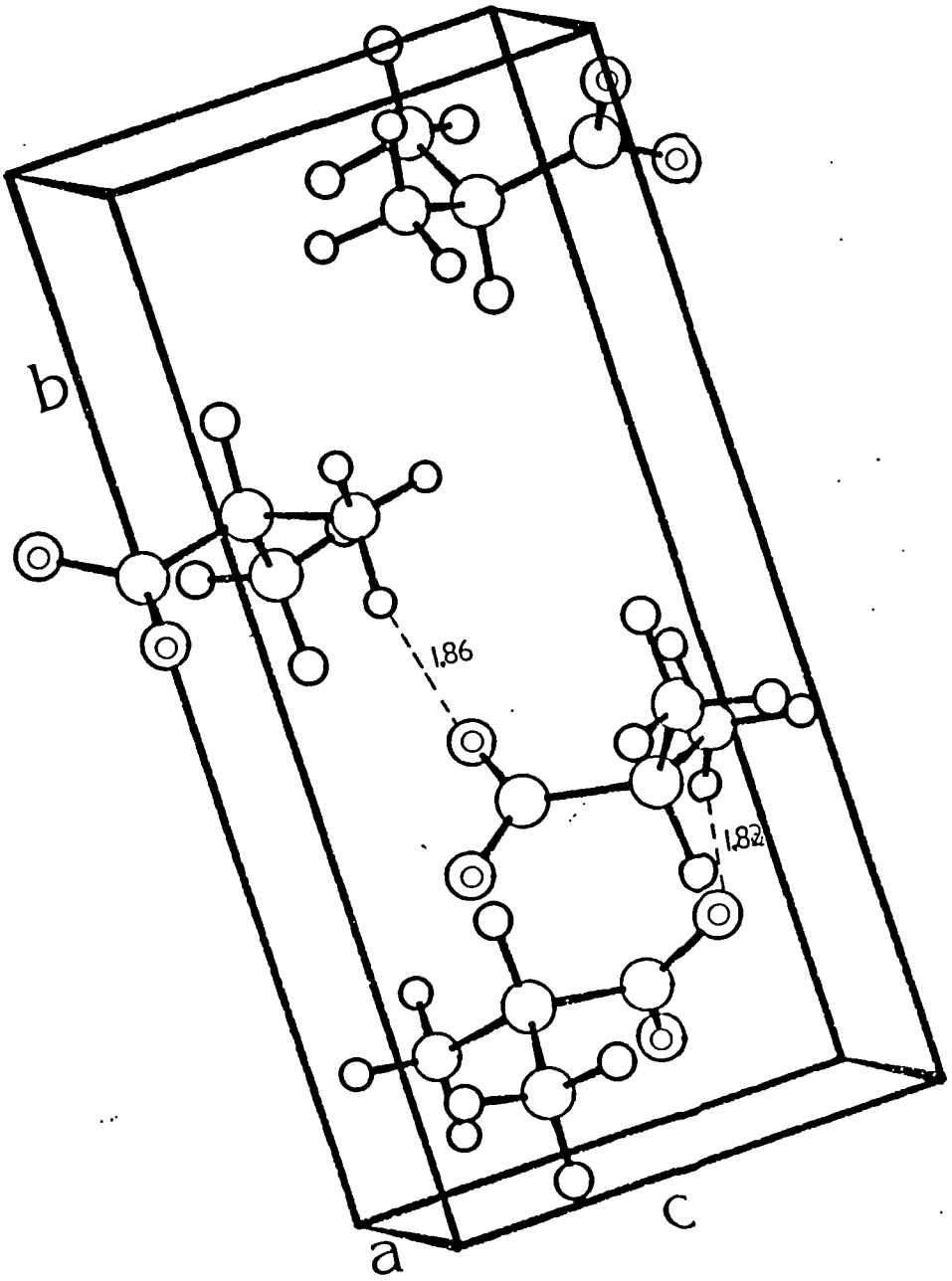

Figure 8.12 L-alanine molecules in the unit cell.

Table 8.5 The important forms identified for l-alanine using Donnay-Harker and attachment energy calculations

FACE	d(hkl) (Angstroms)	Esl (kcal/mol)	Eatt (kcal/mol)
(0 2 0)	6.16	-22.9	-4.5
(1 1 0)	5.41	-21.4	-5.2
(0 1 1)	5.23	-17.0	-7.4
(1 2 0)	4.31	-21.2	-5.3
(0 2 1)	4.22	-10.3	-12.4
(1 0 1)	4.17	-11.5	-10.2
(1 1 $\bar{1}$)	3.95	-11.2	-10.3
(1 2 $\bar{1}$)	3.45	-10.2	-12.8
(1 3 0)	3.39	-21.0	-5.40
(0 3 1)	3.35	-	-

α-glycine R=H.

L-alanine crystallises in the orthorhombic space group $P2_12_12_1$ with four molecules in a unit cell of dimensions a=6.025, b=12.324 and c=5.783Å[10]. Figure 8.11 shows molecules of l-alanine (X) and glycine (Y). The structural similarity is clear differing only where the CH_3 group in alanine replaces one of the H atoms in glycine. Figure 8.12 shows the packing in the unit cell. The four molecules in each unit cell form a network of hydrogen bonding through the l-alanine crystal. Some of the hydrogen bonding distances are labelled in Fig 8.12.

4.1 Morphological Predictions

A Donnay-Harker (DH) model of the morphology was carried out using MORANG and the extinction conditions for the space group $P2_12_12_1$ given in International Tables for X-ray Crystallography [11]. The extinction conditions are

h00 h=2n, 0k0 k=2n, 00l l=2n

The most important forms are given in Table 8.5, the resultant computed morphology is shown in Fig. 8.13(b). The important froms were used in energy calculations using the parameters of Monamy and Carruthers [12]. The lattice energy calculated using PCLEMC of -31.7 kcal/mol is in reasonable agreement with the experimental sublimation enthalpy of 33.0 kcal/mol [13]. The top ten forms identified in the DH analysis were used in the AE calculations. The slice and attachment energies are listed in Table 8.5 and the computed morphology is shown in Fig 8.13(c). The observed morphology determined in chapter 3 is shown in Fig 8.13(a). A more detailed look at the morphology is available in chapter 3 (see Fig 3.4)

4.2 Additive Calculation

α-glycine was considered as an additive using the same approach as adopted in the first two examples in this chapter. The glycine molecule was fitted into the l-alanine unit cell using INTERCHEM [5]. Additive calculations were carried out using PCLEMC in 'ADDT" mode. The resultant changes in incorporation energy for glycine to occupy a site compared to a host l-alanine molecule are given in Table 8.6. The new growth rates with a glycine molecule in the site are also given in Table 8.6. the computed morphology using these new growth rates is shown in Fig 8.14.

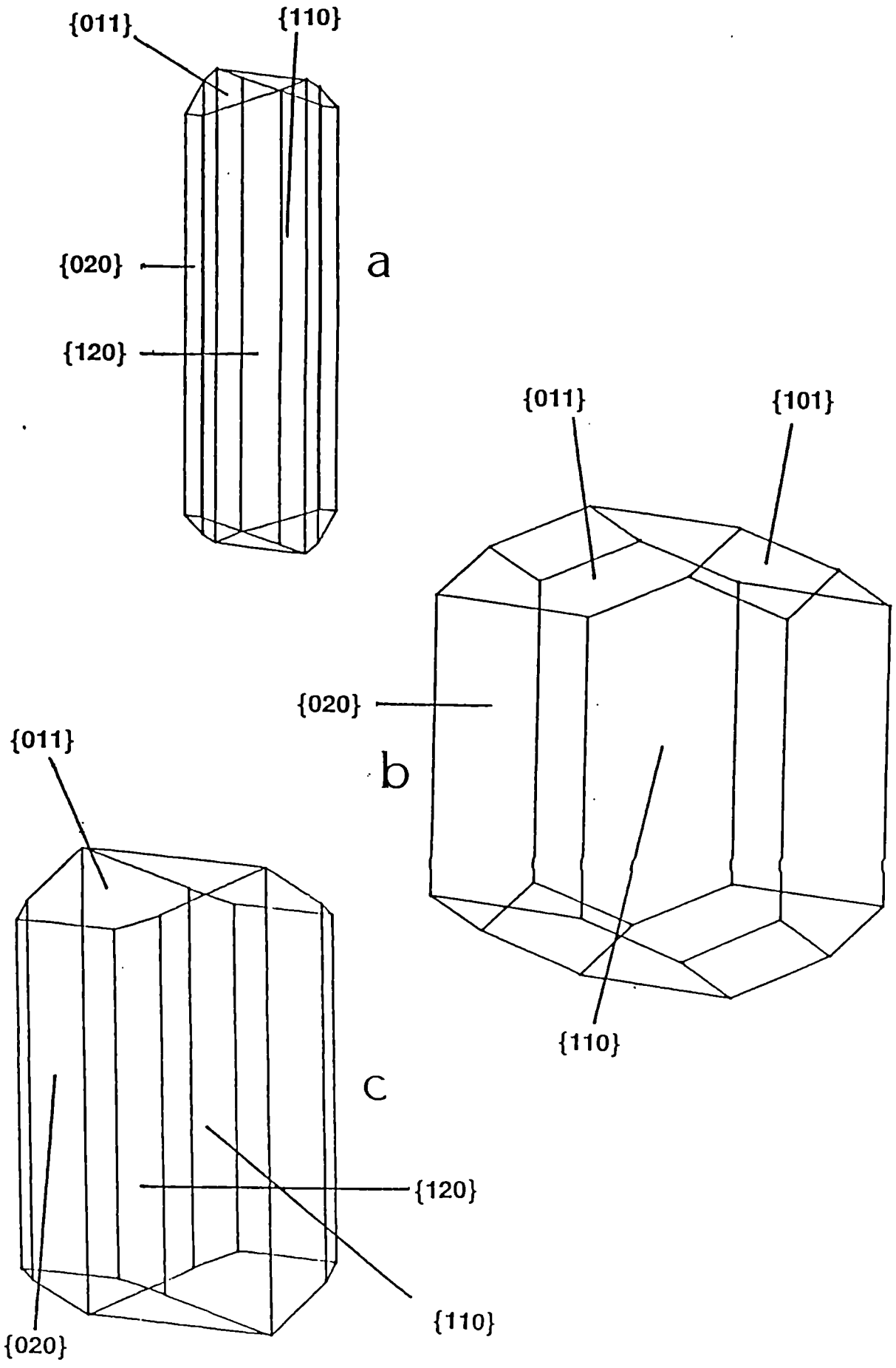

Figure 8.13 Morphologies of l-alanine

a) Observed (see chapter 3) b) Donnay-Harker model

c) Attachment Energy model.

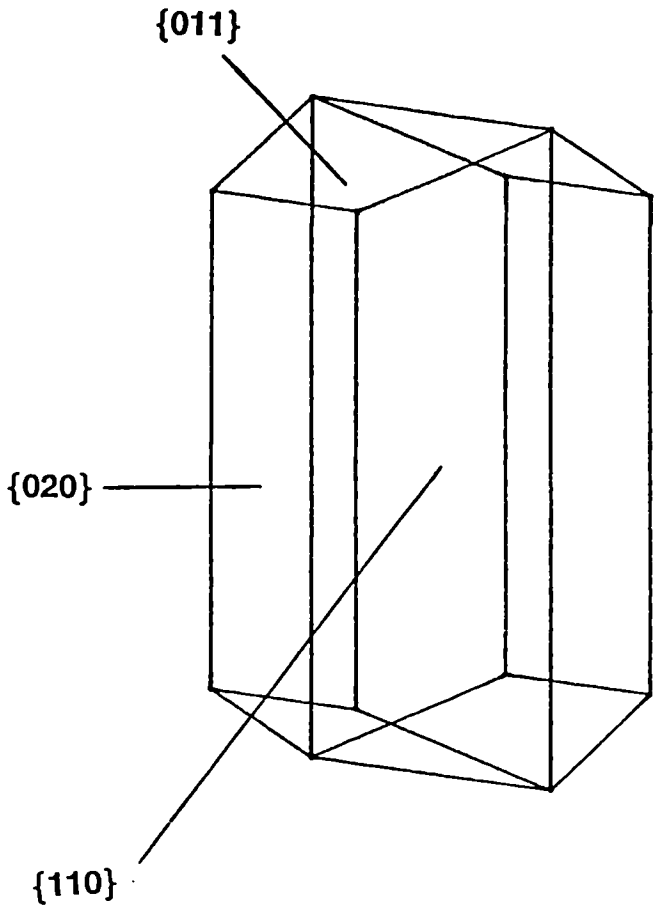

Figure 8.14 The effect of glycine additive on the l-alanine crystal morphology.

Table 8.6 The change in incorporation energy for and the new calculated growth rates for the major faces on an l-alanine crystal with glycine as an additive.

FACE	SYMM	CHANGE IN INCORPORATION ENERGY (kcal/mol)	Eatt'' (kcal/mol)
(020)	1	+1.1	-4.0
	2	+1.1	
	3	+1.1	
	4	+1.1	
(110)	1	+0.8	-4.5
	2	+1.3	
	3	+0.7	
	4	+1.1	
(011)	1	+1.1	-7.0
	2	+1.5	
	3	+1.0	
	4	+1.4	
(120)	1	+0.6	-4.5
	2	+1.3	
	3	+0.6	
	4	+0.9	

4.3 Discussion

The observed morphology exhibits a barrel like morphology with the {120}, {110}, {020} and {011} forms present (see Fig 8.13(a) and Fig 3.4). The {120} form is the major face. The DH model does not identify this face as being present, overestimating as it does the importance of the three remaining forms, the {110},{020} and {011} forms. The DH model also identifies the {101} as being present. The DH model is in general too bulky. The AE model is less bulky and identifies only the faces observed as being present, including the {120} form, not identified by the DH analysis. The results in Table 8.6 indicate that the glycine can get into most faces with only small losses in the incorporation energy. On looking at Fig 8.12 the reasons are clear. The glycine allows the most important strong hydrogen bonding to be completed between the amino and carboxyl groups because of the similarity with alanine. The small loss is only due to replacing a methyl group with a H atom and therefore results in less intermolecular interactions atlonger contact distances. The new growth rates given in Table 8.6 for the situation where an additive is present show only small differences form the pure growth rates given in Table 8.5. This is reflected in the computed morphology shown in Fig 8.14. the only difference has been the loss of the {021} forms.

5 α-glycine/L-alanine

5.1 Structural Details

α-glycine crystallises in the monoclinic space group $P2_1/n$ with four molecules in a unit cell of dimensions a=5.105, b=11.969 and c=5.4644$\mathring{A}$ with $\beta = 111.69°$ [14]. Figure 8.15 shows a glycine molecule beside a l-alanine molecule. Figure 8.15 shows the packing of the molecules of glycine molecule in the unit cell.

5.2 Morphological Predictions

A Donnay-Harker (DH) analysis was carried out, the results are listed in Table 8,7 with the relative morphological importance (M.I.) The computed morphology is shown in Fig 8.16(c). The observed morphologies of α-glycine from sublimation and solution are shown in Figure 8.16(a) and (b) [15]. The AE calculations on the important observed forms were carried out using the parameter of Monamy and Carruthers [12]. The calculated lattice energy of -32.7

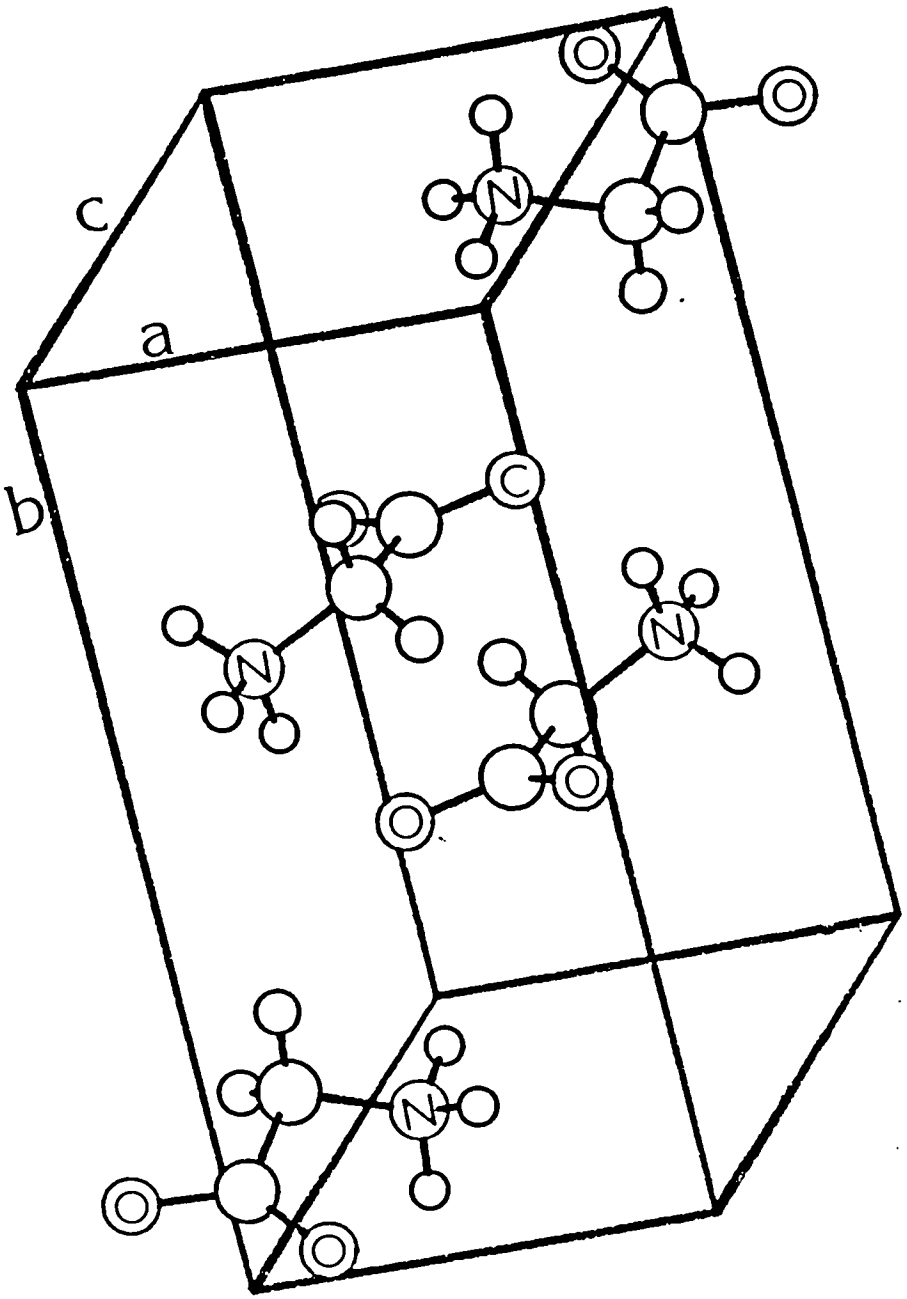

Figure 8.15 Glycine molecules packing in the unit cell

Table 8.7 Important forms identified in the Donnay-Harker analysis of glycine.

FACE	d(hkl) (Angstroms)	RELATIVE MORPHOLOGICAL IMPORTANCE
(0 2 0)	5.98	1.0
(0 1 1)	4.67	0.78
(1 1 0)	4.40	0.73
(1 0 $\bar{1}$)	4.36	0.72
(1 $\bar{1}$ $\bar{1}$)	4.09	0.68
(0 2 $\bar{1}$)	3.87	0.64
(1 2 0)	3.71	0.62
(1 $\bar{2}$ $\bar{1}$)	3.52	0.59
(0 3 $\bar{1}$)	3.13	0.52
(1 $\bar{3}$ 0)	3.05	0.51

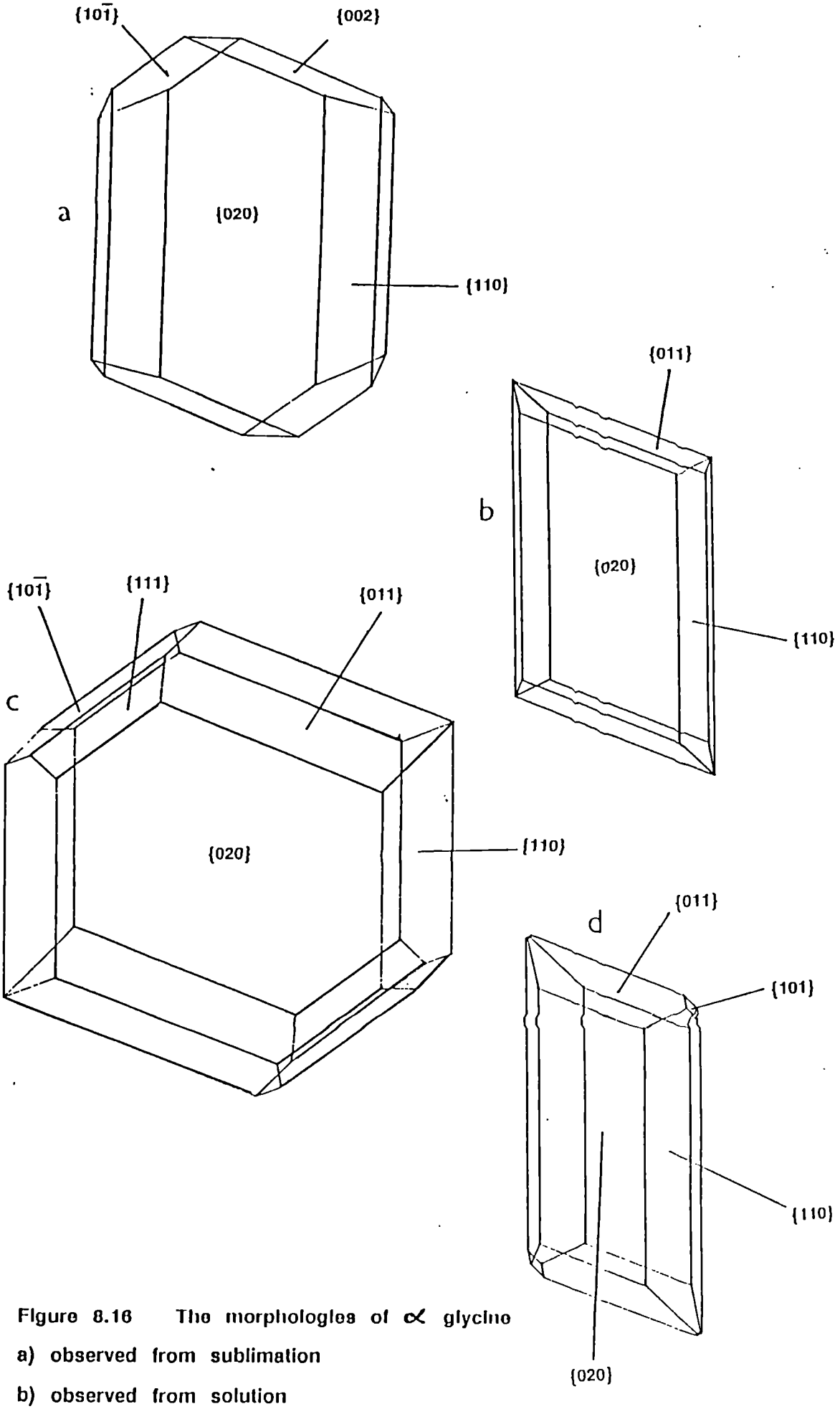

Figure 8.16 The morphologies of ∝ glycine

a) observed from sublimation

b) observed from solution

c) Donnay-Harker model

d) attachment energy calculation

Table 8.8 The calculated slice and attachment energies for the important forms in glycine. Results in kcal/mol

FACE	Esl	Eatt
(020)	-20.3	-6.2
(110)	-21.0	-5.9
(011)	-12.1	-10.3
(101)	-13.2	-9.7
$(10\bar{1})$	-2.5	-15.1
(002)	-6.0	-13.3
(200)	-18.9	-6.9

kcal/mol is in good agreement with the experimental sublimation enthalpy of 32.6 kcal/mol [13]. The slice and attachment energy calculations carried out using PCLEMC are given in Table 8.8, the resultant computed morphology is shown in Fig 8.16(d).

5.3 Additive Calculation

An l-alanine molecule was fitted onto a glycine through the heavy atom backbone and its co-ordinates were obtained in terms of the glycine host system using INTERCHEM and CRYSTLINK. PCLEMC was then used in ADDT mode, the results are listed in Table 8.9. The results include the change in incorporation energy plus the new growth rates with the additive present (the $E_{att''}$ parameter). The The change in incorporation energy indicates that the additive is most likely to get into the (020) face. The additive also appears likely to get into the (011) faces although this is not as favourable as the the (020) face. The binding energies suggest that it is unlikely that the additive gets into the (110) face. The l-alanine/glycine case differs from the previous cases considered in this chapter because the additive molecule is bigger then the host system and the additive is acting as a 'blocker' type. In the previous cases the additives were acting as the disruptive types. In this case the positive $E_{att''}$ values are an indication of the the extent of this blocking ability as it is a measure of the repulsion for the oncoming molecule as it attempts to get into it's rightful position. The E''_{att} parameter is particularily large for the $(0\bar{2}0)$ face and the (011) face. This is in agreement with experimental observations [16] where l-alanine was shown to affect in particular the growth of the $(2\bar{2}0)$ face. The (020) was affected in the same way by d-alanine.

5.4 Discussion

The observed morphologies from sublimation (Fig 8.16(a)) and solution(Fig 8.16(b)) show the same major forms, the {020} and {110}. The sublimation morphology also has the {002} and the $\{10\bar{1}\}$ forms present. The solution morphology has the {011} forms present. Both the DH and AE model have the $\{020\},\{110\}$ and the {011} present. The AE model is in good agreement with the forms observed from solution. Berkovitch-Yellin has carried out similar calculations on glycine [15] and generally found agreement with the calculations here except better agreement with the forms from sublimation. The difference is probably due to a different description of the electrostatic interactions. A more

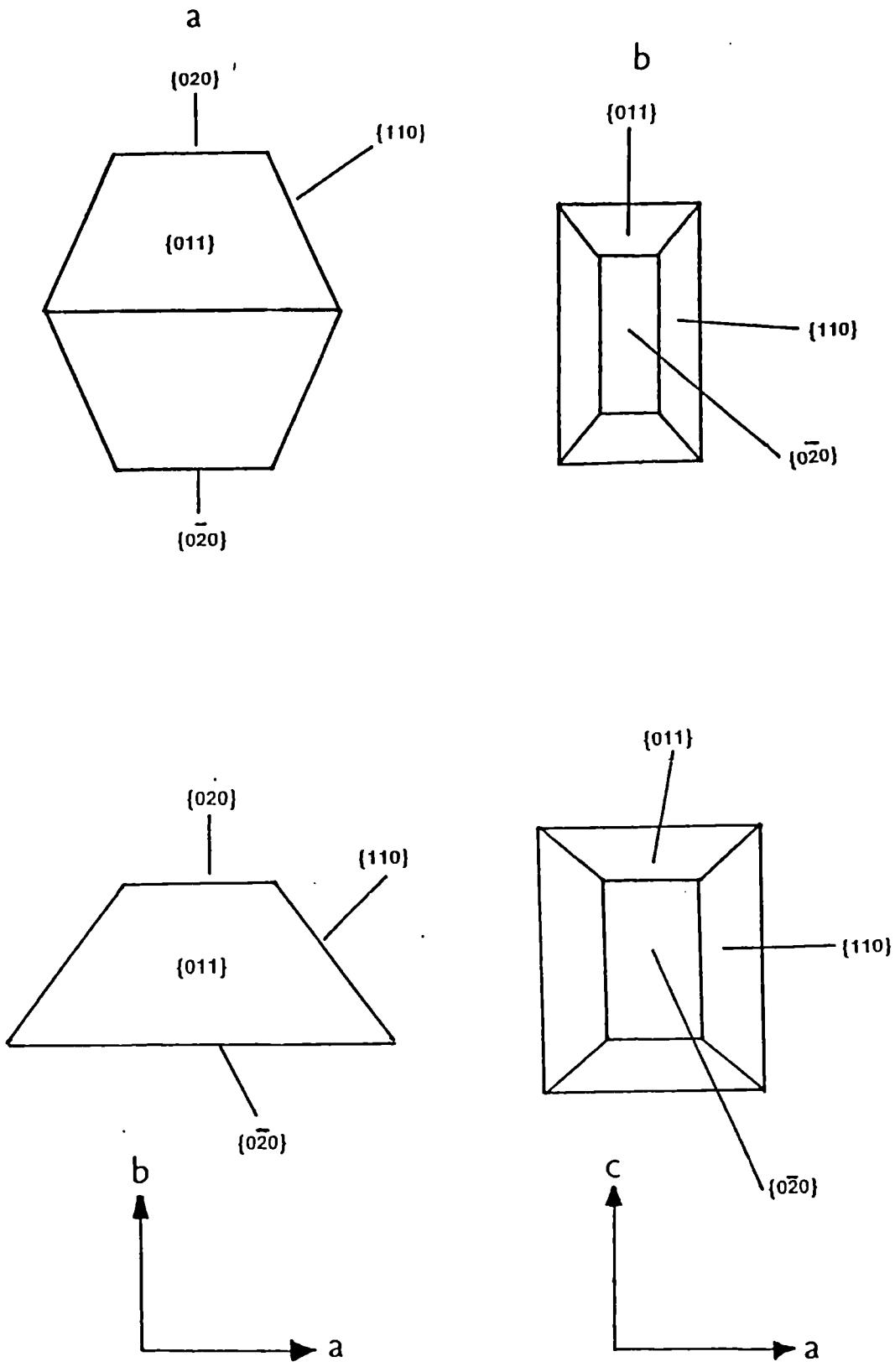

Figure 8.17 Observed morphology of α glycine (a) with l-alanine additive added (b) [16].

Table 8.9 The change in incorporation energy for the main forms on glycine with l-alanine as an additive.

FACE	SYMM	CHANGE IN INCORPORATION ENERGY (kcal/mol)	Eatt'' (kcal/mol)
$(0\bar{2}0)$	1	+1.3	-0.6
	2	+1.9	+94.1
	3	+1.9	+94.1
	4	+1.3	-0.6
(110)	1	+28.6	-3.7
	2	+70.9	+22.8
	3	+29.3	+61.6
	4	+71.5	-7.1
(011)	1	+77.2	-6.7
	2	-17.1	+88.8
	3	+77.2	-3.7
	4	-17.1	-4.9

sophisticated set of parameters particular to glycine obtained from experimental deformation density distributions for glycine from low temperature diffraction has been employed by Berkovitch-Yellin [15].

The additive calculations indicate are in good agreement with what is observed experimentally. The effects of l-alanine on the crystal habit are shown in Fig 8.17. The obvious effect is the increase in the importance of the (020) face. An increase in the surface area of the (011) forms is also noted [16]. This is consistent with the calculations where as it appears likely that the additive can get into these faces. The calculations are in general terms in agreement with the results reported in [16]. The $E_{att''}$ parameter is not nearly as effective for the blocker type additive as it was for the disruptive type. The positive values can be used only as an interpretation of the 'blocking ability' of an additive. Clearly more work is necessary to determine the orientation of the blocker part of the additive with respect to the surface and oncoming layer to produce a more meaningful $E_{att''}$ term.

6 Conclusions

1. The use of $E_{sl'}$ and $E_{att'}$ allows evalulation of the likely sites for additive incorporation.

2. The new parameter ($E_{att''}$) gives a route for quantifying the effects of an additive.

3. The $E_{att''}$ parameter works particularily well for the disruptive type of additive.

4. The $E_{att''}$ parameter is less effective for the blocker additive type although it can be used as a rough guide to blocking ability.

7 References

[1] M. Lahav, L. Leiserowitz, Z. Berkovitch-Yellin, J. van Mil, L. Addadi and M. Idelson, J. Amer. Chem. Soc. 107 (1985) 3111.
[2] C.C.F. Blake and R.W.H. Small, Acta Cryst, B28 (1972) 2201.

[3] S. Lifson, A.T. Hagler and P. Dauber, J. Amer. Chem. Soc. 101 (1979) 5111.
[4] E. Dowty, Amer. Miner. 65 (1980) 465.
[5] INTERCHEM, P. Bladon and R. Breckinridge, University of Strathclyde (1986).
[6] J. Housty, M. Hospital, Acta Cryst. 18 (1965) 693.
[7] J.N. Sherwood and B. McArdle (unpublished results).
[8] A.S. Michaels and A.R. Colville, J. Phys. Chem. 64 (1960) 13.
[9] W.A. Caspari, J. Amer. Chem. Soc. (1928) 3235.
[10] M.S. Lehmann, T.F. Koetzle and W.C. Hamilton. J. Amer. Chem. Soc. 94 (1972) 2657.
[11] International Tables for Crystallography, Vol A, Reidel Dordrecht (1983).
[12] F.A. Monamy, L.M. Carruthers, R.F. McGuire, H.A. Scheraga. J. Phys. Chem. 78 (1974) 1579
[13] J.D. Cox and G. Pilchard, Thermochemistry of Organic and Organometallic Compounds, Academic Press, New York (1970).
[14] J. Almof, A. Kvick and J.O. Thomas, J. Chem. Phys. 59 (1973) 3901.
[15] Z. Berkovitch-Yellin, J. Amer. Chem. Soc. 107 (1985) 8239.
[16] I. Weissbuch, L. Addadi, Z. Berkovitch-Yellin, E. Gati, S. Weinstein, M. Lahav and L. Leiserowitz. J. Am. Chem. Soc. 105 (1982) 6615.

Chapter 9

The Morphology Of Benzophenone. A Comparison Of Donnay-Harker, Hartman-Perdok, Attachment Energy And Ising Models

CONTENTS

1 Introduction

In chapter 2 methods for relating crystal morphology to internal structure were presented. A further review of these methods will be presented elsewhere [1]. The aim of this chapter was to apply all these methods in a study of the organic compound benzophenone. The 'classical' Donnay-Harker (DH) and Attachment Energy (AE) models will be used as for other materials in this thesis. Additionally the Hartman-Perdok (HP) and Ising (IS) approaches will also be applied to benzophenone. Jetten [2] has completed a PBC analysis of benzophenone and derived connected nets for the Ising approach. This work will form a basis for the calculations of the HP and IS models in this chapter. New intermolecular bond strengths calculated as part of this thesis will be introduced into the PBC analysis of Jetten.

The resultant computational models of the morphology were compared and contrasted with each other and with the observed morphology. The results in this chapter will be presented elsewhere [3]. This is the first of a series of systematic studies using all these approaches. Further studies will include paraffin [4] and β-glycerol tristerate [5]. A similar approach to that undertaken for the case of tailor-made additives in the previous chapter was adopted in order to quantify the habit modifying effect of toluene.

2 Benzophenone

Benzophenone ($C_6H_5C = OC_6H_5$) is an aromatic ketone which crystallizes in the orthorhombic non- centrosymetric space group $P2_12_12_1$ with four molecules in a unit cell of dimensions a=10.26Å, b= 12.09Åand c=7.88Å[6]. Only the co-ordinates of heavy atoms were reported [6] and so the hydrogen co-ordinates were fitted assuming sp^2 hybridisation and a standard C-H bond length of 0.11nm using INTERCHEM [7]. The hydrogen positions were then optimised to an energy minimum using MOPAC [8], the co-ordinates of the hydrogen atoms are listed in Table 9.1 along with the heavy atom positions as reported [6]. A discussion of the fitting of hydrogens is given in Appendix D. The co-ordinates of the hydrogen atoms differ only slightly from those of Yoon [9] who added the hydrogens with sp^2 hybridisation but without any minimisation. Figure 9.1 shows a molecule of benzophenone with the atoms labelled. Figure 9.2 shows a unit cell of benzophenone with the hydrogens removed for clarity. Figure 9.3 shows the packing arrangement of benzophenone down the a-axis. In Fig 9.3 the

Table 9.1 Fractional co-ordinates and charge distribution for benzophenone. Heavy atom postions from [6] hydrogens found assuming standard geometry followed by minimisation by MOPAC. Charge distribution from MOPAC.

ATOM	X	Y	Z	CHARGE
CO	0.199	0.217	0.280	0.3138
C1	0.298	0.130	0.304	-0.1400
C2	0.284	0.027	0.220	-0.0158
H2	0.202	0.009	0.137	0.0656
C3	0.383	-0.052	0.237	-0.0744
H3	0.375	-0.131	0.172	0.0656
C4	0.489	-0.028	0.338	-0.0331
H4	0.565	-0.091	0.351	0.0535
C5	0.504	0.070	0.421	-0.0741
H5	0.589	0.087	0.500	0.0705
C6	0.404	0.150	0.403	0.0094
H6	0.417	0.230	0.469	0.0747
C11	0.061	0.193	0.243	-0.1381
C21	-0.003	0.103	0.309	-0.0099
H21	0.048	0.043	0.390	0.0581
C31	-0.134	0.086	0.282	-0.0761
H31	-0.181	0.013	0.337	0.0637
C41	-0.202	0.158	0.186	-0.0331
H41	-0.306	0.143	0.160	0.0535
C51	-0.146	0.254	0.124	-0.0781
H51	-0.203	0.314	0.053	0.0687
C61	-0.012	0.271	0.151	0.0058
H61	0.033	0.345	0.098	0.0757
O1	0.234	0.315	0.291	-0.3131

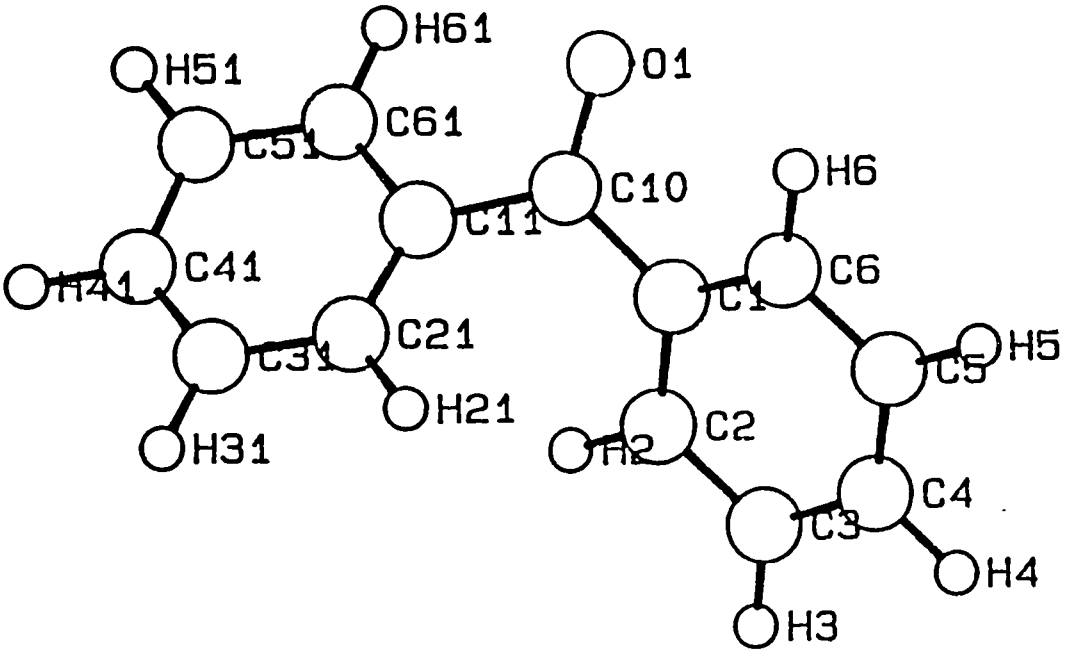

Figure 9.1 Molecule of benzophenone

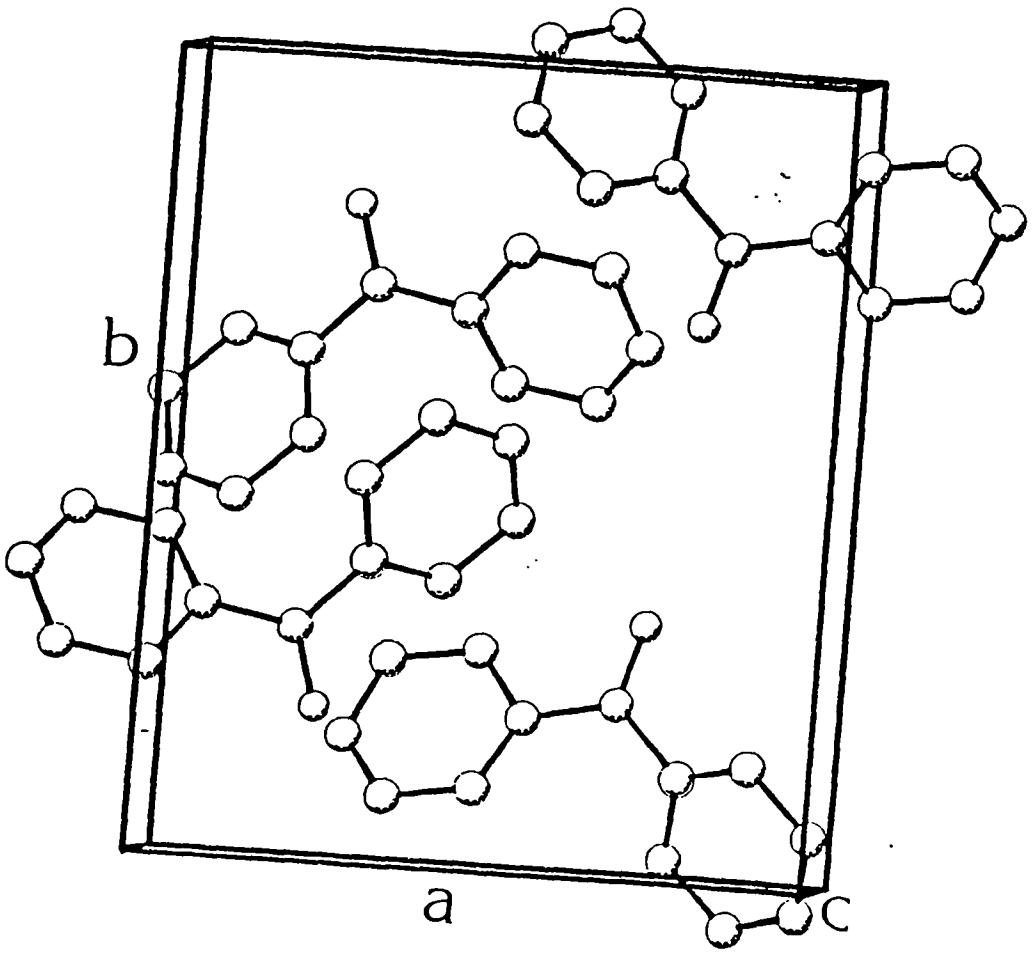

Figure 9.2 Unit cell containing four benzophenone molecules

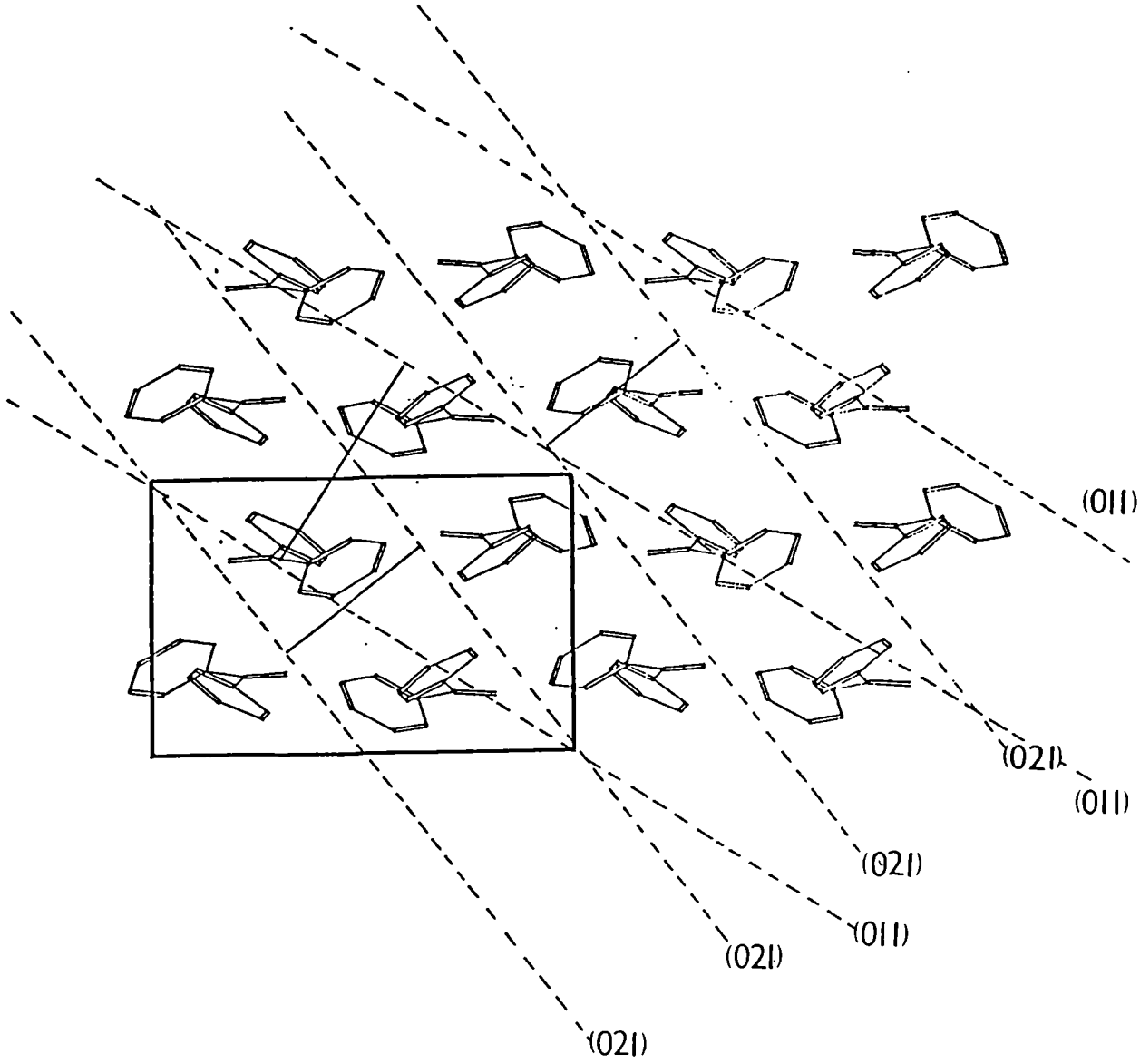

Figure 9.3 Benzophenone packing down the a-axis

hydrogen atoms have been removed for clarity and the double bonds highlighted.

3 Donnay-Harker Approach

For the space group $P2_12_12_1$ the extinction conditions given in International Tables [11] are

(h00) h=2n, (0k0) k=2n, (00l) l=2n

MORANG (Chapter 4 and Appendix A) was used to identify the most important forms according to the interplanar spacing d_{hkl}. The importance of extinction conditions to such calculations has been discussed in Chapter 2. A list of the most important forms for benzophenone according to interplanar spacing is given in Table 9.2 along with the derived relative morphological importance. The computer drawn morphology using these results is given in Figure 9.13(b). The interplanar spacings in terms of the molecular packing can be seen in Fig 9.3 for the (011) and (021) faces. The (011) interplanar spacing is greater than that of (021). This is clearly visable in Figure 9.3.

4 Energy Calculations

A number of authors have derived sets of atom-atom parameters for the study of a variety organic materials. No parameters for the specific study of benzophenone appear to have been published or tested. The parameters of Monamy et al [11] are the most generally applicable used in this thesis. These parameters along with the fractional charges from MOPAC [8] were used to describe the interactions in benzophenone. The charge distribution over a benzophenone molecule is given in Table 9.1. The computer program PCLEMC (Appendix C) was used to calculate the interactions between benzophenone molecules, the results of which are listed in Table 9.3. The calculated lattice energy of - 24.5 kcal/mol is in excellent aggreement with the 'experimental' lattice energy of - 23.9kcal/mol derived from the sublimation enthalpy of of 22.73 kcal/mol [12]. Details of deriving the 'experimental ' lattice energy has been discussed in chapter 6. PCLEMC was then used in debug mode (see Appendix C) to identify the strongest intermolecular 'bonds' in the crystal structure. The strongest bonds are listed in Table 9.3. A similar labelling of molecules and intermolecular interactions to that in Jettens thesis [2] was adopted to allow comparison between the PBC projections and relevant discussions presented by Jetten [2]. There are four molecules in the benzophenone unit cell. The convention adopted by Jetten

Table 9.2 Most important forms in benzophenone according to interplanar spacing. Calculations carried out by MORANG using the cell parameters from [6].

FACE	d(hkl)	Relative Importance
(1 1 0)	7.82	1.00
(0 1 1)	6.60	0.84
(1 0 $\bar{1}$)	6.25	0.80
(0 2 0)	6.04	0.77
(1 1 $\bar{1}$)	5.55	0.71
(1 2 0)	5.21	0.67
(2 0 0)	5.13	0.66
(0 2 1)	4.80	0.61
(2 1 0)	4.72	0.60
(1 $\bar{2}$ 1)	4.34	0.55

Table 9.3 The strongest intermolecular bonds identified in benzophenone using PCLEMC.

Bond	Type	Energy (kcal/mol)	Plotting symbol
1(000)-4(000)	a	-1.9	
1(000)-4(0-10)	a	-1.9	— — — — —
2(000)-3(000)	a	-1.9	
2(000)-3(010)	a	-1.9	
1(000)-4(100)	b	-0.8	
1(000)-4(1-10)	b	-0.8	- - - - - - - - -
2(000)-3(-100)	b	-0.8	
2(000)-3(-110)	b	-0.8	
1(000)-3(000)	c	-2.0	
1(000)-3(-100)	c	-2.0	.....
2(000)-4(001)	c	-2.0	
2(000)-4(101)	c	-2.0	
1(000)-3(00-1)	d	-1.7	
1(000)-3(-10-1)	d	-1.7	- - - - - - - - -
2(000)-4(000)	d	-1.7	
2(000)-4(100)	d	-1.7	
1(000)-2(000)	e	-0.1	
1(000)-2(00-1)	e	-0.1	
3(000)-4(1-10)	e	-0.1	
3(000)-4(1-11)	e	-0.1	
1(000)-2(0-10)	f	-3.4	
1(000)-2(0-1-1)	f	-3.4	— — — — — —
3(000)-4(100)	f	-3.4	
3(000)-4(101)	f	-3.4	
1(000)-2(-1-10)	g	-0.4	
1(000)-2(-1-1-1)	g	-0.4	
3(000)-4(000)	g	-0.4	
3(001)-4(001)	g	-0.4	
1(000)-1(100)	h	-0.9	- + - + - + - +
1(000)-1(001)	j	-0.2	

The plotting symbol is that used in Jettens thesis to aid clarity

means a clear circle represents moleule 1, a clear square molecule 2, a shaded circle molecule 3 and a shaded square molecule 4. The advantage of the current energy calculations are two fold;

1. The calculated lattice energy reported here is in much better agreement with the experimental lattice energy than that calculated by Jetten in his thesis. The lattice energy calculated by Jetten is -18.08kcal/mol. The lattice energy reported in this chapter of -24.55kcal/mol is in much closer to the 'experimental' lattice energy of -23.9kcal/mol.

2. PCLEMC was specifically designed for evaluating the interactions between molecules in the crystal. Jetten used a computer program to calculate the lattice energy. To estimate the intermolecular bond strengths Jetten enlarged one or more molecular axes and reduced the number of molecules in the unit cell. This excluded specific bonds from the summation. Using this approach Jetten was able to estimate intermolecular bond strengths. Using PCLEMC there was no need for such manipulations. All the intermolecular interactions are calculated and identified as a matter of routine in PCLEMC.

A simplified model of the strong and weak intermolecular interactions in the benzophenone unit cell are given in Figures 9.4 and 9.5. The parameters of Monamy et al [11] were also used with PCLEMC for the calculation of slice and attachment energies (see section 6).

5 Hartman-Perdok Approach

The HP approach involves identifying the periodic bond chains formed by the strongest intermolecular interactions in the crystal structure. A discussion of PBC theory has already been given in Chapter 2. A full PBC analysis of benzophenone has already been undertaken by Jetten [2]. The intermolecular bonds in the slices Jetten identified are given in Table 9.4. By fitting the intermolecular bond values calculated using PCLEMC into the slice the slice energy can be calculated by hand, rather than directly as in PCLEMC (see Appendix C). This allows the attachment energies to be estimated . The estimated attachment en-

Table 9.4 Observed center to face distances [15], Hartman-Perdok estimated attachment energies, calculated attachment energies and Ising model results for benzophenone.

Face	Bonds in slice (JETTEN)	Eatt(HP) kcal/mol	Eatt(AE) kcal/mol	ISING $1/\theta^c$	Observed Distance
(110)	a+b+c+d+2f+2j	-10.9	-10.3	0.44	19.5
(101)	2a+c+d+e+f+j	-13.3	-12.9	0.51	30.3
(011)	a+b+2c+e+f+g+2h	-12.1	-12.0	0.55	29.3
(020)	2c+2d+2h+2j	-14.9	-14.6	0.63	27.0
(111)	a+b+c+d+e+f	-14.6	-14.1	0.64	28.5
(021)	2d+f+g+2h	-15.5	-14.9	0.67	29.0
(002)	2a+2b+2h	-17.3	-17.1	0.86	32.5

ergies are given in Table 9.4. A computer drawn model based on this approach is given in Figure 9.13(c)

6 Attachment Energy Model

As described in Chapter 4 and Appendix C, PCLEMC can be used to calculate the slice and attachment energies directly from the crystal structure without having to resort to a full PBC analysis. The slice and attachment energies for the top forms is given in Table 9.4. The morphology constructed from these results is given in Figure 9.13 (d).

7 Ising Models

The important parameter in the Ising model is θ^c. This value is a measure of the stability of a face. The higher the value the more morphologically important the face [13]. Jetten [2] has already derived the connected nets and used his relative bond strengths to calculate θ^c. The value of θ^c will be re-calculated for the faces on the benzophenone crystal using the new evaluated bond strengths obtained from PCLEMC.

Figures 9.4 and 9.5 show the strong bonds in the benzophenone unit cell. The same labelling convention as that used by Jetten [2] has been adopted. Connected nets can be derived from this by looking at the bonding arrangements in the unit cell and following paths across the planes cut out by Miller indices. The connected nets for the faces on the benzophenone crystal (110, 011, 101, 002, 200, and 111) are shown in Figures 9.6(a) - 9.12(a). The nets for (110), (011) and (200) were presented by Jetten [2].

The square planar (MxK) net can be derived from the connected net by introducing bonds of zero or infinite strength. All the paths through the connected net can be traced through the square planar net. An infinite bond strength means zero distance, a zero bond strength indicates no connection [13,14]. The square planar nets derived from the connected nets are given in Figs 9.6(c)-9.12(c). For some connected nets crossing bonds were encountered such as the (011) net where h bonds cross f bonds and e bonds cross h bonds. As is the common practice [2,13,14] the weaker bonds were ignored i.e. the h bonds when h crosses f and the e bonds when e crosses h.

In Table 9.4 the $1/\theta^c$ values calculated using the new bond strengths reported in this chapter. The new values of $1/\theta^c$ are used to compute the Ising

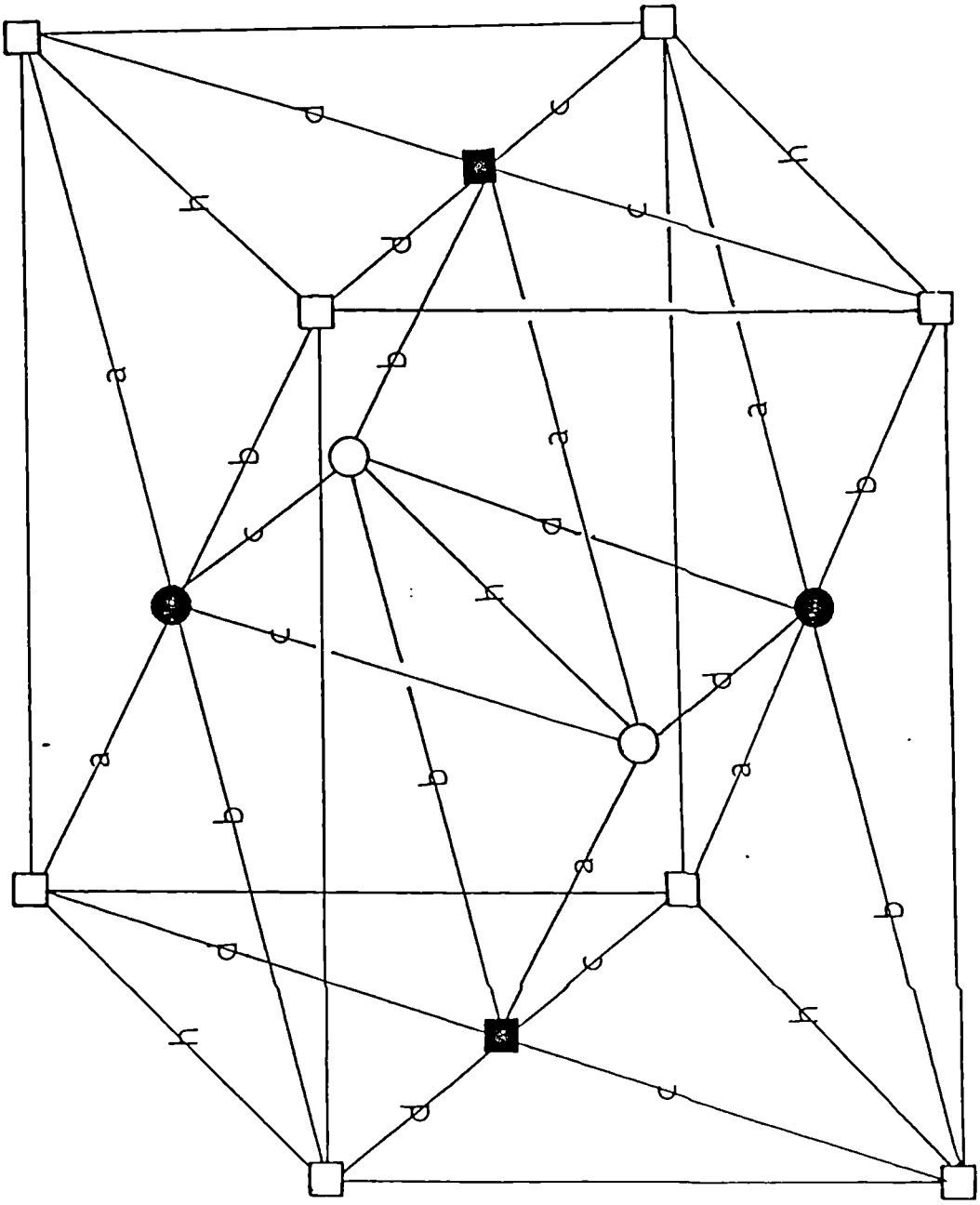

Figure 9.4 The strong intermolecular bonds in benzophenone

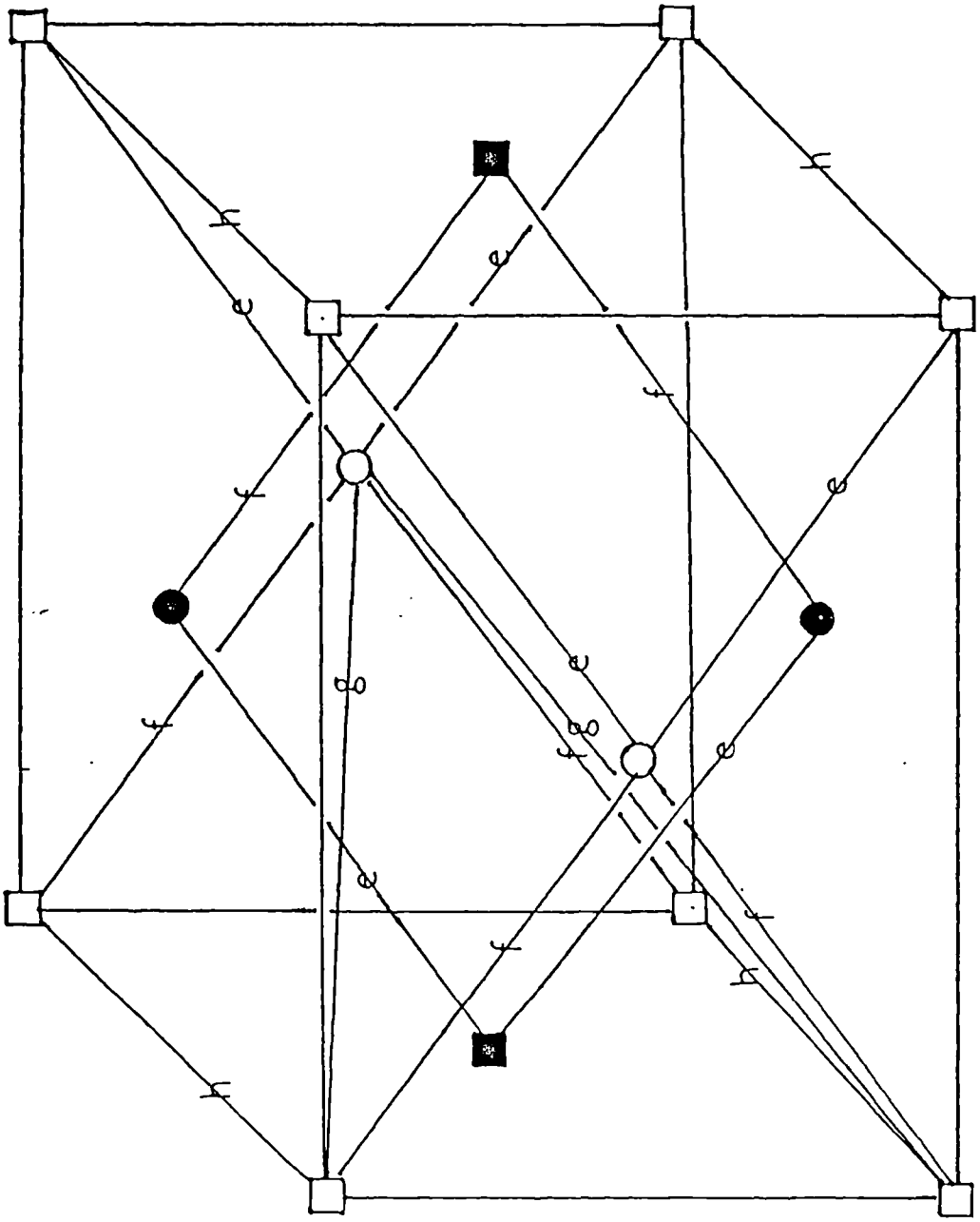

Figure 9.5 The weak intermolecular bonds in benzophenone

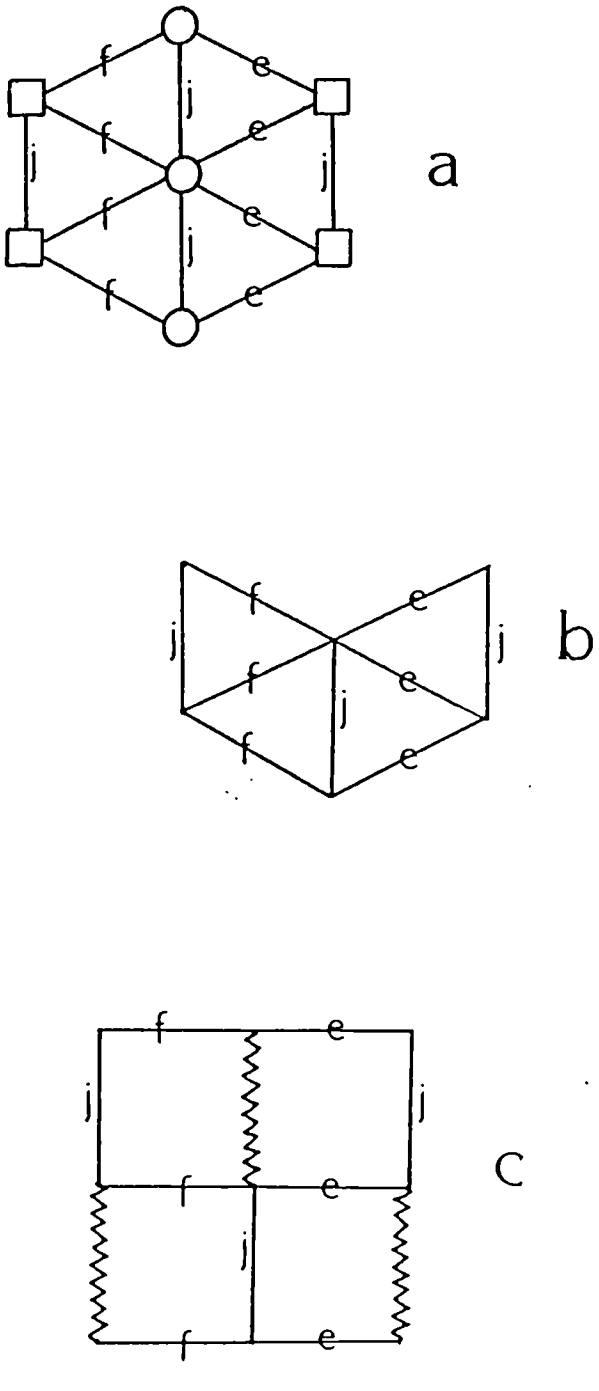

Figure 9.6 The (100) connected net and corresponding rectangular net a), b) connected net c) transformed rectangular net.

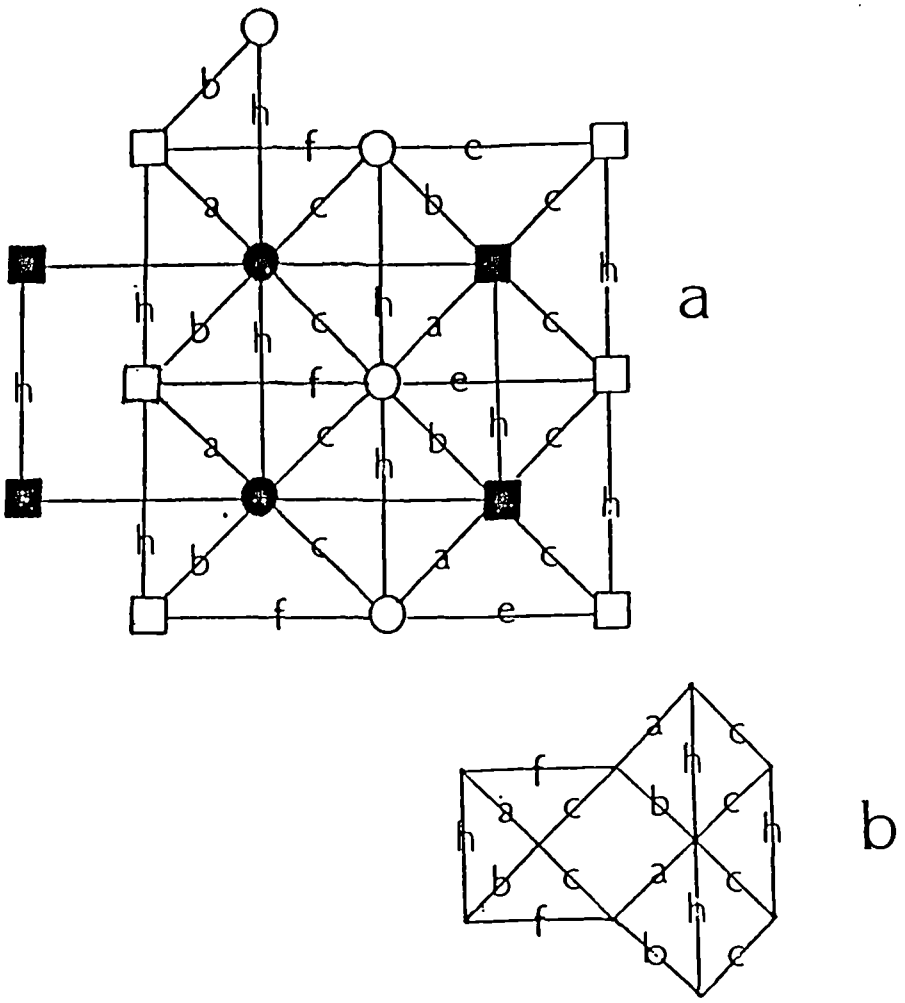

Figure 9.7 The (011) connected net and corresponding rectangular net
a), b) connected net c) transformed rectangular net.

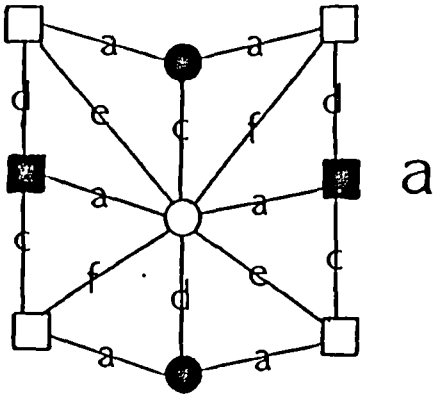

a

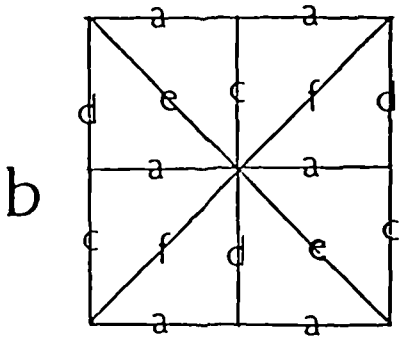

b

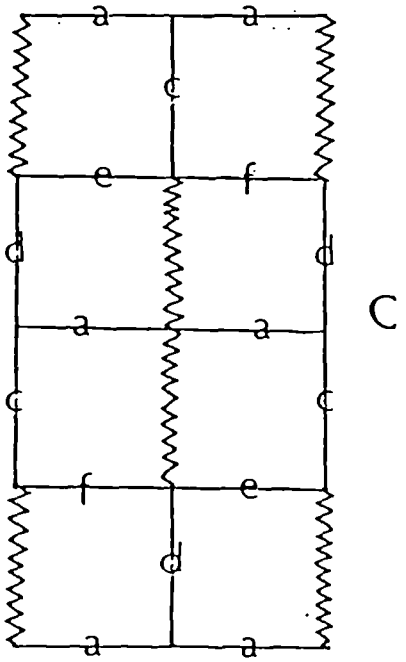

c

Figure 9.8 The (101) connected net and corresponding rectangular net a), b) connected net c) transformed rectangular net.

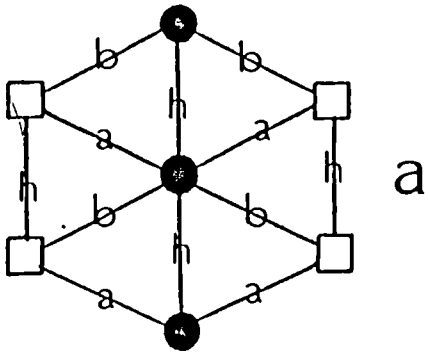

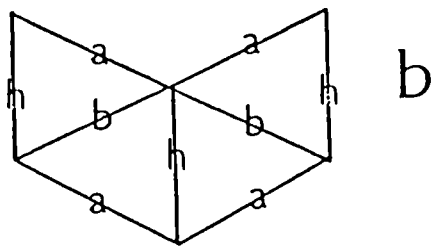

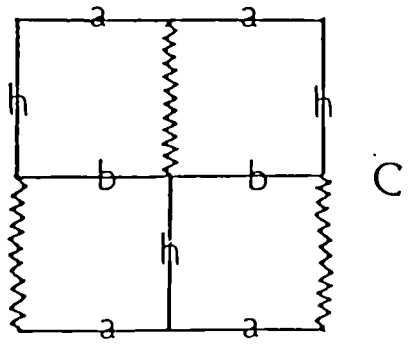

Figure 9.9 The (001) connected net and corresponding rectangular net a), b) connected net c) transformed rectangular net.

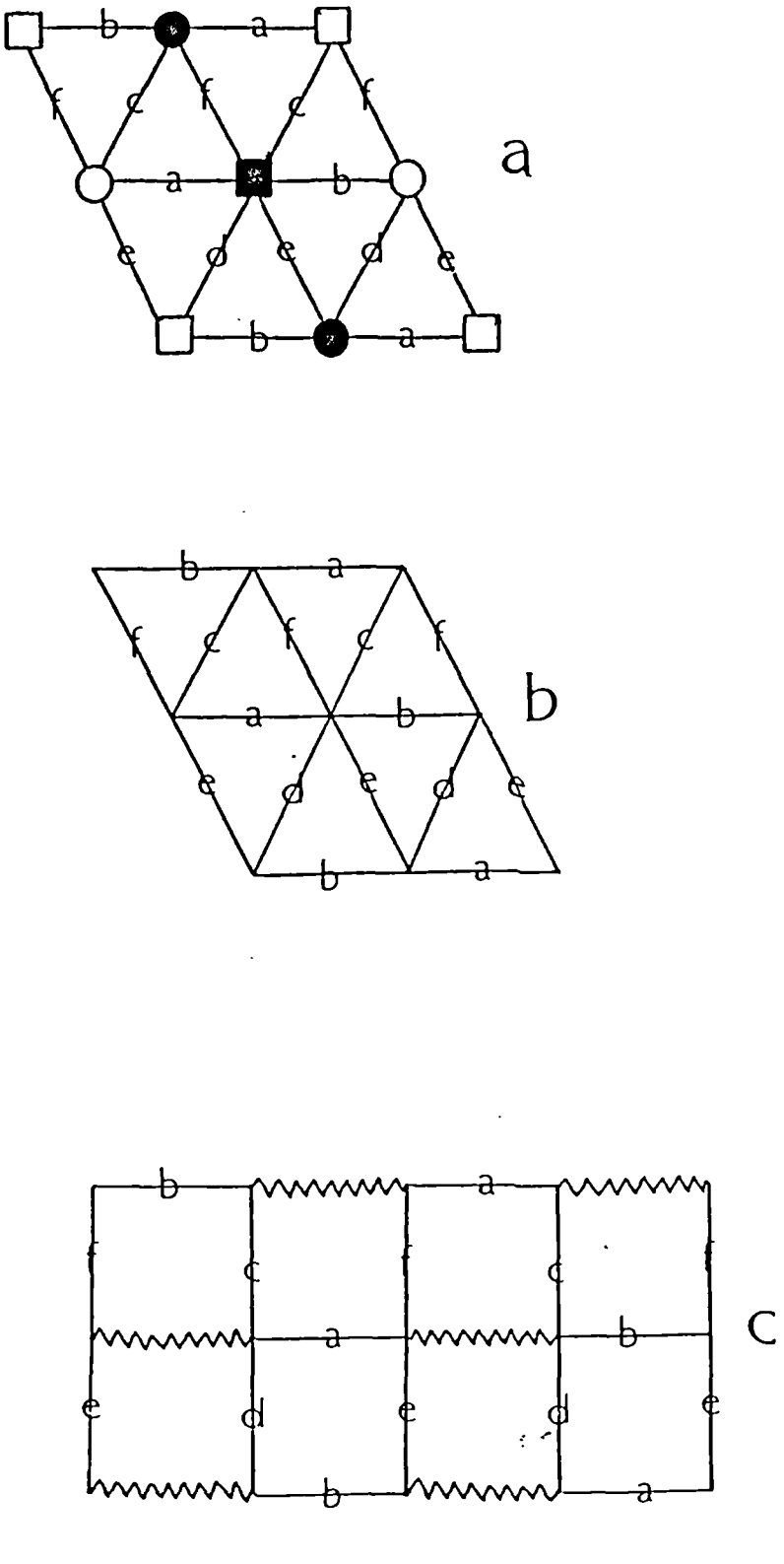

Figure 9.10 The (111) connected net and corresponding rectangular net
a), b) connected net c) transformed rectangular net.

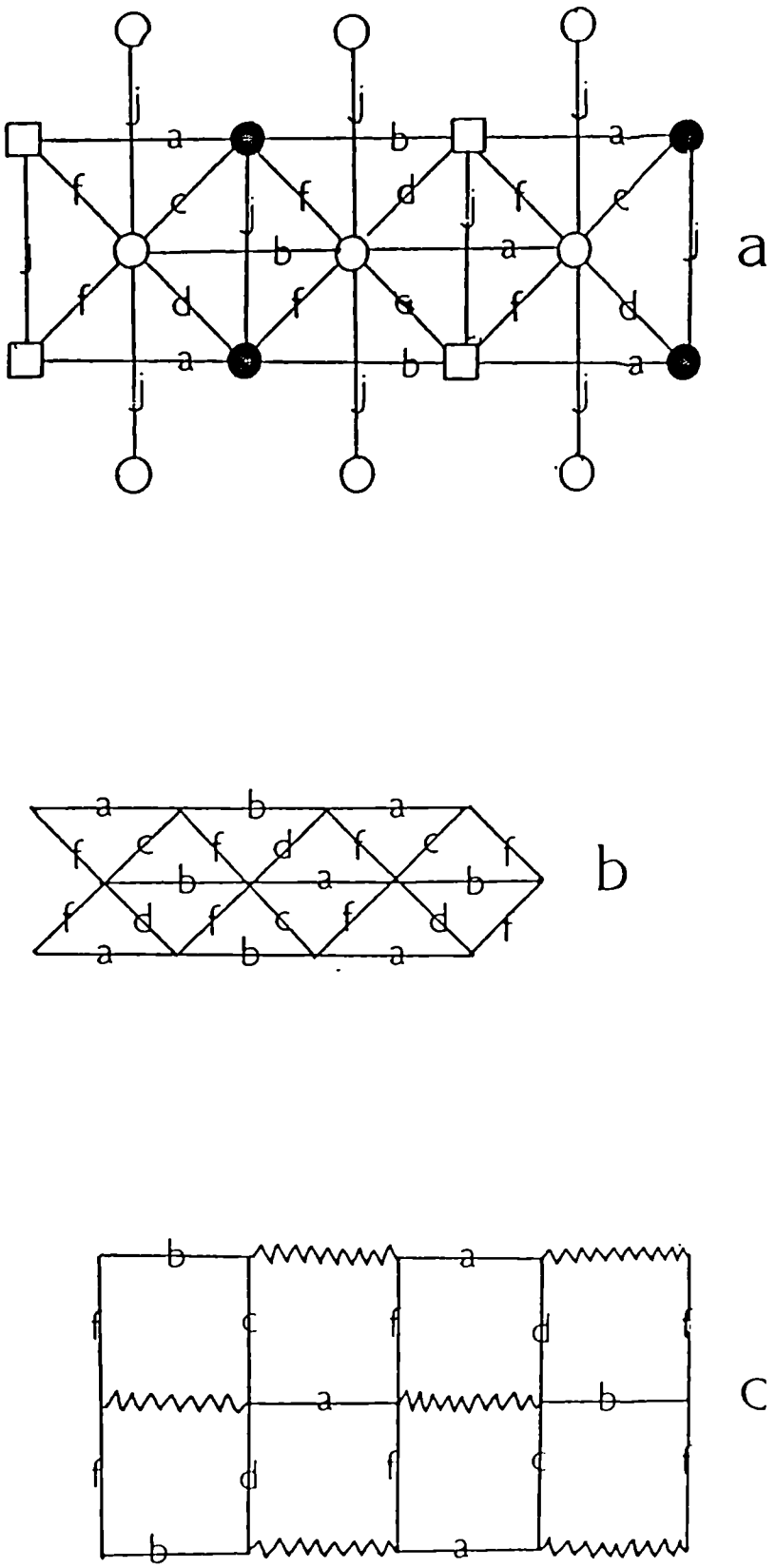

Figure 9.11 The (110) connected net and corresponding rectangular net a), b) connected net c) transformed rectangular net.

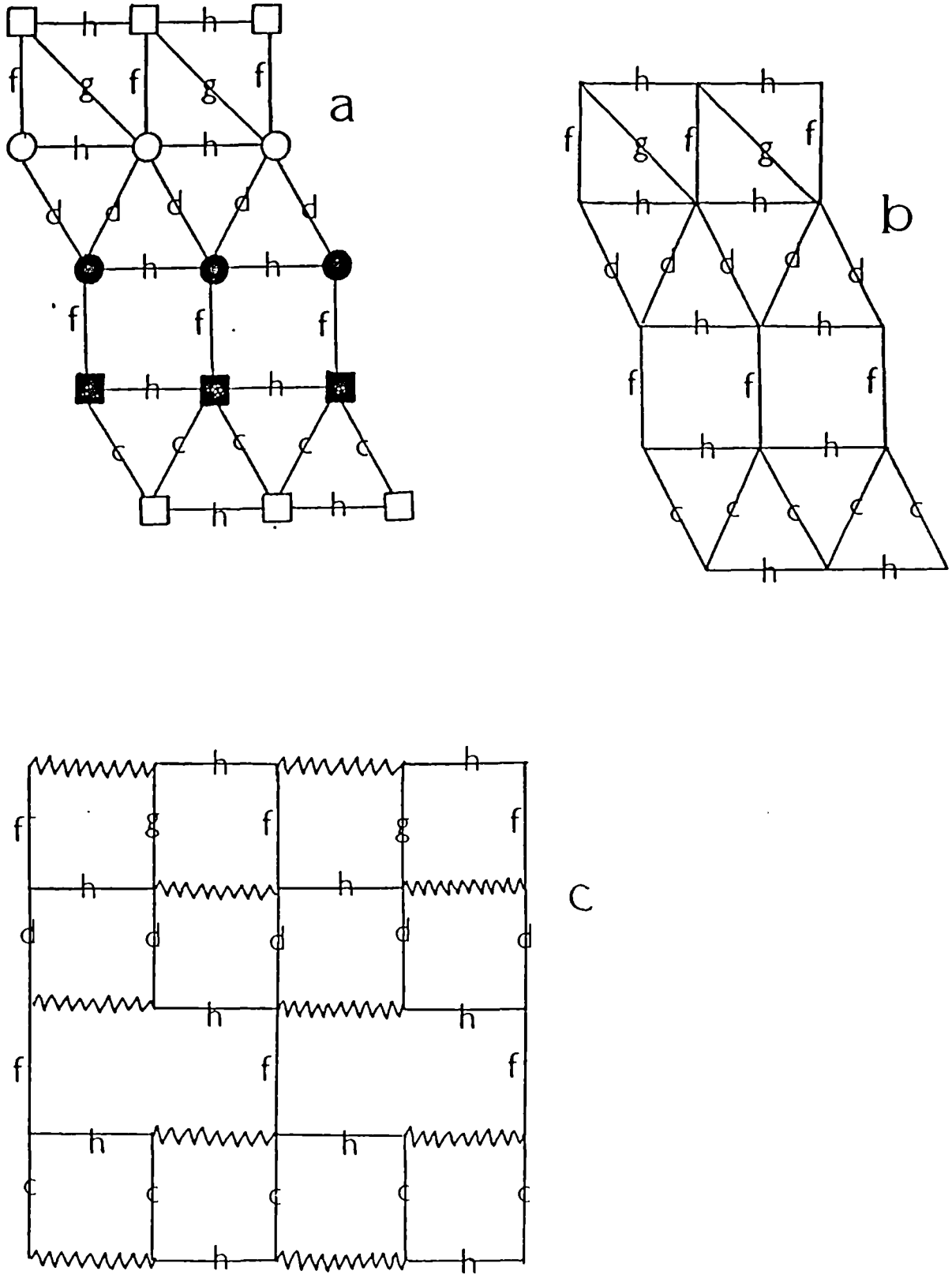

Figure 9.12 The (021) connected net and corresponding rectangular net
a), b) connected net c) transformed rectangular net.

model of the morphology and this is shown in Figure 9.13(e).

8 Comparison Of Morphologies

The observed morphology of benzophenone reported by Becker et al [16] shows a complicated morphology dominated by the {110} faces. The center to face distances for the observed crystal form are listed in Table 9.4 [15], the resultant computer drawn morphology is shown in Fig 9.13(a). The {101}, {111} are the next most important forms. The {002}, {011},{021} and {020} forms are also observed. All the models predict morphologies with {110} dominant and with {101}, {011} and {020} forms present. None of the models predict the presence of the {002}, the IS model and the DH models also do not predict the {111} forms as being present. The AE and HP models show small {111} forms to be present.

Inspection of the computed morphologies shows that the HP and AE models give almost identical results. The HP approach involves identifying the intermolecular bonds in the slice from studying projections. Using these and bond energy values it is possible to estimate the slice energy. The AE model partitions the slice directly from the structure (see PCLEMC, Appendix C). The small differences between the HP estimated and AE calculated E_{att} values are due to the fact that the HP analysis only the stronger intermolecular bonds are considered. In the AE model calculated using PCLEMC all the intermolecular interactions are automatically considered. The HP and AE models both predict small {111} forms to be present. The DH and IS models do not probably due to an overestimation of the importance of the {101} and {011} forms. The DH model gives a largest surface area to the {020} form the IS model giving the smallest importance to the {020} form of all the models.

In general all the predicted morphologies are very similar. All predictions overestimate the importance of the {101} and {011} forms and this results in {021} and {020} not being observed in any predictions. This can be seen by viewing the calculated and observed morphologies down specific zones. Fig 9.14(a) shows the observed and calculated morphologies viewed down the [100] direction. The observed form has the {110} forms dominant at the front with the {020}, {021},{011} and {002} side forms. The calculted morphology shows the {110} main face and the {020} and {011} side faces. It does not show the {021} or the {002} forms. The crystal also appears to be short along the c-axis and long along the b-axis with reference to the observed morphology.

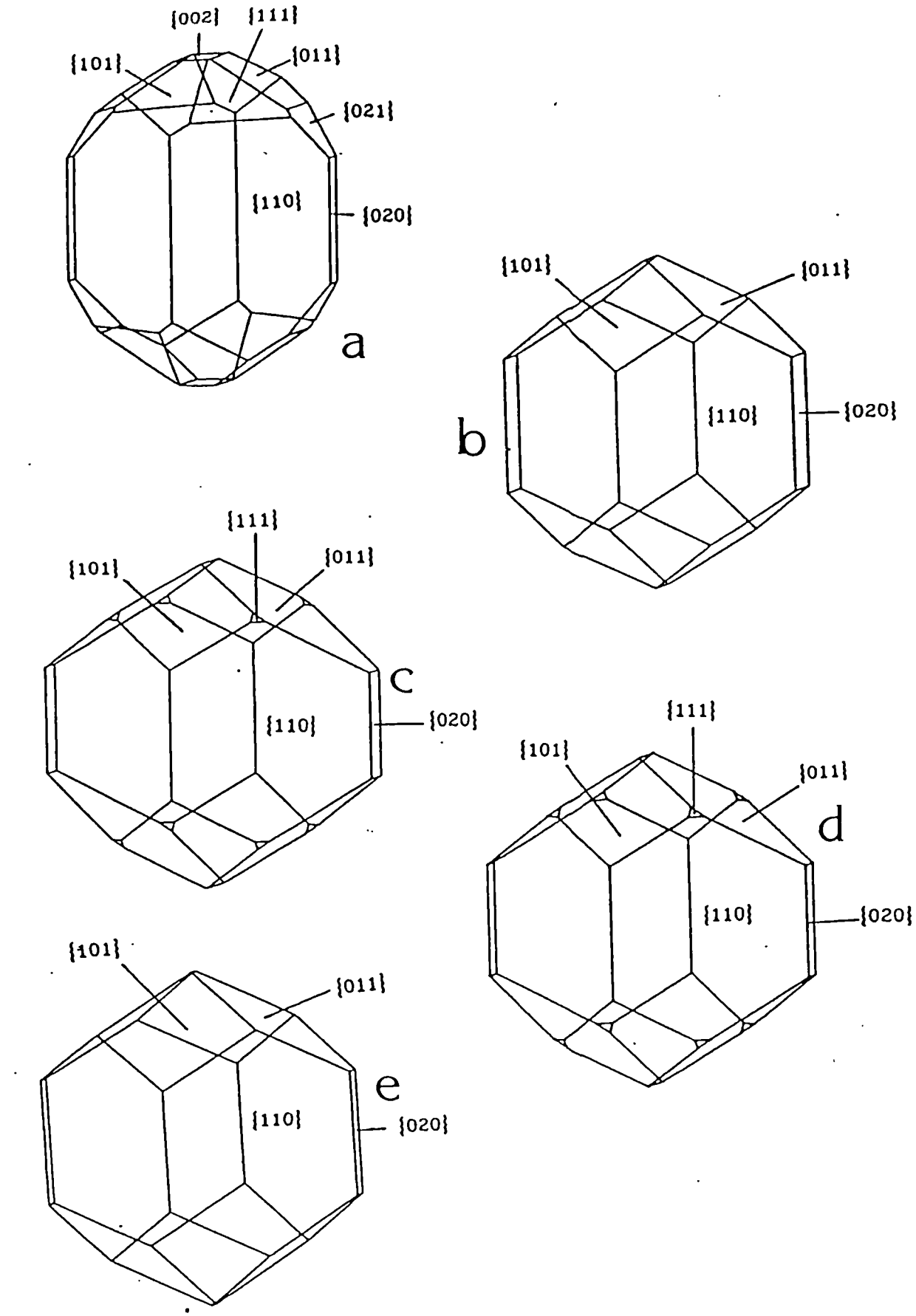

Figure 9.13 The morphologies of benzopheone

a) Observed [15] b) Donnay-Harker model

c) Hartman-Perdok model d) Attachment energy model

e) Ising model

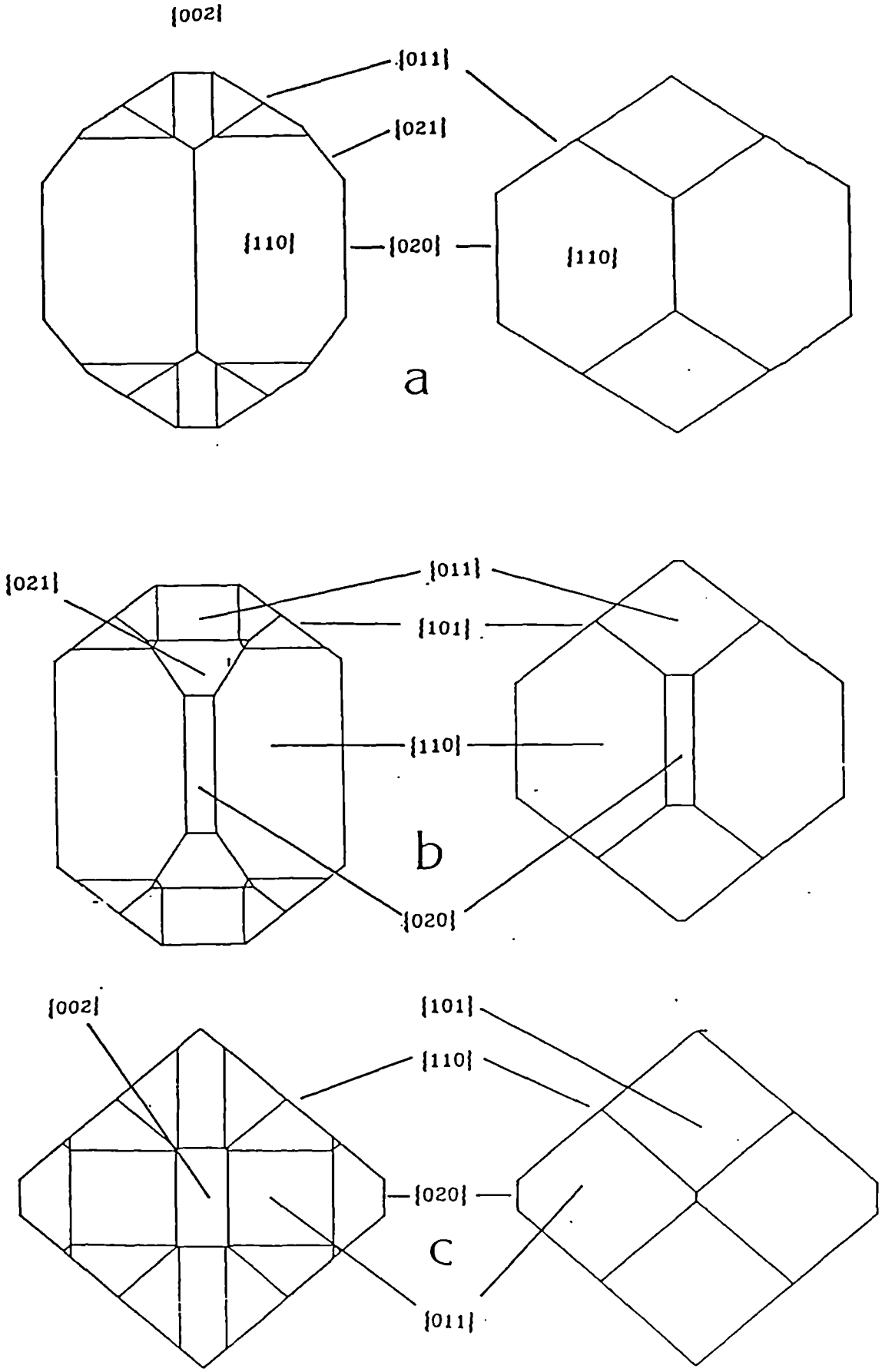

Figure 9.14 Comparsion of observed and calculated projections

a) down the [100]

b) down the [010]

c) down the [001]

Figure 9.14(b) shows the calculated and observed morphologies viewed along the [001] direction. The observed form shows the {020} front face with the {110} forms either side. The {011} and {021} forms can also be seen in this view. The calculated morphology shows the {020} and the {110} faces in a similar arrangement to the observed form. However the calculated morphology does not show the {021} but does show a much larger {011} form which excludes the {021}. These faces are in competition with each other. Overestimation of the importance of the one form results in the second not being observed in th final morphology. The view along the c-axis is a complicated one. The most important faces are the surrounding ones , the {110} and {020}. The calculated morphology shows good agreement down this zone with the same surrounding faces and the same general size and shape with the observed morphology.

The projection down the [001] direction shows the relative rates of the {110} and the {020} are in reasonable agreement with experiment. Using the estimated center to face distances for the observed morphology it is possible to scale, using the {110} form as a base value, 'experimental' attachment energies. This is shown in Table 9.6. Note the excellent agreement between the calculated and experimental values for the {020} and the {002} forms. The {021} and {111} forms are in reasonable agreement. However neither the {002} or the {021} forms appear on the calculated morphologies and this is due to the overestimation of the importance of the {101} and {011} This is clearly shown in Table 9.6

One possible reason for the difference in the calculated and observed morphology for the smaller faces may be the conformational freedom the phenyl rings have in the benzophenone molecule. The crystal structure has the rings tilted at 54° to each other. The rings are tilted at this angle to prevent H2–H21 repulsion which would be encountered at smaller tilt values. The rings could be tilted further apart since the H2–H21 non-bonded interaction is a relatively weak one. Table 9.6 shows the relative change in energy when the rings are tilted further apart. The calculations were carried out using MOPAC [8]. The results indicate that the rings can be tilted up to 85° apart with only a small loss in conformational energy. In the motherphase the benzophenone molecules are likely to have a range of phenyl-phenyl tilt values and some 'conformational correction' is required at the surface for the molecule to achieve the proper tilt for the crystal structure. This is likely to be surface specfic and will depend on the approach path/orientation of the molecule to get into the surface. The changes are likely to be small. However small changes in the growth rates can

have significant effects particularily when a number of faces may be competing. In benzophenone that area concerns the $\{021\}, \{101\}, \{111\}, \{011\}$ and $\{002\}$ forms. If we assume a reasonable description of the [001] zone side faces as indicated by the calculated and observed projections in Fig 9.14(c) then the growth rates of the $\{110\}$ and $\{020\}$ faces can be left fixed. If the importance of the $\{011\}$ and $\{101\}$ forms are reduced by 10 percent and the importance of the other forms in that are increased 10 percent *then the forms not previously* seen are now observed. The computed morphology assuming these corrections is shown in Fig 9.15. This is in excellent agreement with the observed form shown in Fig 9.13(a). This illustrates the sensitivity of a region where there are a number of competing faces to slight changes in relative growth rates.

9 Solvent Effects - Toluene

The morphology of benzophenone grown from toluene near the melting point differs considerably from that of the melt [9,15]. The morphology when grown from toluene is dominated by $\{021\}$ with $\{111\}$ and $\{110\}$ forms completing the morphology [8]. A computer drawn picture of this morphology is shown in Figure 9.16. In a similar approach to that adopted for tailor-made additives a molecule of toluene was built in INTERCHEM [7] and fitted to the phenyl ring in benzophenone. The co-ordinates if the toluene in terms of the host lattice were obtained using CRYSTLINK (see Appendix B). Figure 9.17 shows a toluene molecule fitted into the crystal lattice of benzophenone. The slice and attachment energies were then calculated with toluene as an additive. Table 9.8 shows the change in incorporation energy and the subsequent interaction of the toluene molecule with the oncoming molecules to the surface ($E_{att''}$). A positive value for $E_{att''}$ indicates that toluene is acting like a 'blocker' additive (see chapter 2 and 8) preventing molecules getting to the surface and affecting growth rate. Table 9.7 shows the changes in incorporation energy for all seven faces in benzophenone. Toluene molecules are most likely to get into faces where the least change in incorporation energy results. Toluene appears to be able to get into (021) at sites 2 and 4 with the least loss in energy. (111) at site 4 seems to be another candidate as a site for toluene incorporation and the four sites for (020). When in these sites the interaction with the oncoming molecules is preventing further growth. This indicates that (021) and (111) and possibly (020) should become more important. This is in agreement with what is found experimentally except that the (020) form is not observed. A possible

Table 9.5 Relative stability of benzophenone with different phenyl phenyl tilts. Change in energy relative to conformation in the crystal structure.

Phenyl-Phenyl Angle	Change in Energy (kcal/mol)
54	0
56	0.04
60	0.16
65	0.34
75	0.69
85	1.19

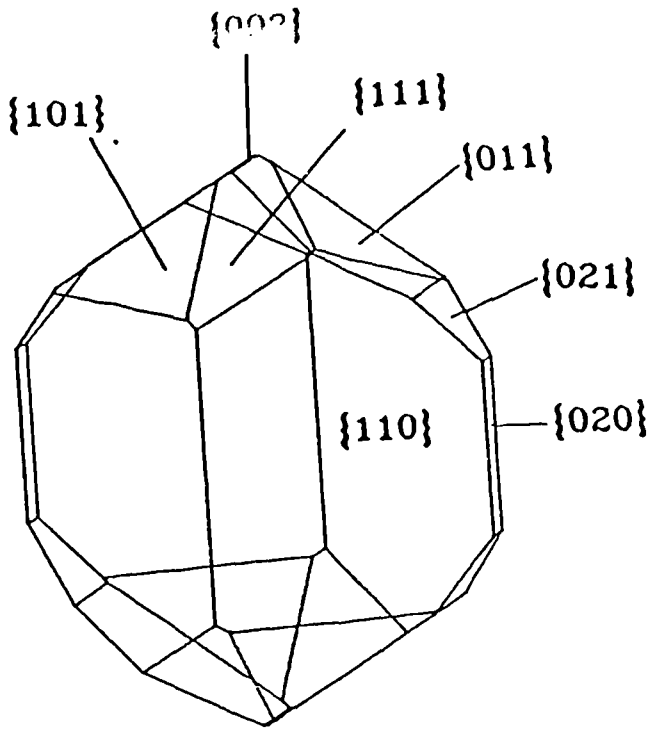

Figure 9.15 Morphology with slight corrections for the faces that were in greatest disagreement with that observed

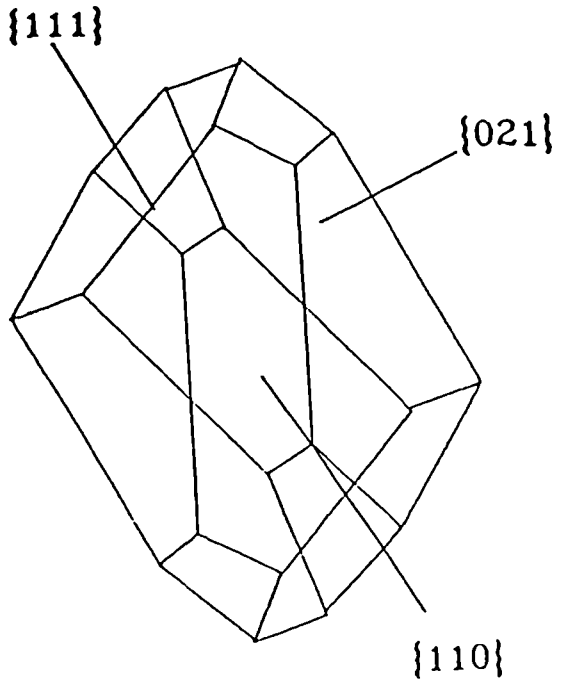

Figure 9.16 The effect of toluene on the crystal habit of benzopheone [9]

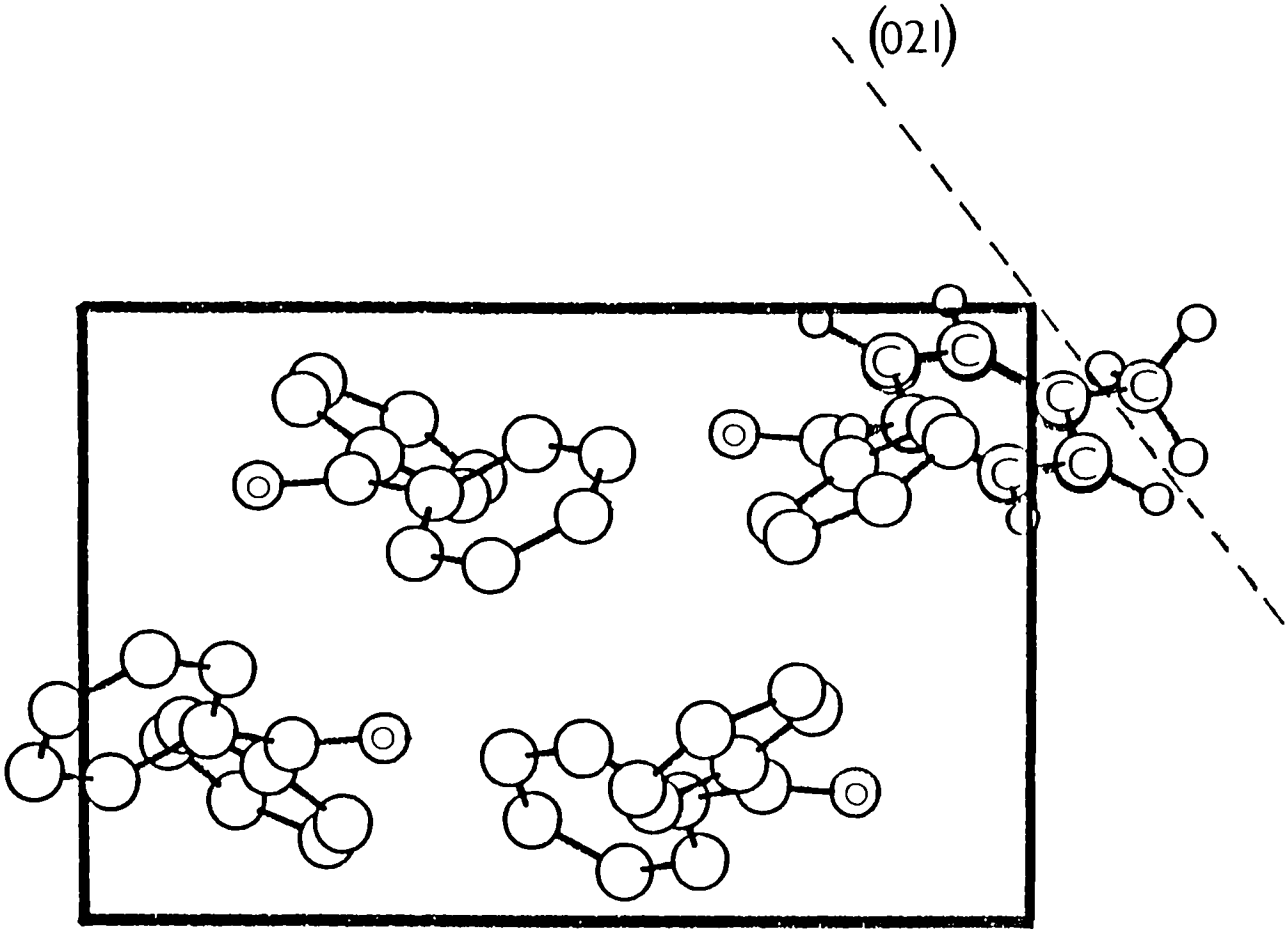

Figure 9.17 Toluene fitted onto one of the phenyl groups in benzophenone and blocking the (021) face. The oxygen and heavy atoms of toluene have been labelled for clarity.

Table 9.6 Calculated attachment energies compared against 'experimental' attachment energies scaled from the main observed form {110}.

FACE	ATTACHMENT ENERGIES (kcal/mol)	
	CALCULATED	EXPERIMENTALLY DERIVED
(110)	-10.3	-10.3
(101)	-12.9	-16.1
(011)	-12.0	-15.1
(020)	-14.6	-14.3
(111)	-14.1	-15.1
(021)	-14.9	-15.4
(002)	-17.1	-17.2

explanation is that (021) and (020) are developing in the same zone (see Fig 9.14(a) and if (021) is dominating then (020) would not be observed.

10 Discussion

All the current methods for interpreting crystal morphology in terms on internal structure give in the case of benzophenone the same predicted morphology which is good agreement with the observed form for the main faces. Overestimation of the importance of some faces results in some of the less important growth forms not being predicted. Slight reductions in the relative importance of these forms results in the smaller faces appearing on the predicted morphology. This example illustrates the sensitivity of a region, where a number of faces are present, to slight changes in relative growth rates.

Conformational calculations indicate that the phenyl rings in benzophenone tilted at 54° in the crystal structure can be tilted further with only slight changes in conformational energies. When a crystal is growing molecules may have a range of phenyl tilts in the motherphase which have to return to the crystal structure value to enter the structure. The degree of 'confomational correction' needed to enter the structure is likely to be surface dependent and may affect the rates of growth of some faces. In the traditional model of crystal growth the main parameters are diffusion to the surface, adsorption onto the surface, diffusion across the surface and incorporation into a kink site. It may be that an additional parameter considering conformational correction is required. Conformational correction may have a significant role in overall crystal shape determination and polymorphism. This is clearly an area where extensive molecular and quantum mechanics calculations could make a significant contribution.

The additive approach detailed in chapters 2,4 and 8 proved useful in interpreting the effect of toluene on the morphology of benzophenone. Calculations indicated that the (021) and (111) faces were the most likely for toluene molecules to get into. Once in these faces the calculations indicated that the toluene molecule is likely to block further molecules getting onto the surface and so alter the crystal shape i.e. make (021) and (111) faces more important. This is in good agreement with what is found experimentally. When grown from toluene the benzophenone morphology is altered with the (021) faces dominating the morphology. The {111} forms also have increased importance in crystals grown from toluene.

Table 9.7 Changes in incorporation energy and interaction with oncoming layer for the seven faces of benzophenone and toluene

FACE	SYMM	CHANGE IN INCORPORATION ENERGY	Eatt''
(101)	1	7.07	-0.42
	2	14.21	1.87
	3	14.24	-0.62
	4	7.10	8.70
(011)	1	15.63	2.57
	2	13.54	-1.98
	3	15.60	-2.24
	4	13.50	4.90
(021)	1	13.50	2.42
	2	5.50	-1.97
	3	13.50	-2.91
	4	5.60	10.07
(002)	1	11.76	-3.76
	2	11.76	-3.76
	3	11.77	3.02
	4	11.77	3.02
(111)	1	20.87	-3.82
	2	12.59	-2.12
	3	12.83	-0.80
	4	5.62	9.14
(110)	1	12.93	-1.46
	2	16.82	-3.93
	3	13.85	-0.71
	4	14.14	5.25
(020)	1	6.51	7.89
	2	6.49	-0.90
	3	6.49	-0.90
	4	6.51	7.89

11 Conclusions

1. All the methods employed essentially give the same predicted morphology.

2. The additive approach can be used to consider the effect of solvents.

3. Conformational correction may have to be considered in modelling crystal growth.

12 References

[1] P. Bennema, R. Docherty and K.J. Roberts (in preparation).

[2] L.M.A.J. Jetten (1983) PhD Thesis, University of Nijmegen.

[3] P. Bennema, L.M.A.J. Jetten, R. Docherty and K.J. Roberts. (in preparation).

[4] P. Bennema, B. Tack, K. Lewtas, J.J.M Rijpkema and K.J. Roberts. (to be published).

[5] P. Bennema and K.J. Roberts. (to be published).

[6] G.M. Lobanova, Sov. Phys. Soc. 13 (1968) 856.

[7] P. Bladon and R. Breckinridge, (1986) INTERCHEM University of Strathclyde.

[8] F.J. Seiler, (1986) MOPAC - Molecular Orbital Package. U.S. Air Force Acadamy, Colorado Springs.

[9] C.S. Yoon, (1986) Thesis University of Strathclyde.

[10] International Tables Vol A (1983) D.Riedel Publishing Company.

[11] L.M. Carruthers, F.A. Momany, R.F. Mc Guire and H.F. Scheraga, J. Phys. Chem. 78 (1978) 1595.

[12] J.G. Blok, C.G. de Kruif and J.C van Miltenburg, J. Chem. Thermodynamics 15 (1983) 129.

[13] P. Bennema and J.P. Van der Eerden. Morphology of Crystals, edited by I. Sunagawa pp (1-75). Terra Publishing Company (1987).

[14] J.J.M. Rijpkema (1984) Thesis, University of Nijmegen.

[15] R. Becker, H. Klapper, H. and T.S. Scheffen-Lauenroth (1983) poster presented at I.C.C.G -7 Stuttgart

Chapter 10

Conclusions and Suggestions for Further Work

CONTENTS

1 Introduction

The aims of this work were,

1. To develop programs in order for morphological investigations based on a knowledge of internal crystal structure to be carried out,

2. To develop a basic approach which contained guidelines for the use of these programs,

3. To use these programs to confront specific problems in relating crystal shape and structure including,

- a comparison of current methods,
- the importance of potential function choice,
- the effect of tailor made additives,
- solvent effects,
- polar morphology.

In the following section the results are summaried and conclusions drawn roughly in the order outlined above. Suggestions for further work are outlined in section 3.

2 Conclusions

2.1 Programs

Three programs have been written to carry out morphological calculations. CRYSTLINK, MORANG and PCLEMC have been tested against a variety of examples and the results presented in this thesis. The programs have also been used by other workers to confront examples of interest to them (see Appendix E). This also served as a useful test of the programs. MORANG has also been

made generally available through the submission of the code to the Computer Physics Communications Library in Belfast (see Appendix A and E).

MORANG and CRYSTLINK are highly sub-routined, menu-driven 'user-friendly' packages. PCLEMC in comparison remains slightly more awkward to use.

2.2 Basic Approach

The basic approach involves using the Donnay-Harker (DH) analysis as an initial guess of the important forms and the energy calculations as a further refinement. Energy calculations are considerably more computationally time consuming and so the calculations are concentrated on the top forms produced from the DH analysis. An arbitrary limit of the top ten forms was choosen. This has proved successful for all but one case. For glycine grown from sublimation one of the observed forms is not present in this top ten cut-off limit.

The calculation of the lattice energy has proved a useful step as it acts as a check of not only the input information but of the potential set being used to describe the intermolecular interactions. This is important test before time consuming slice and attachment energy calculations are undertaken.

The additive approach is basically a variation of the general approach. Particular care must be taken to get the additive co-ordinates in terms of the host lattice. A routine in CRYSTLINK allows this to be achieved if the molecular modelling software employed in the fitting procedure does not carry this to be out. This is the case with INTERCHEM [1].

2.3 Comparison Of Methods

Through all the work there has been a comparison of the Donnay-Harker (DH) morphologies with the attachment energy (AE) morphologies and in one particular chapter other methods currently favoured in the literature were applied to benzophenone. For materials without strong bonding in any directions such as anthracene and biphenyl (see Chapter 6) then the DH model is almost as good as the AE models. However when there is extensive directionally strong bonding such as in l-alanine and succinic acid then the DH model is not as good as the AE model. In both cases the DH analysis identifies the most important forms within the top ten list, however it gets the overall order of importance of these forms wrong. This is shown for l-alanine in Chapter 8 and succinic acid in Chapter 6. There is also some middle ground between these two extremes. For

materials like benzoic acid and benzamide there is some strong bonding but it is limited within dimers. The result is that the DH model is not bad as in the cases where there is extensive networked strong bonding.

In Chapter 9 the common current methods including DH, AE, Hartman-Perdok (HP) and Ising (IS) models were systematically applied to benzophenone. This was the first study of it's kind where all the methods were applied to one material. The result was that all the methods produce the same morphology. A subsequent study by Bennema, Roberts and Tack (unpublished results) has shown similar results for long chain hydrocarbons.

2.4 Importance Of Potentials

The interactions between molecules can be described by using a variety of potentials and a selection of parameter sets. In Chapter 6 a selection of potental functions/parameter sets were used in a study of compounds including anthracene, biphenyl succinic acid and benzoic acid. The result is that the AE method is relatively independent of the potential function choosen as long as the function choosen is giving a reasonable description of the intermolecular bonding. Comparing the lattice energy against the sublimation enthalpy is a simple and reliable check if the sublimation enthalpy is known.

2.5 Tailor-Made Additives

Calculations of the effects of the tailor-made additives are detailed in Chapter 8. The best calculation results were found for the disruptive additive type and the new proposed $E_{att''}$ parameter, which can be used to compute the morphology with an additive present, gave good correlation with experimental observations on the benzamide/benzoic acid host/additive system.

2.6 Solvent Effects

The additive approach gave an opportunity to consider particular solvent effects. Toluene has a significant effect on the morphology of benzophenone. Considering toluene as a tailor-made additive allowed interpretation of this effect. The calculations have been considered in greater detail in Chapter 9.

2.7 Polar Morphology

A number of parameters are thought to be responsible for polar morphology. These include solvent effects at the different surfaces exposed at the opposite ends of a polar direction and the different conformations flexible entities exposed at these surfaces can adopt. None of the current methods employed, whether AE, DH, IS, or HP can account for a polar morphology since they depend on bulk structural properties for their calculation. Urea is a planar molecule in both the solid state the gas phase. Urea grown from sublimation has a polar morphology. The polar morphology is therefore not a result of solvent effects or flexible entities. It was accounted for by considering the charge distributions of a urea molecule in the vapour phase, in the solid bulk and at a crystal surface and using a modification of the current attachment energy approach.

2.8 Conformational Correction

The calculations on benzophenone indicated that this molecule had some degree of conformational freedom. There maybe some need for the molecule to correct itself on entering the crystal structure. This highlighted a wider issue concerning crystal growth of organic molecules. Some organic molecules have a number of conformations which are about the same energy. The molecules are likely to adopt a range of these conformations and this could affect crystal growth. In different solvents different conformations may be adopted. This could explain why different polymorphs can be obtained from different solvents. This is an area which could benefit from extensive molecular mechanics/ quantum chemistry calculations. If the degree to which the molecule has to correct itself is surface dependent then this could explain slight differences in some predicted and observed morphologies.

2.9 Kinetic Roughening

When kinetic roughening occurs a transition takes place between smooth surface ordered growth and rough surface disordered growth (see Chapter 2). This can be observed by growing crystals at different levels of supersaturation. For biphenyl as the supersaturation increases [2] the (020) face disappears. The calculations in chapter 6 show that of the observed froms on biphenyl the {020} has the lowest slice energy and is therefore the weakest face and should be the first to roughen. The calculations suggest that the $(20\bar{1})$ face should be next to

roughen. This is in agreement with experiment [2]. The slice energies calculated therefore can give a feel for the faces that will roughen first and can thefore be used to predict the possible changes in habit which result from changes in supersaturation.

2.10 Competing Faces

When faces are growing out in the same general direction they can be regarded as being in competition. Small changes in the relative growth rates can result in what appears to be significant changes in morphology. For l-alanine the (120) and (110) faces are in competition and only slight changes are necessary to alter the size of each face appearing on the final morphology. For benzoic acid the (100) and $(10\bar{2})$ faces are competing and again only small changes are needed to switch the importance of one over the other. For anthracene the morphology usually has the (110) and $(11\bar{1})$ faces. Occasionally the $(11\bar{1})$ faces are not found. These two faces are competing faces and it only requires slight changes to in the importance of (110) to remove the $(11\bar{1})$ face. A useful feel for the degree of difficulty of changing a crystal shape can be found by altering the relative growth rates and recomputing the crystal shape.

3 Suggestions For Further Work

3.1 Programs

MORANG and CRYSTLINK are highly sub-routined programs which makes them easy to improve and debug. The main code of PCLEMC could be more routined hence making it easier to improve and debug.

In more general terms attempts should be made to produce a system of programs for morphological calculations. This should include the programs presented in this thesis PCLEMC, CRYSTLINK and MORANG as well as additional programs such as SHAPE [3] and TCCALC [4]. This would involve writing interfaces between the programs using the XR format file as the starting point and the means of communication with molecular modelling packages. The interface routines could be built in to CRYSTLINK easily and allow automatic assignment of atom type based on connectivity and bond distances, the picking up of the most common symmetery operators and the use of an extensive selection of potential functions. The aim would be to produce all the models

including Ising models with more reliability and in a shorter space of time than is the norm at present.

3.2 Additive Calculations

The additive calculation routines need improvement to deal with the blocker type of additives. The current approach works well for the disruptive type but gives only the likely sites for where the blocker additive can get into. One possible route would be to minimse the oncoming slice around the surface with the additive present to obtain a more realistic value for E_{att}". The surface and the part of the additive in the crystal surface could be constrained and the oncoming slice and exposed apart of the additive minimised. This would involve combining crystal packing calculations with molecular mechanics methods. Code is being developed under the Collaborative Computing Project (CCP) at Daresbury laboratory [5,6] to carry out these intra and intermolecular calculations.

The dispuptive additive approach works very well in the case on benzamide/benzoic acid but it would be useful to have more experimental information on adipic/succinic acid to confirm the accuracy of this approach.

3.3 Solvent Effects

The additive approach allowed the effects of toluene on the benzopheone crystal habit to be considered. A similar approach could be adopted for the non-linear optic material p-nitro-p'-methyl benzilidine aniline (NMBA). Calculations on this material have already been undertaken (see Appendix E). The habit of this material is known to be affected by toluene.

3.4 Polar Morphology

In the case of urea the polar morphology has beeen accounted for by consideration of surface, bulk and isolated molecule charge distribution. It would be useful to consider the role of these effects in the polar morphology of other materials. γ-glycine might prove to be a useful case study as it exhibits a polar morphology [7] and it is a small enough molecule to consider carrying out extensive quantum chemistry calculations. It does have flexible entities including the NH_3 group which is free to rotate. Quantum chemistry calculations could be employed to determine the degree of freedom of this group, the rest of the molecule could be held rigid. Studies of the crystallographic data on the other

amino acids might also reveal the most favoured conformations of the amino group. Manipulation of the additive code should allow PCLEMC to take into account the 'conformational correction' effect on crystal habit and the extent to which conformation is responsible for polar morphology. The conformational should also be used on other materials like benzophenone to investigate the effect of conformational freedom for the molecule in the motherphase on the final crystal habit.

4 References

[1] INTERCHEM, P. Bladon and R. Breckinridge, University Of Strathclyde (1986).

[2] H.J. Human, J.P. van der Eerden, L.M.A.J. Jetten and J.G.M. Oderkerken. J. Cryst. Growth 51 (1981) 589.

[3] E. Dowty, Amer. Miner. 65 (1980) 465.

[4] TCCALC, J.J.M. Rijpkema, PhD Thesis, University Of Nijmegan (1984).

[5] THBFIT, M. Leslie, SERC Daresbury Laboratory, England, Warrington.

[6] W. Smith, J. Mol. Graphics 5 (1987) 71.

[7] L.J.W. Shimon, M. Lahav and L. Leiserowitz, Nouveau Journal de Chemie (in press).

Appendix A

MORANG

CONTENTS

1 Introduction

One method of determining crystal growth morphology is to compare the observed interfacial angles with calculated interplanar angles, allowing the identification of the forms present on the crystal habit. These calculations can be carried out by hand but it is more convenient to perform the calculations on a computer. A simple Fortran program (MORANG) has been written to help in determining crystal morphology allowing not only the calculation of the angles between planes but also the identification of the forms likely to dominate the crystal habit.

The computer program MORANG described here can be considered to consist of three main routines ANGLE, MORPH2 and MAID. The ANGLE routines carry out the calculation of angles between crystal planes and directions (i.e plane-plane, direction -direction and pole-direction angles). MORPH2, a modified version of MORPH [1] allows the identification of the planes (hkl) likely to dominate the crystal habit, the morphologically important forms {hkl} having the greatest interplanar spacing (d_{hkl}). This approach was pioneered by Bravais-Friedel [2] and later developed by Donnay-Harker [3] to take into account the reduction of interplanar spacings due to space group symmetry. A reduction in the interplanar spacing of a crystallographic form results in a reduction of the morphological importance of that form. This method has been used by a number of workers in predicting crystal morphology [1,2,3,4] and used as an initial guess of the important forms before further refinement of the morphological prediction by energy calculations [5].

MAID is the Morphological Aid section of the program which uses routines called by ANGLE and MORPH2 to obtain the angles between the planes likely to dominate the crystal shape. The user can then obtain the interplanar angles for the morphologically important forms in a given zone and if the user inputs a measured interfacial angle and estimated error, the program searches and outputs the possible planes.

2 Calculation Details

The program uses the relationships for direct and reciprocal lattice along with the equations for calculating the interplanar angles and spacings given for the generalised triclinic case in International Tables for X-ray Crystallography [6].

2.1 Reciprocal Lattice

For a unit cell of dimensions a,b,c,α,β and γ, the unit cell volume V is given by the equation,

$$V = 2abc(sin(S)sin(S-\alpha)sin(S-\beta)sin(S-\gamma))^{1/2} \qquad (A.1)$$

$$S = (\alpha+\beta+\gamma) \qquad (A.2)$$

The reciprocal lattice elements denoted by the * superscript (i.e. a*, b*) can be obtained from the relationships:

$$a^* = bcsin\alpha/V$$

$$b^* = casin\beta/V \qquad (A.3)$$

$$c^* = absin\gamma/V$$

and the cosines of α^* etc are given by:

$$\begin{aligned} cos\alpha^* &= [(cos\beta cos\gamma - cos\alpha)/sin\beta sin\gamma] \\ cos\beta^* &= [(cos\gamma cos\alpha - cos\beta)/sin\gamma sin\alpha] \\ cos\gamma^* &= [(cos\alpha cos\beta - cos\gamma)/sin\alpha sin\beta] \end{aligned} \qquad (A.4)$$

These values are calculated in the sub-routine SETUP (see section 3.3) a sub-routine called by the routines in MORPH2 and ANGLE.

2.2 Interplanar Angles

The interplanar angle ϕ between two planes (hkl) and (h'k'l') can be calculated from the equation

$$\begin{aligned} cos\phi = [(hh'a^*2 + kk'b^* + ll'c^*2 + (kl'+lk')b^*c^*cos\alpha^* + (lh'+hl')c^*a^*cos\beta^* \\ +(hk'+kh')a^*b^*cos\gamma^*)/\sqrt{(Q^*_{hkl}Q^*_{h'k'l'})}] \end{aligned} \qquad (A.5)$$

where Q^*_{hkl} is the so-called quadratic form given in (A.6).

$$Q^*_{hkl} = h^2a^{*2} + k^2b^{*2} + l^2c^{*2} + 2klb^*c^*cos\alpha^* + 2lhc^*a^*cos\beta^* + 2hka^*b^*cos\gamma^* \quad (A.6)$$

The equation for the angle θ between two directions [uvw] and [u'v'w'] is of the same form as equation (A.5) replacing h,k,l,h',k'l' with u,v,w,u',v',w' and the reciprocal lattice elements with direct lattice elements as shown in equation (A.7) and (A.8).

$$cos\theta = [(uu'a^2 + vv'b^2 + ww'c^2 + (vw' + wv')bccos\alpha + (wu' + uw')cacos\beta + (uv' + vw')abcos\gamma)/\sqrt{(Q_{uvw}Q_{u'v'w'})}] \quad (A.7)$$

where Q_{hkl} is the modified quadratic form given in (A.8).

$$Q_{hkl} = u^2a^2 + v^2b^2 + w^2c^2 + 2vwbccos\alpha + 2wucacos\beta + 2uvabcos\gamma \quad (A.8)$$

A plane normal (pole) -direction angle can be calculated from a combination of the plane-plane equation (A.5) and direction- direction equation (A.7) explained above. The angle μ between a crystal pole (hkl) and direction [u,v,w] is, allowing for elimination of combinations of direct and reciprocal lattice given in equation (A.9) These equations are used in the ANGLE routines, ANGPOL, ANGDIR and ANGPDR respectively (see section 3.3).

$$cos\mu = hu + kv + lw/\sqrt{(Q^*_{hkl}Q_{uvw})} \quad (A.9)$$

2.3 Interplanar Spacings

The MORPH2 routines allow the calculation of the interplanar spacing for selective Miller indices or the identification of the most important morphological forms (hkl) according to interplanar spacings. Both these options require the calculation of interplanar spacing d_{hkl} and this is obtained using equation (A.10)

$$d_{hkl} = 1/\sqrt{Q^*_{hkl}} \quad (A.10)$$

where Q^*_{hkl} is as defined in the section 2.2.

2.4 Zone Laws

One of the options in the morphological aid section of the program is the calculation of all the angles for the planes in a given zone. A plane (hkl) lies in a zone [uvw] if the relationship outlined in equation (A.11) holds true [6].

$$hu + kv + lw = 0 \qquad (A.11)$$

3 Program Description

3.1 Machine Requirements

The program is written in standard Fortran-77 (American National Standard ANSI X3.9 1978) and has a code area size of 23.9K. The program has been compiled on a VAX 11/782 with Digital's VAX-11 Fortran Compiler and on an IBM-AT with the IBM Fortran compiler (Version 2.00) without any changes to the source code. It should be possible to run the program on any machine which supports a standard Fortran-77 compiler without any changes. The executable code generated on the IBM was used directly on an AMSTRAD 1512 indicating that it should be possible to run the executable code on a number of 'PC-compatibles' without any need to change and recompile source code.

3.2 Program Operation

The program is interactive and menu driven. The main menu appears after input of a title, crystal system and unit cell information. This input becomes the default cell parameters, users are given the option to change these parameters on entering any of the sub-options. The main menu gives the option to run either ANGLE or MORPH2 individually or to run the MAID routines which call some of the ANGLE and MORPH2 sub-programs. ANGLE gives a menu with options to calculate the angles between crystal planes and directions. MORPH2 allows either the calculation of the interplanar spacing for a given set of Miller indices or the identification of the morphologically important forms according to interplanar spacings. Users will be prompted for the input information required, default values have been supplied where ever possible. The input information for each of the main routines will be discussed in section 4. The program gives the user the option to write results to a file as well as to the screen. The file is opened whilst running the program usually on entering one of the options.

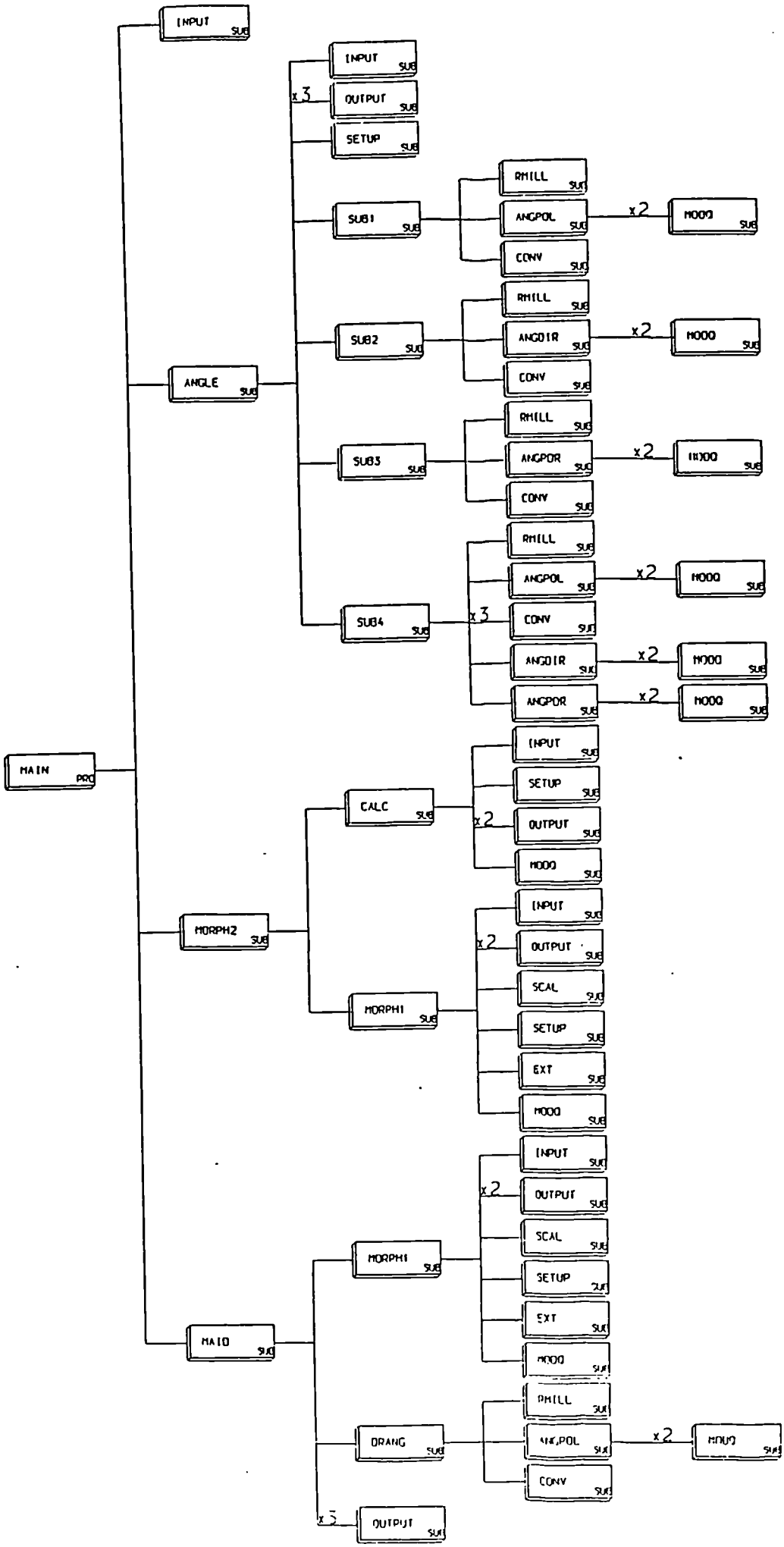

Figure A.1 Schematic of the routines in the program MORANG.

The user will be prompted for the output filename, the file will be automatically closed on the exiting of one of the sub-programs.

3.3 Main Subroutines

The routines used in the MORANG program are outlined in this section. The routines are listed with the MAID routines first, followed by the ANGLE and MORPH2 routines and finally the general routines. Figure A.1 is a schematic of the modules in MORANG. The chart clearly shows the MAIN program and the sub-menus ANGLE, MORPH2, MAID and the various routines used by these options. Routines called more than once are labelled by the number of times they are called. Routine OUTPUT for example is called twice, firstly to open and then to close an output file.

SUBROUTINE MAID - the interface between ANGLE and MORPH2. The program contains the menu for the zone and observed angle options.

SUBROUTINE DRANG - Calculates all the interplanar angles for the likely planes identified as the most important by the MORPH1 routines. This routine is called by MAID.

SUBROUTINE ANGLE - Contains the menu for the ANGLE options.

SUBROUTINE ANGPOL - Calculates the cosine of the angle between two crystal planes.

SUBROUTINE ANGDIR - Calculates the cosine of the angle between two crystal directions.

SUBROUTINE ANGPDR - Calculates the cosine of the angle between a plane normal (pole) and a direction.

SUBROUTINE SUB1 - Interactive routine for calculating the angle between two planes.

SUBROUTINE SUB2 - Interactive routine for calculating the angle between two crystal directions.

SUBROUTINE SUB3 - Interactive routine for calculating the angle between a plane normal and a crystal direction.

SUBROUTINE SUB4 - Interactive routine which uses the functions available in SUB1, SUB2 and SUB3 to calculate the three angles for a given pair of indices.

SUBROUTINE CONV - Converts the cosine of an angle to degrees.

SUBROUTINE RMILL - Converts Miller indices read in as integers to real numbers for calculations.

SUBROUTINE MORPH2 - Contains the menu for MORPH2 routines.

SUBROUTINE MORPH1 - Calculates the interplanar spacings for various faces identifying the most important planes according to interplanar spacings. This is largely the program MORPH [1] with some modifications. Firstly the program now operates in two modes, when called from the MAID routines it assumes some default input values and directs the output into common blocks rather than the screen. Secondly the program calculates interplanar spacings rather than recticular area and thirdly the input and output format has been changed to allow interactive input and output. The actual changes have been highlighted with comments in the source code.
SUBROUTINE EXT - Removes the forbidden reflections according to the extinction conditions for the space group in question.
SUBROUTINE SCAL - Calculates the default scan values for h,k and l based on the unit cell parameters. The smallest unit cell parameter is given a scan value of -7 to +7, the rest are scaled relative to that. The larger the unit cell the smaller the scan required. This routine gives the user the option to replace these default values.
SUBROUTINE CALC - Interactive calculation of the interplanar spacings for selective Miller indices.
SUBROUTINE SETUP - Calculates direct and reciprocal lattice elements as outlined in section 2.1
SUBROUTINE MODQ - Calculates the direct and reciprocal lattice moduli. This routine called by the ANGLE routines and by MORPH1 and CALC.
SUBROUTINE INPUT - Gets the general input information including title, crystal system and unit cell dimensions. This information is used by most routines.
SUBROUTINE OUTPUT - This routine operates in two modes. In the first mode it gets the output filename and opens the file for writing results through channel 6. In mode two the the routine closes the file this occurs after exiting one of the routines.

4 Input Requirements

As mentioned earlier, the program is interactive in nature prompting the user for the information required. Default values are supplied as input options where possible. In this section the input information for the various sections is summarised.

4.1 ANGLE

The angle routines require a title, the unit cell dimensions and the Miller indices to be considered. The user is prompted for the general input information via the INPUT routine (see section above). The user is then presented with a menu and after selecting the option required the user will be prompted for Miller indices of the planes to be considered. Output is to the screen and a file if required, square brackets indicate a crystal direction, round brackets a crystal plane and no brackets a pole (see TEST OUTPUT 2).

4.2 MORPH2

When calculating the selective interplanar spacings the general input is obtained via the INPUT routine. The user will then be prompted for the Miller indices of the planes whose interplanar spacing (d_{hkl}) is to be calculated. When identifying the planes likely to dominate the crystal morphology the general input required is basically the title and unit cell dimensions. Additional input required includes the number of planes to be outputted, the scan values for the Miller indices and the extinction conditions for the space group in question as given in International Tables for Crystallography [6]. These rules for the extinction of x-rays are identical to the conditions when a reduction of the interplanar spacing occurs due to space group symmetry. If the interplanar spacing is reduced the morphological importance of a crystallographic form is also reduced [2]. This input requires a name identifer, an extinction condition and an integer. The name identifiers possible are listed below along with the extinction conditions and their numerical labels.

NAME IDENTIFIERS:

hkl-(1), hhl-(2), hkh-(3), hll-(4), hh0-(5), 0kl-(6), h0l-(7), hk0-(8), h00-(9), 0k0-(10), 00l-(11).

EXTINCTION CONDITIONS:

h+k,k+l= -(1), h+k= -(2), h+l= -(3), k+l= -(4), h+k+l= -(5) -h+k+l= -(6), h= -(7), k= -(8), l= -(9), 2h+l= -(10), 2h+k= -(11), 2l+h= -(12).

Using the numbers to represent the conditions the input to the program consists of a three number code to identify the extinction condition. An example is for organic compound l- alanine which crystallises in the orthorhombic space group $P2_12_12_1$. There are three extinction conditions given in International Tables [6] and these are given below along with the code for entering into the program.

CONDITION	INPUT CODE
h00 h=2n	9 7 2
0k0 k=2n	10 8 2
00l l=2n	11 9 2

4.3 MAID

This routine uses the ANGLE and MORPH2 routines the input required being identical to that outlined in the two previous sections. The user will be prompted for a zone [uvw] or for an observed interfacial angle and estimated error.

5 Output

The program outputs results to the screen and to a file if the user requires it . The file is opened via the OUTPUT routine when entering one of the sub-program units. This file is automatically closed on exiting the routine.

At the end of this appendix samples of the output from the program are given for the organic material l-alanine. An observed interfacial angle of 45.6±0.3°[7] was used as input to the morphological aid routine, the extinction conditions for this material and their input code was given in section 4.2. The unit cell dimensions are given in the test input summary which contains all the information used to generate the test output files given at the end of this appendix and outlined in the test output summary.

6 Test Input Summary

Title: L-alanine
Crystal System: Orthorhombic
Unit cell dimensions: a = 6.025Å, *b* = 12.324*Å*, c = 5.783Å [8]
Extinction Conditions: h00 h=2n, 0k0 k=2n, 00l l=2n.
Observed Angle: 45.6°
Error: 0.3°

7 Test Output Summary

TEST OUTPUT 1 - The identification of the morphologically important forms according to interplanar spacing. Output file created using default options when

TEST OUTPUT 1

l-alanine

CELL PARAMETERS
a = 6.02500(ANGSTROMS)
b = 12.32400(ANGSTROMS)
c = 5.78300(ANGSTROMS)
alpha = 90.00000(DEGREES)
beta = 90.00000(DEGREES)
gamma = 90.00000(DEGREES)

MILLER INDICIES ARE:-
H= -6 TO 6, K= -3 TO 3, L= -7 TO 7

EXTINCTION CONDITIONS

h00: h =2n
0k0: k =2n
001: l =2n

MORPHOLOGICAL IMPORTANCE	FACE H	K	L	MULTIPLICITY	SLICE THICKNESS (ANGSTROMS)
1	0	2	0	2	6.16200
2	1	-1	0	4	5.41278
3	0	1	-1	4	5.23527
4	1	-2	0	4	4.30794
5	0	2	-1	4	4.21682
6	1	0	-1	4	4.17213
7	1	1	-1	8	3.95182
8	1	2	-1	8	3.45474
9	1	-3	0	4	3.39413
10	0	3	-1	4	3.34903
11	2	0	0	2	3.01250

TEST OUTPUT 2

l-alanine

CELL PARAMETERS
a = 6.02500(ANGSTROMS)
b = 12.32400(ANGSTROMS)
c = 5.78300(ANGSTROMS)
alpha = 90.00000(DEGREES)
beta = 90.00000(DEGREES)
gamma = 90.00000(DEGREES)

(0 2 0)	(1 2 0)	ANGLE= 45.64(DEGREES)
(0 2 0)	(1 1 0)	ANGLE= 63.95(DEGREES)
(1 1 0)	(1 2 0)	ANGLE= 18.30(DEGREES)
[0 2 0]	[1 1 0]	ANGLE= 26.05(DEGREES)
[0 2 0]	[1 2 0]	ANGLE= 13.74(DEGREES)

TEST OUTPUT 3

l-alanine

CELL PARAMETERS
a = 6.02500(ANGSTROMS)
b = 12.32400(ANGSTROMS)
c = 5.78300(ANGSTROMS)
alpha = 90.00000(DEGREES)
beta = 90.00000(DEGREES)
gamma = 90.00000(DEGREES)

-- PLANES --						ANGLES (DEGREES)		
						OBSERVED	ERROR	CALCULATED
0	-2	0	-1	-2	0	45.60	.30	45.64
0	-2	0	1	-2	0	45.60	.30	45.64
0	2	0	1	2	0	45.60	.30	45.64
0	2	0	-1	2	0	45.60	.30	45.64
-1	-2	0	0	-2	0	45.60	.30	45.64
1	2	0	0	2	0	45.60	.30	45.64
-1	2	0	0	2	0	45.60	.30	45.64
1	-2	0	0	-2	0	45.60	.30	45.64

possible. The term 'multiplicity' in the output is the number of of symmetrically equivalent forms.
TEST OUTPUT 2 - The file produced during angle option
TEST OUTPUT 3 - Output from the morphological aid option. File created using default options except in the input of error.

8 References

[1] E. Dowty. Amer. Miner. 61 (1976) 448.
[2] A. Bravais. Etudes Crystallographiques Paris (1913).
[3] J.D.H Donnay and D. Harker. Amer. Miner. 22 (1937) 463.
[4] P. Hartman. J.Cryst.Growth 49 (1980) 521.
[5] R.Docherty and K.J.Roberts. J.Cryst. Growth. 88 (1988) 159.
[6] International Tables For X-ray Crystallography Kynoch Press Birmingham. Vol II (1973) p106.
[7] R.Docherty, K.J. Roberts and S.N. Black. (unpublished results).
[8] M.S. Lehmann, T.F. Koetzle and W.C. Hamilton. J. Amer. Chem. Soc. 94 (1972) 2657.

Appendix B

CRYSTLINK

CONTENTS

1 Introduction

As outlined in chapter 4, CRYSTLINK was developed as a support program to the project as the work progressed. It contains a series of routines for data manipulation. A summary of the menus available in CRYSTLINK and where the options provided fit into the overall scheme has been given in chapter 4. In this section details of the program are outlined including a summary of the important routines/variables and how to change CRYSTLINK for other computer systems. Details of the calculations carried out in the program are given in section 2.

2 Calculation Details

2.1 Crystal to Cartesian Co-ordinates

Some of the computer packages used in this work require cartesian co-ordinates rather than crystal co-ordinates as input. This means it is necessary to convert from one co-ordinate system to another. CRYSTLINK uses the same procedure as the VIEW program in Daresbury Laboratory [1]. Crystal co-ordinates (x,y,z) can be converted to cartesian co-ordinates (x',y',z') by multiplication with the matrix A.

$$\begin{pmatrix} x' \\ y' \\ z' \end{pmatrix} = A \begin{pmatrix} x \\ y \\ z \end{pmatrix} \qquad (B.1)$$

$$A = \begin{pmatrix} a & bcos\gamma & ccos\beta \\ 0 & bsin\alpha & M \\ 0 & 0 & N \end{pmatrix} \qquad (B.2)$$

$$M = (c(cos\alpha - cos\beta cos\gamma)/sin\gamma) \qquad (B.3)$$

$$N = (V/(absin\alpha) \qquad (B.4)$$

V is the unit cell volume which can be calculated from equation (A.1) given in Appendix A, a,b,c, α, β and γ are the unit cell dimensions. The matrix is setup in the routine MATRIX , the calculation of cartesian co-ordinates takes place in the routine ORTHOG (see following section).

2.2 Cartesian to Crystal Co-ordinates

One of the major purposes for writing CRYSTLINK was to obtain crystal co-ordinates from molecular graphics packages which work in cartesian co-ordinate systems. After the fitting of hydrogens to incomplete structures or obtaining the co-ordinates of an additive in terms of a host lattice it is necessary to have the co-ordinates in crystal axis system. The importance of this has been discussed in Chapter 4.

This requires a reversal of the procedure carried out in the previous section. Cartesian co-ordinates (x'y'z') can be converted to crystal co-ordinates (x,y,z) by multiplication by the inverse of matrix A.

$$\begin{pmatrix} x \\ y \\ z \end{pmatrix} = A^{-1} \begin{pmatrix} x' \\ y' \\ z' \end{pmatrix} \qquad (B.5)$$

This inversion procedure is carried out by the routine INVERT which calls the NAG library [1] routine F01AAF. The routine will notify the user if the matrix inversion fails. The variable IFAIL is carried into the routine with a value of 0 and flagged to 1 if any problems result during inversion.

2.3 Packing Diagrams

As described in chapter 2 using the co-ordinates of one molecule and the symmetry relations between the molecules in the unit cell it is possible to generate a 3D model of the crystal. This routine uses a standard file from the CSSR database [2] which contains co-ordinates and connectivity and a file containing the symmetry operators from International Tables [3] in the format adopted for PCLEMC (see chapter 5 section 4). The routine generates a unit cell, repeated production of the unit cell in the three crystal directions U, V and W allows a 3D model to be built. The user is prompted for the values of U, V and W. The output file is in the same format as the CSSR input file allowing it to be used as input to a variety of molecular graphics packages and back into the data formatting routines available in CRYSTLINK. The output file contains the new co- ordinates of the atoms in the crystal and the updated connectivity. The file is limited in size to 999 atoms by the format of the CSSR file. This routine was used to produce packing diagrams in this thesis as well as generating the files for simulating quantum chemistry calculations on molecules in the crystal lattice (see chapter 7). This routine is currently being incorporated into the computer

modelling program LEGO [4].

2.4 Slice Diagrams

The generation of the slice diagrams follows the same procedure as that for packing diagrams. The user will be prompted for the same input information as before and the Miller indices of the slice to be considered. The program starts to generate a 3D model of the crystal but utilises the slice definition procedure used in PCLEMC (see Appendix C) to decide which molecules are inside the slice and which are not. The co-ordinates of molecules within a slice are stored in a file, molecules outside the slice are disregarded. The thickness of the slice is defined by the interplanar spacing d_{hkl} (see Chapter 1, section 4), the procedure for deciding which molecules are inside the slice has been given in chapter 5. The output file is in the CSSR format allowing these files to be used as input to a variety of molecular graphics packages.

2.5 Centre of Gravity

The centre of gravity of a molecule (x_g, y_g, z_g) can be calculated from the summations given below.

$$x_g = \sum_{i=1}^{N} x_i A_i / MW$$

$$y_g = \sum_{i=1}^{N} y_i A_i / MW \qquad (B.6)$$

$$z_g = \sum_{i=1}^{N} z_i A_i / MW$$

where (x_i, y_i, z_i) are the fractional co-ordinates of atom i which has an atomic number A_i. N is the number of atoms in the molecule and MW is the molecular weight of the molecule.

3 Program Description

3.1 General Details

The program is written in Vax Fortran [5] and consists almost entirely of subroutines. This allows easy modifications and updates. Important variables are passed into the subroutines via common blocks including CELL for the unit

cell dimensions, COORDS for the co-ordinates of the atoms and CONN for the connectivity. The common blocks are held in the file COMMON.FOR which is included into the program during compilation. The program is currently limited to 2000 atoms and to the most common organic elements. This could be increased if required. The program uses channels 5 and 6 for input and output respectively. The program uses some file handling options particular to the VAX computing system. When reading in a file the program uses the INQUIRE option to check the file exists before opening for reading. If the file does not exist the user is prompted for another file name. When opening a file for writing output the program uses the CARRIAGECONTROL=LIST option. This option determines the type of carriage control processing to be embedded into the file. In essence the use of this particular option creates a data file as output rather than a 'results' file. This allows the outputted file to be changed using the system editor if required (keywords may have to be changed for non-standard calculations).

3.2 Program Operation

On executing the program the user will be faced with the main menu from which four sub-menus may be accessed. On entering a sub-menu the user will be faced with a number of options. On choosing an option the user will be prompted for the input information required. On exiting one of the options any file opened will be closed and the user returned to the current menu. Figure B.1 shows a schematic of the overall structure of the program CRYSTLINK. The diagram clearly shows the four menu's accessible from the main program and the routines called by these menu's. Routines called more than once are highlighted with the number of calls being written alongside the routine box. The external module F01AAF is highlighted in a shaded box. A summary of these routines follows in section 3.4 .

3.3 Program Input

The primary source of input to the program is a file from the CSSR database [2]. A file from the CSSR database is shown in Figure B.2. The file contains the unit cell dimensions on lines 1 and 2, lines 3 and 4 contain information used by the database. The bulk of the information is held in the subsequent lines. It can be divided up into a number of columns. Column 1 is the atom number, column 2 consists of the atom label, columns 3, 4 and 5 are the crystal co-ordinates

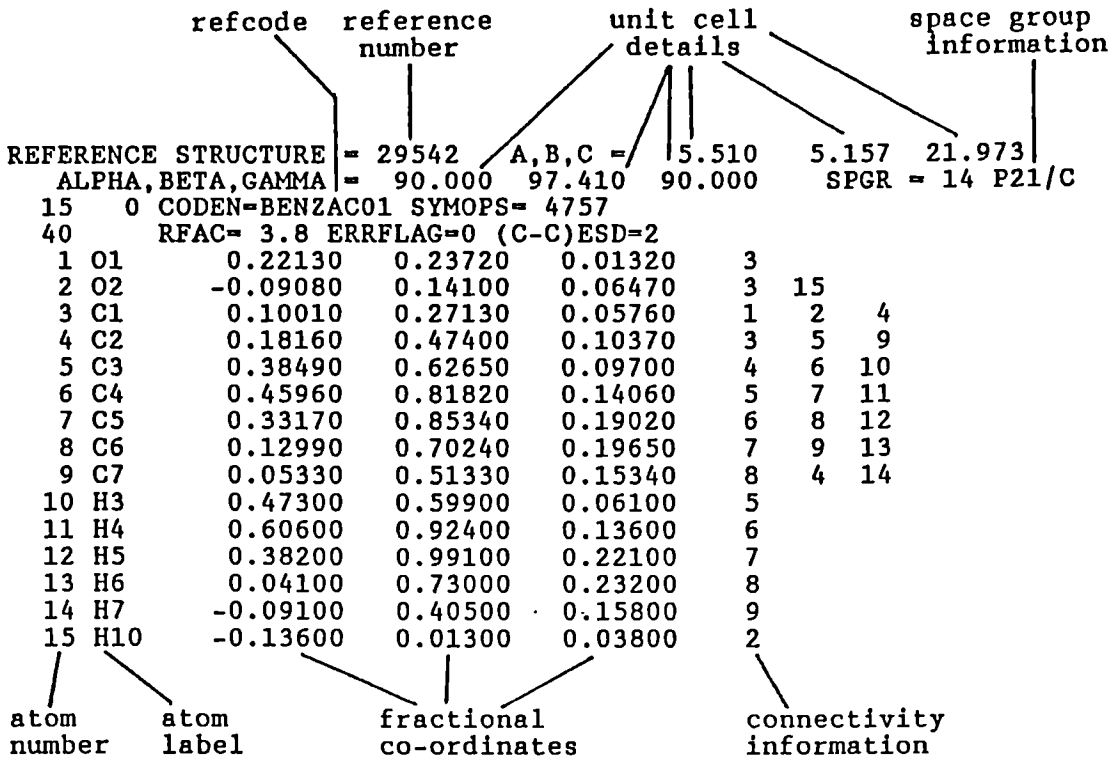

Figure B.2 Typical XR file format.

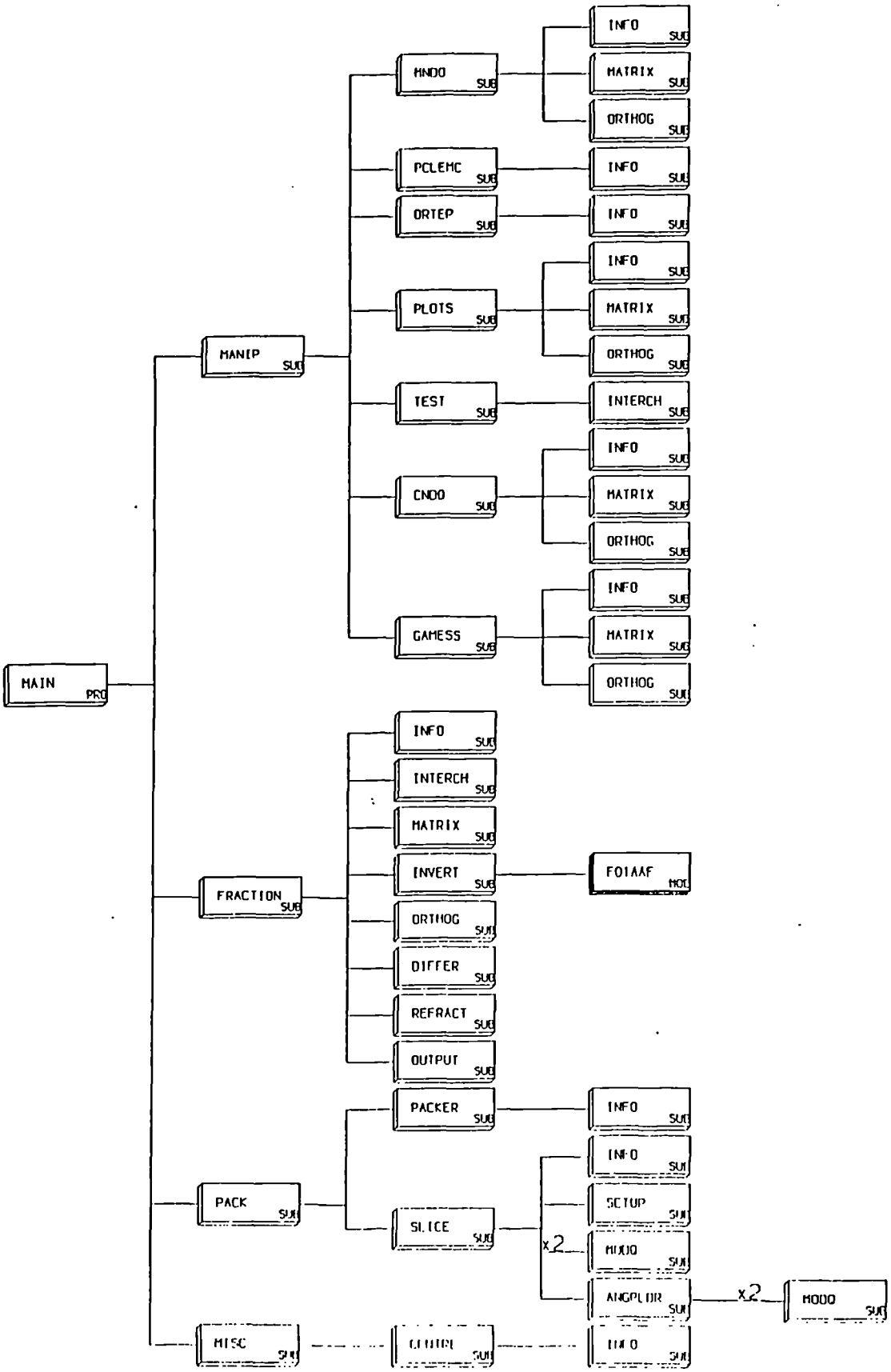

Figure B.1 Schematic of the routines in the program CRYSTLINK.

relative to the unit cell dimensions given in lines 1 and 2. The later columns consist of the connectivity information. This information tells the molecular graphics package which atoms are connected. For organic crystals this usually consists of four columns due to the common tetrahedral arrangement present around carbon atoms. The format of the file allows for the possibility of eight connections.

On entering the packing options the user will be required to input the symmetry operators which relate one molecule to the others in the unit cell. The input format is identical to that adopted for PCLEMC (see chapter 5, section 5). The program will also read in a 'D' type file from INTERCHEM [6].

3.4 Program Routines

The module chart given in Figure B.1 shows where each routine is used. In this section a brief summary of each of the routines is given.
MAIN PROGRAM - The main section of the program contains the main menu.
SUBROUTINE MANIP - This subroutine contains the menu for the data manipulation routines.
SUBROUTINE FRACTION - this is the driver routine which converts cartesian co-ordinates to crystal co-ordinates.
SUBROUTINE PACK - this is the driver routine which provides the sub-menu for packing options.
SUBROUTINE MISC - this is the menu routine containing the miscellaneous options.
SUBROUTINE INFO - this routine reads in the the information from the Daresbury CSSR file, including the unit cell dimensions, atomic co-ordinates and connectivity.
SUBROUTINE MNDO - converts input information from INFO into a format acceptable to MNDO [7].
SUBROUTINE GAMESS - converts information into a format acceptable for the quantum chemistry package GAMESS. Users may have to add keywords for particular types of calculations (see GAMESS [8] manual)
SUBROUTINE ORTEP - prepares information for the program ORTEP-II [9]. The routine prepares a file for drawing a single molecule using standard bond search distances of 0.8Å to 1.5Å. Users may have to change these parameters.
SUBROUTINE TEST - converts a file from INTERCHEM to ORTEP-II format. The same search distance as outlined above are used.

SUBROUTINE INTERCH - reads in the information contained in an INTERCHEM file. The file should be of the 'D' type.
SUBROUTINE MATRIX - this routine sets up the matrix for the conversion of crystal co-ordinates (see section 2.1).
SUBROUTINE INVERT - this routine inverts the matrix generated in the above routine. The matrix is inverted using the NAG routine F01AAF.
SUBROUTINE ORTHOG - this routine converts crystal to cartesian co-ordinates by multiplying with the matrix generated in MATRIX.
SUBROUTINE REFRACT - converts cartesian co-ordinates using the matrix generated by the INVERT routine.
SUBROUTINE DIFFER - checks for difference in cartesian co- ordinates and those read in from INTERCHEM. Checks for any translations particular to INTERCHEM.
SUBROUTINE OUTPUT - This routine outputs the results in a format identical to the CSSR file.
SUBROUTINE CNDO - prepares a file in a format for the program CNDO [10]. Users may have to change keywords for non-standard calculations.
SUBROUTINE PACKER - routine which produces the co-ordinates for packing diagrams. Generates a new file containing new co- ordinates and updated connectivity.
SUBROUTINE PLOTS - Generates a file for use with the plotting program PLOTS [11].
SUBROUTINE SLICE - generates the co-ordinates and connectivity for the molecules that are within the slice of thickness d_{hkl} where (hkl) are the Miller indices input by the user.
SUBROUTINE SETUP - sets up the direct and reciprocal lattice variables as outlined in Appendix A. A similar routine is used by PCLEMC.
SUBROUTINE MODQ - Calculates direct and reciprocal lattice modulli (see chapter 5)
SUBROUTINE ANGPLDR - calculates the aco-sine of the angle between the normal to a plane and a direction. A similar routine is used in PCLEMC.
SUBROUTINE CENTRE - calculates the centre of gravity as outlined in section 2.5.

3.5 Changing CRYSTLINK

The program currently runs on a VAX 11/782. If the program has to be changed to run on another system a number of factors have to be considered.

1. FILE HANDLING OPTIONS - The program uses the 'INQUIRE' option to check the existance of a file before opening for reading. The program also uses the 'CARRIAGECONTROL= LIST' option when writing a results file. This prevents carriage control affecting the output file. Both these options are non-standard. To change this a user must find the equivalent commands on the system of implementation. The other option would be to remove these commands and replace with standard commands.

2. INCLUDE OPTION - The common blocks are held in the file COMMON.FOR, this file is brought into each routine via the 'INCLUDE' command. The format of this command may be system dependent. Slight variations in the format of this command may be required.
i.e VAX INCLUDE 'filename' starting column 6
and IBM INCLUDE 'filename' starting column 1,
where 'filename' is the name of the file containing the information to be brought into the routine.

3. NAG LIBRARY - As mentioned earlier the program requires linking to the NAG library. The command linking the library during compilation will be system and site dependent.

4. INTERFACE TO MOLECULAR GRAPHICS - The current version of the program, has been interfaced to the molecular graphics package INTERCHEM [6], the in-house software at Strathclyde University. The program has been written to accept a file of the 'D' type. In order to interface to other molecular graphics packages this subroutine must be re-written to read in the appropriate information in the format supplied by the package. The important variables are held in the common blocks a summary follows in the next section. Examination of the INTERCH routine should provide the basic structure of the new routine required.

3.6 Important Variable Glossary

The important variables are held in common blocks and passed into each of the routines. A summary of these variables follows.
AA,BB,CC,ALP,BET,GAM - the unit cell dimensions a, b, c, α, β and γ.
X,Y,Z - fractional co-ordinates read in from the CSSR file.
XF,YF,ZF - fractional co-ordinates calculated after fitting hydrogens.
XXO,YYO,ZZO - cartesian co-ordinates calculated from fractional co-ordinates using MATRIX and ORTHOG.
XXI,YYI,ZZI - cartesian co-ordinates read in through the INTERCH option.
AMAT - matrix for converting fractional to cartesian co- ordinates.
AMATINV - inverse of matrix AMAT. For converting cartesian to fractional co-ordinates.
NUM - number of atoms in one molecule. Read in from line 3 of CSSR file.
ACHAR - character array which contains the atom labels.
TITLE1, TITLE2, TITLE3, TITLE4 - all character variables which contain the titles at the top of the CSSR file.
ICONN - Array which contains all the connectivity for the atoms.

4 References

[1] National Alogrithms Group. NAG Central Office, Mayfield House, 256 Banbury Road. Oxford OX2 7DE.
[2] SERC Chemical Databank Systems. CSE Applications Group, Daresbury Laboratory, Warrington, England.
[3] International Tables of X-ray Crystallography. (D. Riedel publishing company, 1983).
[4] LEGO. M. Pantos and G. Mant. Daresbury Laboratory, Warrington, England.
[5] VAX Fortran Reference Manual. (April 1982).
[6] INTERCHEM. P. Bladon and R. Breckinridge. University of Strathclyde.
[7] M. J. S. Dewar and W. Theil. J. Amer. Chem. Soc. 99 (1979) 4899.
[8] GAMESS - General Atomic and Molecular Electronic Structure System. M.F. Guest and J. Kendrick. University of Manchester Regional Computer Centre. (June 1986).
[9] ORTEP-II C.K. Johnson Oak Ridge National Laboratory, Oak Ridge, Tennessee. Rep ORNL-3704 US.

[10] CNDO. QCPE Program Library (Number 19).
[11] V. Docherty, unpublished results University of Strathclyde.

Appendix C

PCLEMC

CONTENTS

1 Introduction

PCLEMC (Program to Calculate the Lattice Energy of Molecular Crystals) was developed as a computational model of molecular crystals. The program consists of a structural description of the crystal and uses the atom-atom approximation to determine the interactions between molecules in the crystal. Calculation of these interactions allows evaluation of lattice, slice and attachment energies, parameters which are used in computing theoretical morphologies. Where these parameters and PCLEMC fits into the overall scheme has been outlined in chapter 4.

In this section details of the calculations are given along with examples of how to run the program in it's various operational modes. Sample input files will be used to illustrate input requirements for each mode. The role of each mode will be related back to the flowcharts in the chapter 4. A full description of the program PCLEMC will also be given. Details of the main program, general sub-routines and the graphical routines are provided in section 4 along with details on how to change PCLEMC for running on different machines.

2 Calculation Details

2.1 Structural Details

The program requires basic structural information to generate the three dimensional model of the crystal. The input required includes the unit cell dimensions (a, b, c, α,β and γ), the co-ordinates of the atoms in one molecule and the symmetry relations between the molecules in the unit cell. This information can be obtained from any conventional x-ray structure analysis as outlined in Chapter 2,section 1.2. The program uses this information to construct a unit cell. The unit cell is the basic building block of a crystal, repeated generation of this unit cell along the crystal directions (U, V and W) allows a three dimensional model of the crystal to be built.

2.2 Lattice Energy

The lattice energy (E_{latt}) can, for molecular crystals, be considered to consist of the summation of all the atom-atom interactions between a central molecule and all the surrounding molecules. For a crystal with a central molecule containing n atoms and N surrounding molecules each containing n' atoms then the lattice

energy can be calculated from the summation given in equation (C.1).

$$E_{latt} = 1/2 \sum_{k=1}^{N} \sum_{i=1}^{n} \sum_{j=1}^{n'} V_{kij} \qquad (C.1)$$

V_{kij} is the interaction energy between atom i of the central molecule and atom j of the k^{th} surrounding molecule. The factor 1/2 is introduced to avoid double counting pairs of interactions. The interaction energy V_{ij} can be calculated by an atom-atom approach as outlined in chapter 1, section 3 and later in chapter 5.

In PCLEMC the number of surrounding molecules is governed by a summation limit. This limit is the radius of the sphere inside which the summation is carried out. In lattice energy mode (see following section) PCLEMC allows a series of limits to be introduced. In the next chapter some profiles of the lattice energy as a function of summation limit are plotted for a variety of organic materials. The calculations show an initial increase in the lattice energy with summation limit. Eventually the lattice energy reaches a plateau beyond which increasing the summation limit has negligible contribution to the calculated lattice energy [1].

Once the lattice energy has been calculated at this summation limit it can be compared to the experimental sublimation enthalpy [2,3]. These values will be of opposite sign but should be of the same order of magnitude. In the following chapter a series of calculated lattice energies are compared to the experimental sublimation enthalpies for a variety of organic compounds, agreement being found between calculated and experimental values. This is a useful test of the input information and of the atom- atom parameters selected to describe the interactions in the material of interest. It serves as a check of of the calculations before more computationally intensive calculations of slice and attachment energies (see flowchart in Fig 4.1).

2.3 Slice and Attachment Energies

Once the lattice energy has been calculated it is possible to carry the calculations one step further and calculate the slice and attachment energies. The program requires the Miller indices (hkl) of the faces to be considered. The program calculates the slice energy by summing the interactions between a central molecule and all the molecules within a layer of thickness d_{hkl}. The layer is centered at each of the symmetrically independent sites in the unit cell in turn

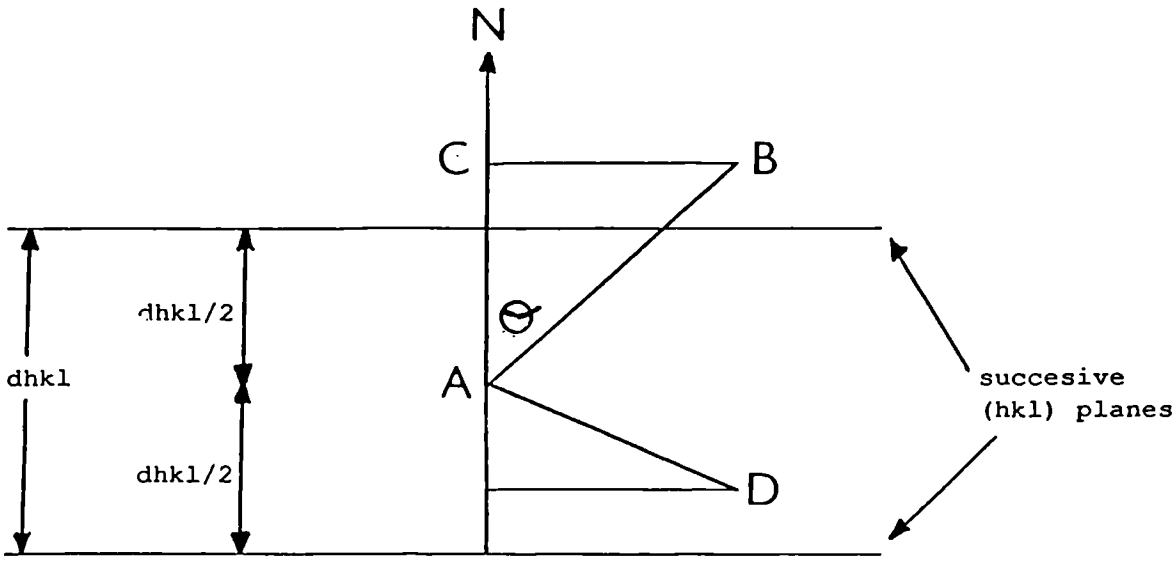

A is the central molecule.

B is a molecule in the crystal out of the slice

D is a molecule in the slice

N is the growth normal to the planes (hkl)

AB and AD are 'bonding vectors'

dhkl is the interplanar spacings

Θ is the angle between the growth normal and the bonding vector.

AC is the component of the vector AB parallel to N the growth normal.

Figure C.1 Outline of the routine for deciding whether molecule is in a slice not.

and then averaged [1]. The attachment energy is calculated by summing all the interactions between a central molecule and all the molecules outwith the slice. These attachment energies can be used as a measure of the relative growth rates normal to the faces being considered [4].

The program decides which molecules are inside the slice by calculating the bonding vector between the central molecule (A) and the molecule under consideration (B) (see Figure C.1). The program calculates the cosine of the angle θ between the normal to the face under consideration and the bonding vector. This allows the magnitude of AC to be calculated (i.e. the size of the bonding vector parallel to the growth normal). Since the slice is centered on the molecule as shown in Figure C.1, if the magnitude of AC is smaller than $d_{hkl}/2$ then the molecule is inside the slice, otherwise the molecule is outside the slice. Figure 1 shows a schematic of this procedure. Molecule B is clearly out of the slice, molecule D is an example of a molecule inside the slice. In order to identify any possible stable growth layers, the program allows the slice to be shifted along the growth normal. A more detailed discussion of this approach has been given by Berkovitch-Yellin [1].

3 Program Operation

3.1 Basic Input and Output

CARD 1 TITLE

The title can be up to eighty characters in length. If 'LAST' the the program terminates. If 'PLO1','PLO2','HIS1',or 'HIS2' then the appropriate graphic routines are activated. The 'POTS' option to obtain general information about the potential functions and parameter sets available in the program.

CARD 2 MODE INFORMATION (A4)

This four letter code switches the program into one of four modes. 'LATT' puts the program into lattice energy mode and 'FULL' puts the program into a mode where it calculates slice and attachment energies. 'POLR' and 'ADDT' switch the program into polar morphology and additive calculation modes respectively.

CARD 3 MNU,MXU,MNV,MXV,MNW,MXW (free format)

The maximum and minimum scan values in the crystal directions U, V and W.

CARD 4 A, B, C, AL, BE, GA (free format)

The unit cell dimensions, the dimensions in angstroms and the angles in degrees.

CARD 5 NZ, NUM, NT, DIEL, IBUG (free format)

NZ = the number of molecules in the unit cell.
NUM = the number of atoms in one molecule (asymmetric unit).
NT = the number of model to be used. This gives a choice of the potential set to be used.
DIEL = the value of the dielectric constant to be used in calculating the electrostatic contribution using a simple coulombic interaction.
IBUG = the debug helper. This controls the amount of output through channel 6. When IBUG = 0 the lattice energy is outputted. This is the minimum amount of output produced. When IBUG is set equal to -1 the intermolecular interactions between the central molecule and surrounding molecules are printed out . Each intermolecular interaction is identified in terms of it's position in the crystal and given a particular number NNUM. When IBUG is set to NNUM the atom-atom interactions for a particular intermolecular interaction are outputted. Using this debug facility can be helpful in identifying the strong bonds in a crystal during a PBC analysis. It is possible to investigate intermolecular and individual atom-atom interactions. This produces a substantial amount of output and should only be used in 'LATT' mode.

CARD 6 NS, STEP (free format)

NS is the number of steps with which to move the growth slice along the growth normal. STEP is the size of the shift in angstroms.

CARD 7 CGX, CGY, CGZ (free format)

Input parameters for the origin of the slice. When 0.0,0.0,0.0, the lattice point is taken as the origin. The center of gravity or the position of an important atom can be used. The input is in fractional co-ordinates.

CARD 8 Two cards repeated NUM times

CARD 8 (a) ID,ND (A4,I3)

ID is the atom label used to identify the atom. This can be useful when the printing control option has been activated.
ND is the atom number. It is used for the selecting the appropriate parameters to describe the atom-atom potential interaction. Using the POTS option allows these potentials to be identified before use.

CARD 8 (b) X,Y,Z.CT (free format)

X, Y and Z are the fractional co-ordinates for the atom described in CARD 8 (a). CT is the partial charge on that atom.

CARD 9 The symmetry operators. Repeated NZ times

The symmetry cards [6], usually one for each molecule in the unit cell. Each

set can be broken up into three component groups of five, one for the symmetry component of each axis. The first three numbers then represent the X,Y and Z components of the X-axis. The last two numbers represent the the translational part.

some examples are:

x,y,z 1 0 0 0 0 0 1 0 0 0 0 0 1 0 0

x+y,y+1/3,-z 1 1 0 0 0 0 1 0 1 3 0 0 -1 0 0

CARD 10 Two cards repeated

CARD 10 (a) H, K and L (free format)

The Miller Indices of the face whoose slice and attachment energy are to be calculated.

CARD 10 (b) ALIM (free format)

The limiting radius, the size of the sphere inside which the potentials are summed.

CARDS 11 Identical to CARD 10

Terminated by 99.0 0.0 0.0

RETURN TO CARD 1

3.2 Output Summary

This is a summary of the input and output channels used in PCLEMC during various calculation modes. Some are common to all types of calculations, unit 5 for example is always used for standard input information. Unit 1 is only used during an additive calculation to write and read information to the file TEMP.DAT.

UNIT=5 Input of the host information PCLEMC.

UNIT=3 Input of additive information.

UNIT=6 Standard output channel for results.

UNIT=1 Output and input channel for file TEMP.DAT. The file is opened and closed by the program. This is only used in additive calculations

UNIT=7 Output channel for file containing summarised output.

UNIT=8 Output channel for line printer histogram.

UNIT=10 Graphical output channel of .RCO plot files [7]. An .RCO file type is a file containing graphical information that can be sent to a variety of output devices.

3.3 Lattice Calculation

This type of calculation can be run interactively. The use of the 'LATT' identifier in line 2 flags the program into lattice energy calculation mode. The sample file for β-succinic acid shows the input to perform a lattice energy calculation on this material. The basic structural information for β- succinic acid is given in Chapter 7. The input file shown in section 6 gives the basic input information for calculating the lattice energy at successive summation limits including 8Å, 10Å, 12Å and 30Å. Example profiles of this type are shown in Figure 5.1 This input file is read in through unit 5, the resultant output summary from unit 7 is also given in section 6. The output information includes the basic structural information, details on potential set selected and results including number of intermolecular contacts, electrostaic contributions and lattice energy.

3.4 Full Calculation

The input for the full calculation mode is essentially the same as that for the lattice energy mode. The difference is that instead of a series of limiting radii a selection of faces can be entered. The limiting radius is usually kept constant for these calculations. At line 2 in the example input file the mode option has been changed to 'FULL'. The input file for β- succinic acid is given at the end of this appendix. The faces to be considered in the sample input file are (100) and (110). The output from this mode is essentially the same as for 'LATT' mode except that slice and attachment energies replace the lattice energy results.

3.5 Polar Calculation

The calculation for polar morphology can be activated using the 'POLR' flag on line two (see example input file). The input is identical to that for the 'FULL' mode except that an extra set of charges have to be inputted. A sample input file for urea has been given at the end of this appendix. The first set of charges is for the molecule in the crystal lattice, the second set of charges is for the isolated molecule. The method of obtaining the distribution over isolated molecules and molecules in the crystal lattice is given in chapter 7. When carrying out the polar morphology calculation the approach is almost identical to the normal calculation, except that the program assigns different distributions to the molecules inside and outside the slice. The lattice charge distribution is assigned to the molecules inside the slice, the monomer distribution to the

molecules outwith the slice i.e. the oncoming molecules.

3.6 Additive Calculation

When carrying out an additive calculation the program currently operates in two modes, switching between these two modes automatically for each crystallographic independent site. In mode 1 the additive is placed in a slice and the familiar slice energy calculated (Esl'). In this mode the attachment energy of a pure slice coming onto an surface containing an additive (Eatt") is also calculated. During these calculations the site of the additive for mode 2 calculations is obtained. The 'site' is defined as the closest position to the slice origin molecule available outwith the slice. The 'site' is recorded in terms of crystal directions (U,V,W) and position in the unit cell (Z) This information is written through channel 1 to the file called TEMP.DAT. In mode 2 the information in the file TEMP.DAT is read through channel 1 and used to locate the additive site. At the 'site' the host molecule is replaced by an additive molecule and the attachment of a layer containing an additive to a pure surface (Eatt') is calculated. The models for Eslice', Eatt' and Eatt" have been detailed in Chapter 2 (see Fig 2.20).

The program requires the standard input for the program in 'FULL' mode. This standard file is read in through channel 5 (see subsections 3.2). In 'ADDT' mode the program requires some information concerning the additive which is read in through channel 3. It was found most convienent to keep input information in this mode in two seperate files, and to read the files in through different channels. This allows a number of additives to be considered for one host system. The additive file was given the .ADD filetype. The program can be flagged into additive calculation in line two of the standard input file. The format of the line would be

ADDT 'filename'

where 'filename' is the name of the file that contains information on the additive. Examples of the two files needed for additive calculations are given in section 6 for the host/additive system of benzamide/benzoic acid [8].

4 Program Description

4.1 General Description

The program has been written in standard Fortran-77 (American National Standard ANSI X3.9 1978) except for the graphic routines which are written using the GINO plotting software. The program has sucessfully been run on a VAX 11/782 with Digital's VAX Fortran Compiler and on an IBM-AT with the IBM Fortran Compiler (V2.0). The main program can be considered to consist of a number of sections. The first section consists of reading in the input information including structural details and program mode. The second section consists of generating the three dimensional model of the crystal by generating the unit cell along the crystal directions U, V and W. The main section of the program consists of identifying atom-atom pairs, calculating their distance apart, evaluating thier interaction energy and deciding whether the calculated intermolecular interaction belongs to the slice energy or not. The final section is the output of results and the routing of appropriate information into the graphical subroutines via the common block GRAPHIC (see graphical subroutines)

4.2 General Sub-routines

SUBROUTINE SETUP - the subroutine uses the unit cell dimensions to calculate the direct and reciprocal lattice information stored in the common blocks TEND, TENR. The mathematics are outlined in the International Tables [6] and in Appendix A.

SUBROUTINE MODQ - Calculates the direct and reciprocal modulii depending on the value of variable T. T=1 ... reciprocal and T=2 ..... direct.

SUBROUTINE ANGPLD - This subroutine calculates the angle between a crystal plane and a crystal direction.

SUBROUTINE DISTAN - This program calculates the distance between two points . It calls the subroutine MODQ in direct mode

SUBROUTINE POTL - This routine directs the program to the appropriate potential subroutine containing the correct data set.

SUBROUTINE POT1 - contains the parameters to describe the interaction between an atom-atom pair. It outputs the attractive and repulsive part of the interaction. The program as supplied contains a number of potential sets. Users can install their own preferred parameter sets. The general structure of the routine can be seen from the program. The output from this program is the at-

tractive and repulsive contributions from an atom-atom interaction. The routine is called at the start to setup the potentials.
SUBROUTINE DETAIL - this routine calls each of the potential sub- routines in turn extracting the general information about each of the potential sets and outputting results to a file. This can be called using the 'POTS' option as described in section 3.1.

4.3 Graphical Sub-routines

The input from the main program to these subroutines are stored in the common block called GRAPH.
SUBROUTINE HIS1 - This produces a histogram of the relative morphological importance based on the attachment energies calculated from the main program. It uses the GINO[9] software and creates a file which can be dumped to a number of graphical devices. This routine creates a graphical file of the RCO type [7].
SUBROUTINE HIS2 - Produces a histogram of the relative morphological importance which can be dumped to a line-printer. It outputs to unit 8 in a file called HIST.DAT.
SUBROUTINE PLO1- plots the lattice energy against the size of the sphere inside which the summation takes place. Again the GINO software is utilised.
SUBROUTINE PLO2 - plots the number of intermolecular contacts against the limiting radius using the GINO software routines.

4.4 Changing PCLEMC

As the program is largely written in standard Fortran-77 (ANSI- X3.9 1978) the program should be easy to implement on any machine which supports a Fortran 77 compiler. The graphical subroutines which are not fundamental to the execution of the program can be replaced with dummy subroutines if the GINO [9] software is not available, or replaced by routines written by the user for the graphics software available on the machine orf implementation. The IBM versions has the graphic routines replaced. The information for the graphical sub-routines are held in the common block GRAPH. Users can change the potential sub-routines to use parameter sets of their own preference. The output from these routines is the attractive and repulsive contributions for an atom-atom interaction. Looking at the form of the routines POT1 and POT2 etc should allow the user to write their own potential routines.

EXAMPLE 1 Succinic acid in 'LATT' mode.

```
SUCCINIC ACID - force field of Hagler      ---- title (80 chars)
LATT                                      ---- program mode
-10 9 -10 9 -10 9                         ---- U,V,W scan values
5.519 8.862 5.101 90.0 91.6 90.0          ---- unit cell dimensions
2 14 1 1 0                                ---- NZ,NUM,MODEL,IDIEL,IBUG
0 0.0                                     ---- growth slice shift
0.0 0.0 0.0                               ---- origin of slice
CAR1  3                                   ---- atom label and identifier
0.08080  -.06640  -.02770  -0.20          ---- fractional co-ords and ch
CAR2  4
0.25990  -.03450  -.23640  0.38
OXY1  6
0.25280  0.07750  -.37600  -0.38
OXY2  7
0.42400  -.13950  -.25700  -0.38
HYD1  1
-.02530  -.16350  -.09240  0.10
HYD1  1
0.18160  -.10350  0.14660  0.10
HYD2  2
0.53550  -.11890  -.40250  0.38
CAR1  3
-.08080  0.06640  0.02770  -0.20
CAR2  4
-.25990  0.03450  0.23640  0.38
HYD1  1
0.02530  0.16350  0.09240  0.10
HYD1  1
-.18160  0.10350  -.14660  0.10
OXY1  6
-.25280  -.07750  0.37600  -0.38
OXY2  7
-.42400  0.13950  0.25700  -0.38
HYD2  2
-.53550  0.11890  0.40250  0.38
1 0 0 0 0 0 1 0 0 0 0 0 1 0 0             ---- symmetry operators
1 0 0 0 0 0 -1 0 1 2 0 0 1 1 2
1 0 0                                     ---- face to be considered
10.0                                      ---- summation limit
1 0 0
15.0
1 0 0
30.0
99 0 0                                    ---- terminate input
LAST                                      ---- program stop
```

EXAMPLE 2 Succinic acid in 'FULL' mode.

```
SUCCINIC ACID - force field of Hagler      ---- title (80 chars)
FULL                                      ---- program mode
-10 9 -10 9 -10 9                         ---- U,V,W scan values
5.519 8.862 5.101 90.0 91.6 90.0          ---- unit cell dimensions
2 14 1 1 0                                ---- NZ,NUM,MODEL,IDIEL,IBUG
0 0.0                                     ---- growth slice shift
0.0 0.0 0.0                               ---- origin of slice
CAR1  3                                   ---- atom label and identifier
0.08080  -.06640  -.02770  -0.20          ---- fractional co-ords and ch
CAR2  4
0.25990  -.03450  -.23640  0.38
OXY1  6
0.25280  0.07750  -.37600  -0.38
OXY2  7
0.42400  -.13950  -.25700  -0.38
HYD1  1
-.02530  -.16350  -.09240  0.10
HYD1  1
0.18160  -.10350  0.14660  0.10
HYD2  2
0.53550  -.11890  -.40250  0.38
CAR1  3
-.08080  0.06640  0.02770  -0.20
CAR2  4
-.25990  0.03450  0.23640  0.38
HYD1  1
0.02530  0.16350  0.09240  0.10
HYD1  1
-.18160  0.10350  -.14660  0.10
OXY1  6
-.25280  -.07750  0.37600  -0.38
OXY2  7
-.42400  0.13950  0.25700  -0.38
HYD2  2
-.53550  0.11890  0.40250  0.38
1 0 0 0 0 0 1 0 0 0 0 0 1 0 0             ---- symmetry operators
1 0 0 0 0 0 -1 0 1 2 0 0 1 1 2
1 0 0                                     ---- face to be considered
30.0                                      ---- lattice limit
1 1 0                                     ---- another face
30.0
1 1 -1
30.0
99 0 0                                    ---- terminate input
LAST                                      ---- program stop
```

EXAMPLE 3 Urea in 'POLR' mode.

```
UREA HAGLERS POTS AND CHARGES - POLAR CALCULATION
POLR
-10 9 -10 9 -10 9
5.565 5.565 4.684  90.0 90.0 90.0
2 8 1 1 0
0 0.0
0.00 0.500 0.316
CAR2  4
  0.00000     0.50000     0.32600     0.38    0.365      <---- fractional co-
OXY1  6                                                        and charges
  0.00000     0.50000     0.59530    -0.38   -0.310
NITR  5
  0.14590     0.64590     0.17660    -0.83    -0.793
HYD2  2
  0.25750     0.75750     0.28270    0.415    0.388
HYD2  2
  0.14410     0.64410    -0.03800    0.415    0.349
NITR  5
 -0.14590     0.35410     0.17660    -0.83    -0.83
HYD2  2
 -0.25750     0.24250     0.28270    0.415    0.388
HYD2  2
 -0.14410     0.35590    -0.03800    0.415    0.349
1 0 0 0 0 0 1 0 0 0 0 0 1 0 0
0 1 0 0 0 -1 0 0 0 0 0 0 -1 1 0
1 1 0
30.0
0 0 1
30.0
1 1 1
99 0 0
LAST
```

EXAMPLE 4 Benzamide in 'ADDT' mode with additive benzoic acid.

```
BENZAMIDE
ADDT BENZOIC.ADD                          ---- program in ADDT mode and name
-10 9 -10 9 -10 9                              file containing additive info
5.590 5.0110 21.930 90.0 90.75 90.00
4 16 1 1 0
0 0.0
-0.5 0.076  0.115
CAR1  3
-.17772  0.13046  0.19814  -0.1
CAR1  3
-.34743  -.06584  0.20369  -0.1
CAR1  3
-.52163  -.09500  0.15844  -0.1
CAR1  3
-.52547  0.07294  0.10909   0.0
CAR1  3
-.35564  0.27025  0.10439  -0.1
CAR1  3
-.15858  0.29596  0.14893  -0.1
CAR2  4
-.71288  0.03114  0.06120  0.38
HYD1  1
-.05504  0.15513  0.22906  0.1
HYD1  1
-.36226  -.18055  0.24069  0.1
HYD1  1
-.64295  -.23486  0.16391  0.1
HYD1  1
-.34756  0.37927  0.06838  0.1
HYD1  1
-.04949  0.43365  0.14257  0.1
HYD2  2
-.90713  0.23037  0.00075  0.415
HYD2  2
-.74808  0.40960  0.04141  0.415
NITR  5
-.78003  0.24030  0.02826  -0.83
OXY1  6
-.80214  -.19107  0.05309  -0.38
1 0 0 0 0 0 1 0 0 0 0 0 1 0 0
-1 0 0 0 0 0 1 0 1 2 0 0 -1 1 2
-1 0 0 0 0 0 -1 0 0 0 0 0 -1 0 0
1 0 0 0 0 0 -1 0 1 2 0 0 1 1 2
0 0 2
30.0
1 0 0
30.0
99 0 0
LAST
```

EXAMPLE 5 Benzoic additive input information.

```
benzoic acid                                  ---- additive title
15                                             ----- no of atoms in additive
CAR1  3                                        ----- atom label and identifier
-.17772  0.13046  0.19814  -0.1               ----- co-ordinates and charge on
CAR1  3
-.34743  -.06583  0.20369  -0.1
CAR1  3
-.52163  -.09499  0.15844  -0.1
CAR1  3
-.52547  0.07295  0.10909  0.0
CAR1  3
-.35564  0.27025  0.10439  -0.1
CAR1  3
-.15858  0.29598  0.14893  -0.1
CAR2  4
-.71289  0.03115  0.06120  0.38
HYD1  1
-.05504  0.15513  0.22906  0.1
HYD1  1
-.36227  -.18054  0.24069  0.1
HYD1  1
-.64296  -.23486  0.16391  0.1
HYD1  1
-.34757  0.37927  0.06838  0.1
HYD1  1
-.04949  0.43365  0.14257  0.1
HYD2  2
-.90714  0.23038  0.00075  0.38
OXY2  7
-.78003  0.24031  0.02826  -0.38
OXY1  6
-.80214  -.19106  0.05309  -0.38
```

5 Sample Input

The sample input files are given at the end of this appendix. Example 1 is for the program operating in 'LATT' mode with a range of limiting radii.. Example 2 is a 'FULL' calculation on succinic acid with a number of faces being considered. Example 3 is for the program operating in 'POLR' mode. Examples 4 and 5 are concerning the program operating in additive calculation mode. Example 4 shows the input for the main file and Example 5 shows the input information for an additive file. The example shown is for benzamide with benzoic acid the additive.

6 References

[1] Z. Berkovitch-Yellin. J. Am. Chem. Soc. 107 (1985) 8239.

[2] F.A. Momany, L.M. Carruthers, R.F. McGuire and H.A. Scheraga. J. Phys. Chem. 78 (1974) 1579.

[3] S. Lifson, A.T. Hagler and P. Dauber. J. Amer. Chem. Soc. 101 (1979) 5111.

[4] P. Bennema and P. Hartman. J. Cryst. Growth 49 (1980) 145.

[5] P.Hartman and W.G. Perdok. Acta Cryst. 8 (1955) 49.

[6] International Tables of X-ray Crystallography. vol A (D. Riedel Publishing Company, 1983).

[7] RCO plot file format laid down by Regional Computing Organisations of the Universities of Edinburgh, Glasgow and Strathclyde.

[8] Z. Berkovitch-Yellin, J. van Mil, L. Addadi, M. Idelson, M. Lahav and L. Leiserowitz. J. Am. Chem. Soc. 107 (1985) 3111.

[9] GINO plotting system. Computer Aided Design Centre, Cambridge, England.

Appendix D

Fitting Hydrogens To Incomplete Structures

CONTENTS

1 Introduction

In a number of cases the published crystal structure of an organic compound is not complete and does not have the positions of the hydrogens reported. In such cases an attempt can be made to predict the positions of the hydrogens by fitting the hydrogens to the skeletal structure assuming standard bond lengths and geometry and then minimsing the interaction energy with respect to the hydrogen positions.

In a crystal the positions of the hydrogens are governed by both the inter and intramolecular interactions. Since the minimisation of the positions deals only with the intramolecular interactions then the validity of such an approach must be tested.

2 Procedure

The crystal structures of both l-alanine and anthracene have been reported in the literature [1,2]. In both cases the hydrogen positions have been reported. In the case of l-alanine the structure determination was carried out using neutron diffraction rather than conventional x-ray diffraction. A neutron diffraction study is generally accepted as being a more accurate method of determing the positions of hydrogens since the scattering results from interactions with the nucleus rather than with the electrons as is the case with conventional x-ray diffraction (see Chapter 2). The cases of l-alanine and anthracene were considered as there are different degrees of intra and intermolecular bonding present.

The hydrogen atoms were removed from the l-alanine and anthracene structures and then fitted back onto the skeletal structure assuming standard bond lengths and geometry using the molecular graphics routines available in INTERCHEM [3]. The positions of the hydrogens were then minimised using MOPAC [4]. The resultant cartesian co-ordinates were then converted back to fractional co-ordinates using INTERCHEM and CRYSTLINK (see Chapter 4 and Appendix B).

3 Results

The reported hydrogen co-ordinates are compared to the fitted co- ordinates for l-alanine and anthacene in Tables D.1 and D.2. In these and subsequent tables in this appendix the * means fitted value. The results are in reasonable

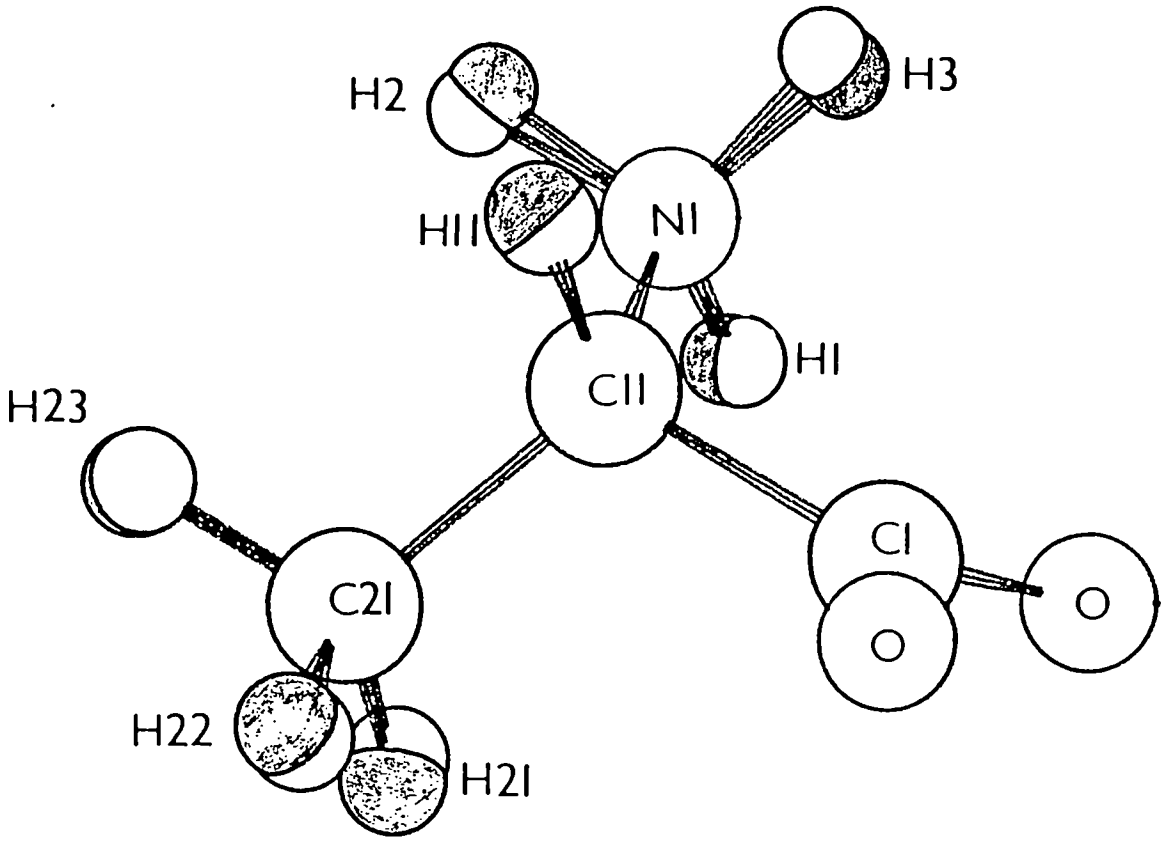

Figure D.1 Molecule of l-alanine with fitted and reported hydrogens Shaded atoms are fitted hydrogens.

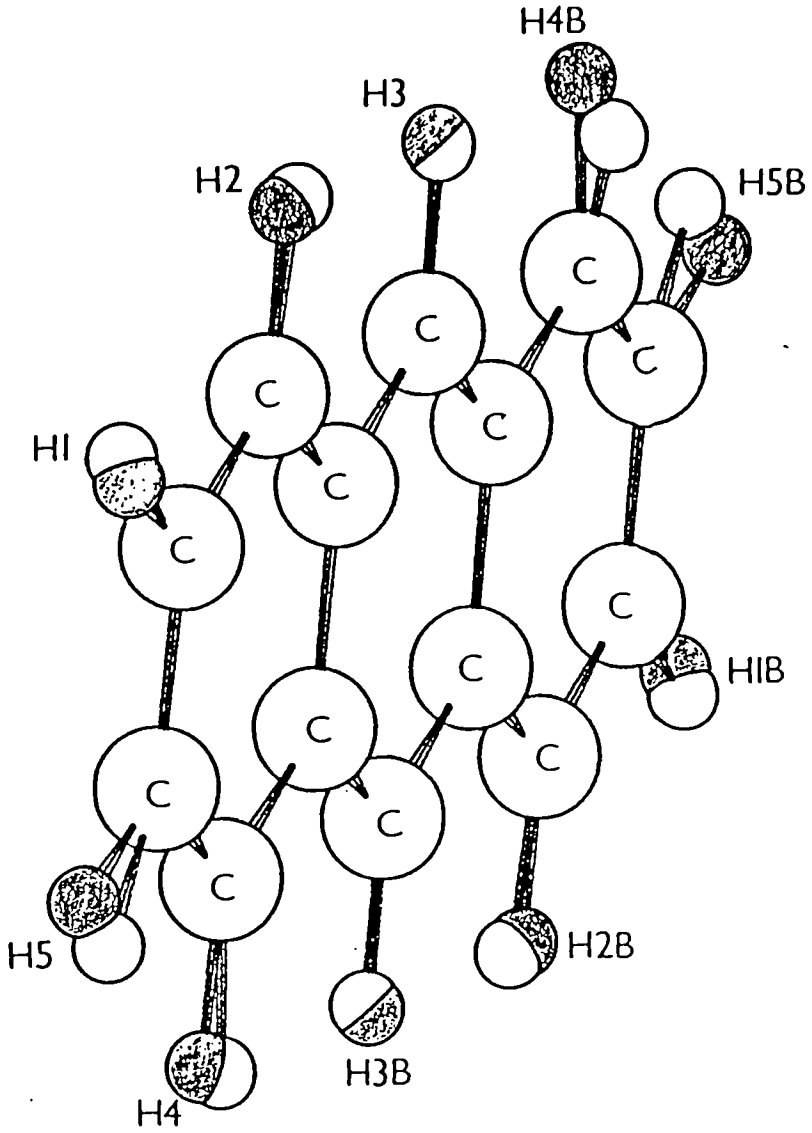

Figure D.2 Molecule of anthracene with fitted and reported hydrogens. Shaded atoms are fitted hydrogens.

Table D.1 Fitted and reported hydrogen fractional co-ordinates for l-alanine (* = fitted).

ATOM	FRACTIONAL CO-ORDINATES					
	X	X*	Y	Y*	Z	Z*
H1	-0.2893	-0.2957	0.0593	0.0581	-0.7997	-0.8109
H11	-0.5643	-0.5663	0.2473	0.2484	-0.6624	-0.6676
H21	-0.6811	-0.6921	0.0067	0.0033	-0.6943	-0.6826
H2	-0.4052	-0.3894	0.1489	0.1553	-0.9822	-0.9807
H22	-0.8541	-0.8619	0.10501	0.1111	-0.5705	-0.5757
H3	-0.2158	-0.2053	0.1917	0.1831	-0.7889	-0.7793
H23	-0.7900	-0.7904	0.1106	0.1066	-0.8671	-0.8746

Table D.2 Fitted and reported hydrogen fractional co-ordinates for anthracene (* = fitted).

ATOM	FRACTIONAL CO-ORDINATES					
	X	X*	Y	Y*	Z	Z*
H1	0.1308	0.1323	0.1084	0.0836	0.4718	0.4737
H2	0.1959	0.1882	0.3246	0.3182	0.3167	0.3193
H3	0.1546	0.1559	0.3764	0.3711	0.0852	0.0848
H4	-0.1207	-0.1300	-0.4304	-0.4207	0.1432	0.1463
H5	-0.0239	-0.0263	-0.3239	-0.2774	0.3791	0.3879
H1B	-0.1308	-0.1325	-0.1083	-0.0837	-0.4718	-0.4737
H2B	-0.1959	-0.1884	-0.3246	-0.3183	-0.3167	-0.3193
H3B	-0.1546	-0.1561	-0.3764	-0.3712	-0.0852	-0.0847
H4B	0.1207	0.1298	0.4304	-0.4207	-0.1432	-0.1463
H5B	0.0239	0.0262	0.3239	0.2773	-0.3791	-0.3880

Table D.3 Comparison of bond lengths and angles between fitted and reported hydrogens for l-alanine (* = fitted).

ATOMS A	B	C	BOND LENGTHS (B-C)	(B-C)* (Angstroms)	BOND ANGLES (ABC)	(ABC)*
C11	C21	H21	1.097	1.110	110.3	113.3
C11	C21	H22	1.081	1.110	110.5	110.0
C11	C21	H23	1.080	1.113	110.4	111.9
C11	N1	H1	1.028	1.027	111.3	112.8
C11	N1	H2	1.047	1.022	109.5	112.8
N1	C11	H11	1.091	1.123	106.9	106.1

Table D.4 Comparison of bond lengths and angles between fitted and reported hydrogens for anthracene (* = fitted).

ATOMS A	B	C	BOND LENGTHS (B-C)	(B-C)* (Angstroms)	BOND ANGLES (ABC)	(ABC)*
C7	C6	H4	1.127	1.092	123.8	120.5
C1	C7	H5	1.187	1.094	130.7	118.6
C3	C4	H3	1.117	1.091	119.2	119.6
C2	C1	H1	1.134	1.093	113.5	120.0
C5	C4B	H3B	1.117	1.092	120.4	119.7
C3	C2	H2	1.145	1.089	116.3	119.7
C5B	C6B	H4B	1.127	1.091	115.7	119.2
C1B	C7B	H5B	1.187	1.093	130.7	118.6
C2B	C1B	H1B	1.134	1.093	113.5	120.0
C3B	C2B	H2B	1.145	1.090	116.3	119.7

agreement with each other. The bond distances and bond angles in the reported and fitted cases were also calculated and are shown in Tables D.3 and D.4. The bond distances are again in reasonable agreement with each other the bond angles also showing good agreement perhaps the best agreement being found in the l-alanine. The deviations in the case of l-alanine were very small differing by 4° at most. in anthracene the deviations were slightly greater 12° at maximum. Figures D.1 and D.2 are the molecules of l-alanine and anthracene, the shaded atoms indicating fitted hydrogens. The theoretical bond lengths are in excellent agreement with those observed. In the l-alanine case they tend to be slightly overestimated and in the anthracene case underestimated. This could be corrected by using the average of the bond lengths determined from crystallographic studies of related compounds rather than the default values supplied by INTERCHEM [1]. A comprehensive study of the bond distances determined by x-ray and neutron diffraction has already been undertaken [5].

4 References

[1] M.S. Lehmann, T.F. Koetzle and W.C. Hamilton. J. Amer. Chem. Soc. 94 (1972) 2657.

[2] R. Mason. Acta Cryst 17 (1964) 547.

[3] INTERCHEM. P. Bladon and R.Breckinridge. University of Strathclyde (1986).

[4] MOPAC. F.J. Sieler. Res. Lab. U.S. Air Force Academy Colorado Springs.

[5] F.H. Allen, O. Kennard, D.G. Watson, L. Brammer, A. Guy Opren and R. Taylor, J. Chem. Soc. Perkin Trans. II (1987) S1.

Appendix E

Publications and Reports

1 Publications From Thesis

[1] Modelling The Morphology of Molecular Crystals. Application To Anthracene, Biphenyl and β-Succinic Acid.
R. Docherty and K.J. Roberts
Journal Of Crystal Growth 88 (1988) 159

[2] MORANG - A Computer Program Designed To Aid In The Determinations of Crystal Morphology.
R. Docherty, K.J. Roberts and E. Dowty
Computer Physics Communications 51 (1988) 9

2 Publications and Reports Using Programs

[1] Experimental and Theoretical Morphology of p-Nitro-p'-methyl Benzilidine Aniline, A Non Linear Optic Material.
S.N. Black, R.J. Davey and T.D. McLean
Mol. Cryst. Liq. Inc. Non Lin. Opt. 161 (1988) 283

[2] A Theoretical Study Of The Crystal Morphology Of Ibuprofen P. Meenan
Final Year Project, University of Strathclyde (1988)

[3] The Energetics Of Hydrogen-Bonded Proton Exchange in Terephthalic Acid.
S.N. Black and D. Pullen.
Journal Of Solid State Chemistry 79 (1989) 293.

3 Presentations at Meetings Attended

[1] 'Modelling The Morphology Of Molecular Crystals'

presented at,

British Crystallographic Association, Spring Meeting, Edinburgh, April 1986.

Eighth International Conference On Crystal Growth, York, August 1986.

Second International Conference On The Crystal Growth Of Biological Macromolecules, Bischenberg, France, July 1987.

[2] 'Modelling Polar Morphology - Urea As A Case Study'

presented at

British Crystallographic Association, Spring Meeting, Warwick, April (1988)

Crystal Science Workshop, University Of Strathclyde, July (1989).

4 Papers In Preparation

[1] Modelling The Morphology Of Molecular Crystals. The Principles Behind Donnay-Harker, Hartman-Perdok, Attachment Energy and Ising Models.
P. Bennema, R. Docherty and K.J. Roberts.

[2] Modelling The Morphology of Molecular Crystals. Application Of Donnay-Harker, Hartman-Perdok, Attachment Energy and Ising Models To Benzophenone.
R. Docherty, K.J. Roberts, P. Bennema and L.M.A.J. Jetten.

[3] Modelling Polar Morphology. An Investigation Of Urea.
R. Docherty, K.J. Roberts, V. Saunders, R.J. Davey and S.N. Black.

[4] PCLEMC, Program For Calculating The Lattice Energy Of Molecular Crystals
R. Docherty and K.J. Roberts